STUDIES OF PNP AND PCP PINCER COMPLEXES: SYNTHESIS AND C-H ACTIVATION POTENTIAL OF PNP PINCER COMPLEXES AND A PCP PINCER COMPLEX APPLIED TO ALKENE HYDROGENATION

by

ELIZABETH MARIE PELCZAR

A Dissertation submitted to the

Graduate School-New Brunswick

Rutgers, The State University of New Jersey

in partial fulfillment of the requirements

for the degree of

Doctor of Philosophy

Graduate Program in Chemistry

written under the direction of

Professor Alan S. Goldman

and approved by

_____

_____

_____

_____

New Brunswick, New Jersey

January 2008

ABSTRACT OF THE DISSERTATION

STUDIES OF PNP AND PCP PINCER COMPLEXES: SYNTHESIS AND C-H

ACTIVATION POTENTIAL OF PNP PINCER COMPLEXES AND A PCP PINCER

COMPLEX APPLIED TO ALKENE HYDROGENATION

By: Elizabeth Marie Pelczar

Dissertation Director:

Professor Alan S. Goldman

The ability to break the C-H bond, which is considered one of the most inert bonds in chemistry, has vast applications in a wide variety of chemical processes. (^{R}PCP)Ir pincer complexes have been shown to be highly effective catalysts for C-H activation, in particular in the context of dehydrogenation reactions. Related to the (^{R}PCP)Ir complexes are (^{R}PNP)M complexes which have not been examined in terms of C-H activation potential.

Chapter 2 presents the synthesis and full characterization of two new iron PNP pincer complexes, (^{tBu}PNP)FeCl$_2$ and (^{tBu}PNP)Fe(CO)$_2$. The dichloride complex is paramagnetic with an unusually long Fe-N bond. The blue dicarbonyl complex has significantly bent Fe-C-O angles in the solid state and in solution, and appears to be an equilibrium mixture between square pyramidal and trigonal bipyramidal structures.

Chapter 3 presents the synthesis and full characterization of two new osmium ^{tBu}PNP pincer complexes, (^{tBu}PNP)OsCl$_3$ and (^{tBu}PNP)OsH$_4$. The crystal structure of the hydride complex shows that the complex is a purely classical hydride in the solid state.

Chapter 4 follows up on (^{tBu}PNP)OsH$_4$ by discussing the reactivity of this complex. Unlike the (^{R}PCP)Ir complexes, (^{tBu}PNP)OsH$_4$ was not found to be an active catalyst for C-H activation, dehydrogenation, or phenylacetylene dimerization. The difference in reactivity most likely comes from the difference in metal-hydride bond strength.

Chapter 5 discusses the hydrogenation kinetics of *trans*-5-decene by (^{tBu}PCP)IrH$_2$. The reaction follows second order kinetics and appears to be largely temperature independent. The room temperature activation energy, activation enthalpy, and activation entropy were calculated and show that the main barrier comes from entropic factors.

Chapter 6 presents the synthesis and characterization of a new (^{tBu}PCP)IrH-μ^2-Cl$_2$-Ir(COD) dimer. This complex can be thought of as the oxidative addition product of (^{tBu}PCP) with ½ [Ir(COD)Cl]$_2$. The complex was found to be an Ir(I) / Ir(III) dimer with the hydride atom coordinated to the Ir(III) atom that was coordinated to the PCP ligand.

ACKNOWLEDGEMENTS

DEDICATION

To my family.
Thanks for everything.

TABLE OF CONTENTS

LIST OF FIGURES

LIST OF TABLES

LIST OF SCHEMES

Chapter 1

Introduction to the Thesis

The ability to selectively activate carbon-hydrogen (C-H) bonds, has great potential in the context of a wide range of chemical processes. One of the main goals of transition metal chemistry in the past two decades has been to develop organometallic catalysts that can selectively and catalytically manipulate the C-H bond.

In 1965 Chatt reported the first example of C-H bond activation by a transition metal complex.[1] A ruthenium(0) complex was found to activate a ligand C-H bond to give a ruthenium(II) dimer and, perhaps even more significantly, activated a C-H bond of naphthalene to give the ruthenium(II) naphthyl hydride complex (Scheme 1.1). Shortly after that, H/D exchange reactions between methane and D_2O by Shilov showed that platinum could also activate C-H bonds.[2] Similar to Chatt's complex, where ruthenium(0) activated a ligand C-H bond, $Ir(PPh_3)Cl$ was found to activate a phenyl C-H bond to give a cyclometalated iridium hydride complex as shown in Scheme 1.2.[3] Ruthenium, rhodium, iridium and platinum are all late transition metals but early transition metal complexes can also activate C-H bonds. For example, photolysis of Cp_2WH_2 in the presence of benzene was found to give $Cp_2W(Ph)H$ (Scheme 1.3).[4]

Scheme 1.1: First example of transition metal C—H activation[1]
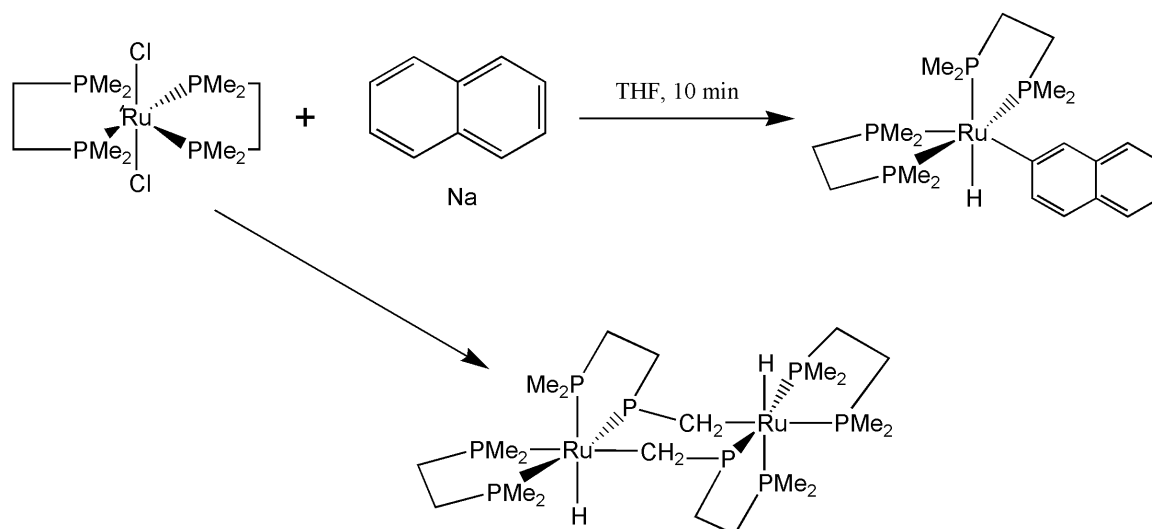
Scheme 1.2: C—H activation by Ir(PPh₃)₃Cl[3]
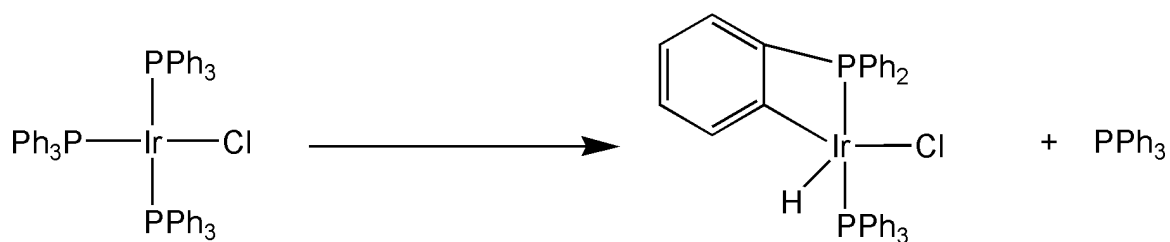
Scheme 1.3: C—H activation by the early transition metal complex Cp₂WH₂[4]
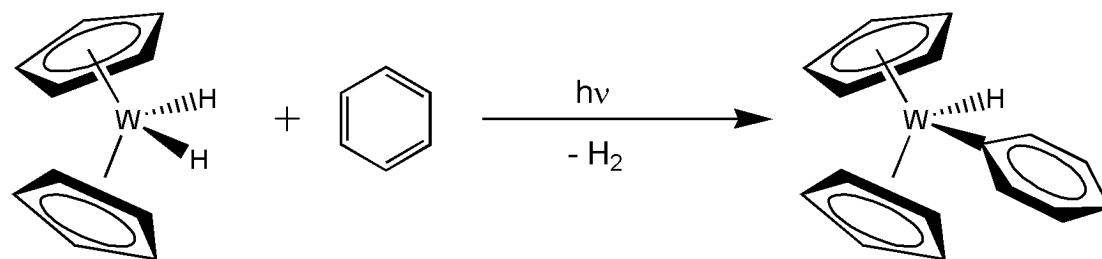
These early examples of C-H activation mostly involved aryl C-H bonds; however activation of the less reactive alkane C-H bonds has also been observed. The first examples of alkane C-H activation were reported by Bergman[5] and then Graham,[6] who observed that Cp*Ir(PMe$_3$)H$_2$, presumably after losing H$_2$, activated cyclohexane to give the cyclohexyl iridium hydride species Cp*IrH(PMe$_3$)(C$_6$H$_{11}$) (Scheme 1.4).

Scheme 1.4: First example of alkane C-H activation[5,6]
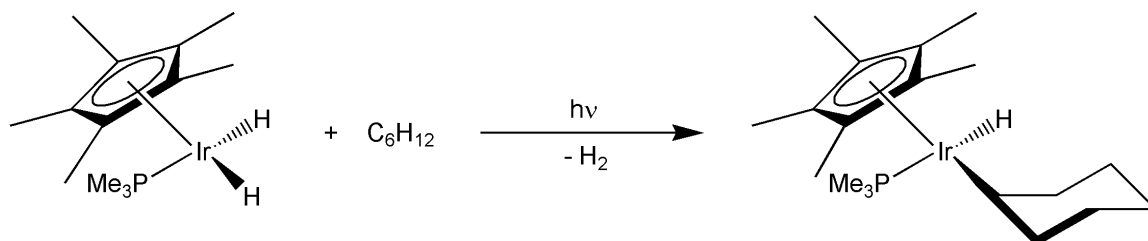
C-H activation by complexes without Cp ligands has frequently been reported in metal complexes containing phosphine ligands. [Os(PMe$_3$)$_4$(CH$_2$^{t}Bu)(H)] was found to oxidatively add C-H bonds of various molecules as was [Os(PMe$_3$)$_4$(R)(H)].[7,8] Another complex containing a group 8 metal, Fe(depe)$_2$ (depe = bis(diethylphosphino)ethane) selectively added the primary C-H bond of *n*-pentane.[9] When [(cyclooctene)$_2$IrCl]$_2$ was dissolved in benzene and P^{i}Pr$_3$ was added, (P^{i}Pr$_3$)$_2$Ir(Cl)(Ph)(H) was obtained and crystallographically characterized.[10] Nitrogen based ligands have been found to be effective for promoting C-H activation with platinum complexes. [(tmeda)Pt(CH$_3$)(NC$_5$F$_5$)]$^+$ reacted with ^{13}C-labeled methane to give [(tmeda)Pt(^{13}CH$_3$)(NC$_5$F$_5$)]$^+$, and [(diimine)Pt(CH$_3$)(OH$_2$)]$^+$ was also found to activate C-H bonds.[11,12]

In attempting to exploit the ability of organometallic complexes to activate C-H bonds dehydrogenation is a particularly attractive option. Alkanes are the most abundant organic chemicals but they are also among the least useful for chemical synthesis. Alkenes, by contrast, are very valuable in a variety of areas including synthetic organic and petroleum-related chemistry. The ability to catalytically dehydrogenate alkanes to the much more useful alkenes has become one of the main focuses of organometallic chemistry.

The first examples of transfer dehydrogenation were by Crabtree who reported that $[(Me_2CO)_2IrH_2(PPh_3)_2]^+$ dehydrogenated cycloalkanes to give the cycloalkadiene iridium complexes.[13] In this reaction *tert*-butylethylene (TBE) was used as an acceptor and hydrogenated to 2,2-dimethylbutane (*tert*-butylethane), while the cycloalkane was dehydrogenated (Scheme 1.5).[13]

Scheme 1.5: First example of transfer dehydrogenation[13]
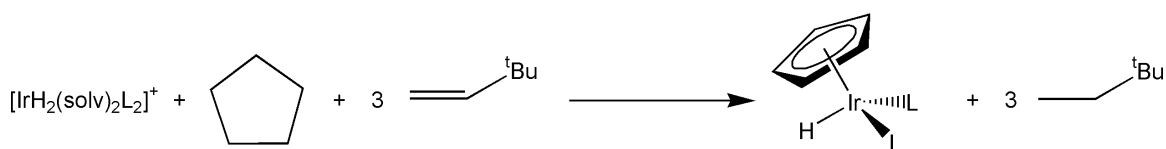
The first mechanistically studied alkane dehydrogenation system used $(P(p\text{-}FC_6H_4)_3)_2Ir(H)_2(\kappa^2\text{-}O_2CCF_3)$ (Figure 1.1) as the catalyst for dehydrogenation of *n*-hexane and a variety of cycloalkanes.[14] In this complex, dehydrogenation could be effected either by using TBE as an acceptor or by photolysis.[14] In both cases, the turnover numbers were fair at best and catalyst decomposition was the primary reason for the low

activity.[14] Nevertheless, the system showed that catalytic alkane dehydrogenation was possible.

Figure 1.1:   (P(p-FC$_6$H$_4$)$_3$)$_2$Ir(H)$_2$(κ^2-O$_2$CCF$_3$), the catalyst used to study alkane dehydrogenation mechanistically.[14]
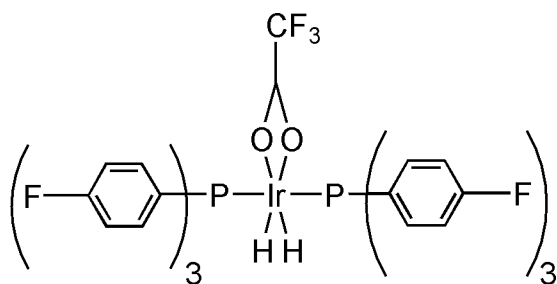
In 1976, Moulton and Shaw introduced what have come to be known as "pincer" ligands and from these a variety of pincer complexes have been synthesized (Figure 1.2).[15] It should be noted that although the term pincer is now used to describe a wide variety of tridentate ligands, for this thesis, it will be used to refer to the original structure developed by Moulton and Shaw a benzene-based, meridionally bound, tridentate ligand.

Figure 1.2: The pincer ligand as developed by Moulton and Shaw[15]
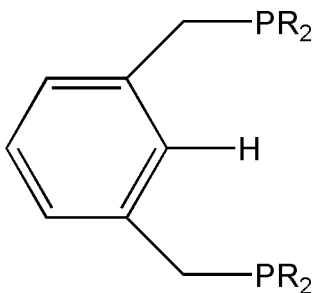
Pincer complexes have had a great impact in the development of catalytic dehydrogenation. In 1996, two pincer catalysts were independently screened for dehydrogenation potential. Goldman began working with (^{tBu}PCP)RhL pincer complexes,[16] while Kaska and Jensen were working with the iridium analogue (^{tBu}PCP)IrH$_2$.[17,18] The rhodium complexes were not found to be good dehydrogenation catalysts, however the iridium complexes were. DFT calculations showed that the difference in activity seems to derive from the greater strength of the Ir-H (or Ir-C) bonds.[19] (^{tBu}PCP)IrH$_2$ was found to give high rates and turnover numbers for both transfer and acceptorless dehydrogenation.[19] Varying the phosphine group from *tert*-butyl to isopropyl to give (^{iPr}PCP)IrH$_2$ resulted in even higher yields and turnover numbers,[20] but more importantly (and perhaps more excitingly), this ligand selectively dehydrogenated *n*-alkanes at the primary position to give α-olefins (Figure 1.3).[21]

In an effort to improve the catalyst, almost every position in the original ^{R}PCP pincer fragment has been varied (Figure 1.4). In addition to changing the alkyl phosphine, pincer complexes have been made where nitrogen[22] or oxygen[23] atoms replace the methylene carbons. Pincer complexes have also been made where groups are added to the para position of the aryl ring, such as OMe[24] or NMe$_2$.[25] Even the aryl ring itself has changed, as benzene rings have been substituted with pyridine rings to give a new class of ^{R}PNP pincer complexes that are also being screened for catalytic activity.[26-32]

Figure 1.3: Mechanism of n-alkane dehydrogenation by (^{iPr}PCP)IrH$_2$ to give α-olefins[21]
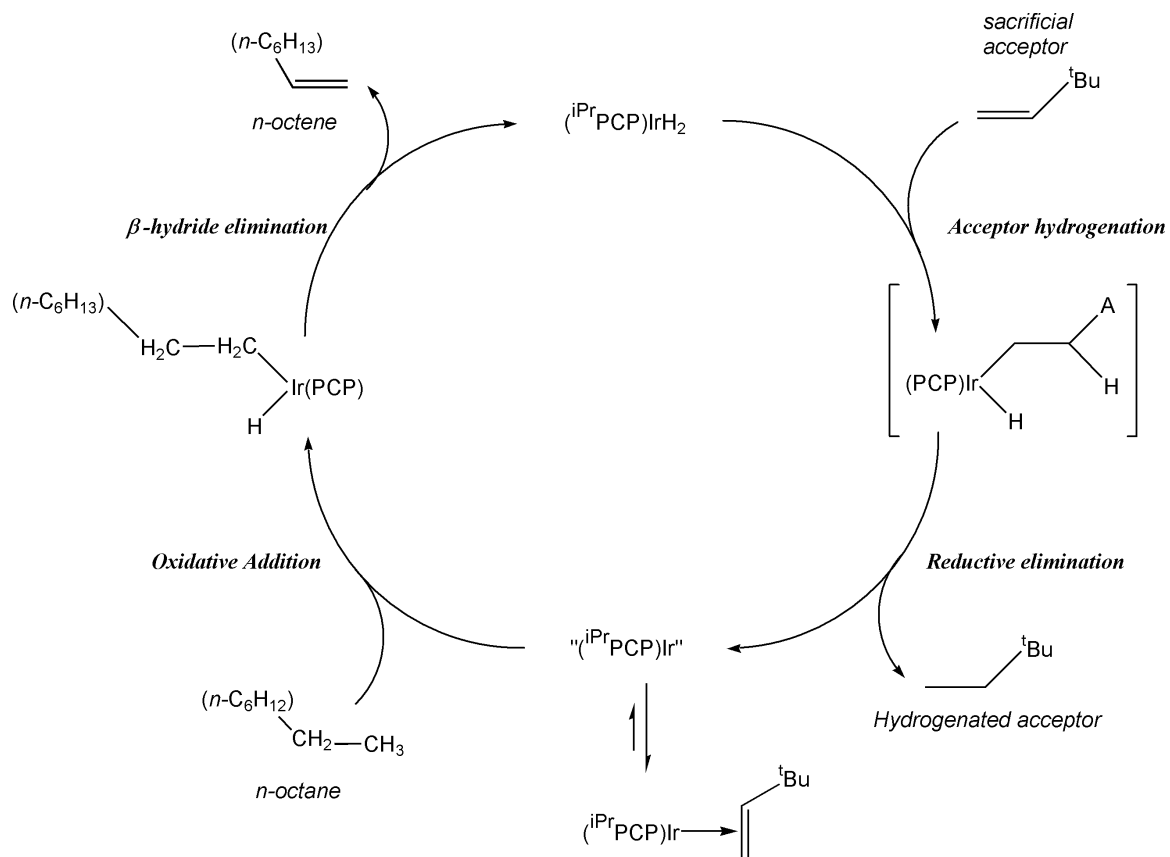
Figure 1.4: Variations in the pincer ligand

M = Ni, Pd, Pt[21]

M = Ir[22]

R = OMe[23], NMe$_2$[24]

M = Ir

M = Ru, Os, Ir, Rh, Fe

Ni, Co, Pd[25-31]
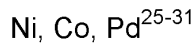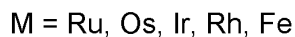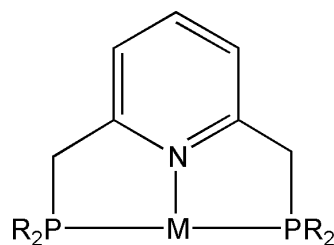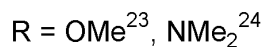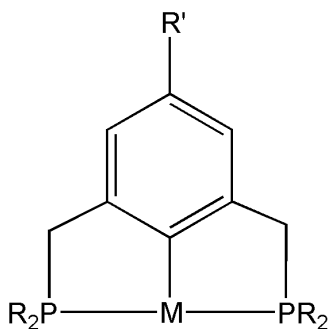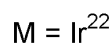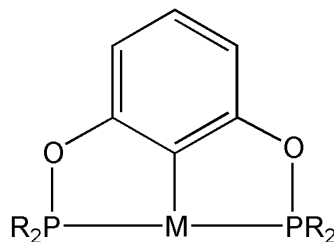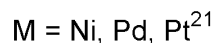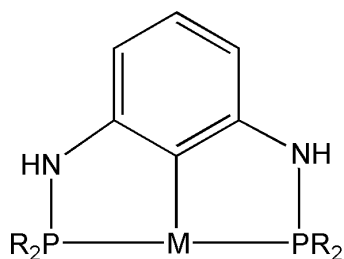
This thesis can be viewed as divided into two parts. The first part comprising Chapters 2 through 4 introduces new [tBu]PNP pincer complexes. Chapter 2 presents the synthesis and characterization of new iron PNP pincer complexes. Two new pincer complexes, ([tBu]PNP)FeCl$_2$ and ([tBu]PNP)Fe(CO)$_2$ were made and fully characterized. The dichloride complex is paramagnetic with an unusually long Fe-N bond. The dicarbonyl complex is an unusually blue colored iron(0) complex. The complex has significantly bent Fe-C-O angles in the solid state and in solution appears to be an equilibrium mixture between square pyramidal and trigonal bipyramidal structures.

Chapter 3 presents the synthesis and characterization of new osmium ^{tBu}PNP pincer complexes. Two complexes, (^{tBu}PNP)OsCl$_3$ and (^{tBu}PNP)OsH$_4$, were synthesized and fully characterized. The trichloride complex is paramagnetic with the expected octahedral geometry around osmium in the solid state. At room temperature, the hydride atoms of (^{tBu}PNP)OsH$_4$ exchange in solution. The low-temperature NMR spectrum and crystal structure show two distinct sets of hydrides in the complex. The crystal structure also shows that the complex is a purely classical hydride in the solid state.

Chapter 4 follows up on (^{tBu}PNP)OsH$_4$ by discussing the reactivity of this complex. Unlike the (^{R}PCP)Ir complexes, (^{tBu}PNP)OsH$_4$ was not found to be an active catalyst for C-H activation, dehydrogenation, or phenylacetylene dimerization. The difference in reactivity likely derives from a difference in metal-hydride bond strength.

Chapters 5 and 6 comprise the second part and return to the well characterized (^{tBu}PCP)Ir systems. Chapter 5 discusses the hydrogenation kinetics of *trans*-5-decene by (^{tBu}PCP)IrH$_2$. The reaction follows second order kinetics and appears to be virtually temperature independent. The activation enthalpy and activation entropy were calculated; TΔS‡ is the major factor contributing to ΔG‡.

Chapter 6 presents the synthesis and characterization of a new (^{tBu}PCP)IrH(μ^2-Cl)$_2$Ir(COD) dimer. This complex, an Ir(I)/Ir(III) dimmer, can be thought of as the oxidative addition product of (^{tBu}PCP-H) with one of the two Ir(COD)Cl units in [Ir(COD)Cl]$_2$.

References

(1)   Chatt, J.; Davidson, J. M. *J. Chem. Soc.* **1965**, 843-855.

(2)   Gol'dshleger, N. F.; Tyabin, M. B.; Shilov, A. E.; Shteinman, A. A. *Zhurnal Fizicheskoi Khimii* **1969**, *43*, 2174-2175.

(3)   Bennett, M. A.; Milner, D. L. *Chem. Commun.* **1967**, *12*, 581-582.

(4)   Green, M. L. H.; Knowles, P. J. *J. Chem. Soc. (D): Chem. Commun.* **1970**, *24*, 1677.

(5)   Janowicz, A. H.; Bergman, R. G. *J. Am. Chem. Soc.* **1982**, *104*, 352-354.

(6)   Hoyano, J. K.; Graham, W. A. G. *J. Am. Chem. Soc.* **1982**, *104*, 3723-3725.

(7)   Harper, T. G. P.; Shinomoto, R. S.; Deming, M. A.; Flood, T. C. *J. Am. Chem. Soc.* **1988**, *110*, 7915-7916.

(8)   Desrosiers, P. J.; Shinomoto, R. S.; Flood, T. C. *J. Am. Chem. Soc.* **1986**, *108*, 7964-7970.

(9)   Baker, M. V.; Field, L. D. *Organometallics* **1986**, *5*, 821-823.

(10)   Werner, H.; Hoehn, A.; Dziallas, M. *Angew. Chem.* **1986**, *98*, 1112-1114.

(11)   Holtcamp, M. W.; Labinger, J. A.; Bercaw, J. E. *J. Am. Chem. Soc.* **1997**, *119*, 848-849.

(12)   Johansson, L.; Tilset, M.; Labinger, J. A.; Bercaw, J. E. *J. Am. Chem. Soc.* **2000**, *122*, 10846-10855.

(13)   Crabtree, R. H.; Mihelcic, J. M.; Quirk, J. M. *J. Am. Chem. Soc.* **1979**, *101*, 7738-7740.

(14)   Burk, M. J.; Crabtree, R. H. *J. Am. Chem. Soc.* **1987**, *109*.

(15)   Moulton, C. J.; Shaw, B. L. *J. Chem. Soc. Dalt. Trans.* **1976**, *11*, 1020-1024.

(16)   Wang, K.; Goldman, M. E.; Emge, T. J.; Goldman, A. S. *J. Organomet. Chem.* **1996**, *518*, 55-68.

(17)   Gupta, M.; Hagen, C.; Flesher, R. J.; Kaska, W. C.; Jensen, C. M. *Chem. Commun.* **1996**, 2083-2084.

(18)   Gupta, M.; Hagen, C.; Kaska, W. C.; Cramer, R. E.; Jensen, C. M. *J. Am. Chem. Soc.* **1997**, *119*, 840-841.

(19)   Xu, W.-W.; Rosini, G. P.; Krogh-Jespersen, K.; Goldman, A. S.; Gupta, M.; Jensen, C. M.; Kaska, W. C. *Chem. Commun.* **1997**, *23*, 2273-2274.

(20)   Liu, F.; Goldman, A. S. *Chem. Commun.* **1999**, 655-656.

(21)   Liu, F.; Pak, E. B.; Singh, B.; Jensen, C. M.; Goldman, A. S. *J. Am. Chem. Soc.* **1999**, *121*, 4086-4087.

(22)   Benito-Garagorri, D.; Bocokic, V.; Mereiter, K.; Kirchner, K. *Organometallics* **2006**, *25*, 3817-3823.

(23)   Gottker-Schnetmann, I.; White, P.; Brookhart, M. *J. Am. Chem. Soc.* **2004**, *126*, 1804-1811.

(24)   Zhu, K.; Achord, P. D.; Zhang, X.; Krogh-Jespersen, K.; Goldman, A. S. *J. Am. Chem. Soc.* **2004**, *126*, 13044-13053.

(25)   Ray, A., Rutgers, 2007.

(26)   Prechtl, M. H. G.; Hoelscher, M.; Ben-David, Y.; Theyssen, N.; Loschen, R.; Milstein, D.; Leitner, W. *Angew. Chem. Int. Ed.* **2007**, *46*, 2269-2272.

(27)   Ben-Ari, E.; Leitus, G.; Shimon, L. J. W.; Milstein, D. *J. Am. Chem. Soc.* **2006**, *128*, 15390-15391.

(28)   Trovitch, R. J.; Emil, L.; Chirik, P. J. *Inorg. Chem.* **2006**, *45*, 7252-7260.

(29)   Dahlhoff, W. V.; Nelson, S. M. *J. Chem. Soc. (A): Inorg. Phys. Theor.* **1971**, *13*, 2184-2190.

(30)   Vasapollo, G.; Giannoccaro, P.; Nobile, C. F.; Sacco, A. *Inorg. Chim. Acta.* **1981**, *48*, 125-128.

(31)   Hahn, C.; Vitagliano, A.; Giordano, F.; Taube, R. *Organometallics* **1998**, *17*, 2060-2066.

(32)   Li, Z.; Che, C.; Poon, C. *Wuhan Univ. J. Nat. Sci.* **1996**, *1*, 230-234.

Chapter 2

Synthesis and Characterization of Iron (PNP) Pincer Complexes

Abstract

Iridium (^{R}PCP) pincer complexes have proven to be some of the most effective catalysts to date for the dehydrogenation of alkanes. In the search for new pincer type catalysts, and to expand our knowledge of pincer complexes, two new PNP-iron pincer complexes of the type (^{tBu}PNP)FeX$_2$ (X = Cl, CO) were synthesized and fully characterized. (^{tBu}PNP)FeCl$_2$ is a high spin, paramagnetic complex. The paramagnetism of the complex leads to broad signals over a wide range in the ^{1}H NMR spectrum. The x-ray crystal structure of this complex shows that it has an unusually long Fe-N bond distance of approximately 2.3 Å. (^{tBu}PNP)Fe(CO)$_2$ is a strikingly bright blue complex. Infrared and computational data on this complex indicate that, in solution, it is a mixture of two structural isomers: approximately trigonal bipyramidal and square planar. An x-ray crystal structure was obtained in which the geometry around iron in the solid state is distorted square pyramidal. This is the inferred geometry of the major isomer in solution and contrasts with the trigonal bipyramidal structure found by Chirik[1] for the ^{iPr}PNP analogue (a single isomer). The x-ray structure of the square pyramidal isomer also reveals that the Fe-C-O bonds are noticeably bent away from linear. Calculations on the

truncated ^{Me}PNP analogue done by Krogh-Jespersen[2] also predict non-linear Fe-C-O angles, so this is apparently not a purely steric effect.

2.1 Introduction

Since 1998 when Brookhart and Gibson independently reported that iron(II) bis(imino)pyridyldichlorides (NNN) are highly active catalysts for polymerization reactions, there has been much interest in (NNN)Fe pincer complexes.[3,4] In addition to the earlier work reported by Brookhart and Gibson, Qian has studied the effects of varying the structure of the bis(imino)pyridyl ligand on the ability to polymerize ethylene.[5] More recently, Chirik has used the iron(II) bis(imino)pyridyldihalides as precursors to iron zero bis(imino)pyridyl –dinitrogen and -dicarbonyl complexes (Figure 2.1).[6] These iron zero bis(imino)pyridyl complexes were then investigated as catalysts in hydrogenation and hydrosilation reactions.[6]

Figure 2.1: Fe(II) and Fe(0) bis(imino)pyridyl complexes[6]
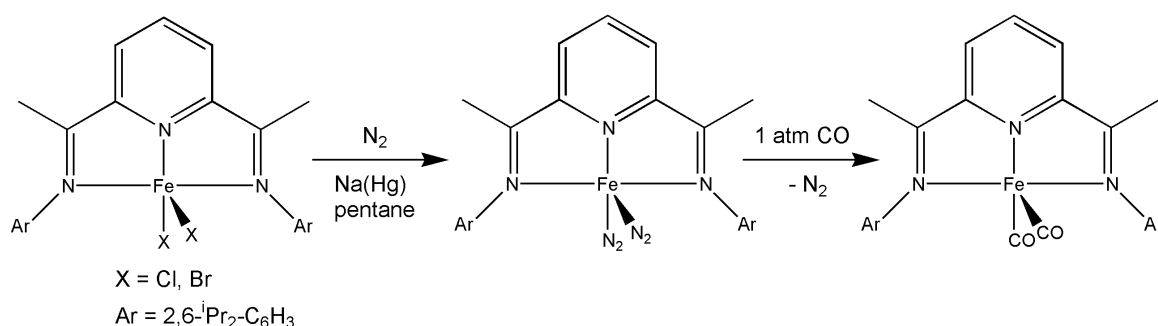
(^{R}PNP)Fe complexes share the central pyridine of the tridentate NNN ligands; however, the two other nitrogen ligands are replaced by phosphorus as shown in Figure 2.2. Until recently, most of the wide variety of work done with (PNP)Fe complexes have used only the ^{Ph}PNP ligand. For example, Sacco has done a comparative study of

(^{Ph}PNP)M complexes, where M = Ni(II), Co(II), or Fe(II).[7] A series of (^{Ph}PNP)FeX$_2$ (X=Cl, Br, I, NCS) complexes were made by Dahlhoff and Nelson for the study of electronic structure.[8] Based on the polymerization work done by Brookhart and Gibson with (NNN)Fe catalysts, Reiger has examined (^{Ph}PNP)FeCl$_2$ and similar complexes for ethylene polymerization activity.[9]

Figure 2.2: Comparison of (^{Ar}NNN)Fe and (^RPNP)Fe complexes

Until recently, there were no published x-ray crystal structures of (PNP)Fe complexes. None of the complexes previously mentioned were characterized crystallographically and it was not until 2003, that we reported the crystal structure of (^{tBu}PNP)FeCl$_2$[10] (Milstein also later published this same structure[11]) and in 2006 the structure of (^{iPr}PNP)Fe(CO)$_2$ was published.[1] These two complexes also represent a shift from the popular ^{Ph}PNP ligand and an expansion into new ^RPNP type ligands.

In an effort to develop possible new dehydrogenation catalysts, and to further the development of pincer complexes, a series of iron-based (^{tBu}PNP) pincer complexes were synthesized and characterized. This chapter will present the synthesis and full characterization of (^{tBu}PNP)FeCl$_2$ (**1**)[10,12-14] and (^{tBu}PNP)Fe(CO)$_2$ (**3**).[13,14] The attempted

synthesis and partial characterization of (^{tBu}PNP)Fe(hydride) (**2**) will also be discussed as will be the attempts to make (^{tBu}PNP)Fe(alkyl) complexes.

2.2 Results and Discussion

2.2.1 (^{tBu}PNP)FeCl$_2$

Following a method similar to the reported synthesis of (^{Ph}PNP)Fe(NO$_3$)$_2$, FeCl$_2$·4H$_2$O was reacted with the ^{tBu}PNP ligand in a 1:1 mixture of benzene and ethanol according to Scheme 2.1.[7] The reaction gave a bright yellow crystalline precipitate that was collected and recrystalized from cold ethanol to give yellow crystals of (^{tBu}PNP)FeCl$_2$ (**1**).

*Scheme 2.1: Synthesis of (^{tBu}PNP)FeCl$_2$ (**1**)*
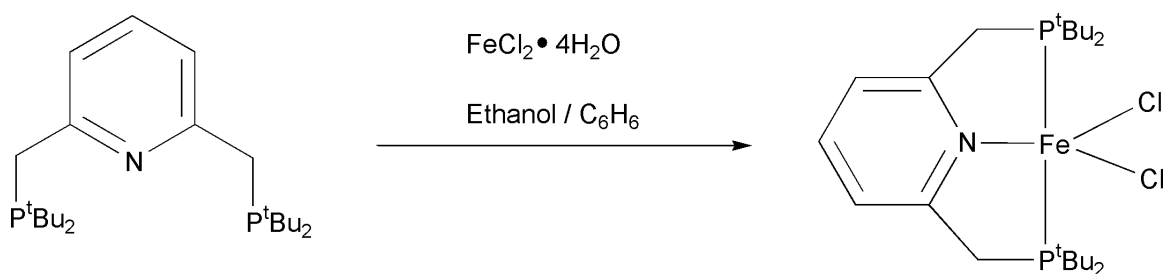
Characterization of **1** by NMR spectroscopy was difficult. The ^{31}P{^{1}H} NMR spectrum showed no signals while the ^{1}H NMR spectrum showed broad signals with unusual chemical shifts (Figure 2.3). Nonetheless, based on integration values and splitting patterns the signals in the ^{1}H spectrum were assigned. The signals at δ 54.9 ppm

and δ −10.0 ppm integrated in a 2:1 ratio and were respectively assigned to the meta and para pyridine protons. The methylene protons appeared as a very broad signal from approximately δ 18 to 14 ppm and the *tert*-butyl protons appeared at δ 10.7 ppm.

Figure 2.3: ^{1}H NMR of (^{tBu}PNP)FeCl$_2$ (**1**)
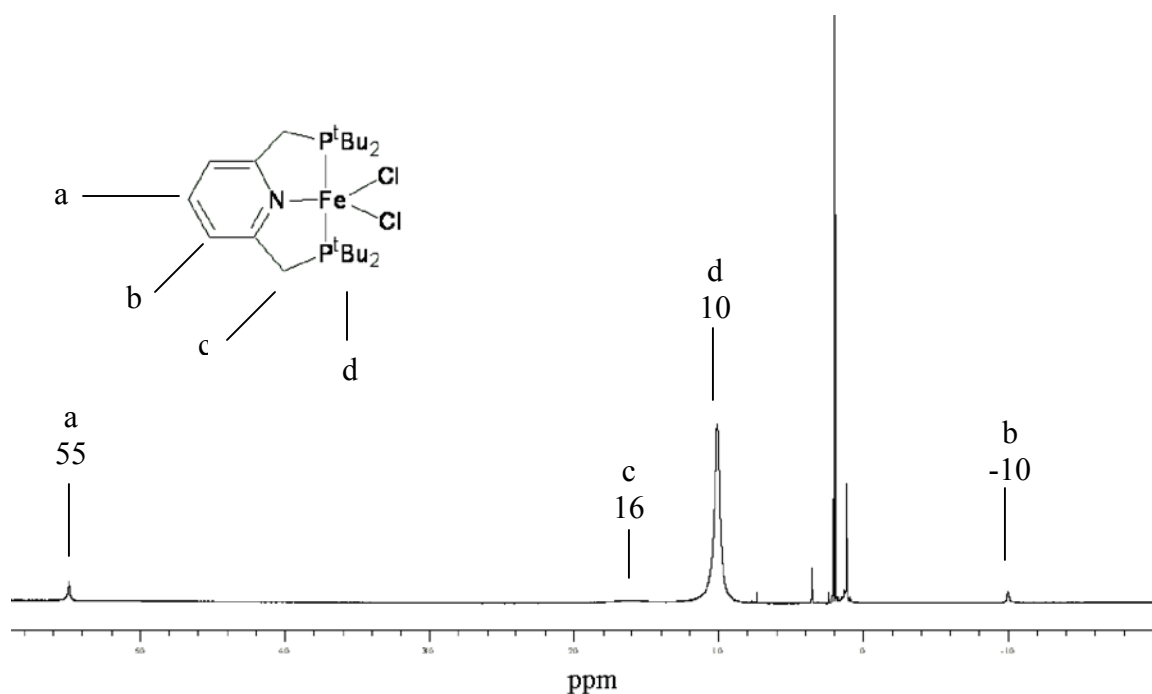
The broadness of the signals of the NMR spectrum and the unusual chemical shifts indicated the complex is a paramagnetic, iron (II) complex such as those reported by Dalhoff and Nelson.[8] The (NNN)Fe complexes published by Brookhart and Gibson are also paramagnetic.[3,4] To determine whether (^{tBu}PNP)FeCl$_2$ was high or low spin, magnetic susceptibility was measured. The theoretical magnetic moment can be calculated from equation 1 where n is the number of unpaired electrons.

$$\mu_{calc} = \sqrt{n(n+2)} \qquad\qquad (1)$$

Based on equation 1, a high spin complex that has four unpaired electrons would have a magnetic moment of 4.899 BM.

The plot of magnetic susceptibility versus temperature, shown in Figure 2.4, remained linear at high temperature in accord with the Curie Law, which is typical of paramagnetic complexes where the molecules are well isolated from each other.[15] The μ_{eff} value for (^{tBu}PNP)FeCl$_2$ was found to be 5.143 BM and was determined using equation 2, where C is equal to the reciprocal of the slope (1/ 0.3024 = 3.31).

$$\mu_{eff} = \sqrt{8C} \qquad\qquad (2)$$

This value is similar to the value of 5.22 BM that was measured for (^{Ph}PNP)FeCl$_2$[8] and 5.38 BM for (^{tBu}PNP)FeCl$_2$.[11] The value is also in good agreement with the calculated magnetic moment of 4.899 BM.

*Figure 2.4: Magnetic Susceptibility of (^{tBu}PNP)FeCl$_2$ (**1**)*

Magnetic Susceptibility of (tBuPNP)FeCl2

$y = 0.3024x + 2.2526$
$R^2 = 0.9991$
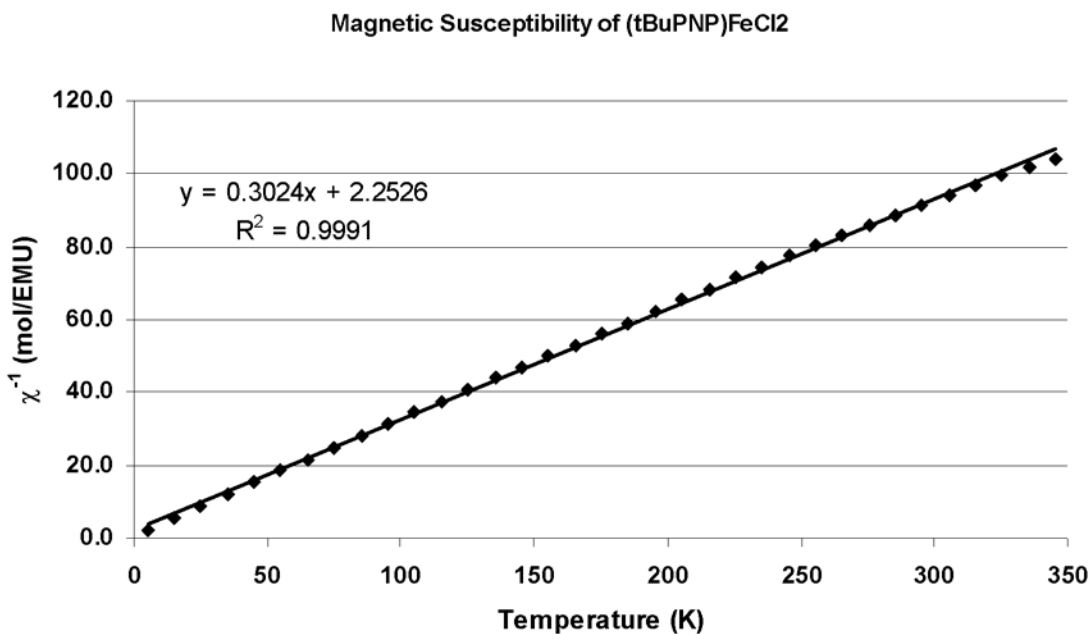
Crystals suitable for x-ray diffraction were obtained by recrystalization from cold

ethanol. The x-ray diffraction pattern showed that the crystals were monoclinic and in

the P2(1)/n space group (Figure 2.5, Table 2.1. Full crystallographic details are in the

Appendix). The iron atom is five coordinate and shows an unusually long Fe-N bond

length of 2.33(13) Å (Table 2.2), which is consistent with the value of 2.303(1) Å

reported by Milstein for the same bond in this complex.[11] For comparison the

(NNN)FeCl$_2$ complex developed by Brookhart has an Fe-N(py) bond length of 2.091(4)

Å[3] and Gibson reports an Fe-N(py) bond length of 2.088 Å[4] for (NNN)FeCl$_2$. It should

be noted that in the (NNN)Fe complexes the apical phosphorus atoms have been replaced

by nitrogen atoms. The smaller size of the apical nitrogen atoms as compared to

phosphorus atoms in the same positions should lead to a decrease in the Fe-N(py) bond length.

Figure 2.5: Crystal structure of (^{tBu}PNP)FeCl$_2$ (1)
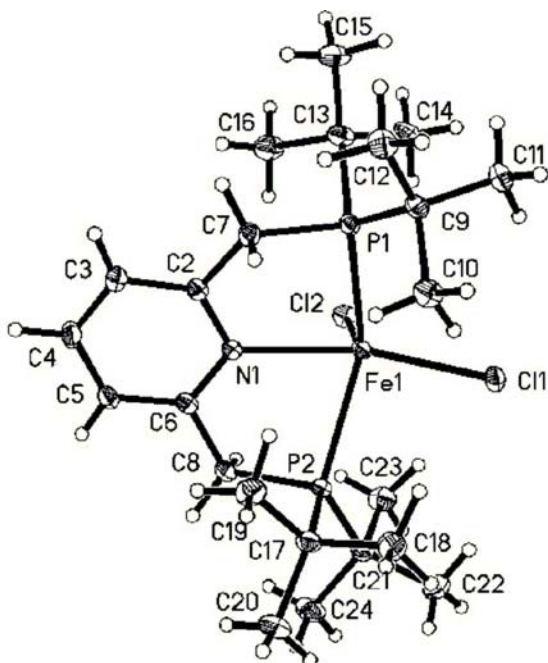
DFT calculations by Krogh-Jespersen show that when nitrogen atoms are replaced by phosphorus atoms, the Fe-N(py) bond length increases (Figure 2.6). The value obtained by calculations for the Fe-N(py) bond length in a 2,6-bis(dimethylamino)pyridineFe complex is 2.045 Å[2] which is close to the values obtained by Brookhart and Gibson for their (NNN)Fe complexes. When one nitrogen is replaced by a phosphorus, the bond length increases to 2.112 Å and when both nitrogens have been replaced the bond length is 2.178 Å.[2] While these calculations support the idea that the Fe-N(py) bond length should increase the calculated value of 2.178 Å is still much

shorter than the observed value of 2.329 Å. The difference may be attributed to the fact that these calculations were done with ^{Me}PNP as the ligand as opposed to the ^{tBu}PNP ligand. When the calculations were done with (^{tBu}PNP)FeCl$_2$, the Fe-N bond length was calculated to be 2.363 Å, which is in good agreement with the experimental value of 2.329 Å.

Table 2.1: Crystal data and structure refinement for (^{tBu}PNP)FeCl$_2$ (**1**)

Identification code	fecl2pnp
Empirical formula	C23 H43 Cl2 Fe N P2
Formula weight	522.27
Temperature	100(2) K
Wavelength	0.71073 Å
Crystal system	Monoclinic
Space group	P2(1)/n
Unit cell dimensions	a = 12.0831(9) Å α= 90°.
	b = 15.5084(12) Å β= 91.093(2)°.
	c = 14.5049(11) Å γ = 90°.
Volume	2717.6(4) Å^3
Z	4
Density (calculated)	1.277 Mg/m^3
Absorption coefficient	0.880 mm^{-1}
F(000)	1112
Crystal size	0.21 x 0.06 x 0.03 mm^3
Theta range for data collection	1.92 to 30.57°.
Index ranges	-17<=h<=17, -22<=k<=22, -20<=l<=20
Reflections collected	31924
Independent reflections	8292 [R(int) = 0.0456]
Completeness to theta = 30.57°	99.4 %
Absorption correction	Semi-empirical from equivalents
Max. and min. transmission	0.9999 and 0.8338
Refinement method	Full-matrix least-squares on F^2
Data / restraints / parameters	8292 / 0 / 434
Goodness-of-fit on F^2	1.012
Final R indices [I>2sigma(I)]	R1 = 0.0349, wR2 = 0.0753
R indices (all data)	R1 = 0.0534, wR2 = 0.0823
Largest diff. peak and hole	0.618 and -0.300 e.Å^{-3}

Table 2.2: Selected bond lengths (Å) and angles (º) for (^{tBu}PNP)FeCl$_2$ (**1**)

Fe(1)-Cl(2)	2.3028(5)	Fe(1)-N(1)	2.3286(13)
Fe(1)-Cl(1)	2.3816(5)	Fe(1)-P(1)	2.5149(5)
Fe(1)-P(2)	2.5168(5)		

Cl(2)-Fe(1)-N(1)	97.61(3)	Cl(2)-Fe(1)-Cl(1)	107.628(17)
N(1)-Fe(1)-Cl(1)	153.95(3)	Cl(2)-Fe(1)-P(1)	106.190(16)
N(1)-Fe(1)-P(1)	77.13(3)	Cl(1)-Fe(1)-P(1)	101.249(16)
Cl(2)-Fe(1)-P(2)	104.774(16)	N(1)-Fe(1)-P(2)	73.59(3)
Cl(1)-Fe(1)-P(2)	93.402(16)	P(1)-Fe(1)-P(2)	139.582(16)
C(7)-P(1)-Fe(1)	101.54(5)	C(9)-P(1)-Fe(1)	118.08(5)
C(13)-P(1)-Fe(1)	116.14(5)	C(8)-P(2)-Fe(1)	96.66(5)
C(21)-P(2)-Fe(1)	118.84(5)	C(17)-P(2)-Fe(1)	117.92(5)
C(2)-N(1)-Fe(1)	121.78(10)	C(6)-N(1)-Fe(1)	118.70(10)

Figure 2.6: Change in the Fe-N(py) bond length as (PNP)Fe goes to 2,6-bis(dimethylamino)pyridineFe as calculated by Krogh-Jespersen[2]

2.178 Å	2.112 Å	2.045 Å

*2.2.2 Attempted synthesis of a (*tBu*PNP)Fe hydride complex*

Several attempts were made to convert (*tBu*PNP)FeCl$_2$ to an iron hydride complex. In the synthesis of (*R*PCP)IrH$_4$, (*R*PCP)IrHCl is reduced using LiEt$_3$BH under a hydrogen atmosphere (Scheme 2.2).[16]   This method, however, was not applicable to the PNP system, since LiEt$_3$BH can reduce pyridine rings.[17]   Using the sodium salt instead, reaction with NaEt$_3$BH gave a gray unidentified solid.   Another attempt involved using ethanol and triethylamine; this only gave a gray unidentified.

*Scheme 2.2: Synthesis of (*tBu*PCP)IrH$_4$*[16,18]
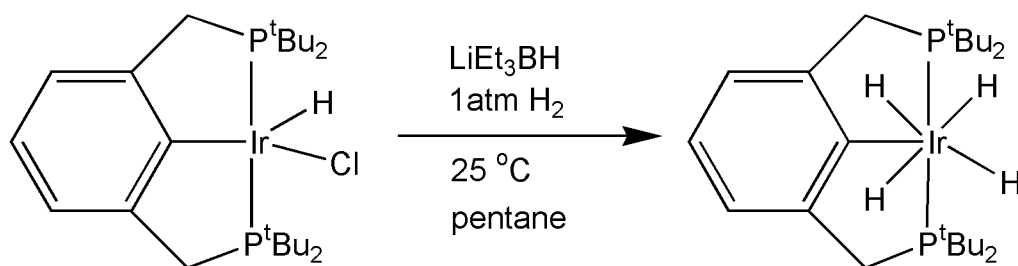
The next two attempts involved using alkyl lithium reagents in the hope of obtaining either an iron hydride or an iron dialkyl complex.   These complexes had the advantage that the lithium chloride side product might be easily separated from the iron pincer complex.   To make the iron dialkyl complex, methyllithium was used.   The small methyl groups should not encounter any significant steric resistance in binding to the iron center.   However, the reaction produced a dark solid that was insoluable in pentane.   A similar reaction using *n*-butyl lithium was also run.   In this case, if an iron butyl species

were produced it might be capable of β-hydride elimination to produce an iron hydride. When the reaction was run, a dark solid that was most likely iron metal was obtained.

2.2.3 (^{tBu}PNP)FeClH

Addition of 4 equivalents of NEt$_4$BH$_4$ or NaBH$_4$ to (^{tBu}PNP)FeCl$_2$ gave a slow color change from a yellow to dark red solution with the production of a white solid. Once the white solid was removed NMR characterizations on the red solution were performed. The ^{1}H NMR showed the presence of a new hydride triplet at −13.64 ppm (Figure 2.7) and, unlike for the (^{tBu}PNP)FeCl$_2$, all signals were sharp and within a chemical shift range typical of diamagnetic complexes. The ^{31}P{^{1}H} NMR showed a new, sharp singlet at 103.40 ppm while the selectively decoupled ^{31}P NMR showed a doublet with J_{P-H} = 51 Hz (Figure 2.8). This data allows inferences as to the structure of the complex. Firstly, the two phosphorus nuclei of the PNP ligand are still equivalent and secondly, since the ^{31}P NMR is a doublet, they are apparently coupled to one hydride.

Figure 2.7: ^1H NMR of (^{tBu}PNP)FeHCl

-13.64 ppm
J = 58
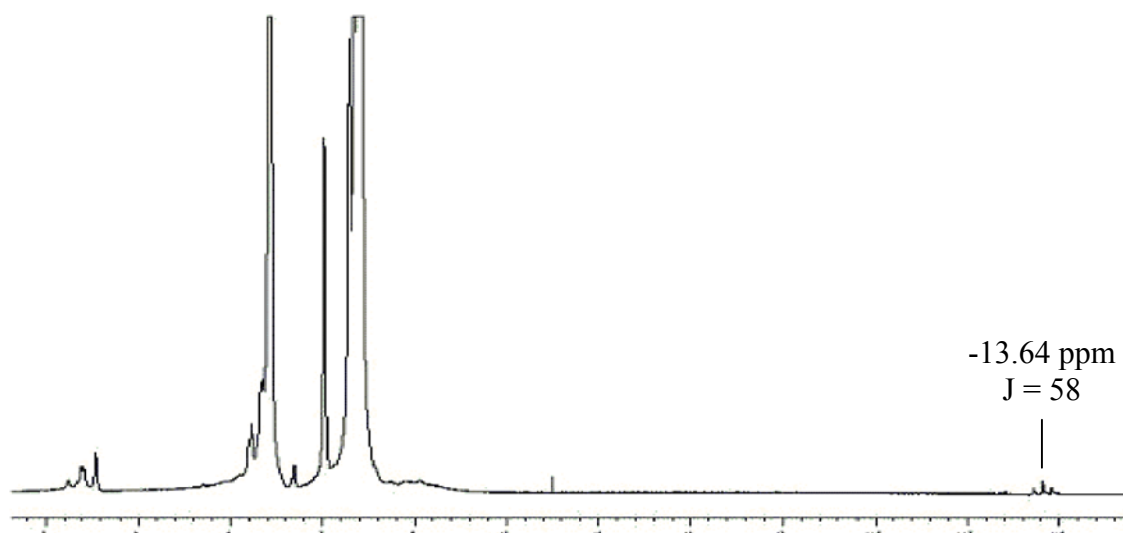
Figure 2.8: ^{31}P NMR of (^{tBu}PNP)FeHCl
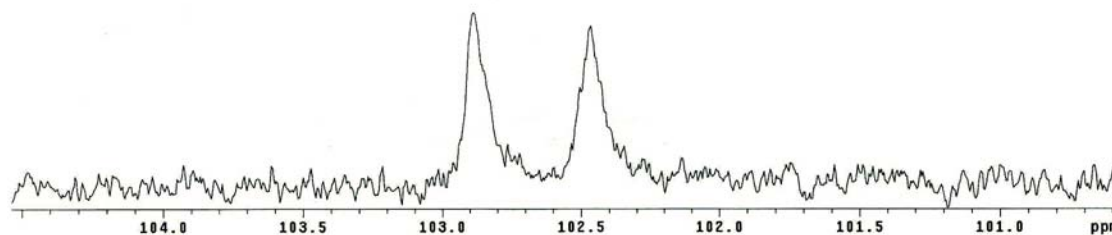
Due to the instability of the complex, attempts to isolate it for structural analysis have been unsuccessful; however, based on the NMR data a proposed structure is possible. The fragment (^{tBu}PNP)FeH has a 15 valence-electron Fe count. The complex is apparently diamagnetic; likely a 16-electron Fe(VI). Thus, it seems plausible that one chlorine atom remained bound to the iron resulting in (^{tBu}PNP)FeHCl (**2**) or an adduct

thereof. This complex matches the NMR data, since the two PNP phosphorus nuclei are equivalent and give a doublet when coupled to the hydride. The presence of either a bound solvent ligand, or if no solvent were bound, donation of a lone pair from a chloride atom into an empty d orbital of iron, would lead to a more stable 18-electron complex.

2.2.4 (^{tBu}PNP)Fe(CO)$_2$

The complex, (^{tBu}PNP)Fe(CO)$_2$ (**3**), was first made in an effort to trap the putative (^{tBu}PNP)FeHCl. We reacted (^{tBu}PNP)FeCl$_2$ with excess NEt$_4$BH$_4$ under 1 atm of CO at low temperature (Scheme 2.3). The resulting product was (^{tBu}PNP)Fe(CO)$_2$, an 18-electron Fe(0) complex. A second method to produce (^{tBu}PNP)Fe(CO)$_2$ follows the synthesis used to makde (^{iPr}PNP)Fe(CO)$_2$ that was reported during the course of this work.[1] This method uses a sodium mercury amalgam to abstract the chlorides from (^{tBu}PNP)FeCl$_2$ and produces a cleaner product than using either NEt$_4$BH$_4$ or NaBH$_4$.[1]

Scheme 2.3: Synthesis of (^{tBu}PNP)Fe(CO)$_2$ (3)
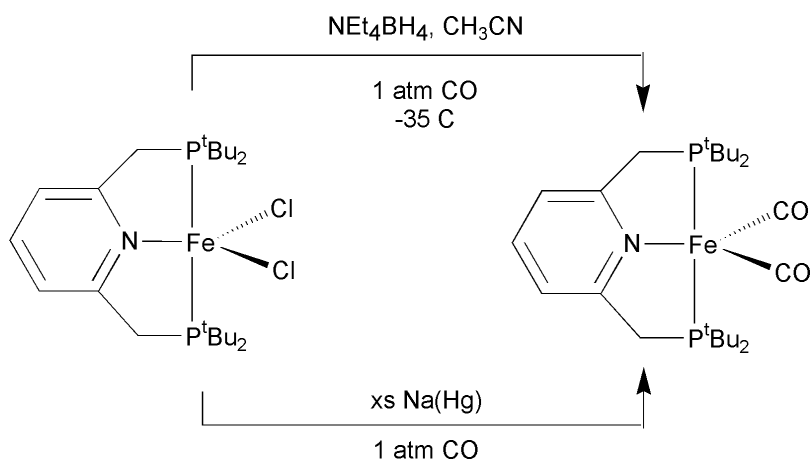
Unlike (^{iPr}PNP)Fe(CO)$_2$ which has sharp signals at room temperature in both the ^{31}P{^{1}H} and ^{1}H NMR spectra, (^{tBu}PNP)Fe(CO)$_2$ has broad signals at room temperature.[1] The room temperature ^{31}P{^{1}H} NMR spectrum of (^{tBu}PNP)Fe(CO)$_2$ showed a sharp signal for free ^{tBu}PNP at δ 35 ppm and a broad signal at δ 120 ppm that sharpened to a singlet, in a 1:1 ratio with the free ^{tBu}PNP signal, at −80 ºC (Figure 2.9). The room temperature ^{1}H NMR of (^{tBu}PNP)Fe(CO)$_2$ displayed broad signals that remained broad even at −80 ºC (Figure 2.10). The room temperature ^{1}H NMR was assigned based on integration; however, the signal for the para pyridine proton was broadened into the baseline and not observed at this temperature. This signal is observed as a very broad peak from approximately δ 6.8 to 6.6 ppm at −80 ºC and integrates to 1H against the meta protons, which appear at δ 6.21 ppm and methylene protons which are at δ 2.79 ppm. The *tert*-butyl protons are difficult to integrate at both room temperature and low temperature, since they overlap with *tert*-butyl signal for the free ^{tBu}PNP ligand.

Figure 2.9: ^{31}P *NMR spectra of ($^{tBu}PNP)Fe(CO)_2$ (3) at $-80\ ^{\circ}C$ and room temperature*

-80 °C

PNP

(^{tBu}PNP)Fe(CO)$_2$


```
      200        150        100         50          0         -50        -100
ppm (f1)
```

PNP

Room Temperature

(^{tBu}PNP)Fe(CO)$_2$

PNP


```
      200        150        100         50          0         -50        -100
ppm (f1)
```
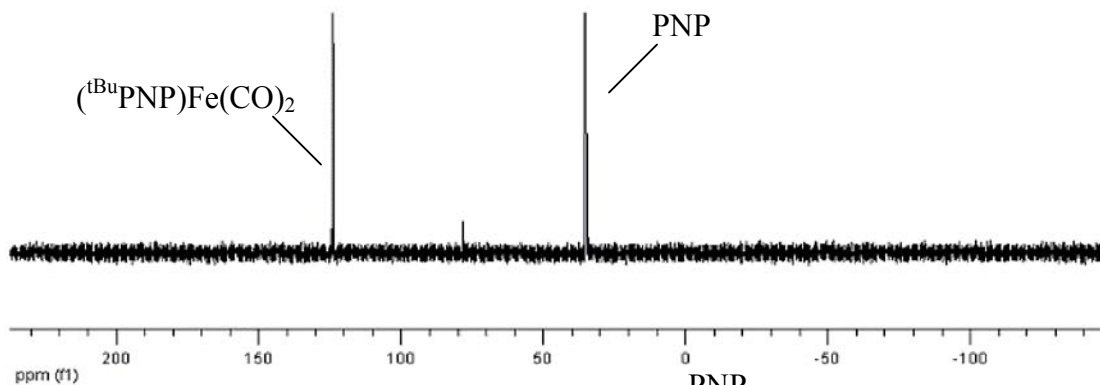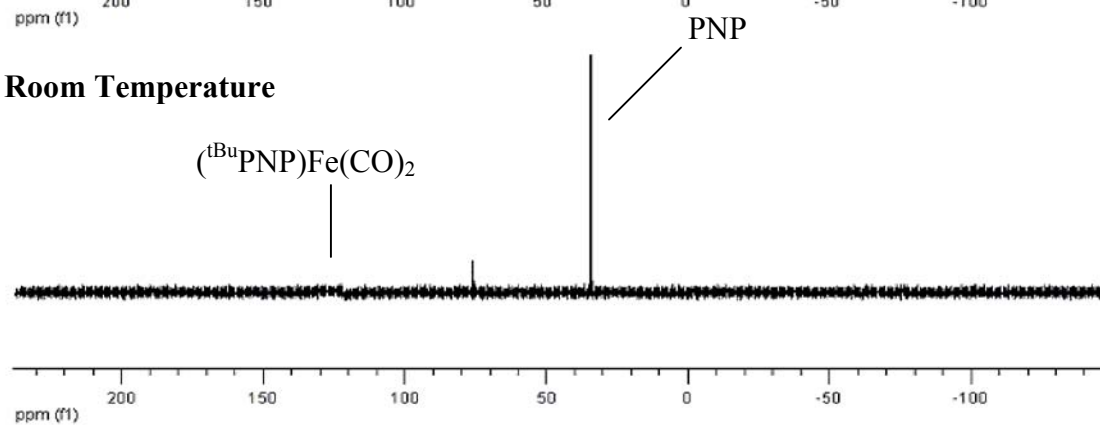
Figure 2.10: ^{1}*H NMR spectra of (*^{tBu}*PNP)Fe(CO)$_2$ (3) at room temperature and* $-80\ ^oC$
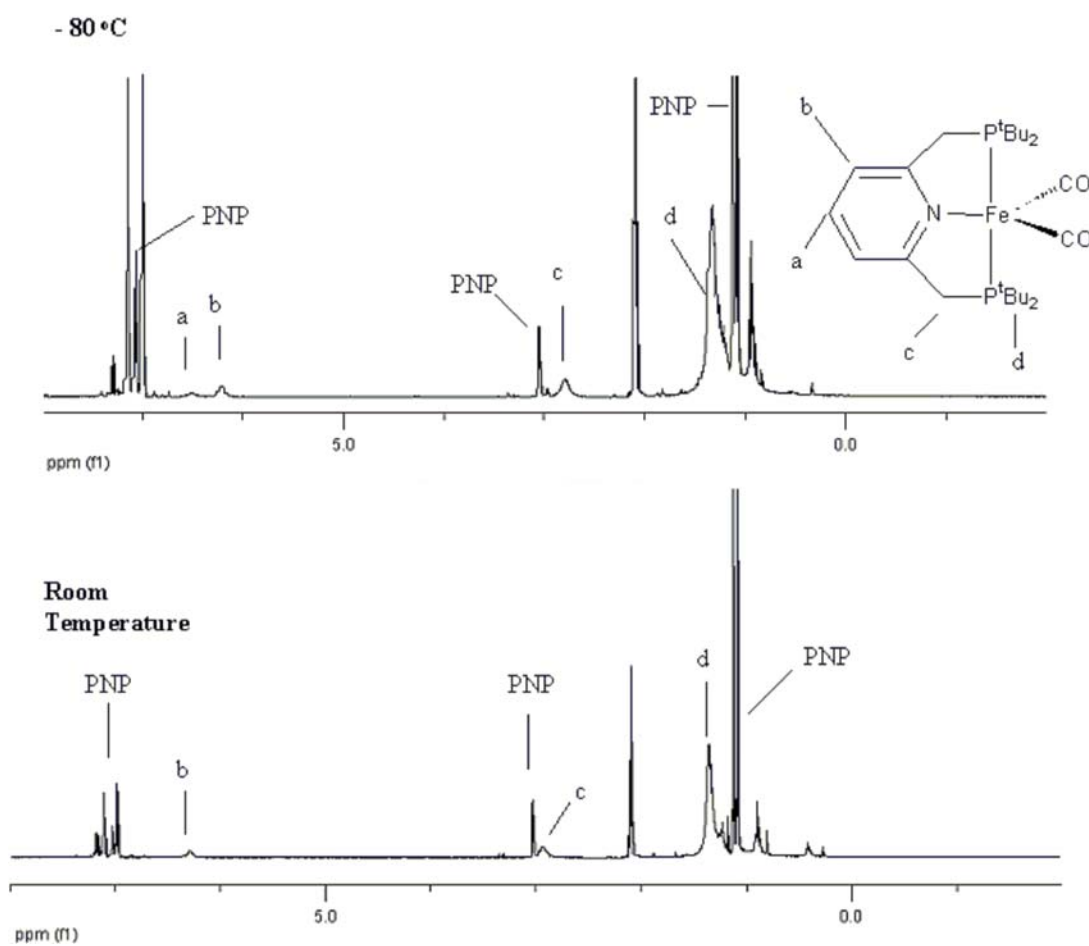
The broadness of the NMR signals pointed to a possible equilibrium in solution. The first equilibrium that was considered was one between the mono and dicarbonyl species as shown in Scheme 2.4. Labeling experiments with (tBuPNP)Fe(^{13}CO)$_2$ were done in this context. The ^{13}C NMR of (tBuPNP)Fe(CO)$_2$ and (tBuPNP)Fe(^{13}CO)$_2$ clearly showed the presence of the carbonyl signal as a triplet at δ 230.74 ppm, proving that the labeled ^{13}CO was bound to the iron atom (Figure 2.11). The ^{31}P{^{1}H} NMR was also split into a triplet, meaning that the phosphorus resonance was split by two ^{13}C atoms (Figure 2.12). This suggested that the two carbonyl ligands remained bound to the iron atom in solution, and that the broadness was due to a different process.

Scheme 2.4: Potential equilibrium between (tBuPNP)Fe(CO)$_2$ and (tBuPNP)Fe(CO)
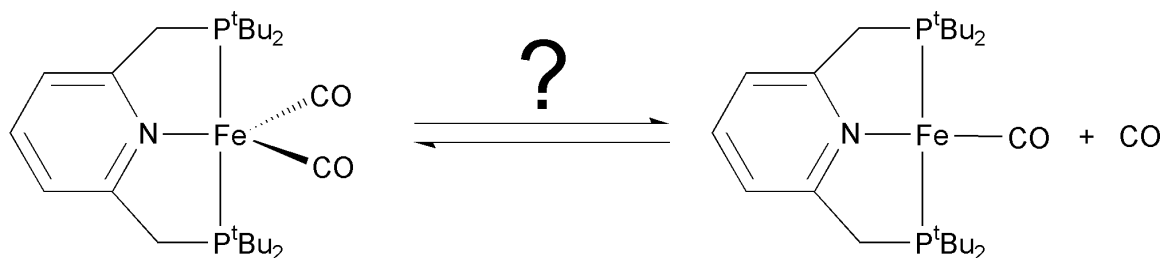
Figure 2.11: ^{13}C *NMR spectra of (*^{tBu}*PNP)Fe(CO)$_2$ and (*^{tBu}*PNP)Fe(*^{13}*CO)$_2$*
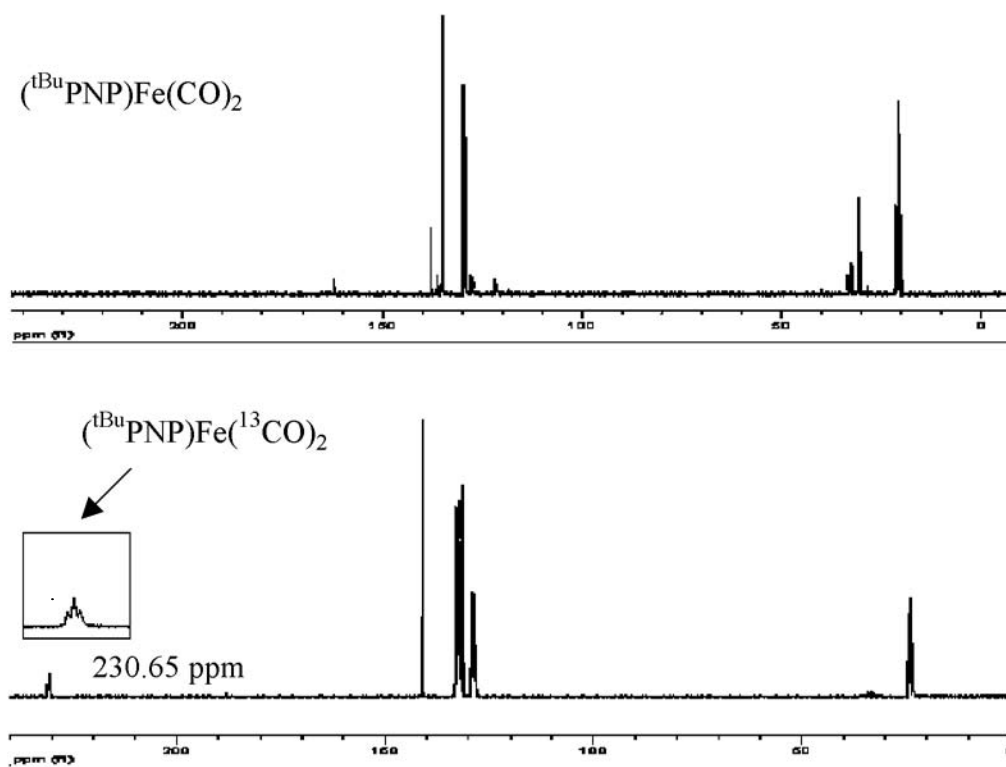
Figure 2.12: $^{31}P\{^{1}H\}$ and ^{13}C NMR of $(^{tBu}PNP)Fe(^{13}CO)_2$

$^{31}P\{^{1}H\}$ Spectrum

Free PNP

J = 21

$(^{tBu}PNP)Fe(^{13}CO)_2$

ppm (f1)

^{13}C Spectrum

J = 21

ppm (f1)
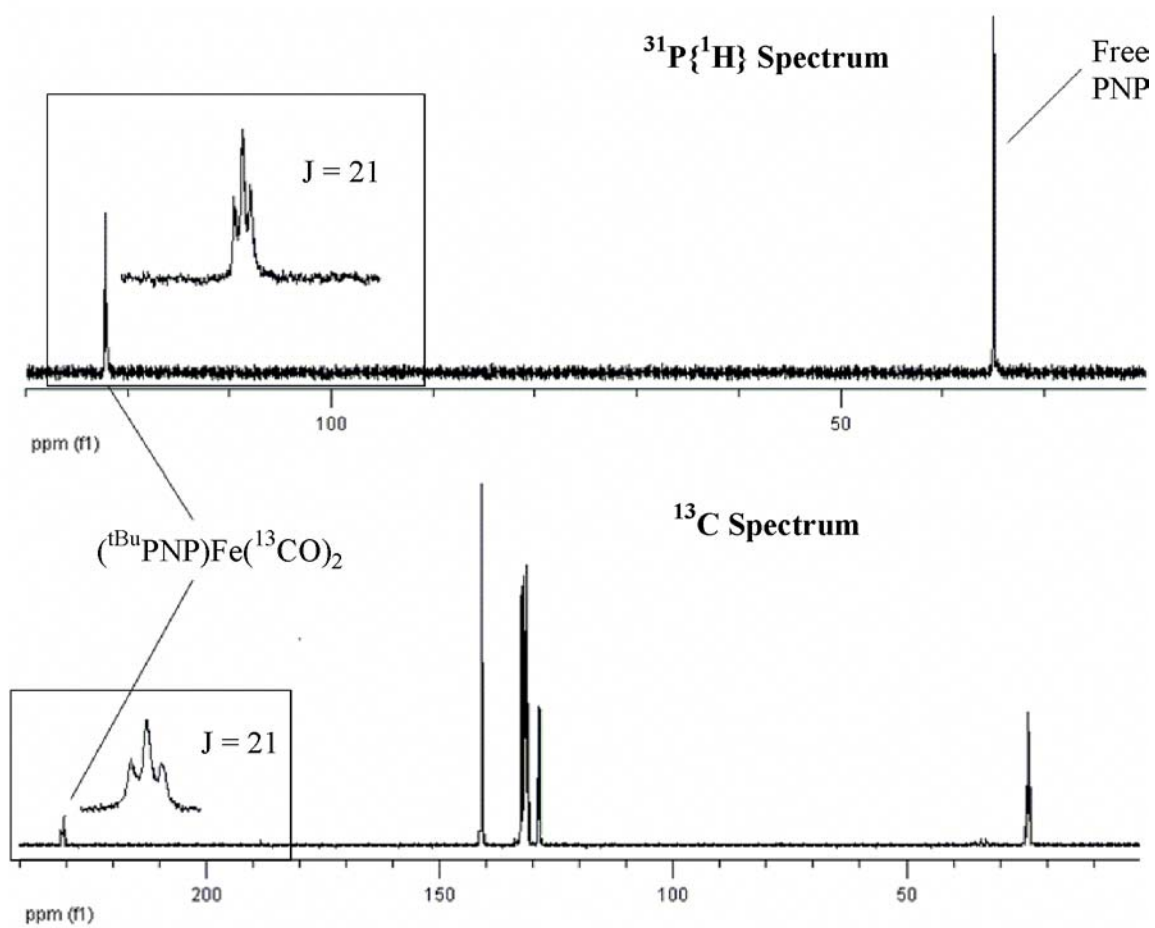
A comparison of the crystal structures of (^{tBu}PNP)Fe(CO)$_2$ and Chirik's (^{iPr}PNP)Fe(CO)$_2$ species shows a striking contrast and also suggests a second possible equilibrium to explain the broad NMR spectra of the former. (^{tBu}PNP)Fe(CO)$_2$ is orthorhombic and in the P2(1)2(1)2(1) space group (Table 2.3. Full crystallographic details are in the appendix). In contrast with Chirik's trigonal bipyramidal complex, the geometry around the five coordinate iron in (^{tBu}PNP)Fe(CO)$_2$ is somewhere between trigonal bipyramidal and square pyramidal (Figure 2.13). For example, the C(24)-Fe-C(25) angle is 105.78(5)º . If the complex were a perfect trigonal bipyramidal structure this angle should be 120º, while if it were a square pyramid the angle should be 90º. In (^{iPr}PNP)Fe(CO)$_2$ the equivalent angle is 119.91(7)º, which is almost perfect for a trigonal bipyramidal structure.[1] (Indeed, Chirik characterizes this complex as having an "idealized trigonal bipyramidal structure."[1]) The difference in the solid state structures of both complexes lead to the idea that a possible equilibrium between the two isomers, trigonal bipyramidal and square pyramidal, is the cause of the broadness in the NMR spectra.

*Figure 2.13: Crystal Structure of (^{tBu}PNP)Fe(CO)$_2$ (**3**)*
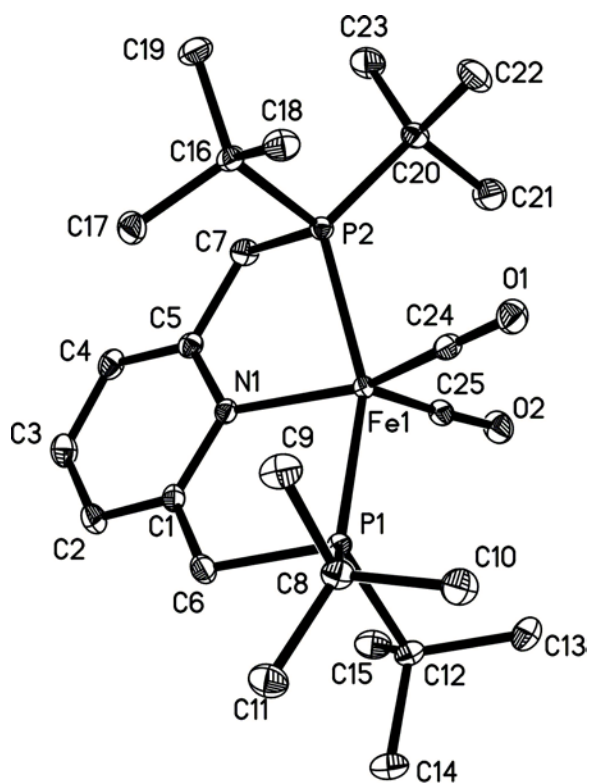
Table 2.3: Crystal data and structure refinement for (^{tBu}PNP)Fe(CO)$_2$ (**3**)

Identification code	fehco
Empirical formula	C25 H43 Fe N O2 P2
Formula weight	507.39
Temperature	100(2) K
Wavelength	0.71073 Å
Crystal system	Orthorhombic
Space group	P2(1)2(1)2(1)
Unit cell dimensions	a = 11.7404(12) Å $\quad$ α= 90°.
	b = 14.5944(14) Å $\quad$ β= 90°.
	c = 15.3327(15) Å $\quad$ γ = 90°.
Volume	2627.2(4) Å^3
Z	4
Density (calculated)	1.283 Mg/m^3
Absorption coefficient	0.717 mm^{-1}
F(000)	1088
Crystal size	0.29 x 0.25 x 0.18 mm^3
Theta range for data collection	1.93 to 30.56°.
Index ranges	-16<=h<=16, -20<=k<=20, -21<=l<=21
Reflections collected	31387
Independent reflections	8025 [R(int) = 0.0228]
Completeness to theta = 30.56°	99.9 %
Absorption correction	Semi-empirical from equivalents
Max. and min. transmission	0.9999 and 0.9146
Refinement method	Full-matrix least-squares on F^2
Data / restraints / parameters	8025 / 0 / 335
Goodness-of-fit on F^2	1.041
Final R indices [I>2sigma(I)]	R1 = 0.0219, wR2 = 0.0561
R indices (all data)	R1 = 0.0230, wR2 = 0.0565
Absolute structure parameter	0.002(6)
Largest diff. peak and hole	0.362 and -0.180 e.Å^{-3}

Table 2.4: Selected bond lengths (Å) and angles (º) for (^{tBu}PNP)Fe(CO)$_2$ (**3**)

Fe(1)-C(24)   1.7310(12)   Fe(1)-C(25)   1.7708(12)

Fe(1)-N(1)   2.0503(9)   Fe(1)-P(2)   2.2066(4)

Fe(1)-P(1)   2.2322(3)   C(24)-O(1)   1.1717(14)

C(25)-O(2)   1.1679(14)

C(24)-Fe(1)-C(25)   105.78(5)   C(24)-Fe(1)-N(1)   152.52(5)

C(25)-Fe(1)-N(1)   101.57(4)   C(24)-Fe(1)-P(2)   90.13(4)

C(25)-Fe(1)-P(2)   101.94(4)   N(1)-Fe(1)-P(2)   81.55(3)

C(24)-Fe(1)-P(1)   92.21(4)   C(25)-Fe(1)-P(1)   103.35(4)

N(1)-Fe(1)-P(1)   84.04(3)   P(2)-Fe(1)-P(1)   152.917(13)

C(6)-P(1)-Fe(1)   101.92(4)   C(12)-P(1)-Fe(1)   116.69(4)

C(8)-P(1)-Fe(1)   121.45(4)   C(7)-P(2)-Fe(1)   99.58(4)

C(20)-P(2)-Fe(1)   122.20(4)   C(16)-P(2)-Fe(1)   116.38(4)

C(1)-N(1)-C(5)   117.24(9)   C(1)-N(1)-Fe(1)   122.15(7)

C(5)-N(1)-Fe(1)   120.37(7)   O(1)-C(24)-Fe(1)   176.68(10)

O(2)-C(25)-Fe(1)   171.87(10)

To examine this possibility, DFT calculations were done by Krogh-Jespersen,[2] and infrared studies were done in our group. The solution infrared spectrum of $(^{tBu}PNP)Fe(CO)_2$ taken in THF shows four bands in the carbonyl region (Figure 2.14). An intense set of bands appears at 1869.8 and 1819.0 cm^{-1} and a weaker set at 1846.2 and 1791.2 cm^{-1} (Table 2.5). The solid state IR of the trigonal bipyramidal $(^{iPr}PNP)Fe(CO)_2$, taken using a KBr pellet, has one set of bands in the infrared spectrum at 1842 and 1794 cm^{-1}.[1] These values are close to the weaker set of bands in the IR spectrum of $(^{tBu}PNP)Fe(CO)_2$ suggesting that these bands derive from a trigonal bipyramidal isomer.

Table 2.5: Comparison of the CO frequency for $(^{tBu}PNP)Fe(CO)_2$ in the IR spectrum

Structure	DFT Predicted v_{CO} Value $(cm^{-1})^a$	Equation 4 v_{CO} Value $(cm^{-1})^b$	Experimental v_{CO} Value (cm^{-1})
$(^{tBu}PNP)Fe(CO)_2$ Square Pyramid	1874, 1829		1869, 1819
$(^{tBu}PNP)Fe(^{13}CO)_2$ Square Pyramid		1824, 1775	1827, 1775
$(^{tBu}PNP)Fe(CO)_2$ Trigonal Bipyramidal	1850, 1807		1846, 1797
$(^{tBu}PNP)Fe(^{13}CO)_2$ Trigonal Bipyramidal		1801,1753	1803, 1756
$(^{iPr}PNP)Fe(CO)_2$			1842, 1794[c]

[a]Calculated by DFT.[2] [b]Calculated from experimental values using reduced mass equations 3 and 4. [c]Previously published.[1]

*Figure 2.14: IR spectrum of (^{tBu}PNP)Fe(CO)$_2$ (**3**)*
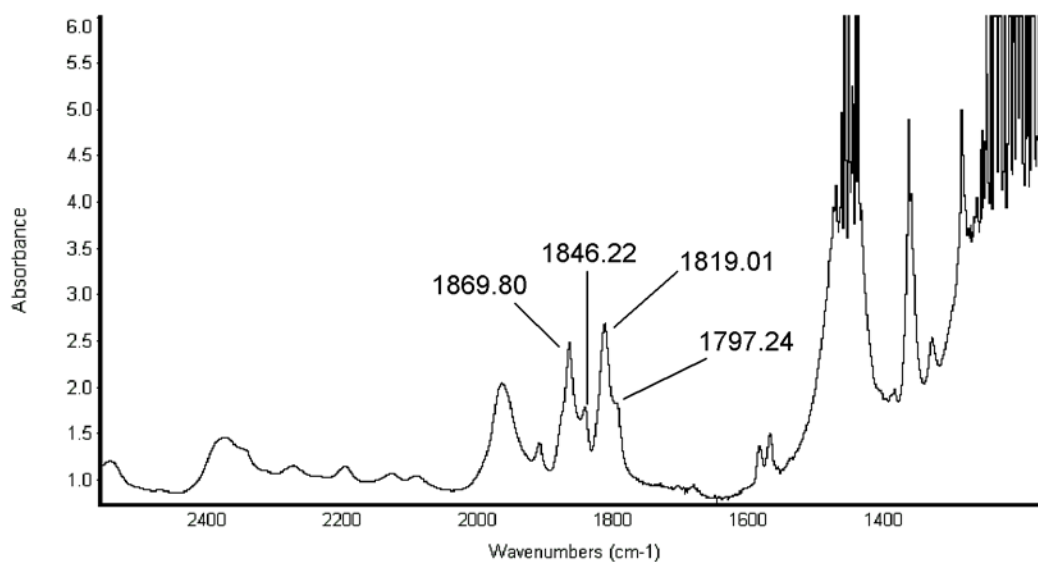
As a means to test whether all four bands were due to carbonyl ligands, labeling experiments with (^{tBu}PNP)Fe(^{13}CO)$_2$ were done. Using equation 3 to determine reduced mass (μ), the expected wavenumbers of the carbonyl signals in (^{tBu}PNP)Fe(^{13}CO)$_2$ can be calculated from the carbonyl signals in (^{tBu}PNP)Fe(CO)$_2$ using equation 4.

$$\mu = (m_1 m_2)/ (m_1 + m_2) = m_C m_O/ (m_C + m_O) \qquad (3)$$

$$\nu(^{13}CO)= \sqrt{\mu(^{12}CO)/ \mu(^{13}CO)} \ \times \nu(^{12}CO) \qquad (4)$$

The calculated values are all within three wavenumbers of the experimental values (Table 2.5), demonstrating that the four bands in the IR spectrum are all due to (^{tBu}PNP)Fe(CO)$_2$ carbonyl ligands (Figure 2.15).

*Figure 2.15: IR spectrum of (*tBu*PNP)Fe(*13*CO)₂*
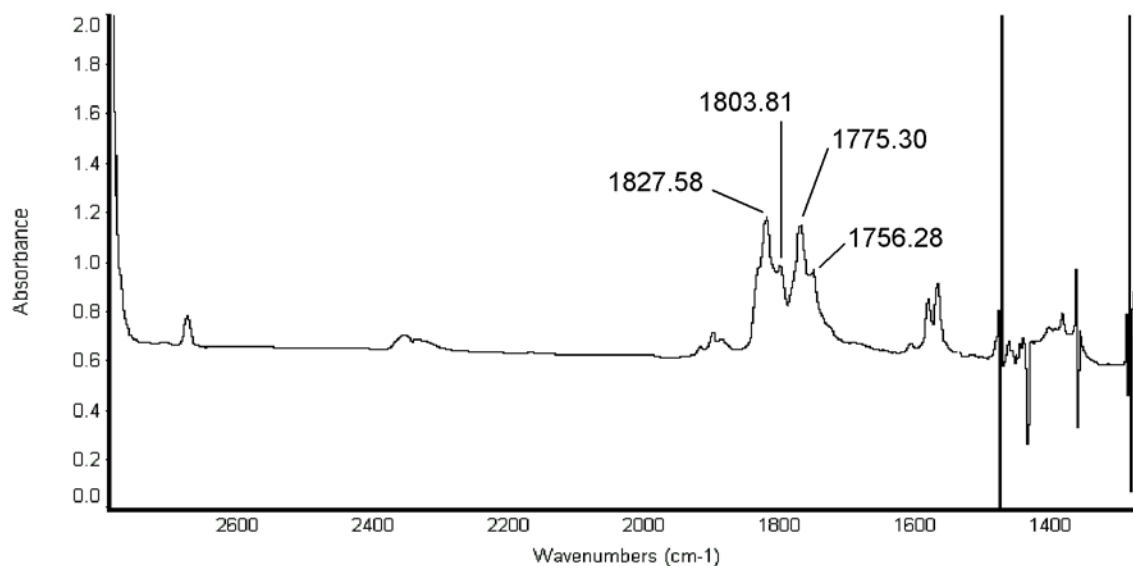
Solution DFT calculations by Krogh-Jespersen of (*tBu*PNP)Fe(CO)₂ give two energy minima that correspond to a trigonal bipyramidal structure and a square pyramidal structure, with the square pyramidal structure being only slightly lower in energy by 0.57 kcal/mol.[2] (*iPr*PNP)Fe(CO)₂ has only one calculated minima that corresponds to a trigonal bipyramidal structure.[2] The calculations also give wavenumbers in the infrared spectrum that are close to the values obtained experimentally (Table 2.5). This combination of computational results, ^{1}H and ^{13}C NMR and IR spectroscopic data, and the contrasting solid-state structures of (*tBu*PNP)Fe(CO)₂ and its *iPr*PNP analogue, all support the conclusion that there is an equilibrium between trigonal bipyramidal and square pyramidal (*tBu*PNP)Fe(CO)₂ isomers in solution.

There are other notable differences between the (*tBu*PNP)Fe(CO)₂ and (*iPr*PNP)Fe(CO)₂. (*tBu*PNP)Fe(CO)₂ is blue both in solution and as a solid. Other Fe(0)

complexes of the form $(PR_3)_3Fe(CO)_2$ in the literature range in color from yellow to orange to red.[19-23]   Interestingly, $(^{iPr}PNP)Fe(CO)_2$ is reported as being "royal blue" in solution but red in the solid state.[1]   The electronic spectrum of $(^{tBu}PNP)Fe(CO)_2$ shows a low broad absorbance at 640 nm which produces the blue color (Figure 2.16).[24]   DFT calculations by Krogh-Jespersen,[2] agree with this number with a computed HOMO-LUMO absorption occurring at 598 nm.[2]

Figure 2.16: Electronic absorption spectrum of (^{tBu}PNP)Fe(CO)$_2$
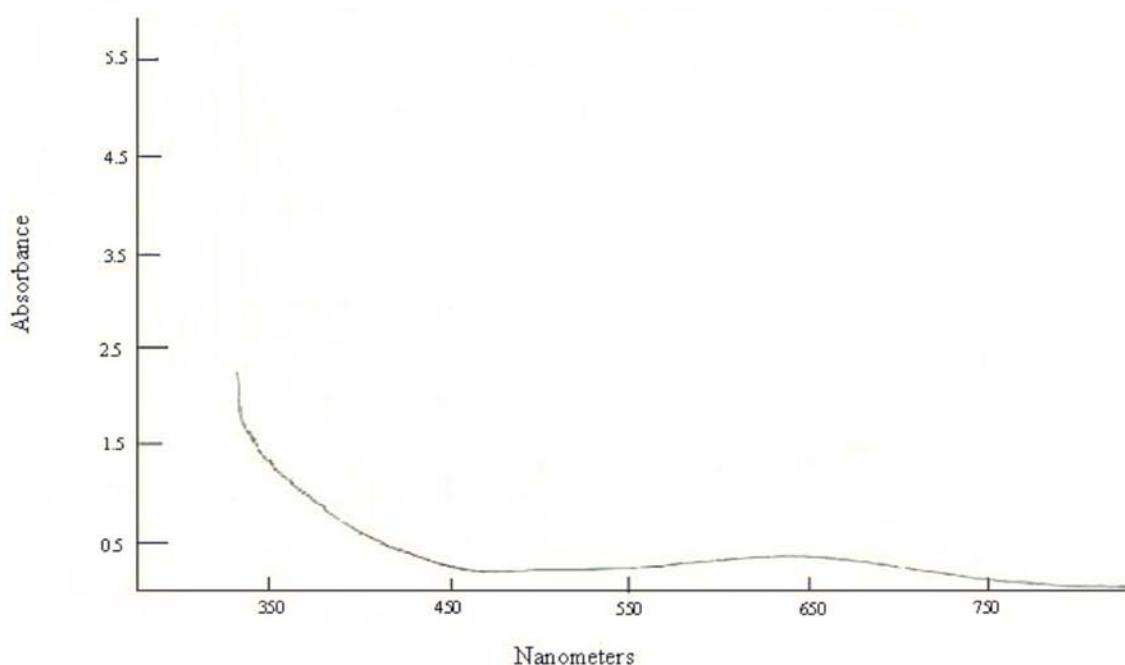
The Fe-C-O angles of $(^{tBu}PNP)Fe(CO)_2$ are also quite noteworthy particularly in the context of biologically important d^8 iron carbonyls.[25-30]   In particular, the O(2)-C(25)-Fe(1) angle of 171.87º (the apical CO of the distorted square pyramid) deviates significantly from linearity.   The O(1)-C(24)-Fe(1) angle is much closer to linear,

176.68º. In a literature survey of published metal complexes with bent O-C-M angles, the values ranged from 178-172º.[31-44] In contrast, the (^{iPr}PNP)Fe(CO)$_2$ complex has two equivalent CO ligands with Fe-C-O bond angles of 174.5º (which is the average of the two bond angles observed in **3**.[1])

Figure 2.17 shows the interatomic distances between select hydrogen atoms and the carbonyl oxygen atoms. The intra-molecular steric interactions between these atoms most likely contribute to the deviation from linearity of the carbonyl group. O(1) has an average distance of 2.68 Å to H(10B) and H(9C) as opposed to an average distance of 2.83 Å to H(18B) and H(22A), while O(2) has an average of distance of 2.69 Å to H(13B) and H(15B) but an average distance of 2.80 Å to H(21C) and H(2B). Interestingly, both of the shorter (~ 2.70 Å) contact distances are on one side of the NFe(CO)$_2$ plane, while the longer contact distances (~2.80 Å) are on the opposite side.

Figure 2.17: Interatomic distances in (^{tBu}PNP)Fe(CO)$_2$ (3)
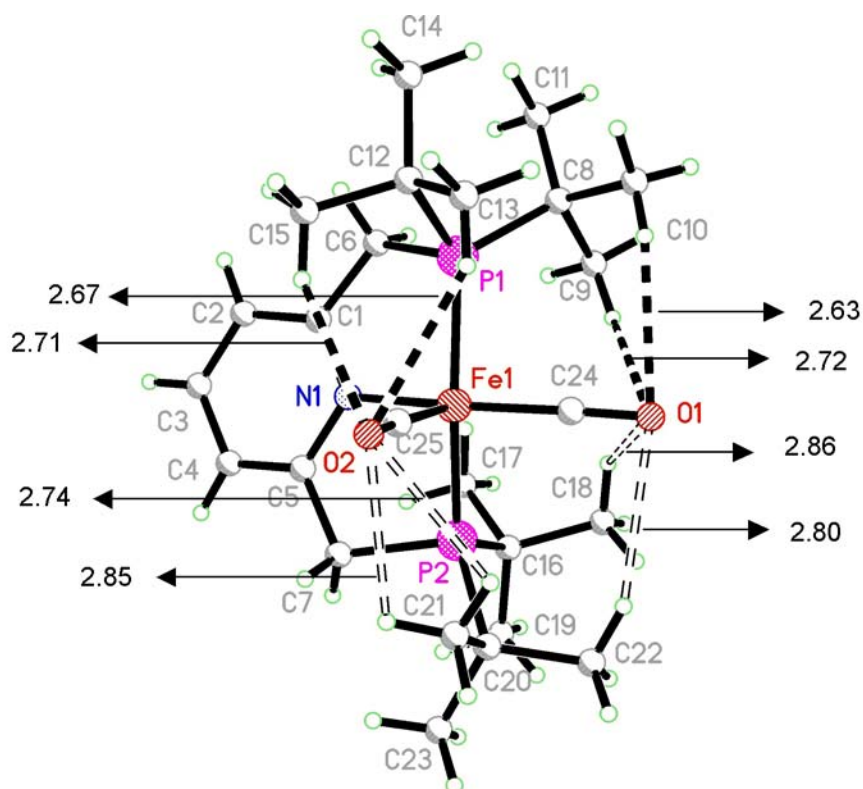
2.2.5 Attempted Reactions

Brookhart has shown that (PCP)IrHCl and (POCOP)IrHCl (Figure 2.18) will both generate catalysts that are active for the dehydrogenation of cyclooctane in the presence of NaO^{t}Bu.[45]   Based on this work (^{tBu}PNP)FeHCl (**2**) was used as a potential catalyst precursor in the dehydrogenation of alkyl groups. After **2** was generated, a solution of diisopropylethylamine and KO^{t}Bu was added. NMR spectra taken after 40 minutes of stirring at room temperature, 1 hour of heating at 75 ºC, and overnight heating at 85 ºC showed no dehydrogenation had taken place.

Figure 2.18: Structure of (^{tBu}POCOP)IrHCl[45]
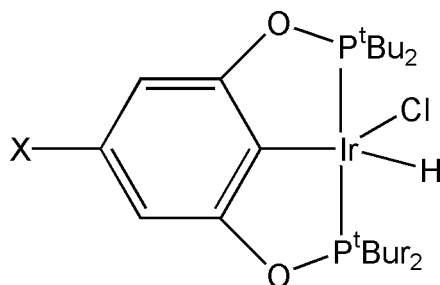
2.3 Conclusions

(^{tBu}PNP)FeCl$_2$ was synthesized and fully characterized. Magnetic susceptibility measurements done on the complex confirm that it is a paramagnetic, high spin, iron (II) complex with four unpaired electrons. X-ray diffraction shows that the Fe-N bond length is unusually long, at 2.303 Å in the structure, and this is due to a combination of steric as well as electronic factors. The pincer ligand places the nitrogen atom in a position where bonding to the iron is favorable; however, since iron is relatively small, there is not enough room for the nitrogen to be brought closer.

(^{tBu}PNP)FeHCl was also synthesized; however, due to the instability of the complex, we were unable to fully characterize it. The tentative structural assignment is based on the observance of a new hydride signal in the ^{1}H NMR and the commensurate observation of a doublet in the selectively ^{1}H decoupled ^{31}P NMR spectrum.

The last complex made in this series was the bright blue (tBuPNP)Fe(CO)$_2$. Infrared and NMR (^{1}H and ^{31}P) spectroscopy and DFT calculations all indicate that this complex exists in equilibrium between a trigonal bipyramidal and square pyramidal structure in solution with the square pyramidal structure being lower in energy by 0.57 kcal/mol (DFT). The solid state structure is a distorted square pyramid, where one Fe-C-O bond angle is surprisingly bent at 171.87º. While the analogous complex (iPrPNP)Fe(CO)$_2$ does have a bent CO, the similarities end there. (iPrPNP)Fe(CO)$_2$ is red with almost perfect trigonal bipyramidal geometry in the solid state and also only shows one set of carbonyl bands in the solid state infrared spectrum, corresponding to a trigonal bipyramidal structure.

2.4 Experimental

All reactions were conducted under an argon atmosphere unless otherwise noted. All solvents were purchased as anhydrous from Aldrich and degassed with argon. NMR spectra were recorded on Varian 400 MHz and 300 MHz spectrometers. ^{1}H NMR signals are calibrated using the residual proton peaks of the deuterated solvent (they are referenced to TMS). ^{31}P NMR signals are calibrated with an external reference, a capillary with a solution of para-xylene-d_{10} and PMe$_3$ (δ –62.4 ppm). Elemental Analysis was performed by Robertson Microlit Laboratories. X-Ray diffraction data by Dr. Thomas Emge (Rutgers) was obtained from an oil coated crystal mounted on a glass fiber. X-Ray intensity measurements were made using a Bruker-AXS Smart APEX CCD diffractometer with graphite monochromatized Mo Kα radiation at 100 K. Magnetic susceptibility measurements were obtained on a Quantum Design superconducting

quantum interference device (SQID) magnetometer (MPMS-*XL)*. Electronic adsorption data was collected using a Perkin Elmer Lambda 40 UV-Vis spectrometer. IR data was collected on an Avatar 360 FT-IR.

^{tBu}PNP: The ligand was synthesized according to the literature;[46] purification, however, was achieved by extracting the crude material with benzene, filtering, and removing the solvent. The same procedure was repeated using diethyl ether to obtain the product as white microcrystals (yield 44 %).

(^{tBu}PNP)FeCl$_2$ (1): FeCl$_2$·4H$_2$O (0.25 g, 1.26 mmol) was placed in a vial and dissolved in 5 mL of ethanol. In a separate vial, ^{tBu}PNP (0.50 g, 1.26 mmol) was dissolved in 10 mL of benzene. The ^{tBu}PNP solution was added to the FeCl$_2$·4H$_2$O solution resulting in an orange solution. The solvent was removed by vacuum to give a yellow solid. Ethanol (10 mL) was added to the solid and the slurry was placed at –48 $^{\circ}$C overnight, which resulted in the formation of yellow crystals. The crystals were collected on a frit, and washed with pentane (3 x 5 mL). Yield = 0.40 g (60 %). ^{1}H NMR (300 MHz, CD$_3$CN): δ 54.9 (broad, 2H, *m*-py), 18-14 (very broad, 4H, CH$_2$), 10.1 (broad, 36H, *tert*-butyl), -10.0 (broad, 1H, *p*-py). Anal. Calcd. for FeP$_2$NCl$_2$C$_{23}$H$_{43}$: C, 52.89; H, 8.29, N, 2.68; Cl, 13.58. Found: C, 52.01; H, 8.47; N, 2.50; Cl, 13.62.

(^{tBu}PNP)FeHCl (2): (^{tBu}PNP)FeCl$_2$ (10.0 mg, 1.914 x 10^{-2} mmol) was placed in a vial and dissolved in 0.5 mL of acetonitrile to give a yellow solution. In a separate vial a solution of NEt$_4$BH$_4$ (10.0 mg, 6.892 x 10^{-2} mmol) in 0.5 mL of acetonitrile was made and added to the (^{tBu}PNP)FeCl$_2$ solution and left to stand at room temperature overnight. The resulting bright red solution was filtered to remove precipitates. ^{1}H NMR (300 MHz,

CD$_3$CN): -13.623 (t, hydride, J$_{P-H}$ = 58). ^{31}P NMR (121) MHz, CD$_3$CN): δ 102.7 (d, J$_{P-H}$ = 51).

(^{tBu}PNP)Fe(CO)$_2$ (3)   **Method 1:** (^{tBu}PNP)FeCl$_2$ (20.0 mg, 3.829 x 10-2 mmol) was dissolved in 0.7 mL of CD$_3$CN and placed in a J. Young NMR tube. CO (1 atm) was added and the tube inverted 3 times to mix before being placed in an isopropanol/ice bath overnight. The solution was filtered through a pipet with glass wool into a vial and the solvent was slowly evaporated to give blue crystals suitable for x-ray diffraction (5.2 mg, 27 %).   **Method 2:**[1]   A 5% sodium amalgam was made and placed in a cuvette bottomed schlenk flask with a large head space that contained a magnetic stir bar. The flask was placed under 1 atm of CO. In the glovebox, a solution of (^{tBu}PNP)FeCl$_2$ in toluene was made. The solution was taken up by syringe and injected into the flask with CO. The solution was stirred vigorously overnight resulting in the formation of a dark blue solution. Slow evaporation of the solvent lead to the formation of a dark blue solid. ^{1}H NMR (400 MHz, toluene-d_8, room temperature): δ 6.29 (broad, 2H, *m*-pyridine), 2.95 (broad, 4H, CH$_2$), 1.36 (broad, 36H, *tert*-butyl). ^{1}H NMR (400 MHz, toluene-d_8, -80 °C): δ 6.50 (broad, 1H, *p*-pyridine), 6.21 (broad, 2H, *m*-pyridine), 2.79 (broad, 4H, CH$_2$), 1.33 (broad, 36H, *tert*-butyl). ^{31}P{^{1}H} (121 MHz, toluene-d_8, room temperature): δ 123 -119 (very broad, (^{tBu}PNPFe(CO)$_2$), 76.18, 34.63 (free ^{tBu}PNP). ^{31}P{^{1}H} (121 MHz, toluene-d_8, -80 °C): δ 124.10, 78.52, 35.00 (^{tBu}PNP). IR(THF): ν$_{co}$ = 1870, 1846, 1819, 1797 cm^{-1}.   Electronic absorption 640 nm (very broad, low intensity). (^{tBu}PNP)Fe(^{13}CO)$_2$: ^{1}H NMR (400 MHz, toluene-d_8, room temperature): δ 6.45 (broad, 1H, *p*-pyridine), 6.27 (broad, 2H, *m*-pyridine), 2.94 (broad, 4H, CH$_2$), 1.34 (broad, 36H, *tert*-butyl). ^{1}H NMR (400 MHz, toluene-d_8, -80 °C): δ 6.22 (broad, 2H, *m*-pyridine),

2.71 (broad, 4H, CH$_2$), 1.32 (broad, 36H, *tert*-butyl). ^{31}P{^{1}H} NMR (162 MHz, toluene-d_8, room temperature): δ 122.15 (t, J$_{P-C}$ = 19), 35.00 (free ^{tBu}PNP). ^{31}P{^{1}H} NMR (162 MHz, toluene-d_8, -80 ºC): δ 123.43 (broad), 35.00 (free ^{tBu}PNP). ^{13}C NMR (101 MHz, toluene-d_8, room temperature): δ 230.65. ^{13}C NMR (101 MHz, toluene-d_8, -80 ºC): δ 230.74 (t, J$_{P-C}$ = 19). IR(THF): ν$_{co}$ = 1828, 1804, 1775, 1756.

2.5 References

(1)   Trovitch, R. J.; Emil, L.; Chirik, P. J. *Inorg. Chem.* **2006**, *45*, 7252-7260.

(2)   Krogh-Jespersen, K., Personal Communication.

(3)   Small, B. L.; Brookhart, M.; Bennett, A. M. A. *J. Am. Chem. Soc.* **1998**, *120*, 4049-4050.

(4)   Britovsek, G., J.P.; Gibson, V. C.; Kimberley, B. S.; Maddox, P. J.; McTavish, S.; Solan, G. A.; White, A. J. P.; Williams, D. J. *Chem. Commun.* **1998**, 849-850.

(5)   Chen, Y.; Chen, R.; Qian, C.; Dong, X.; Sun, J. *Organometallics* **2003**, *22*, 4312-4321.

(6)   Bart, S. C.; Lobkovsky, E.; Chirik, P. J. *J. Am. Chem. Soc.* **2004**, *126*, 13749-13807.

(7)   Giannoccaro, P.; Vasapollo, G.; Nobile, C. F.; Sacco, A. *Inorg. Chim. Acta.* **1982**, *61*, 69-75.

(8)   Dahlhoff, W. V.; Nelson, S. M. *J. Chem. Soc. (A): Inorg. Phys. Theor.* **1971**, *13*, 2184-2190.

(9)   Muller, G.; Klinga, M.; Leskela, M.; Rieger, B. *Z. Anorg. Allg. Chem.* **2002**, *628*, 2839-2846.

(10)   Pelczar, E. M.; Goldman, A. S. In *Abstracts of Papers, 226th ACS National Meeting, New York, NY, United States, September 7-11, 2003*; American Chemical Society: Washington, D.C., 2003.

(11)   Zhang, J.; Gandelman, M.; Herrman, D.; Leitus, G.; Shimon, L. J. W.; Ben-David, Y.; Milstein, D. *Inorg. Chim. Acta.* **2006**, *359*, 1955-1960.

(12)   Pelczar, E. M.; Goldman, A. S. In *Abstracts of Papers, 228th ACS National Meeting, Philadelphia, PA, United States, August 22-26, 2004*; American Chemical Society: Washington, D.C., 2004.

(13)   Pelczar, E. M.; Emge, T. J.; Goldman, A. S. In *Abstracts, 37th Middle Atlantic Regional Meeting of the American Chemical Society, New Brunswick, NJ, United States, May 22-25*; American Chemical Society: Washington, D.C., 2005.

(14)   Pelczar, E. M.; Emge, T. J.; Krogh-Jespersen, K.; Goldman, A. S. In *Abstracts, 39th Middle Atlantic Regional Meeting of the American Chemical Society,*

Collegeville, PA, United States, May 16-18 (2007),; American Chemical Society: Washington, D.C., 2007.

(15)   Cox, P. A.; Oxford University Press: New York, 1987, p 154-157.

(16)   Gupta, M.; Hagen, C.; Flesher, R. J.; Kaska, W. C.; Jensen, C. M. *Chem. Commun.* **1996**, 2083-2084.

(17)   Blough, B. E.; Carroll, F. I. *Tet. Let.* **1993**, *34*, 7239-7242.

(18)   Gupta, M.; Hagen, C.; Kaska, W. C.; Cramer, R. E.; Jensen, C. M. *J. Am. Chem. Soc.* **1997**, *119*, 840-841.

(19)   Jaunky, P.; Schmalle, H. W.; Blacque, O.; Fox, T.; Berke, H. *J. Orgmet. Chem.* **2005**, *690*, 1429-1455.

(20)   Jaunky, P.; Schmalle, H. W.; Alfonso, M.; Fox, T.; Berke, H. *J. Orgmet. Chem.* **2004**, *689*, 801-810.

(21)   Kandler, H.; Gauss, C.; Bidell, W.; Rosenberger, S.; Burgi, T.; Eremenko, I. L.; Veghini, D.; Orama, O.; Burger, P.; Berke, H. *Chem. Eur. J.* **1995**, *1*, 541-548.

(22)   Birk, R.; Berke, H.; Hund, H.-U.; Huttner, G.; Zsolnai, L.; Dahlenburg, L.; Behrens, U.; Sielisch, T. *J. Orgmet. Chem.* **1989**, *372*, 397-410.

(23)   Vancheesan, S. *Indian J. Chem.* **1982**, *21A*, 579-582.

(24)   http://www.cem.msu.edu/~reusch/VirtualText/Spectrpy/UV-Vis/spectrum.htm

(25)   Spiro, T. G.; Kozlowski, P. M. *Acc. Chem. Res.* **2001**, *34*, 137-144.

(26)   Spiro, T. G.; Kozlowski, P. M. *JBIC, J. Bio. Inorg. Chem.* **1997**, *2*, 516-520.

(27)   Yu, N.-T.; Benko, B.; Kerr, E. A.; Gersonde, K. *Proc. Natl. Acad. Sci. USA* **1984**, *81*, 5106-5110.

(28)   Scheidt, R. W.; Haller, K. J.; Fons, M.; Mashiko, T.; Reed, C. A. *Biochemistry* **1981**, *20*, 3653-3657.

(29)   Peng, S.-M.; Iber, J. A. *J. Am. Chem. Soc.* **1976**, *98*, 8032-8036.

(30)   Goedken, V. L.; Peng, S.-M.; Molin-Norris, J.; Park, Y.-a. *J. Am. Chem. Soc.* **1976**, *98*, 8391-8400.

(31)   Atwood, J. L.; Beveridge, K. A.; Bushnell, G. W.; Dixon, K. R.; Eadie, D. T.; Stobart, S. R.; Worotko, M. J. *Inorg. Chem.* **1984**, *23*, 4050-4057.

(32)   Schumann, H.; Heisler, M.; Pickardt, J. *Chem. Ber.* **1977**, *110*, 1020-1026.

(33)   Stewart, K. R.; Levine, S. G.; Bordner, J. *J. Org. Chem.* **1984**, *49*, 4082-4084.

(34)   Bradley, F. C.; Wong, E. H.; Gabe, E. J.; F.L., L. *Inorg. Chim. Acta.* **1986**, *120*, L21-L22.

(35)   Klufers, P. *Z. fur. Kristall.* **1984**, *167*, 253-260.

(36)   Williams, G. M.; Rudisill, D. E.; Barnum, B. A.; Hardcastle, K.; Heyn, R. H.; Kozak, C. J.; McMillan, J. W. *J. Am. Chem. Soc.* **1990**, *112*, 205-215.

(37)   Rickard, C. E. F.; Roper, W. R.; Taylor, G. E.; Waters, J. M.; Wright, L. J. *J. Orgmet. Chem.* **1990**, *389*, 375-388.

(38)   Sabat, M.; Reynolds, K. A.; Finn, M. G. *Organometallics* **1994**, *13*, 2084-2087.

(39)   Ooyama, D.; Tomon, T.; Tsuge, K.; Tanaka, K. *J. Orgmet. Chem.* **2001**, *619*, 299-304.

(40)   Denis, B.; Massoud, A.; Parlier, A.; Rudler, H.; Daran, J. C.; Vaissermann, J.; Alvarez, C.; Patino, R.; Toscano, R. A. *J. Orgmet. Chem.* **1990**, *386*, 51-62.

(41)   Lin, J. T.; Sun, S.-S.; Wu, J. J.; Liaw, Y.-C.; Lin, K.-J. *J. Orgmet. Chem.* **1996**, *517*, 217-226.

(42)   Mague, J. T.; Johnson, M. P. *Organometallics* **1990**, *9*, 1254-1269.

(43)   Yang, J.; Yin, J.; Abboud, K. A.; Jones, W. M. *Organometallics* **1994**, *13*, 971-978.

(44)   Adams, R. D.; Huang, M. *Organometallics* **1995**, *14*, 2887-2891.

(45)   Gottker-Schnetmann, I.; White, P.; Brookhart, M. *J. Am. Chem. Soc.* **2004**, *126*, 1804-1811.

(46)   Hermann, D.; Gandelman, M.; Rozenberg, H.; Shimon, L. J. W.; Milstein, D. *Organometallics* **2002**, *21*, 812-818.

Chapter 3

Synthesis and Characterization of Osmium (PNP) Pincer Complexes

Abstract

As part of our efforts to expand our knowledge of pincer complexes and potentially develop new catalysts, two new ^{R}PNP-osmium pincer complexes of the type (^{tBu}PNP)OsX$_n$ (X = Cl, n = 3; X = H; n = 4) were synthesized and fully characterized. (^{tBu}PNP)OsCl$_3$ is paramagnetic and gives broad signals in the ^{1}H NMR spectrum. X-ray diffraction studies show that the geometry around osmium is distorted octahedral, and the Os-Cl bond lengths are within the expected range for an Os(III)-Cl complex.   The (^{tBu}PNP)OsCl$_3$ compound was converted into (^{tBu}PNP)OsH$_4$. Variable temperature NMR studies show that this complex has hydrides that exchange at room temperature, but resolve into two separate signals at low temperature. The x-ray crystal structure shows that there are two distinct sets of hydrides in the complex in accord with the low temperature NMR data. Interestingly, the crystal structure also shows that this complex is a purely classical hydride with no evidence of dihydrogen character in the H···H distances. This is in contrast to the isoelectronic (^{R}PCP)IrH$_4$ complexes where one set of H···H distances are consistent with a hydride species, while the other set is much shorter and more consistent with a dihydrogen complex.

3.1 Introduction

For many years osmium has been viewed as a potential catalyst for several types of reactions. Most of the research in this area has focused on developing catalysts that hydrogenate olefins;[1-3] however, applications of osmium catalysts to other reactions such as hydroformylation,[4] hydrogenolysis,[5-7] and C-H and C-C activation[8] have also been examined. In the realm of asymmetric catalysis, osmium tetraoxide has been studied for its ability to asymmetrically dihydroxylate olefins; however, OsO_4 is not an attractive catalyst due to its high toxicity.[9,10]

A wide variety of osmium complexes have also been investigated for their photo- and electro-chemistry. The electronic absorption and redox potential of a series of mononuclear *trans*-dihalogen osmium complexes have been studied by Webster.[11] This group later expanded their research to include cationic osmium diphosphine and diarsine complexes.[12] Again these studies focused on the electronic absorption spectra and redox potentials determined by cyclic voltammetry.

Terpyridine (Figure 3.1) or (tpy) based pincer ligands are also popular as bridges for forming arrays of osmium complexes to be used as switches. Araki's group has made several of these complexes using a terpyridine based linker to make Os-Os and Os-Ru dinuclear and trinuclear complexes.[13] Electron transport is another area of research that uses terpyridine based osmium complexes. One such structure, that has been studied for this purpose, is an osmium bis(terpyridine)tetrathienyl complex shown in Figure 3.2.[14] This can be converted into a polymer that has the repeat unit shown in Figure 3.2 and will transport an electron through the polymer chain by a series of Os^{2+} to Os^{3+} oxidations.[14]

There is also work being done that studies the photo- and electro-chemical properties of these arrayed type complexes in both solution and in solid matrices.[15]

Figure 3.1: Structure of terpyridine (tpy)
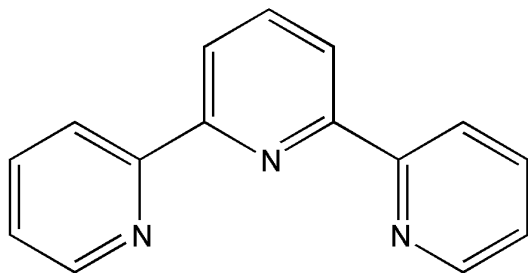
Figure 3.2: Os(tpy) complex and reaction to Os(tpy) polymer
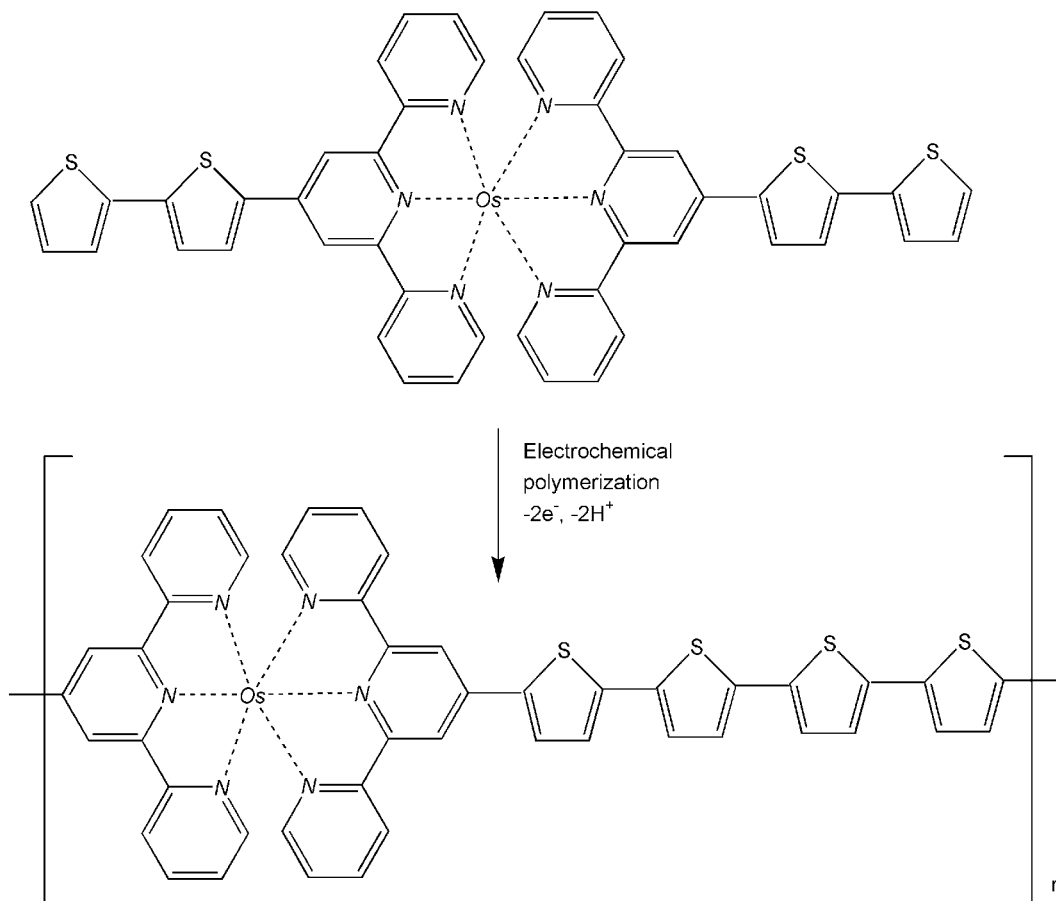
Another pincer type ligand that is frequently used with osmium is [R]PCP (PCP = 2,6-C$_6$H$_3$(PR$_2$)$_2$) (Figure 3.3). For example, a series of ([R]PCP)Os complexes were synthesized and characterized by Gusev's group.[16] This work was later extended to include studies on ([R]PCP)Os alkylidene and vinylidene complexes,[17] followed by an investigation into the corresponding silylene complexes.[18] Gia's group has made ([R]PCP)Os vinylidene and carbyne complexes[19] and has also used a ([R]PCP)Os complex to couple phenylacetylene.[20] In addition to coupling reactions, ([R]PCP)Os complexes have been looked at for their ability to activate C-C bonds.[21]

Figure 3.3: Structure of [R]PCP and [R]PNP pincer ligands
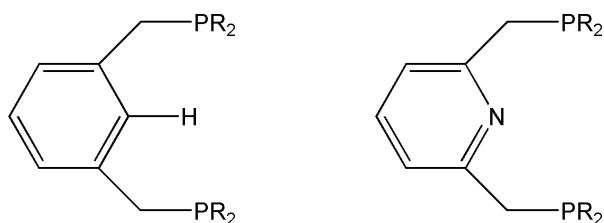
While much work has been done with ([R]PCP)Os complexes, relatively little has been done with the corresponding ([R]PNP)Os complexes. The ([R]PNP)Os unit is isoelectronic with the ([R]PCP)Ir unit which has proven to be catalytically valuable. ([Ph]PNP)OsCl$_2$ has been reportedly synthesized but characterized only by elemental analysis and infrared spectroscopy.[22] Using ([Ph]PNP)OsCl$_2$(PPh$_3$) as a starting material, a tetradentate ([R]PNP)Os complex, whose acidity properties have been studied, was made (Figure 3.4).[23] The cationic [([Ph]PNP)OsCl(H$_2$)]BF$_4$ complex has also been synthesized and used in a comparison acidity study.[24]

Figure 3.4: Synthesis of tetradentate (^{R}PNP)Os complexes[23]
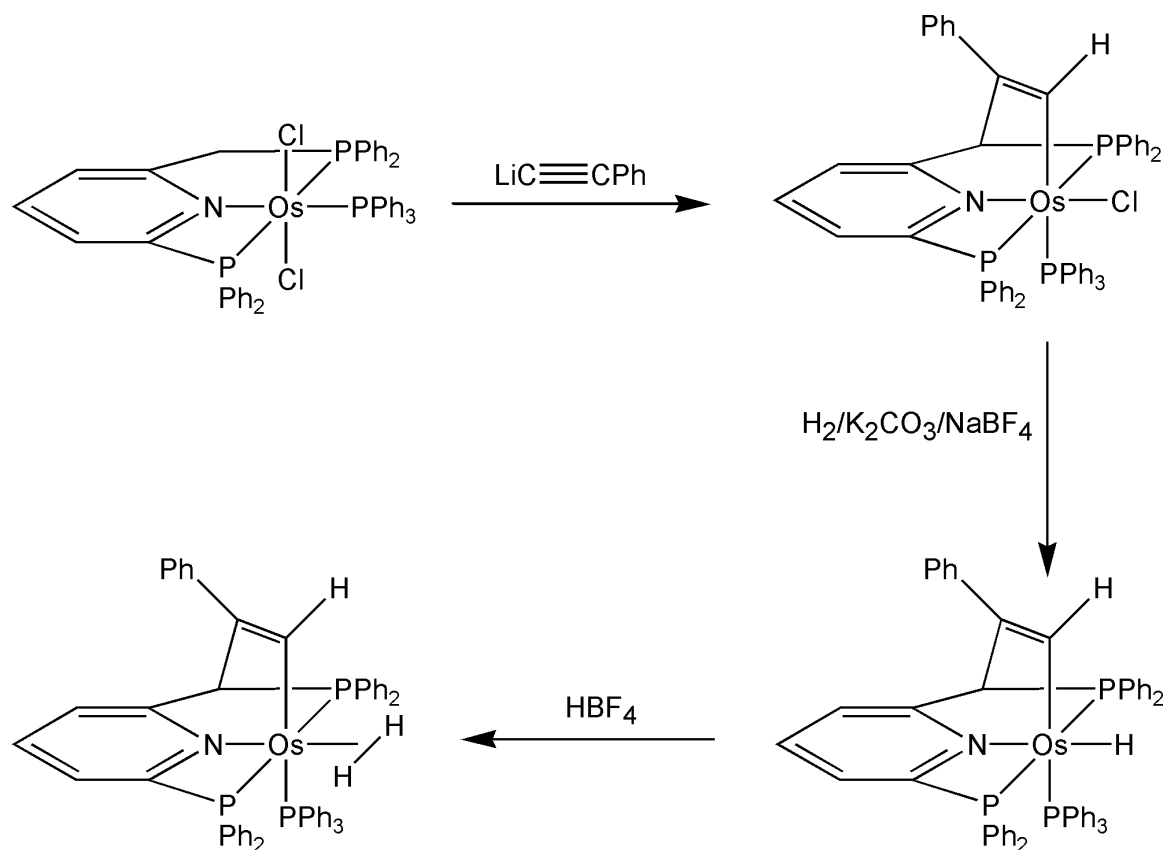
In an effort to search for new catalysts, perhaps with activity related to that of (^{R}PCP)Ir based species, and to deepen the understanding of pincer complexes in general, two new osmium pincer complexes were developed. The first was (^{tBu}PNP)OsCl$_3$ (**4**) which was then converted into (^{tBu}PNP)OsH$_4$ (**5**), a complex that is formally related to the already well characterized, highly active, dehydrogenation catalyst (PCP)IrH$_4$. This chapter will present the synthesis and characterization of these complexes as well as compare the bond lengths, angles, and H···H distances in various (PCP)Ir-based hydride complexes to those in (^{tBu}PNP)OsH$_4$.

3.2 Results and Discussion

3.2.1 (^{tBu}PNP)OsCl$_3$

Poon's group has published the synthesis of a complex that they have identified as (^{Ph}PNP)OsCl$_2$ based solely on elemental analysis and infrared data.[22] Following their method, Na$_2$OsCl$_6$·6H$_2$O and ^{tBu}PNP were dissolved in 2-methoxyethanol and then refluxed (Scheme 3.1). After filtering to remove insoluble material, the solution was concentrated and cooled to give (^{tBu}PNP)OsCl$_3$ (**4**) as red crystals.

Scheme 3.1:   Synthesis of (^{tBu}PNP)OsCl$_3$
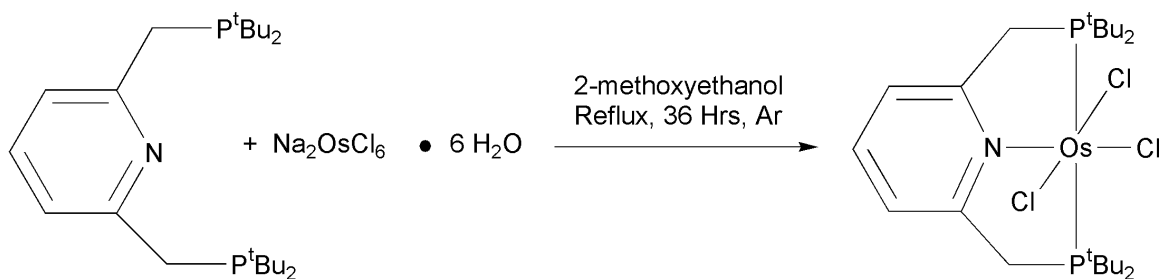
Characterization of the Os(III) complex **4** by NMR methods was difficult since it is paramagnetic. The ^{31}P{^{1}H} NMR showed no signals. The ^{1}H NMR showed signals that were outside the usual range (0-10 ppm) of chemical shifts (Figure 3.5). The para proton on the pyridine ring gave the sharpest signal with shoulders that gave the appearance of a possible triplet. This is consistent with coupling to the two meta protons of the pyridine ring, but the shoulders were not well enough defined to be used to calculate a coupling constant. This semi-sharp signal was assigned an integration value

of 1.00 for the para proton, and the other signals in the spectrum were integrated against this value.

Figure 3.5: ^1H NMR spectrum of (^{tBu}PNP)OsCl$_3$
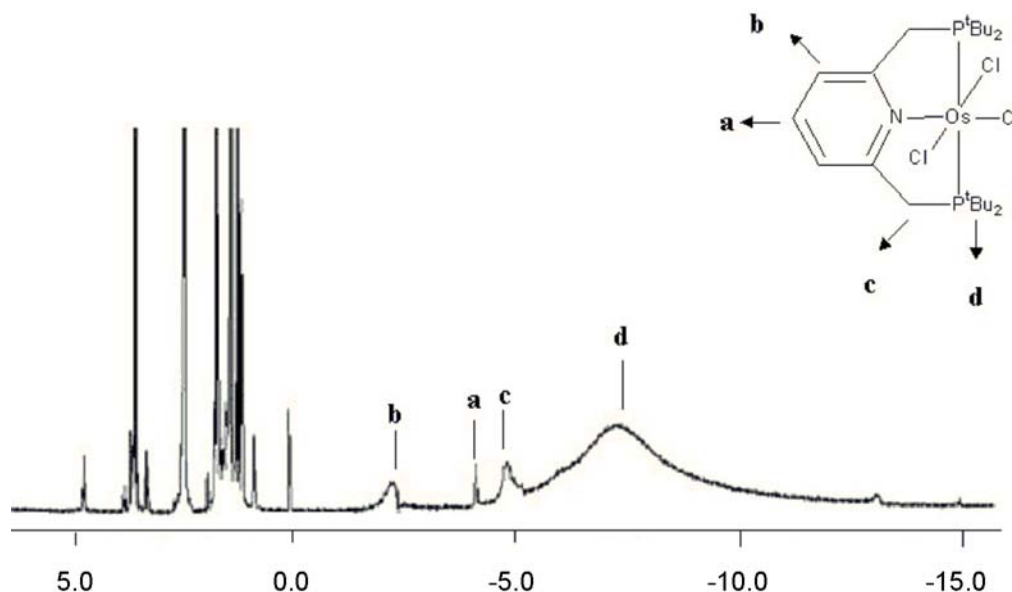
Despite the broadness of the signals, the integrations matched very well and allowed the remaining signals to be assigned to other hydrogen atoms in the complex. The very broad signal at δ −2.19 ppm integrated to 2H and was assigned to the meta protons of the pyridine ring. The sharpest signal at δ −4.10 ppm was assigned to the para proton of the pyridine ring. Another broad signal at δ −4.81 ppm integrated to 4H and was assigned to the methylene protons and an extremely broad signal from δ −5 ppm to −8 ppm integrated to 36H and was assigned to the *tert*-butyl groups on the PNP.

An x-ray diffraction study of a single crystal of **4** revealed that the crystal was orthorhombic and in the P2(1)2(1)2(1) space group (Table 3.1). The geometry around

the osmium center was only slightly distorted away from octahedral (Figure 3.6). As

seen in Table 3.2 and Figure 3.6 the major source of distortion is due to the acuteness of

the N-Os-P angles (ca 81°). The Os-Cl bond lengths of 2.3597(12) − 2.3777(13) Å

(average = 2.3698 Å) are similar to those found in other Os(III)-Cl$_3$ complexes.[25,26] The

structure proves that there are three chlorides bound to the osmium in contrast with the

reported characterization of (^{Ph}PNP)OsCl$_2$.[22] Full crystallographic data may be found in

the appendix.

Figure 3.6: Crystal structure of (^{tBu}PNP)OsCl$_3$ (4)
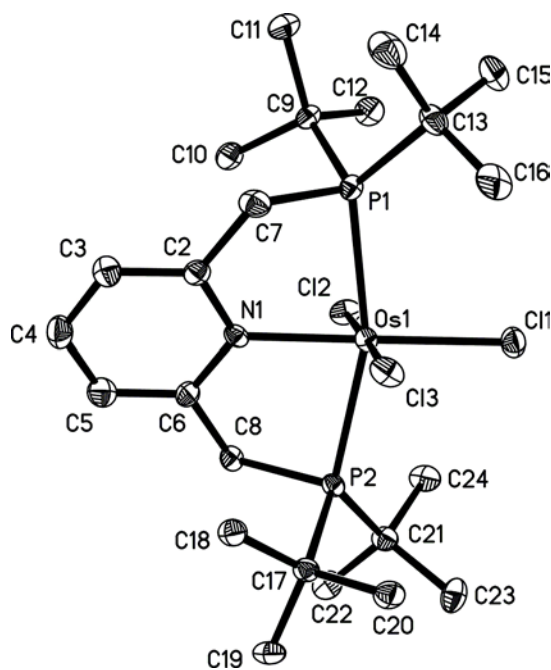
Table 3.1: Crystal data and structure refinement for (^{tBu}PNP)OsCl$_3$ (**4**)

Identification code	ospnpcl
Empirical formula	C23 H43 Cl3 N Os P2
Formula weight	692.07
Temperature	100(2) K
Wavelength	0.71073 Å
Crystal system	Orthorhombic
Space group	P2(1)2(1)2(1)
Unit cell dimensions	a = 13.1011(6) Å α= 90°.
	b = 14.1488(7) Å β= 90°.
	c = 15.0599(7) Å γ = 90°.
Volume	2791.6(2) Å^3
Z	4
Density (calculated)	1.647 Mg/m^3
Absorption coefficient	4.981 mm^{-1}
F(000)	1380
Crystal size	0.16 x 0.09 x 0.04 mm^3
Theta range for data collection	1.97 to 30.51°.
Index ranges	-18<=h<=18, -20<=k<=20, -21<=l<=21
Reflections collected	33378
Independent reflections	8522 [R(int) = 0.0388]
Completeness to theta = 30.51°	99.9 %
Absorption correction	None
Refinement method	Full-matrix least-squares on F^2
Data / restraints / parameters	8522 / 0 / 283
Goodness-of-fit on F^2	1.004
Final R indices [I>2sigma(I)]	R1 = 0.0396, wR2 = 0.0889
R indices (all data)	R1 = 0.0426, wR2 = 0.0903
Absolute structure parameter	0.007(7)
Largest diff. peak and hole	7.495 and -2.106 e.Å^{-3}

Table 3.2: Selected Bond Lengths (Å) and angles (°) for (^{tBu}PNP)OsCl$_3$ (**4**)

Os(1)-N(1)	2.066(4)	Os(1)-Cl(3)	2.3597(12)
Os(1)-Cl(2)	2.3721(12)	Os(1)-Cl(1)	2.3777(13)
Os(1)-P(2)	2.4374(14)	Os(1)-P(1)	2.4440(13)
P(1)-C(7)	1.841(6)	P(1)-C(9)	1.905(6)
P(1)-C(13)	1.906(6)	P(2)-C(8)	1.848(5)
P(2)-C(21)	1.896(6)	P(2)-C(17)	1.908(5)
N(1)-C(6)	1.370(7)	N(1)-C(2)	1.375(7)

N(1)-Os(1)-Cl(3)	89.43(12)	N(1)-Os(1)-Cl(2)	89.41(12)
Cl(3)-Os(1)-Cl(2)	178.78(5)	N(1)-Os(1)-Cl(1)	179.53(14)
Cl(3)-Os(1)-Cl(1)	90.82(5)	Cl(2)-Os(1)-Cl(1)	90.35(5)
N(1)-Os(1)-P(2)	80.75(13)	Cl(3)-Os(1)-P(2)	91.52(5)
Cl(2)-Os(1)-P(2)	87.95(5)	Cl(1)-Os(1)-P(2)	99.65(5)
N(1)-Os(1)-P(1)	81.00(13)	Cl(3)-Os(1)-P(1)	87.73(5)
Cl(2)-Os(1)-P(1)	92.43(5)	Cl(1)-Os(1)-P(1)	98.61(5)
P(2)-Os(1)-P(1)	161.74(4)	C(7)-P(1)-Os(1)	93.32(18)
C(9)-P(1)-Os(1)	119.60(18)	C(13)-P(1)-Os(1)	123.5(2)
C(8)-P(2)-Os(1)	93.81(17)	C(21)-P(2)-Os(1)	123.02(18)
C(17)-P(2)-Os(1)	120.07(16)	C(6)-N(1)-Os(1)	120.8(4)
C(2)-N(1)-Os(1)	120.3(4)		

3.2.2 (^{tBu}PNP)OsH$_4$

After synthesizing (^{tBu}PNP)OsCl$_3$ the next step was to convert the complex into a potentially catalytic hydride. In the synthesis of (^{R}PCP)IrH$_n$ complexes, shown in Scheme 3.2, (^{R}PCP)IrHCl is reacted with LiEt$_3$BH under an H$_2$ atmosphere.[27] When this procedure was tried using **4** as the starting material, the result was a sticky red/orange solid. LiEt$_3$BH is used to reduce pyridine rings and most likely reduced the pyridine backbone instead of, or in addition to, the metal center.[28] Reacting **4** with NaEt$_3$BH instead, in THF under an H$_2$ atmosphere according to Scheme 3.3, successfully gave the complex (^{tBu}PNP)OsH$_4$ (**5**).[29]

Scheme 3.2: Synthesis of (^{tBu}PCP)IrH$_4$[27,30]
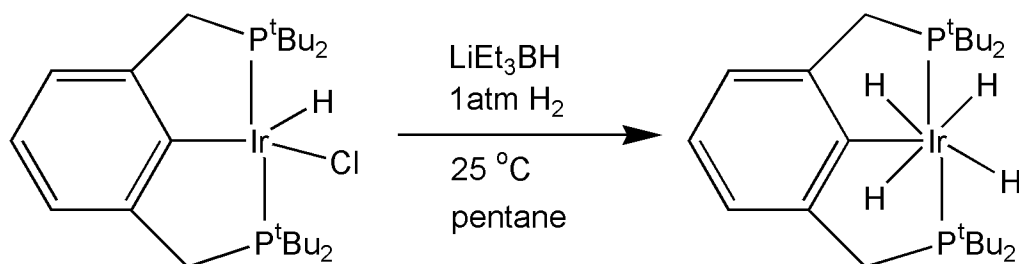
Scheme 3.3: Synthesis of (^{tBu}PNP)OsH$_4$ (**5**)
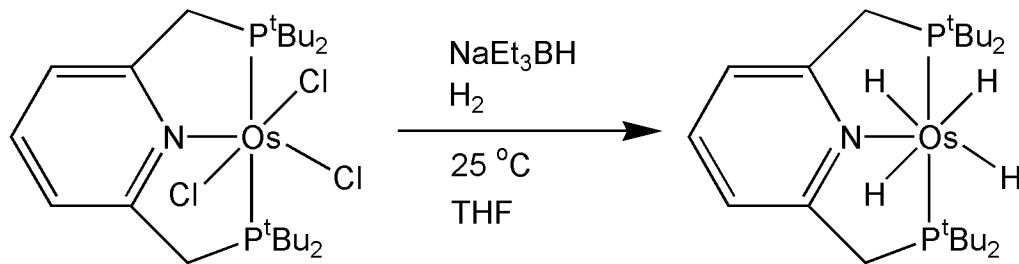
The ^{31}P NMR spectrum showed a singlet at δ 76.71 ppm. This value is close to the chemical shift of ([tBu]PCP)IrH₄, δ 73.1 ppm.[27,30] In the ^{1}H NMR spectrum (Figure 3.7), the para proton on the pyridine ring is a triplet centered at δ 6.84 ppm. The meta protons were assigned as a doublet at δ 6.59 ppm, while the methylene and *tert*-butyl protons were both triplets at δ 3.33 ppm and δ 1.32 ppm, respectively. While the splitting patterns and integration values made assignment of the [tBu]PNP protons straightforward, there was a question as to the number of hydrides on the complex, since they appeared as a broad signal at δ −8.7 ppm and integrated to 3H. Based on analogies drawn from the similar ([R]PCP)IrH$_n$ complexes, either 4 or 2 hydrides seemed more likely.

Figure 3.7: Room Temperature ^{1}H NMR spectrum of ([tBu]PNP)OsH₄ (5)
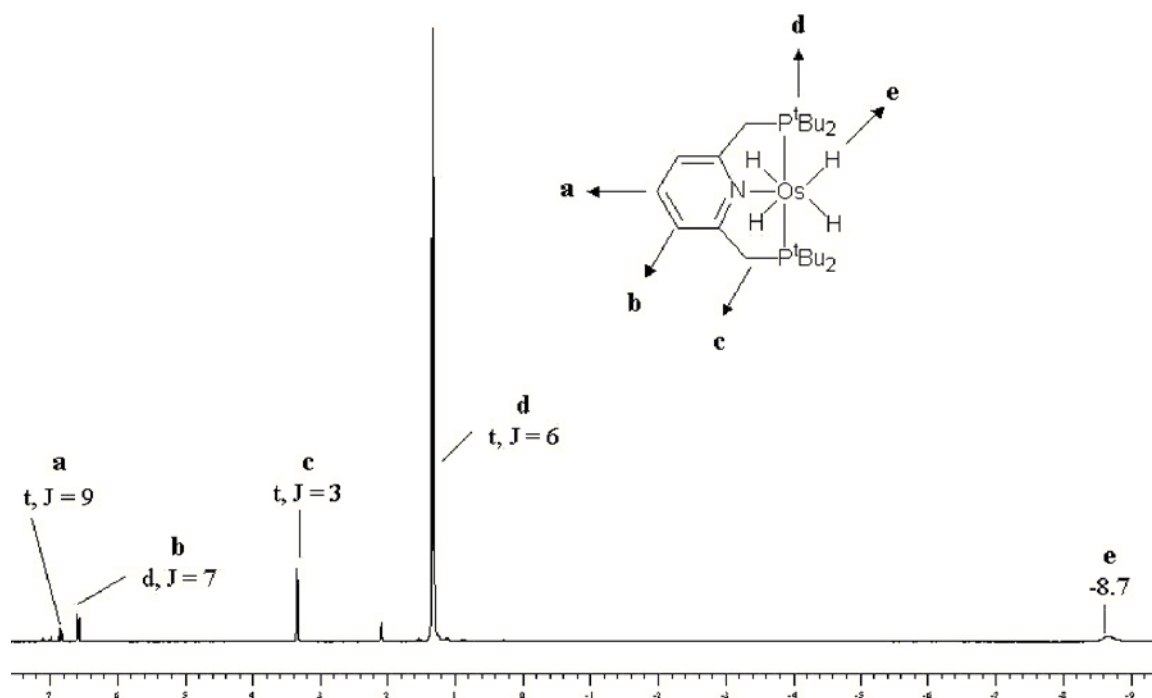
A series of variable temperature NMR studies were undertaken. The first set involved heating the complex to 60 °C. At this temperature, in the proton spectrum the hydrides sharpen to give a triplet at δ −8.68 ppm that integrated to 4H suggesting the complex was a tetrahydride (Figure 3.8a). The selectively decoupled ^{31}P NMR spectrum taken at this temperature was split into a quintet centered at δ 77.21 ppm in support of this conclusion (Figure 3.8b).

*Figure 3.8: High Temperature Spectra (60 °C) of (^{tBu}PNP)OsH$_4$ (**5**).   a. ^{1}H NMR Spectrum*

a.

b. ³¹P NMR Spectrum

J_{P-H} = 10 Hz
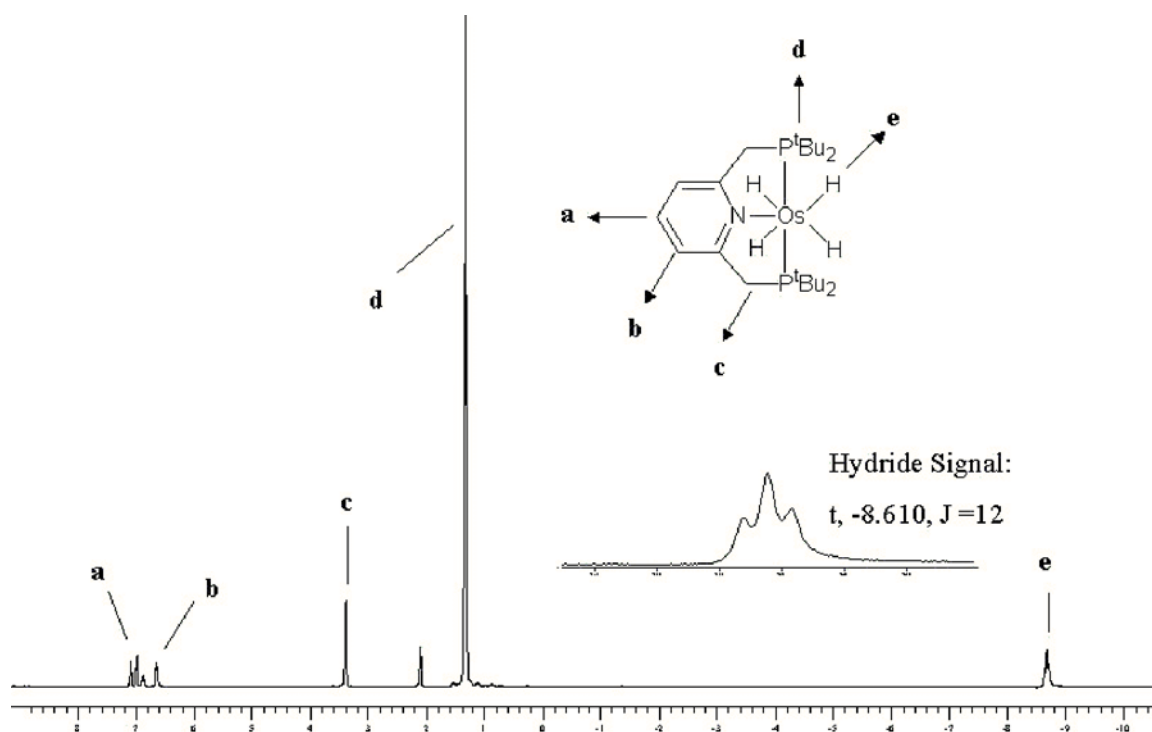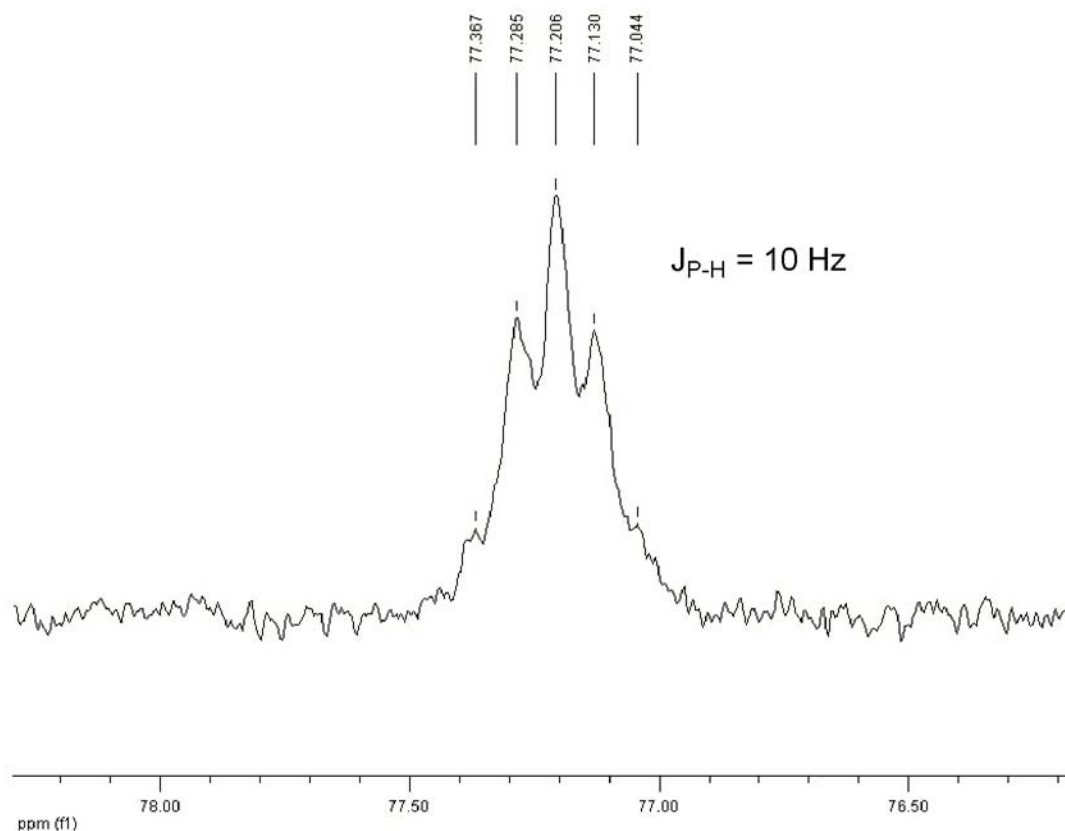
In a second set of variable temperature experiments, the sample was cooled to -80 ºC in 20-degree increments. At −20 ºC, the hydride signal broadened into the baseline and at −40 ºC the appearance of two small new broad signals is first seen. At −80 ºC, these have resolved into two broad, but easily discernible, singlets at δ -5.04 ppm and δ −11.97 ppm, that integrate to two protons each (Figure 3.9). This suggests that not only is there a total of four hydrides in the complex, but also that they are divided into two inequivalent sets of two hydrides.

Figure 3.9: Low Temperature (-80 °C) Spectrum of (^{tBu}PNP)OsH$_4$ (5)
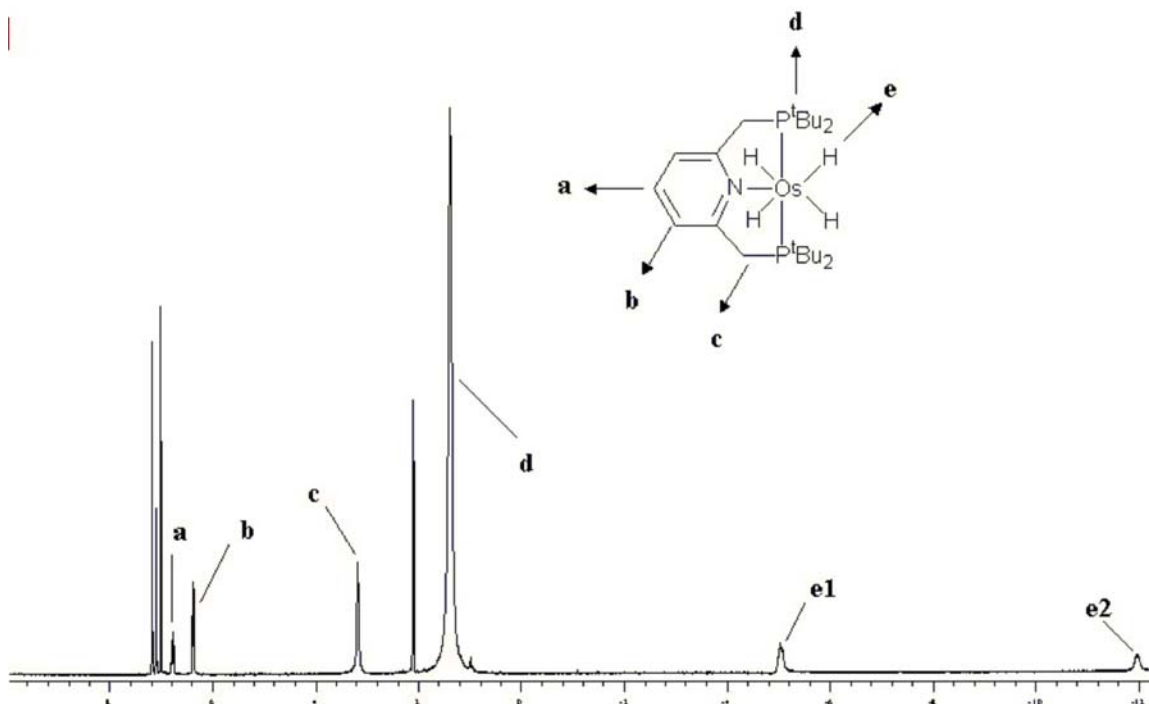
The solid state x-ray crystal structure of **5** confirmed that there were two sets of two hydrides (Figure 3.10). The crystal was tetragonal and in the P4$_2$ space group. As is the case in the similar (^{R}PCP)Ir complexes, the P(1)-Os(1)-P(1A) angle is decidedly not linear at 165.11° (Table 3.4). The H(2)/H(2A) hydrides are approximately trans to each other, while the H1/H1A pair may be viewed as "partially trans" to the PNP nitrogen atom. Since hydride is a strong trans influence ligand the Os-H(2) distances may be expected to be longer than the Os-H(1) distances. This is quite evident in the crystal data where the Os-H(2) distance is 1.846(19) Å, while the Os-H(1) distance is significantly shorter at 1.62(2) Å. This shorter distance is consistent with the Os-H distances of 1.66 – 1.68 Å that were found by neutron diffraction for the four hydrides of Os(PMe$_2$Ph)$_3$H$_4$,

although in this structure both sets of hydrides were found as essentially trans to each other.[31] Full crystallographic data may be found in the Appendix.

Figure 3.10: Crystal Structure of (^{tBu}PNP)OsH₄ (5)
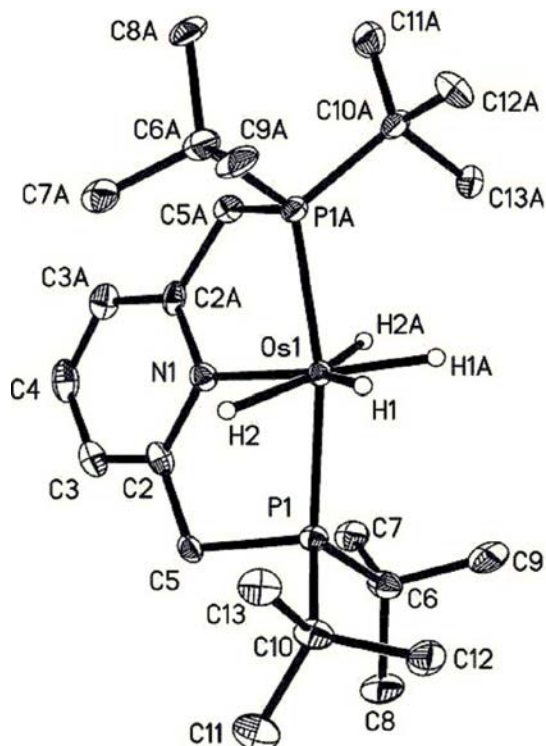
Table 3.3: Crystal Collection Data for (^{tBu}PNP)OsH$_4$ (**5**)

Identification code	osh4
Empirical formula	C23 H47 N Os P2
Formula weight	589.76
Temperature	100(2) K
Wavelength	0.71073 Å
Crystal system	Tetragonal
Space group	P4$_2$ (#77)
Unit cell dimensions	a = 11.6422(10) Å $\quad$ α= 90°.
	b = 11.6422 Å $\quad$ β= 90°.
	c = 9.4519(8) Å $\quad$ γ = 90°.
Volume	1281.12(15) Å^3
Z	2
Density (calculated)	1.529 Mg/m^3
Absorption coefficient	5.110 mm^{-1}
F(000)	596
Crystal size	0.30 x 0.15 x 0.07 mm^3
Theta range for data collection	1.75 to 30.49°.
Index ranges	-16<=h<=16, -16<=k<=16, -13<=l<=13
Reflections collected	15756
Independent reflections	3901 [R(int) = 0.0224]
Completeness to theta = 30.49°	100.0 %
Absorption correction	Semi-empirical from equivalents
Max. and min. transmission	0.7324 and 0.3093
Refinement method	Full-matrix least-squares on F^2
Data / restraints / parameters	3901 / 1 / 218
Goodness-of-fit on F^2	1.007
Final R indices [I>2sigma(I)]	R1 = 0.0129, wR2 = 0.0352
R indices (all data)	R1 = 0.0147, wR2 = 0.0362
Absolute structure parameter	0.022(7)
Largest diff. peak and hole	0.927 and -0.264 e.Å^{-3}

Table 3.4: Selected bond lengths and angles for (^{tBu}PNP)OsH$_4$ (**5**)

Os(1)-N(1)	2.153(3)	Os(1)-P(1A)	2.2864(4)
Os(1)-P(1)	2.2865(4)	Os(1)-H(1)	1.62(2)
Os(1)-H(2)	1.846(19)	P(1)-C(5)	1.8592(17)
P(1)-C(10)	1.8953(16)	P(1)-C(6)	1.8985(15)
N(1)-C(2)	1.361(2)	N(1)-C(2A)	1.361(2)

N(1)-Os(1)-P(1A)	82.555(17)	N(1)-Os(1)-P(1)	82.556(17)
P(1A)-Os(1)-P(1)	165.11(3)	N(1)-Os(1)-H(1)	145.2(8)
P(1A)Os(1)-H(1)	97.2(6)	P(1)-Os(1)-H(1)	95.0(6)
N(1)-Os(1)-H(2)	80.2(9)	P(1A)-Os(1)-H(2)	92.0(6)
P(1)-Os(1)-H(2)	85.4(6)	H(1)-Os(1)-H(2)	65.0(12)
C(5)-P(1)-Os(1)	100.04(5)	C(10)-P(1)-Os(1)	120.65(5)
C(6)-P(1)-Os(1)	117.93(5)	C(2)-N(1)-Os(1)	120.47(13)
C(2A)-N(1)-Os(1)	120.47(13)		

The residual electron density map clearly shows the presence of the four hydrogen atoms bound to the osmium center (Figure 3.11). The clear presence of the four hydrogens in this map also allows the determination of H···H distances and some deeper insight into the structure. The H(1)···H(2) distance is 1.87 Å and the H(1)···H(1A) distance is 1.85 Å. These distances are consistent with the H···H distances of 1.84 - 1.91 Å found in Os(PMe$_2$Ph)$_3$H$_4$.[31] Thus **5** is a purely classical hydride complex, which is in agreement with DFT calculations made by Ziegler that found for Os(PPh$_3$)$_3$H$_4$ the hydride complex is more stable than the dihydrogen complex.[32]

This classical tetrahydride character is in contrast to (^{R}PCP)IrH$_4$ complexes which clearly show some dihydrogen character. Table 3.5 shows some (^{R}PCP)IrH$_4$ complexes with their corresponding H···H distances. From this table it is apparent that the

(PCP)IrH$_4$ complexes have one set of two purely terminal (classical)hydride ligands and one set (the "endo" hydrides) with dihydrogen character.

Figure 3.11: Residual Electron Density Map of (^{tBu}PNP)OsH$_4$ (5) showing the hydride signals
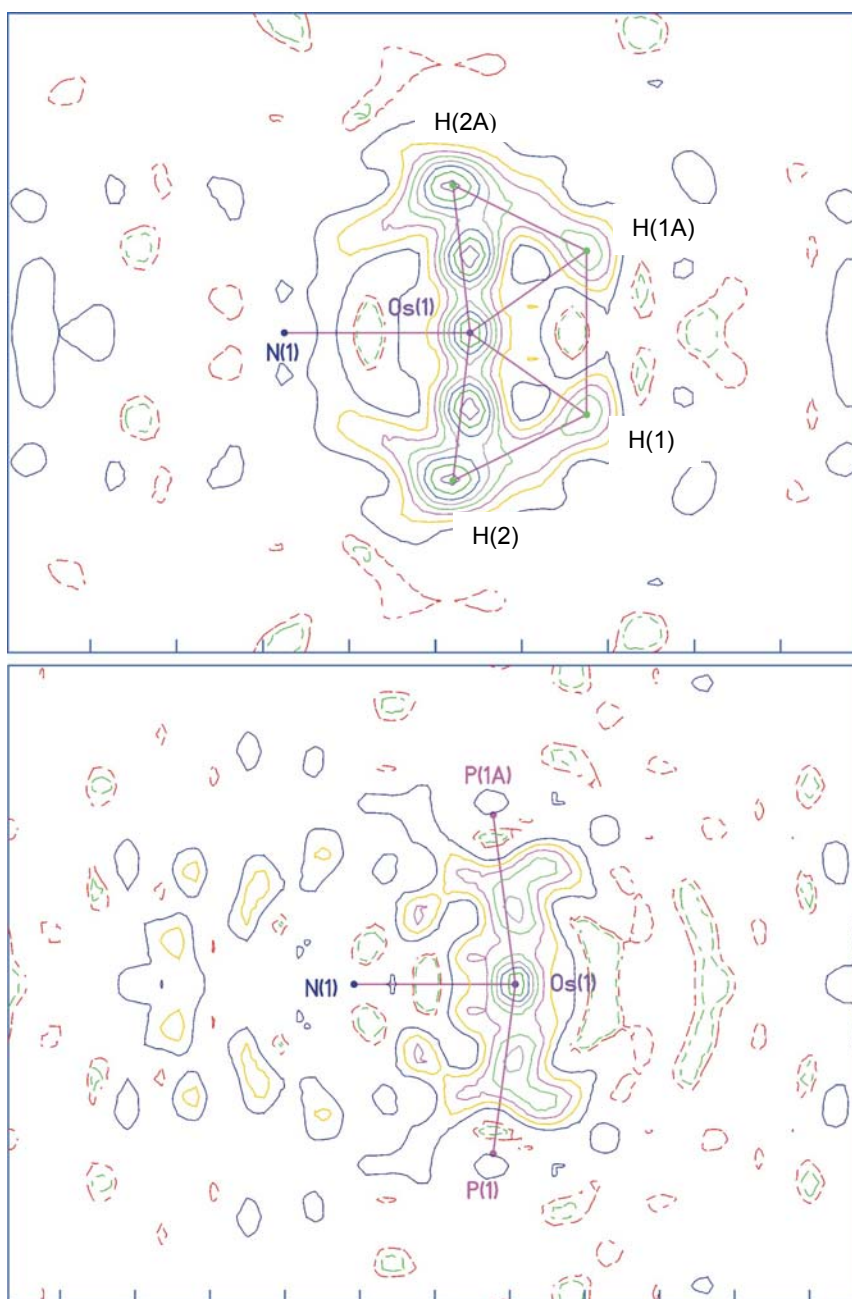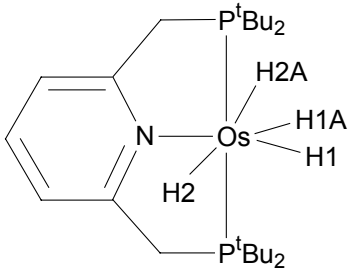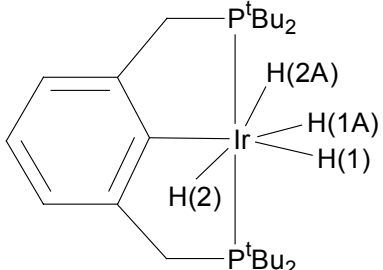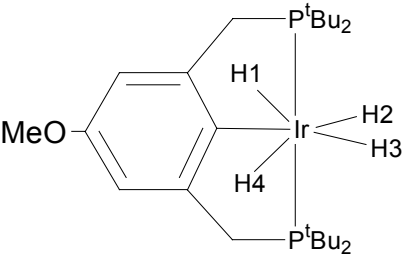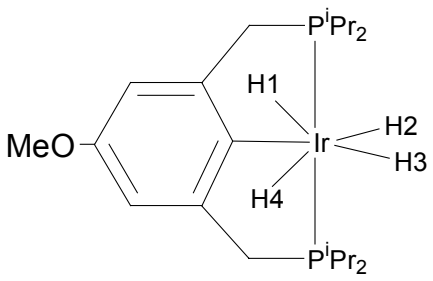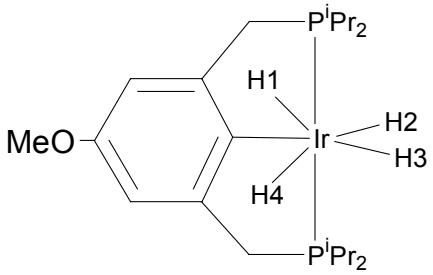
Table 3.5: Comparison of (^{tBu}PNP)OsH$_4$ (**5**) with (PCP)IrH$_4$ complexes

Pincer Complex	H···H Distance (Å)	M-H Distance (Å)	H-M-H Angles (º)
	H(1)···H(2) 1.87 H(2)···H(2A) 1.85	Os-H(1) 1.62 (2) Os-H(2) 1.846 (19)	H(1)-Os-H(2) 65.0 (12)
* 	H(1)···H(1A) 1.488 (16) H(1)···H(2) 1.92 (2) H(1A)···H(2A) 1.92 (2)	Ir-H(1) 1.55 (1) Ir-H(2) 1.70 (1)	H(1)-Ir-H(1A) 57.5 (9) H(1)-Ir-H(2) 72.4 (6) H(1)-Ir-H(2A) 129.9 (6) H(2)-Ir-H(2A) 157.7 (7)
	H(2)···H(3) 1.44	Ir-H(1) 1.531 (19) Ir-H(2) 1.587 (18) Ir-H(3) 1.559 (18) Ir-H(4) 1.534 (19)	H(2)-Ir-H(3) 55.8 (7) H(1)-Ir-H(2) 78 (3) H(1)-Ir-H(3) 134 (3)

*Data for (^{tBu}PCP)IrH$_4$ is from Neutron Diffraction

Table 3.5: Continued Comparison of (^{tBu}PNP)OsH$_4$ (**5**) with (PCP)IrH$_4$ Complexes

Pincer Complex	H···H Distance (Å)	M-H Distance (Å)	H-M-H Angles (°)
 Monoclinic	H(2)···H(3) 1.42 (5) H(3)···H(4) 1.70 (5) H(1)···H(2) 1.98 (6)	Ir-H(1) 1.57 (2) Ir-H(2) 1.59 (2) Ir-H(3) 1.58 (2) Ir-H(4) 1.60 (2)	H(2)-Ir-H(3) 53 (2) H(1)-Ir-H(3) 130 (2)
 Triclinic	H(2)···H(3) 1.30 (5) H(1)···H(2) 1.80 (5) H(3)···H(4) 1.99 (4)	Ir-H(1) 1.570 (17) Ir-H(2) 1.592 (18) Ir-H(3) 1.603 (18) Ir-H(4) 1.583 (18)	H(2)-Ir-H(3) 47.9 (18) H(4)-Ir-H(3) 117 (2)

3.3 Conclusions

(^{tBu}PNP)OsCl$_3$ was synthesized and fully characterized. Since this complex is paramagnetic the signals in the ^{1}H NMR were very broad and had unusual chemical shifts. The Os-Cl bond lengths in the crystal structure were consistent with the Os-Cl bond lengths of known osmium(III) chlorides.[25,26] The crystal structure of this complex also confirmed that there were three chlorides bound to the osmium center, which is in contrast to the structure for (^{Ph}PNP)OsCl$_2$ which was characterized only by elemental analysis and infrared data.[22]

(^{tBu}PNP)OsH$_4$ was also synthesized and fully characterized. The ^{1}H NMR spectrum shows that all four hydrides are exchanging at room temperature. In the low temperature ^{1}H NMR spectrum, they separate into two sets of inequivalent hydrides. X-ray diffraction measurements show that there are indeed two sets of two hydrides in the complex. One of these is a set that is trans to each other and has longer Os-H bond lengths than the second set. The residual electron density map shows that the H⋯H distances between all four hydrides are approximately equal (1.86 ± 0.01 Å). Thus (^{tBu}PNP)OsH$_4$ is a classical hydride species, in contrast to the related (^{R}PCP)IrH$_4$ complexes that clearly show some degree of dihydrogen character in the endo set of hydrides.

3.4 Experimental

All reactions were conducted under an argon atmosphere unless otherwise noted. All solvents were purchased as anhydrous from Aldrich and degassed with argon. NMR spectra were recorded on a Varian 300-MHz spectrometer. ^{1}H NMR signals are calibrated using the residual proton peaks of the deuterated solvent (they are referenced to TMS). ^{31}P NMR signals are calibrated with an external reference, a capillary with a solution of para-xylene-d_{10} and PMe$_3$ (δ –62.4 ppm). Elemental Analysis was performed by Robertson Microlit Laboratories. X-Ray diffraction by Dr. Thomas Emge (Rutgers) was obtained from an oil coated crystal mounted on a glass fiber. X-Ray intensity measurements were made using a Bruker-AXS Smart APEX CCD diffractometer with graphite monochromatized Mo Kα radiation at 100 K. ^{tBu}PNP was synthesized according to a method published by Milstein[33] with the modifications noted in Chapter 2.

(^{tBu}**PNP)OsCl$_3$ (4)**: Na$_2$OsCl$_6$·6H$_2$O (2.683 g, 5.985 mmol) and ^{tBu}PNP (2.367 g, 5.985 mmol) were placed in a three-neck 1-L flask with a magnetic stir bar. 2-methoxyethanol (420 mL) was added to the flask, resulting in a dark green solution that was refluxed for 36 hours during which time the solution turned dark orange/brown. The flask was cooled to room temperature and the solution was filtered through a course frit. The solution was concentrated by vacuum and placed in the freezer; **4** precipitated out as red/orange crystals. Yield = 1.883 g (45%). ^{1}H NMR (300 MHz, THF-d_8): δ -2.19 (broad, 2H, *m*-py), -4.10 (broad, 1H, *p*-py), -4.81(broad, 4H, CH$_2$), -5 to –8 (very broad, 36H, *tert*-butyl). Anal. Calcd. for OsP$_2$NCl$_3$C$_{23}$H$_{43}$: C, 39.91; H, 6.26; N, 2.02; Cl, 15.36. Found: C, 39.75; H, 6.47; N, 1.94; Cl, 15.50.

(^{tBu}PNP)OsH$_4$ (5): (^{tBu}PNP)OsCl$_3$ (1.000 g, 1.445 mmol) was placed in a 250-mL Schlenk flask with a magnetic stir bar. Tetrahydrofuran (140 mL) was added resulting in an orange/brown solution with some undissolved solid. Hydrogen was bubbled through the solution for 5 minutes before addition of 5.78 mL of 1 M NaEt$_3$BH THF solution (5.780 mmol). The solution immediately turned a dark green color but slowly (lightening of the dark green was seen within a couple of hours) turned back to red/orange with the formation of a light colored precipitate with hydrogen flowing over the flask overnight. The solvent was removed by vacuum and 25 mL of benzene was added resulting in a red solution. Pentane (100 mL) was added to the solution resulting in the precipitation of a dark red solid that was removed by filtration. The pentane was removed by flowing argon over the solution resulting in the formation of **5** as small yellow crystals. Yield = 0.358 g (42%). ^{1}H NMR (300 MHz, toluene-d_8, room temperature): δ 6.84 (t, J = 8, 1H, *p*-py), 6.58 (d, J = 7, 2H, *m*-py), 3.33 (t, J = 3, 4H, CH$_2$), 1.32 (t, J = 6, 36H, *tert*-butyl), -8.66 (broad, 3H, Os-H). ^{1}H NMR (300 MHz, toluene-d_8, -80 ºC): δ 6.77 (t, J = 8, 1H, *p*-py), 6.37 (d, J = 8, 2H, *m*-py), 3.17 (4H, CH$_2$), 1.38 (36H, *tert*-butyl), -5.04 (broad, 2H, Os-H), -11.97 (broad, 2H, Os-H). ^{1}H NMR (300 MHz, toluene-d_8, 60 ºC): δ 6.97 (t, J = 7, 1H, *p*-py), 6.64 (d, J = 7, 2H, *m*-py), 3.38 (4H, CH$_2$), 1.32 (t, J = 6, 36H, *tert*-butyl), -8.68 (t, J = 12, 4H, Os-H). ^{31}P{^{1}H}NMR (121 MHz, p-xylene-d_{10}, room temperature): δ 76.86. ^{31}P NMR (121 MHz, p-xylene-d_{10}, 60 ºC): δ 77.21 (quin, J_{P-H} = 10). Anal. Calcd. for OsP$_2$NCl$_3$C$_{23}$H$_{47}$: C, 46.84; H, 8.03; N, 2.37. Found: C, 46.24; H, 7.67; N, 2.31.

3.5 References

(1)   Parent, J. S.; McManus, N. T.; Rempel, G. L. *Indust. & Eng. Chem. Res.* **1998**, *37*, 4253-4261.

(2)   Odebunmi, E. O. *Bull. Chem. Soc. Ethiopia* **1993**, *7*, 43-52.

(3)   Farnetti, E.; Graziani, M.; Mezzetti, A.; Del Zotto, A. *J. Molec. Cat.* **1992**, *73*, 147-155.

(4)   Johnson, T. J.; Albinati, A.; Koetzle, T., F.; Ricci, J.; Eisenstein, O.; Huffman, J. C.; Caulton, K. G. *Inorg. Chem.* **1994**, *33*, 4966-4976.

(5)   Kobayashi, S.; Sugiura, M. *Adv. Synth. & Cat.* **2006**, *348*, 1496-1504.

(6)   Kockritz, A.; Bartoszek, M.; Dobler, C.; Beller, M.; Magerlein, W.; Militzer, H.-C. *J. Molec. Cat. A: Chem.* **2004**, *218*, 55-66.

(7)   Norrby, P.-O.; Kolb, H. C.; Sharpless, B. K. *J. Am. Chem. Soc.* **1994**, *116*, 8470-8478.

(8)   Akherem, I. S.; Chistovalova, N. M.; Polubentseva, M. F.; Pikersky, I. E.; Dubinsky, Y. G.; Vol'pin, M. E. *Cat. Let.* **1993**, *19*, 361-367.

(9)   Yang, J. W.; Han, H.; Roh, E. J.; Lee, S.; Song, C. E. *Org. Let.* **2002**, *4*, 4685-4688.

(10)   Choudary, B. M.; Chowdari, N. S.; Kantam, M. L.; Raghayan, K. V. *J. Am. Chem. Soc.* **2001**, *123*, 9220-9221.

(11)   Champness, N. R.; Levason, W.; Mould, R. A. S.; Pletcher, D.; Webster, M. *J. Chem. Soc. Dalt. Trans. Inorg. Chem.* **1991**, *10*, 2777-2783.

(12)   Champness, N. R.; Levason, W.; Pletcher, D.; Spicer, M. D.; Webster, M. *J. Chem. Soc. Dalt. Trans. Inorg. Chem.* **1992**, *14*, 2201-2207.

(13)   Akasaka, T.; Mutai, T.; Otsuki, J.; Araki, K. *Dalton Trans.* **2003**, *8*, 1537-1544.

(14)   Hjelm, J.; Handel, R. W.; Hagfeldt, A.; Constable, E. C.; Housecroft, C. E.; Forster, R. J. *J. Phys. Chem. B* **2003**, *107*, 10431-10439.

(15)   Bassani, D. M.; Lehn, J.-M.; Serroni, S.; Puntoriero, F.; Campagna, S. *Chem. Eur. J.* **2003**, *9*, 5936-5946.

(16)   Gusev, D. G.; Dolgushin, F. M.; Antipin, M. Y. *Organometallics* **2001**, *20*, 1001-1007.

(17)   Gusev, D. G.; Maxwell, T.; Dolgushin, F. M.; Lyssenko, M.; Lough, A. J. *Organometallics* **2002**, *21*, 1095-1100.

(18)   Gusev, D. G.; Fontaine, F.-G.; Lough, A. J.; Zargarian, D. *Angew. Chem. Int. Ed.* **2003**, *42*, 216-219.

(19)   Wen, T. B.; Cheung, Y. K.; Yao, J.; Wong, W.-T.; Zhou, Z. Y.; Jia, G. *Organometallics* **2000**, *19*, 3803-3809.

(20)   Wen, T. B.; Zhou, Z. Y.; Jia, G. *Organometallics* **2003**, *22*, 4947-4951.

(21)   Gauvin, R. M.; Rozenberg, H.; Shimon, L. J. W.; Milstein, D. *Organometallics* **2001**, *20*, 1719-1724.

(22)   Li, Z.; Che, C.; Poon, C. *Wuhan Univ. J. Nat. Sci.* **1996**, *1*, 230-234.

(23)   Liu, S. H.; Lo, S. T.; Wen, T. B.; Zhou, Z. Y.; Lau, C. P.; Jia, G. *Organometallics* **2001**, *20*, 667-672.

(24)   Jia, G.; Lee, H. M.; Williams, I. D.; Lau, C. P.; Chen, Y. *Organometallics* **1997**, *16*, 3941-3949.

(25)   Demadis, K. D.; El-Samanody, E.-S.; Meyer, T. J.; White, P. S. *Polyhedron* **1999**, *18*, 1587-1594.

(26)   Bright, D.; Ibers, J. A. *Inorg. Chem.* **1969**, *8*, 1078-1083.

(27)   Gupta, M.; Hagen, C.; Kaska, W. C.; Cramer, R. E.; Jensen, C. M. *J. Am. Chem. Soc.* **1997**, *119*, 840-841.

(28)   Blough, B. E.; Carroll, F. I. *Tet. Let.* **1993**, *34*, 7239-7242.

(29)   Milstein, D. Personal Communication

(30)   Gupta, M.; Hagen, C.; Flesher, R. J.; Kaska, W. C.; Jensen, C. M. *Chem. Commun.* **1996**, 2083-2084.

(31)   Hart, D. W.; Bau, R.; Koetzle, T. F. *J. Am. Chem. Soc.* **1977**, 7557-7564.

(32)   Li, J.; Dickson, R. M.; Ziegler, T. *J. Am. Chem. Soc.* **1995**, *117*, 11482-11487.

(33)   Hermann, D.; Gandelman, M.; Rozenberg, H.; Shimon, L. J. W.; Milstein, D. *Organometallics* **2002**, *21*, 812-818.

Chapter 4

Reactions Using (^{tBu}PNP)OsH$_4$

Abstract

(^{tBu}PNP)OsH$_4$ was screened for reactivity with two potential hydrogen acceptors, then tested as a catalyst in dehydrogenation and phenylacetylene dimerization reactions. Both reactions were stoichiometic in osmium. The dimerization reaction did have a strong preference for the formation of the Z isomer with the ratio between the Z and E isomer being 15:1. The complex was also examined for C-H addition ability, in particular the ability to form metalloaromatic complexes. These reactions were unsuccessful and no C-H activation products were observed. The most likely reason for the lower activity of (^{tBu}PNP)OsH$_4$ compared to (^{tBu}PCP)IrH$_4$ is that the Os(IV)-H bonds are stronger than Ir(V)-H bonds.

4.1 Introduction

C-H bond activation has vast applications in both synthetic chemistry and petroleum research. In the synthetic arena, it is possible to imagine C-H activation being followed by C-C coupling to give larger organic products or dehydrogenation to give alkenes that are easily functionalized. Petroleum consists mostly of alkanes; thus the ability to transform alkanes into the chemically much more useful alkenes, via dehydrogenation, is potentially very valuable. As such, the search for catalysts for such reactions has been extensive.

In 1965 Chatt reported the first example of C-H activation by a transition metal complex.[1] The complex was ruthenium(0) based and activated a C-H bond of either the ligand to give a ruthenium(II) dimer or, perhaps more excitingly, the C-H bond of a molecule of naphthalene to form a ruthenium(II) aryl hydride complex as shown in Scheme 4.1.[1] Since that time, other early and late transition metal complexes have been shown to activate C-H bonds of a variety of substrates.[2] Pincer complexes have been a particularly important area of focus.

Scheme 4.1: First example of transition metal C-H activation[1]
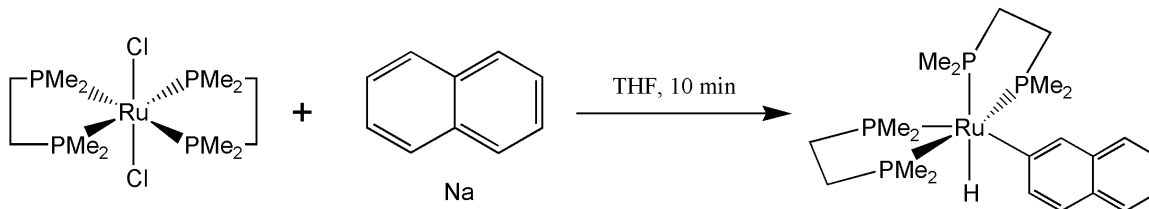
In particular, (^RPCP)Ir complexes have been studied extensively for their ability to catalyze reactions of C-H bond activation. Recently work has been published that is based on Murai chemistry, where (^RPCP)Ir complexes have produced metalloaromatic products from C-H activation of a reactant with an electron donor group, such as nitrobenzene (Scheme 4.2).[3] (^RPCP)Ir pincer complexes have also been used in C-C coupling. In particular, they have been shown to dimerize acetylenes resulting in various enyne complexes.[4] These dimerization reactions usually give a mixture of the E and Z conformers with the E being the preferred product.[4] This is the trend that is echoed in the literature, where the E-enyne is the preferred isomer.[4-13]

The most substantial amount of work with (^RPCP)Ir complexes focuses on their ability to dehydrogenate alkanes to form α-olefins (Scheme 4.3).[14-18] The first step of this mechanism is the C-H activation of an alkane to form an alkyl hydride complex (Figure 4.1).[16] This step is followed by β-hydride elimination from the alkyl chain to produce the desired α-olefin.[16]

Scheme 4.2: Formation of a metalloaromatic products by C-H activation[3]

A = norbornene, TBE
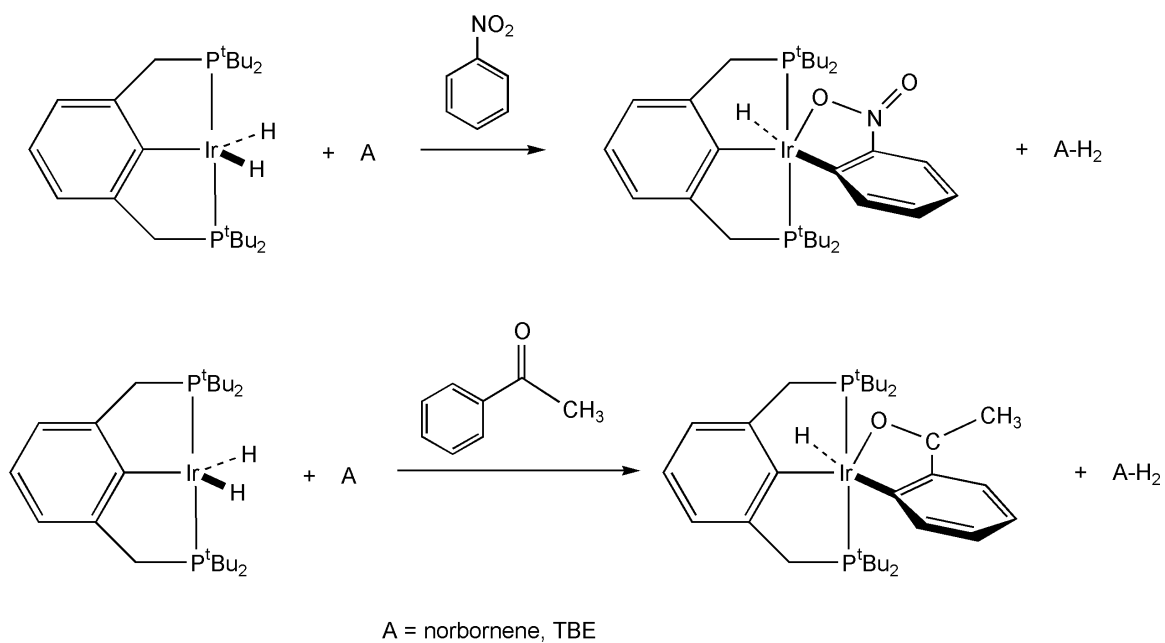
Scheme 4.3: General dehydrogenation reaction
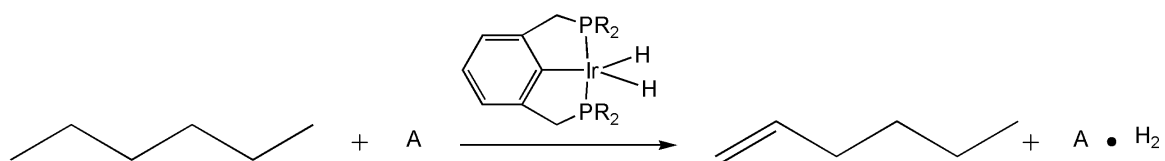
Figure 4.1: General mechanism for the dehydrogenation of alkanes[16]

(n-C$_6$H$_{13}$)

n-octene

β-hydride elimination

(^{iPr}PCP)IrH$_2$

sacrificial acceptor

^{t}Bu

Acceptor hydrogenation

(n-C$_6$H$_{13}$)

H$_2$C—H$_2$C

Ir(PCP)

H

$[$ (PCP)Ir ... A, H, H $]$

Oxidative Addition

Reductive elimination

(n-C$_6$H$_{12}$)

CH$_2$—CH$_3$

n-octane

"(^{iPr}PCP)Ir"

(^{iPr}PCP)Ir

^{t}Bu

^{t}Bu

Hydrogenated acceptor
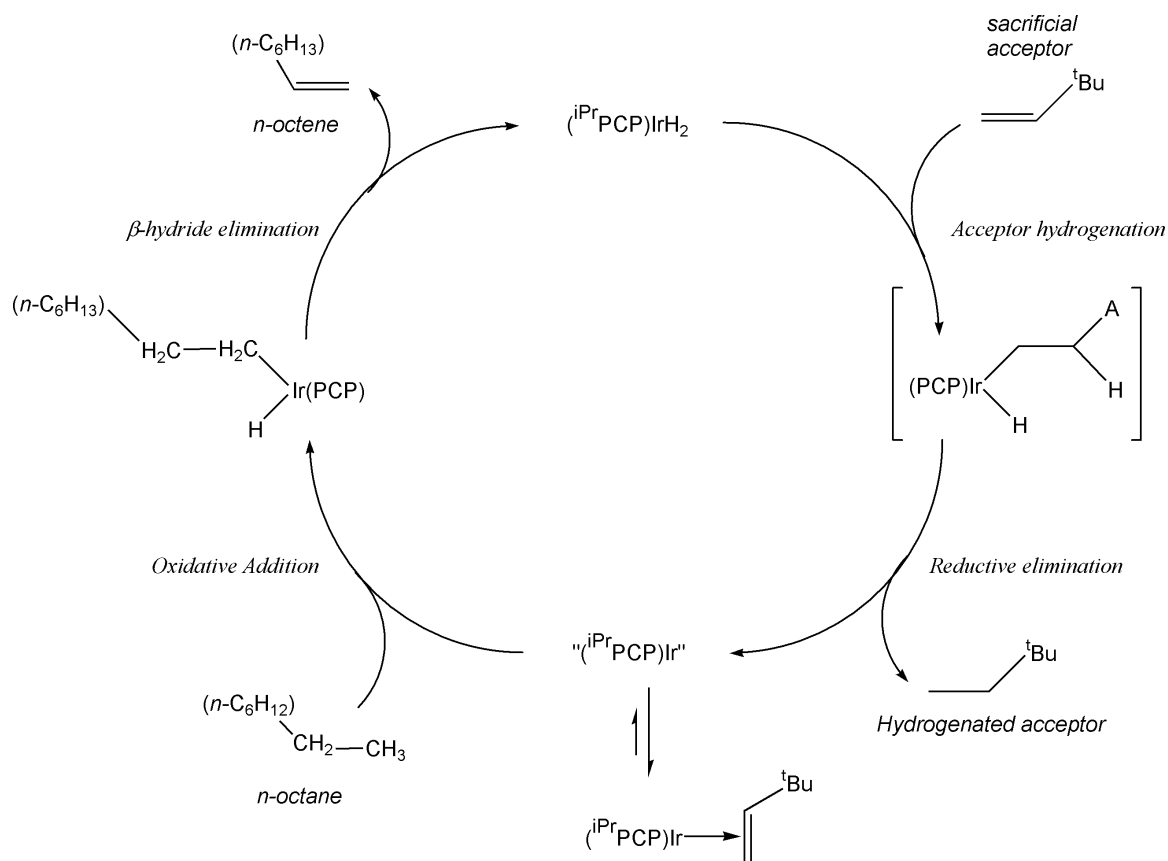
There are two classes of dehydrogenations: acceptorless dehydrogenation and transfer dehydrogenation. In acceptorless dehydrogenation reactions, H$_2$(g) is released and removed from the system. Transfer dehydrogenation requires the use of a sacrificial acceptor olefin that is hydrogenated during the reaction. For research purposes, two common choices for a sacrificial acceptor are norbornene (NBE) and *tert*-butylethylene (TBE), although in reality simpler alkenes may be used.

Chapter 2 presented the synthesis and characterization of (^{tBu}PNP)OsH$_4$. This complex is isoelectronic to (^{tBu}PCP)IrH$_4$, which has been shown to act as a catalyst

precursor for C-H activation,[3,19] alkane dehydrogenation[14-18] and C-C coupling reactions leading to enyne dimers of phenylacetylene.[4] This chapter will present experiments designed to test the reactivity of the isoelectronic complex (^{tBu}PNP)OsH$_4$ in the areas of C-H activation, dehydrogenation, and C-C coupling. The first section presents experiments that were performed to find a suitable acceptor to use with (^{tBu}PNP)OsH$_4$. The second section explores the possibility of hydrides being removed from the complex in the form of H/D exchange between (^{tBu}PNP)OsH$_4$ and solvent. The third section presents attempted C-H activation reactions and the final section examines the dimerization of phenyl acetylene.

4.2 Results and Discussion

4.2.1 The Search for a Sacrificial Acceptor

As evidenced by the classical hydride structure of (^{tBu}PNP)OsH$_4$, the Os(IV)-H bonds are most likely stronger than the Ir(V)-H bonds of (^{tBu}PCP)IrH$_4$. This is reflected in the ease that (^{tBu}PCP)IrH$_4$ will loose H$_2$ to give (^{tBu}PCP)IrH$_2$; this reaction will occur in the solid state at room temperature without the addition of an acceptor. (^{tBu}PNP)OsH$_4$, by contrast, has shown no signs of spontaneously losing H$_2$(g) to form (^{tBu}PNP)OsH$_2$. Since the Os-H bonds are strong, the use of an acceptor would be needed to remove hydrides from the osmium to create vacant sites for C-H activation to occur. To test the reactivity and stability of (^{tBu}PNP)OsH$_4$ with possible acceptors, screening reactions were run that contained only (^{tBu}PNP)OsH$_4$ and acceptor. The reactions were monitored by ^{1}H and ^{31}P NMR spectroscopy to look for catalyst decomposition or reaction with acceptor.

In the first reaction, $(^{tBu}PNP)OsH_4$ and *tert*-butylethylene (TBE) were placed in an NMR tube with para-xylene-d_{10} that was heated at 105 ºC (Scheme 4.4). The second reaction was similar but with norbornene (NBE) used instead of TBE (Scheme 4.4). After 1 hour, the NMR tube with TBE showed formation of a dark precipitate that was likely due to the formation of osmium metal. The NMR tube with NBE did not show formation of the dark precipitate until ca. 32 hours. Due to the slower decomposition of the $(^{tBu}PNP)OsH_4$ with norbornene, norbornene was chosen as the sacrificial acceptor for the next set of reactions.

Scheme 4.4: Reactions to screen potential acceptors
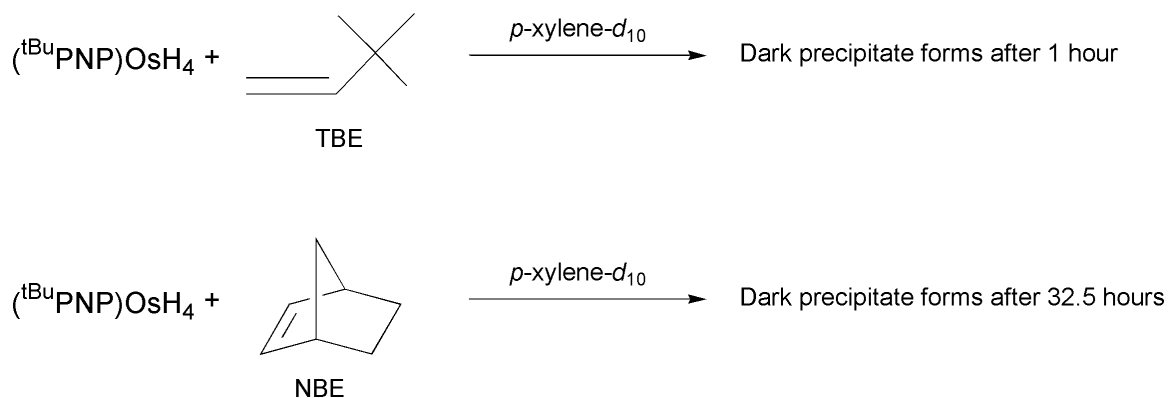
4.2.2 H/D Exchange Reactions between (^{tBu}PNP)OsH$_4$ and solvent

Since (^{tBu}PNP)OsH$_4$ is an 18-electron species, hydrides must presumably be removed before any potential dehydrogenation or C-C coupling reactions will occur. To test if hydride removal were possible, H/D exchange reactions were run with (^{tBu}PNP)OsH$_4$ and a deuterated solvent. The first experiment that was run was a control experiment, where (^{tBu}PNP)OsH$_4$ was placed in para-xylene and heated for 22 hrs while monitoring by NMR spectroscopy. An external capillary of PMe$_3$ was used as a reference. As shown in Figure 4.2, the graph showing the ^{1}H NMR integration values of (^{tBu}PNP)OsH$_4$ remained approximately constant, although with a small amount of decay over time most likely due to catalyst decomposition. Due to the intensity of the para-xylene signals, the protons in the meta and para positions of the PNP ring could not be found.

Figure 4.2: a. Graph of the ^{1}H NMR integration values of para-xylene when (tBuPNP)OsH4 is heated at 85 °C for 15 hours in para-xylene b. Graph of the ^{1}H NMR integration values of the tert-butyl and hydride signals of (tBuPNP)OsH4 when heated at 85 °C for 15 hours in para-xylene. Both are referenced against an external capillary of PMe3

a.
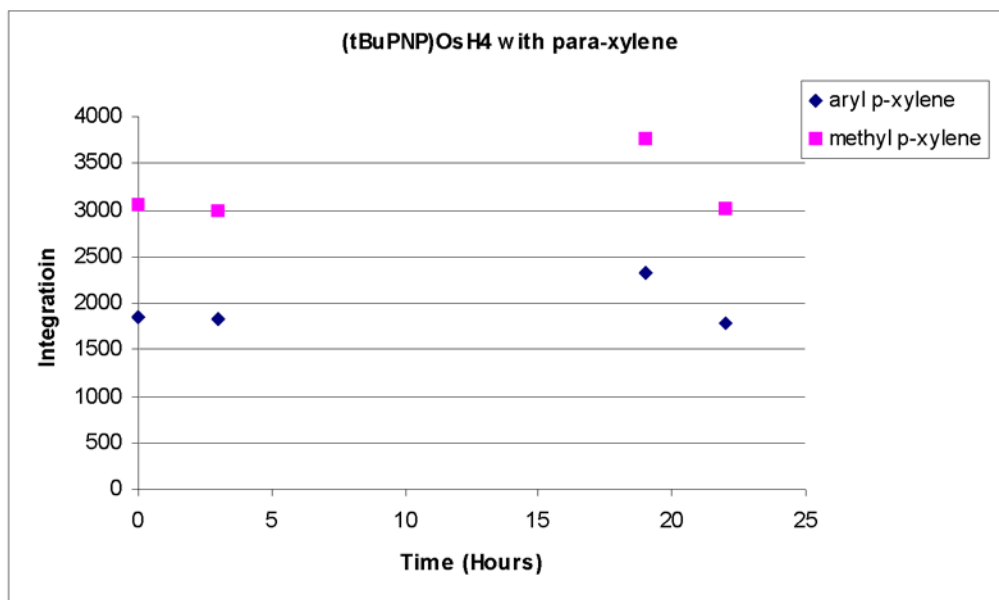
$(^{tBu}PNP)OsH_4 = 24$ mM

b.
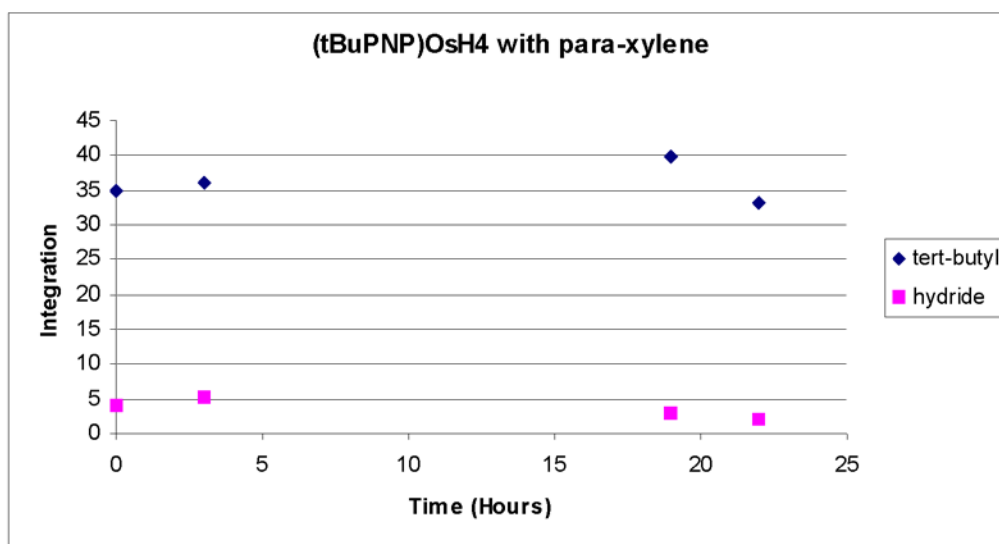
$(^{tBu}PNP)OsH_4 = 24$ mM

The next two reactions involved placing (^{tBu}PNP)OsH$_4$ in para-xylene-d_{10} and heating the reaction; one reaction was done in the presence of 0.5 equivalents of NBE and the other contained no NBE. Little clear evidence of either decomposition or H/D exchange was observed in the absence of NBE.

Figure 4.3: Graph of the ^{1}H NMR integration of para-xylene-d_{10} and (^{tBu}PNP)OsH$_4$ when (^{tBu}PNP)OsH$_4$ is heated in para-xylene-d_{10} at 125 °C
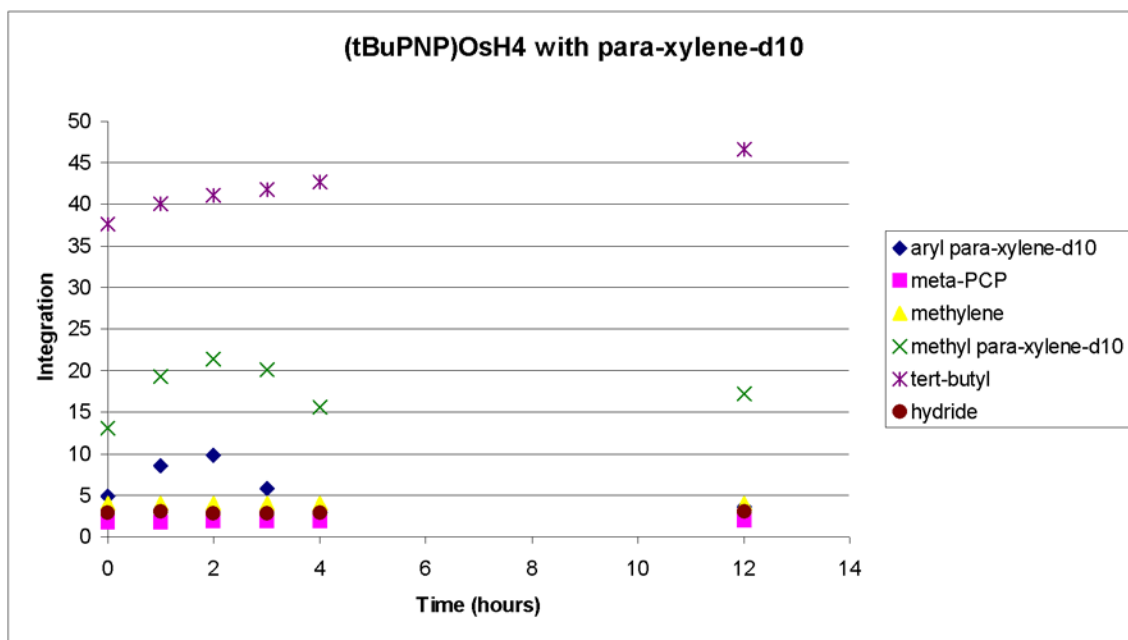
(^{tBu}PNP)OsH$_4$ = 24 mM

The reaction in which 0.5 equivalents of NBE was added to (^{tBu}PNP)OsH$_4$ and para-xylene-d_{10} showed much more reactivity (Figure 4.4). The first trend is a decrease in the *tert*-butyl integration as deuterium atoms from the solvent replace the hydrogens in the *tert*-butyl groups. Concurrent with this drop is an increase in the methyl groups of the para-xylene-d_{10} solvent, as they exchange with hydrogens in (^{tBu}PNP)OsH$_4$.

Interestingly, in this graph there is also a decrease in the integration values of the meta proton on the PNP and the hydride signals, meaning that these protons were also exchanging with solvent.

Figure 4.4:   *Graph of the ^1H NMR integration of para-xylene-d$_{10}$ and (^{tBu}PNP)OsH$_4$ when (^{tBu}PNP)OsH$_4$ is reacted with NBE in p-xylene-d$_{10}$*
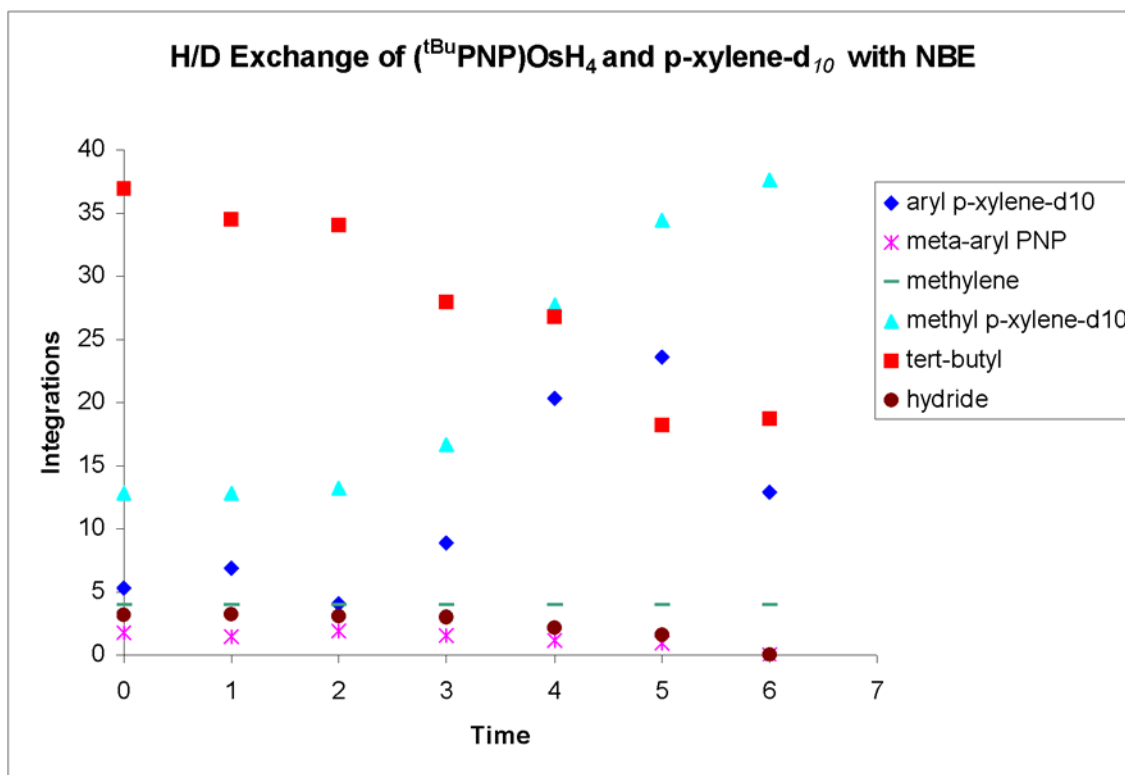
(^{tBu}PNP)OsH$_4$ = 24mM, NBE = 12 mM

In preparation for a competition experiment, a control reaction with (^{tBu}PNP)OsH$_4$ and C$_6$D$_6$ was run. As expected, based on the previous results, after 28 hours there was a significant decrease in the integration values of *tert*-butyl and para hydrogen on the PNP ring signals. The PNP meta hydrogens and the hydride signals did not show a significant decrease until 148 hours of heating.

The last set of experiments in this series was a competition experiment with C_6H_6 and toluene-d_8. Again two sets of experiments were done. One used just (^{tBu}PNP)OsH$_4$, C_6H_6 and toluene-d_8 and the other used (^{tBu}PNP)OsH$_4$, C_6H_6, toluene-d_8 and 0.5 equivalents of NBE. In these experiments, the aryl signals of the PNP ligand were not found due to overlap with the C_6H_6 signal. In the case without NBE (Figure 4.5), the methylene signal was held constant and the remaining signals integrated against it. The toluene-d_8 signal showed a slight increase in integration value. In the second case, with NBE added (Figure 4.6), the integrations were made against a PMe$_3$ standard. In this reaction, similar to the case where NBE was added to the para-xylene-d_{10} reaction, there is a significant decrease in the C_6H_6 and *tert*-butyl signals while the toluene-d_8 shows a significant increase in integration value. The methylene and meta PNP hydrogen signals also showed decreases in their integration values, while the hydride signal went to zero. This result shows that scrambling is occurring in the whole molecule.

Figure 4.5: Graph of the ^1H NMR integration of C_6H_6 in the competition experiment between C_6H_6 and toluene-d_8 using (^{tBu}PNP)OsH$_4$ as catalyst   a.   Showing the C_6H_6 integration b. Showing the integration of the toluene-d_8 and (^{tBu}PNP)OsH$_4$ protons

a.

b.
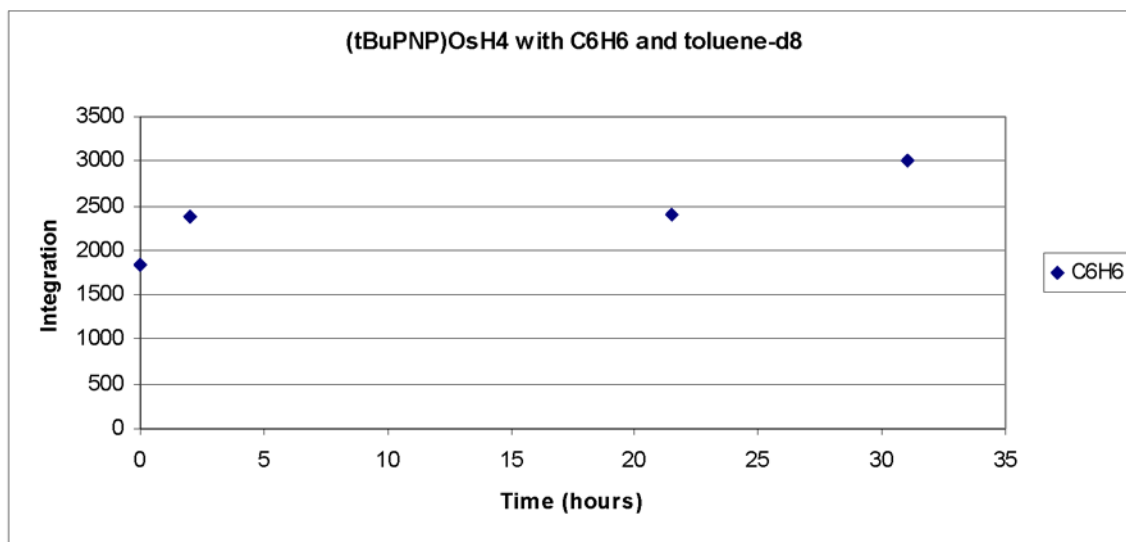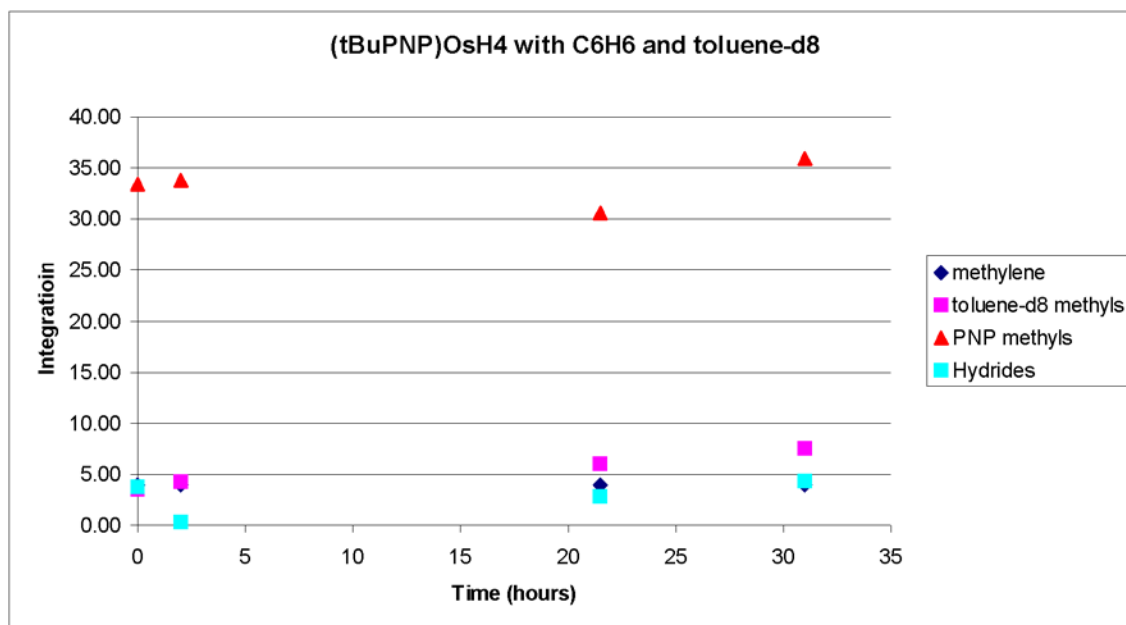
(^{tBu}PNP)OsH$_4$ = 24 mM, toluene-d_8 = 5M, C_6H_6 = 5M

Figure 4.6: ^1H *NMR integration of* $(^{tBu}PNP)OsH_4$ *with NBE,* C_6H_6 *and toluene-d_8 a. Showing the integration of C_6H_6 and toluene-d_8 b.   Showing the integration of $(^{tBu}PNP)OsH_4$ signals*

a.
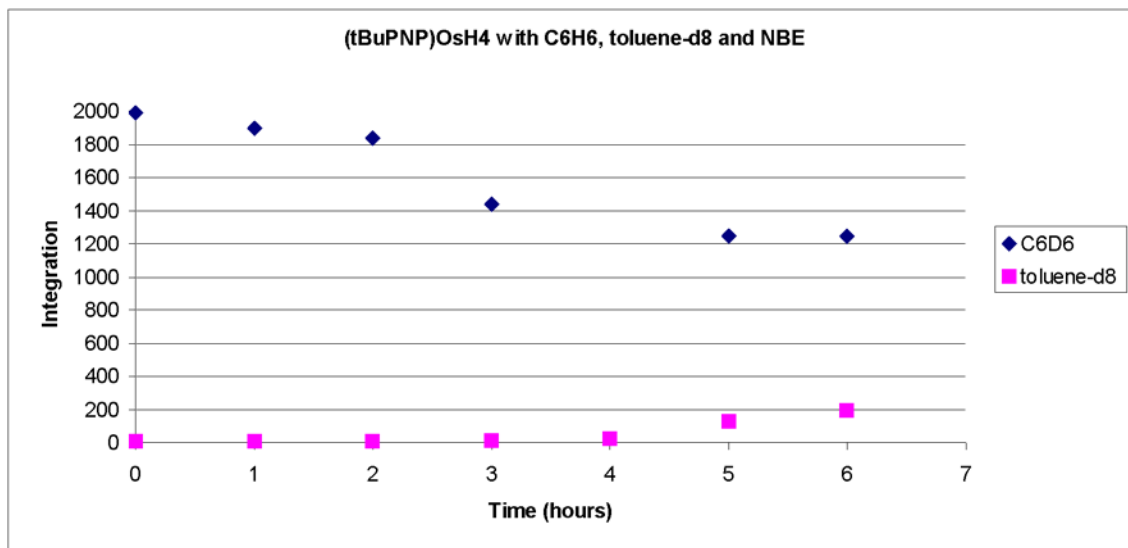
b.
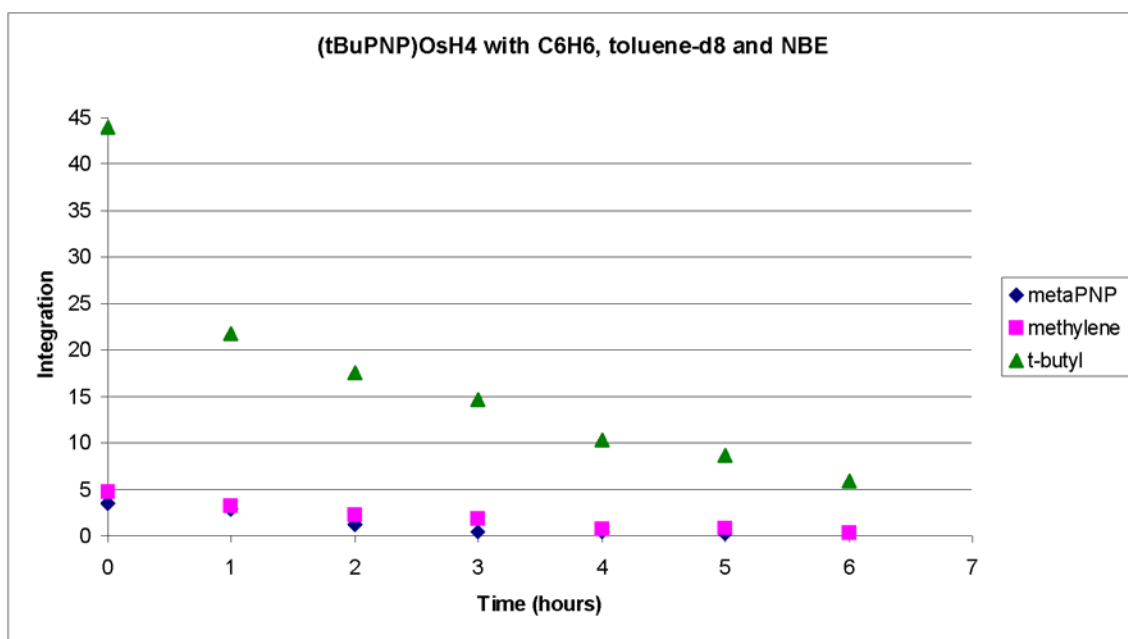
$(^{tBu}PNP)OsH_4 = 24$ mM, $C_6H_6 = 5$ M, toluene-$d_8 = 5$ M, NBE $= 12$ mM

In both reactions where NBE was added, the results obtained were much more consistent with the expected results. Since NBE is added to remove some of the hydrides from (^{tBu}PNP)OsH$_4$, this suggests that a certain amount of vacant coordination sites need to be produced before C-H activation will take place. This also suggests that in order for any C-H activation reactions to occur, the use of a sacrificial acceptor will be needed.

4.2.3 Attempted Dehydrogenation Reactions

With a suitable acceptor chosen, the dehydrogenation of alkanes was looked at. Dehydrogenating alkanes to alkenes has vast potential in chemical reactions. In organic chemistry, the C=C bond is easily functionalized into a variety of groups. In petroleum research, alkenes are needed to transform otherwise useless short chain alkanes into more useful longer alkyl chains. The basic test molecule used for initial dehydrogenation studies is cyclooctane as the cyclic complex avoids isomerization reactions.[17,18,20,21]

This reaction was done by placing (^{tBu}PNP)OsH$_4$ in neat cyclooctane and monitoring the reaction by ^{1}H and ^{31}P NMR spectroscopy. After heating at 120 ºC for 4 hours a new signal appeared in the olefin region of the ^{1}H NMR spectrum. After 8 hours at 120 ºC the solution turned to a dark brown with a dark solid precipitating out and after 24 hours of heating at 120 ºC, there were no signals in the ^{31}P NMR and no sign of the (^{tBu}PNP)OsH$_4$ signals in the ^{1}H NMR. The small amount of cyclooctene that formed was found by integration to be in a 1:1 ratio with the amount of (^{tBu}PNP)OsH$_4$ used, meaning that the reaction was stoichiometric.

Since the solid that formed was most likely coming from the reaction of (^{tBu}PNP)OsH$_4$, a second attempt was made using 1-octene as the acceptor. In this case

the reaction was heated at 90 °C over a period of 8 hours. After only 3 hours of heating, a color change to red/brown was observed along with the appearance of a new signal in the olefin region of the ^{1}H NMR spectrum. After the full 9 hours, the ^{31}P NMR spectrum showed the presence of (^{tBu}PNP)OsH$_4$ (48 %) along with the appearance of a new signal at 55.42 ppm (52 %), that was most likely a π-bound olefin complex. GC analysis of the organic portion of the sample showed that the new olefin signal was due to isomerization of the 1-octene acceptor to *cis*- and *trans*- 2-octene and that very little cyclooctene had actually formed in the reaction.

The next several experiments were designed to explore the possibility of C-H activation occurring in stoichiometric amounts. Murai has shown that Ru(0) catalysts selectively insert olefins into ortho C-H bonds.[22] Milstein has shown that cationic (PNP)Ir complexes also selectively activate the ortho C-H bond of halobenzene complexes[23] (Figure 4.7) and previous work from our group has shown that (^{tBu}PCP)IrH$_2$ selectively adds aryl C-H bonds to give metalloaromatic complexes of iridium.[3]

Figure 4.7: Example of Ortho C-H bond activation by a cationic (^{R}PNP)Ir complex[23]

X = Cl, Br
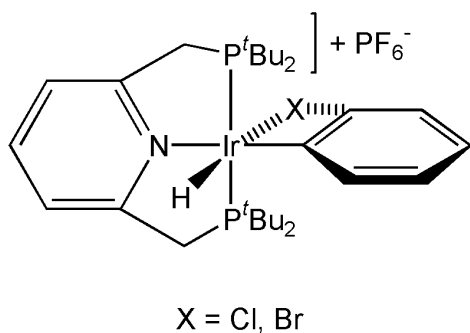
Based on the previous literature, (^{tBu}PNP)OsH$_4$ was tested for the possibility of selective ortho C-H bond activation and the possible formation of metalloaromatic complexes. In the first reaction, (^{tBu}PNP)OsH$_4$ was placed with NBE in nitrobenzene, similar to a previously published reaction.[3] The reaction was heated to 60 ºC to slow the decomposition of (^{tBu}PNP)OsH$_4$ that occurs in the presence of NBE, and the reaction was monitored over a period of 3 days. At the end of 3 days the solution had turned dark brown and the ^{1}H NMR spectrum showed only starting material, while the ^{31}P NMR spectrum showed (^{tBu}PNP)OsH$_4$ and the presence of a new signal at δ 56.70 ppm. Although this substance was not isolated, the chemical shift is consistent with that of an olefin bound metal complex.

The next reaction was done in a similar fashion with (^{tBu}PNP)OsH$_4$, NBE and 3-pentanone. The use of 3-pentanone eliminates the possibility for selective ortho C-H activation, however the possibility of forming a metalloaromatic complex is still viable. This reaction was done in two parts. In the first part of the experiment the NMR tube was heated in a GC oven at 110 ºC for 10 days. After 10 days, the temperature was increased to 120 ºC for 36 hours. Throughout the experiment, the reaction was monitored by ^{1}H and ^{31}P NMR spectroscopy. After 6 hours of heating at 110 ºC, a color change from yellow to red was observed. (^{tBu}PNP)OsH$_4$ was still present in the solution as evidenced by the broad hydride signal at δ –8.97 in the ^{1}H NMR spectrum. The ^{31}P NMR spectrum showed the presence of (^{tBu}PNP)OsH$_4$ as a singlet at δ 76.55 ppm, however normalized integration showed that the signal was only about 49 % of the spectrum. The rest of the ^{31}P NMR spectrum consisted of a doublet at δ 64.08 ppm (36 %) and a singlet at δ 54.27 ppm (15 %). These signals remained for the course of heating

at 110 ºC with the ratios after 10 days being 35 % (^{tBu}PNP)OsH$_4$, 19 % (δ 64.08 ppm),

and 40 % (δ 54.27 ppm). The signals at δ 64.08 ppm and δ 54.27 ppm are most likely

due to π–bound olefin complexes. Further heating at 120 ºC caused a decomposition of

the complex with all signals decreasing drastically in the ^{31}P NMR spectrum along with

the appearance of multiple new signals.

4.2.4 Dimerization of Phenylacetylene

Research by Jia's group has shown that (^{R}PCP)Os complexes can couple

phenylacetylene to give a variety of products, with the most interesting to this research

being the enyne bound osmium complex.[13,24,25] In general, complexes that dimerize

phenylacetylene favored the formation of the E-enyne;[4-8,10,12] however there are some

ruthenium[26] and lanthanide based[9] complexes that favor formation of the Z-enyne. The Z

isomer can also be formed by a Suzuki-Sonogashira coupling that uses copper and

palladium/copper catalysts.[11] (^{tBu}PCP)IrH$_4$ has also been shown to dimerize

phenylacetylene. The catalytic reaction shows that the E-enyne product is slightly

favored over the Z-enyne product with the ratio between the two being 3:1.[4] Since

(^{tBu}PCP)IrH$_4$ can dimerize phenylacetylene, the same reaction was attempted using

(^{tBu}PNP)OsH$_4$. In this reaction there is no need to add an acceptor as excess

phenylacetylene will act as an acceptor. The first step of the mechanism also involves a

C-H activation to coordinate the phenylacetylene to the osmium center.

The reaction was performed by placing (^{tBu}PNP)OsH$_4$ in an NMR tube with 10

equivalents of phenylacetylene. The NMR tube was then heated in an oil bath at 85 ºC,

and the reaction was monitored by ^{1}H and ^{31}P NMR spectroscopy over 45 hours. After

only 3 hours of heating, a color change from yellow to orange is observed, and the appearance of signals due to the E- and Z- enynes are seen in the ^{1}H NMR spectrum with the Z-enyne being only slightly favored over the E-enyne. The ^{31}P NMR spectrum shows that all of the (^{tBu}PNP)OsH$_4$ has been converted into a new complex with a signal at δ 37.67 ppm after 6 hours of heating. Although this new complex was not isolated, a proposed structure would be that of the bound di-yne, before hydrogenation of one triple bond. After the full 45 hours, the solution has an orange/red color and the Z-enyne is the clearly favored isomer with the ratio between the Z- and E- enynes being 15:1 (Figure 4.8).

Figure 4.8: ^{1}H NMR spectrum showing the cis- and trans- enyne formation
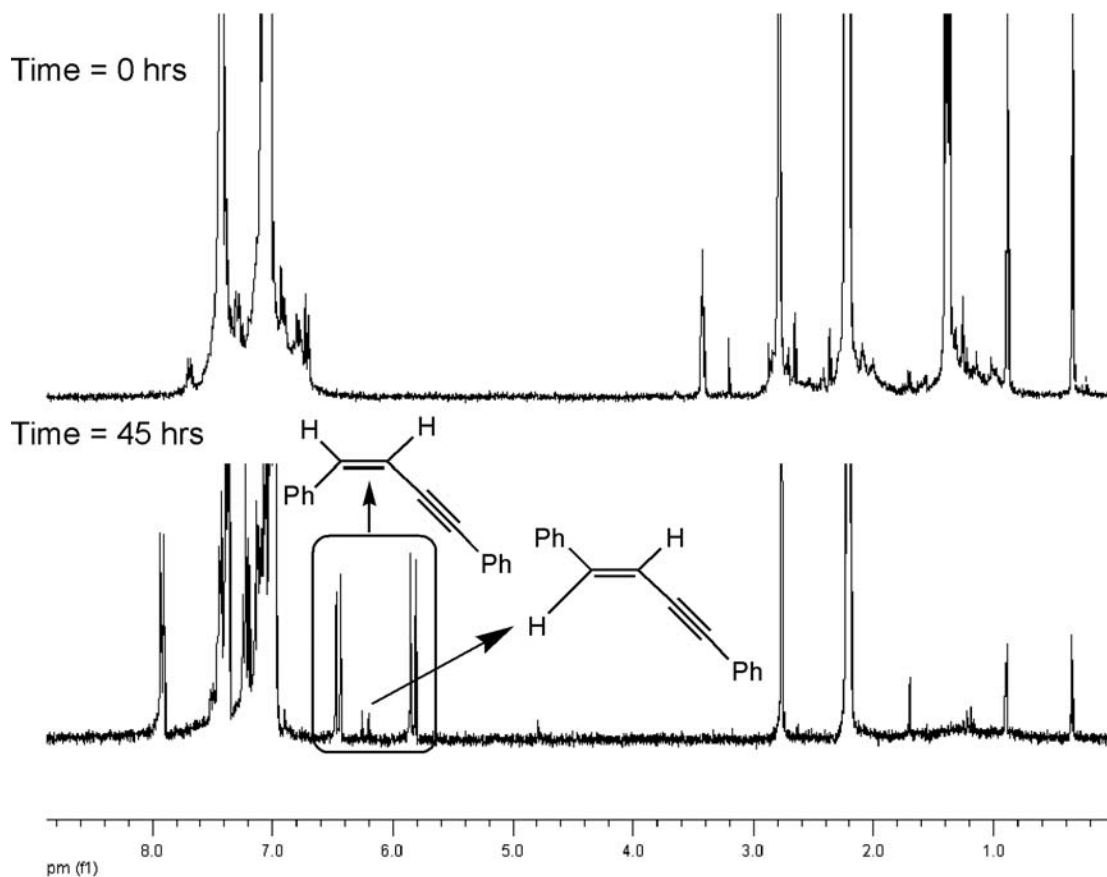
A proposed mechanism (Figure 4.9) for the Z-enyne formation would be initial generation of "(^{tBu}PNP)Os" by removing the 4 hydrides with 2 equivalents of phenylacetylene. This is supported by the ^{1}H NMR spectrum that shows a small amount of styrene forming in the reaction. "(^{tBu}PNP)Os" can then oxidatively add two equivalents of phenyl acetylene to give the (^{tBu}PNP)osmium dialkyldihydride complex. C-C coupling between the two alkyl chains leads to the bound dialkyne species, which may then have one triple bond hydrogenated to give the enyne species. Despite the fact that excess phenylacetylene was used, integration of the NMR spectra shows that only two equivalents of phenylacetylene were consumed per one mole of (^{tBu}PNP)OsH$_4$, meaning that the reaction was stoichiometeric in osmium.

Figure 4.9: Proposed mechanism for the formation of Z-enyne product
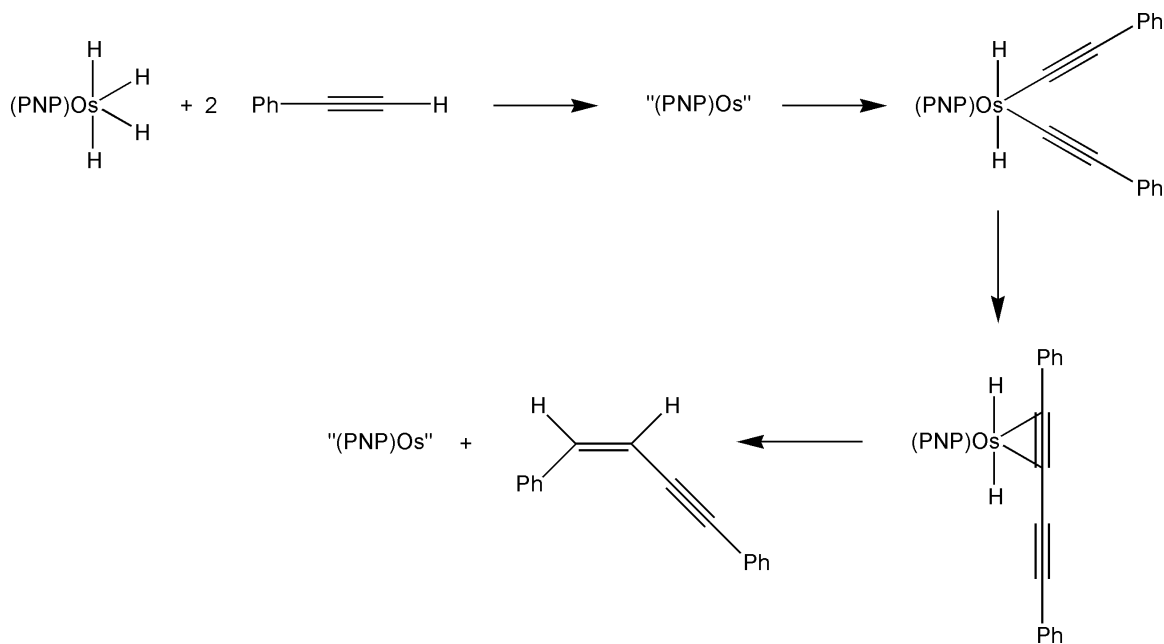
4.3 Conclusion

The stronger metal hydride bonds found in (^{tBu}PNP)OsH$_4$, where the osmium is +4 as opposed to the Ir +5 metal in (^{tBu}PCP)IrH$_4$, make (^{tBu}PNP)OsH$_4$ much less reactive than (^{tBu}PCP)IrH$_4$. H/D exchange reactions show that it is possible to remove the hydrides from (^{tBu}PNP)OsH$_4$ with norbornene and that deuterium scrambling occurs through the whole molecule. Attempts at C-H addition reactions to give metalloaromatic complexes of (^{tBu}PNP)Os were unsuccessful, and dehydrogenation reactions were minimally successful. Cyclooctane was dehydrogenated, however the reaction was stoichiometric in osmium. Attempts to dimerize phenylacetylene were also minimally successful. As was the case with the dehydrogenation, the dimerization reaction was stoichiometric in osmium; however the reaction did show a preference for the less common Z-1,4-diphenylbuta-1-en-3-yne.

4.4 Experimental

All reactions were conducted under an argon atmosphere unless otherwise noted. All solvents were purchased as anhydrous from Aldrich and degassed with argon. NMR spectra were recorded on Varian 300- and 400-MHz spectrometers. ^{1}H NMR signals are calibrated using the residual proton peaks of the deuterated solvent (they are referenced to TMS). ^{31}P NMR signals are calibrated with an external reference, a capillary with a solution of para-xylene-d_{10} and PMe$_3$ (δ −62.4 ppm). Gas chromatographs were run on a

Thermo Focus GC. (^{tBu}PNP)OsH$_4$ was made according to the method reported in Chapter 2.

Sample Preparation for Acceptor Screening: (^{tBu}PNP)OsH$_4$ (10 mg, 1.696 x 10^{-2} mmol) and acceptor (2.004 x 10^{-2} mmol) were placed in 1 mL of para-xylene-d_{10} in an NMR tube. The NMR tube was placed in an oil bath at 85 ºC and the reaction was monitored by ^{1}H and ^{31}P NMR{^{1}H} for 15 hours.

Sample H/D Exchange Reaction: (^{tBu}PNP)OsH$_4$ (10 mg, 1.696 x 10^{-2} mmol) and norbornene (0.16 mL, 8.48 x 10^{-3} mmol) were placed in 0.7 mL of para-xylene-d_{10} and sealed in an NMR tube. The NMR tube was heated in a GC oven at 125 ºC and cooled to 25 ºC before the ^{31}P{^{1}H} and ^{1}H NMR spectra were taken.

Sample C-H Activation Reaction: (^{tBu}PNP)OsH$_4$ (10 mg, 1.696 x 10^{-2} mmol) was dissolved in 0.8 mL of sample to be tested. The solution was sealed in an NMR tube and heated in a GC oven at 110 ºC. The NMR tube was cooled to room temperature before ^{31}P{^{1}H} and ^{1}H NMR spectra were run.

Dehydrogenation of Cyclooctane: (^{tBu}PNP)OsH$_4$ (2 mg, 3.391 x 10^{-3} mmol) and norbornene (6 mg, 6.40 x 10^{-2} mmol) were dissolved in 0.8 mL of cyclooctane. The solution was heated in an oil bath at 110 ºC for 96 hours, with ^{31}P{^{1}H} and ^{1}H NMR spectra taken every 24 hours.

(^{tBu}PNP)OsH$_4$ (5 mg, 8.478 x 10^{-3} mmol) and 1-octene (33.2 μL, 0.212 mmol) were placed in 0.7 mL of cyclooctane. The reaction was heated at 90 ºC in for 8 hours. NMR spectra were recorded every hour and GC analysis run after 9 hours.

Phenylacetylene Dimerization: A solution of 0.7 mL of para-xylene-d_{10} and phenylacetylene (74 μL, 0.678 mmol) was made in a vial in the box. This solution was

added to (^{tBu}PNP)OsH$_4$ (4 mg, 6.782 x 10^{-3} mmol) resulting in a yellow solution that was transferred to a J. Young NMR tube. The NMR tube was heated in an oil bath at 85 ºC for 45 hours with ^{31}P{^{1}H} and ^{1}H NMR spectra taken at times 0, 3, 6, 27 and 45 hours.

4.5 References

(1)   Chatt, J.; Davidson, J. M. *J. Chem. Soc.* **1965**, 843-855.

(2)   Shilov, A. E.; Shul'pin, G. B. *Chem. Rev.* **1997**, *97*, 2879-2932.

(3)   Zhang, X.; Kanzelberger, M.; Emge, T. J.; Goldman, A. S. *J. Am. Chem. Soc.* **2004**, *126*, 13192-13193.

(4)   Ghosh, R.; Xiawei, Z.; Achord, P. D.; Emge, T. J.; Krogh-Jespersen, K.; Goldman, A. S. *J. Am. Chem. Soc.* **2007**, *129*, 853-866.

(5)   Li, J.-H.; Li, J.-L.; Wang, D.-P.; Pi, S.-F.; Xie, Y.-X.; Zhang, M.-B.; Hu, H.-C. *J. Org. Chem.* **2007**, *72*, 2053-2057.

(6)   Feuerstein, M.; Chahen, L.; Doucet, H.; Santelli, M. *Tetrahedron* **2005**, *62*, 112-120.

(7)   Weng, W.; guo, C.; Celenligil-Cetin, R.; Foxman, B. M.; Ozerove, O. V. *Chem. Commun.* **2006**, *2*, 197-199.

(8)   Hilt, G.; Hess, W.; Vogler, T.; Hengst, C. *J. Organmet. Chem.* **2005**, *690*, 5170-5181.

(9)   Komeyama, K.; Kawabata, T.; Takehira, K.; Takaki, K. *J. Org. Chem.* **2005**, *70*, 7260-7266.

(10)   Cai, M.; Chen, J. *J. Chem. Res.* **2004**, *12*, 840-842.

(11)   Hoshi, M.; Nakayabu, H.; Shirakawa, K. *Synthesis* **2005**, *12*.

(12)   Saejueng, P.; Bates, C. G.; Venkataraman, D. *Synthesis* **2005**, *10*, 1706-1712.

(13)   Wen, T. B.; Zhou, Z. Y.; Jia, G. *Organometallics* **2003**, *22*, 4947-4951.

(14)   Goldman, A. S.; Roy, A. H.; Huang, Z.; Ahuja, R.; Schinski, W.; Brookhart, M. *Science* **2006**, *312*, 257-261.

(15)   Liu, F.; Goldman, A. S. *Chem. Commun.* **1999**, 655-656.

(16)   Liu, F.; Pak, E. B.; Singh, B.; Jensen, C. M.; Goldman, A. S. *J. Am. Chem. Soc.* **1999**, *121*, 4086-4087.

(17)   Wei-wei, X.; Rosini, G. P.; Gupta, M.; Jensen, C. M.; Kaska, W. C.; Krogh-

Jespersen, K.; Goldman, A. S. *Chem. Commun.* **1997**, 2273-2274.

(18)   Zhu, K.; Achord, P. D.; Zhang, X.; Krogh-Jespersen, K.; Goldman, A. S. *J. Am. Chem. Soc.* **2004**, *126*, 13044-13053.

(19)   Kanzelberger, M.; Singh, B.; Czerw, M.; Krogh-Jespersen, K.; Goldman, A. S. *J. Am. Chem. Soc.* **2000**, *122*, 11017-11018.

(20)   Crabtree, R. H.; Mihelcic, J. M.; Quirk, J. M. *J. Am. Chem. Soc.* **1979**, *101*, 7738-7740.

(21)   Gottker-Schnetmann, I.; White, P.; Brookhart, M. *J. Am. Chem. Soc.* **2004**, *126*, 1804-1811.

(22)   Kakiuchi, F.; Murai, S. *Acc. Chem. Res.* **2002**, *35*, 826-834.

(23)   Ben-Ari, E.; Gandelman, M.; Rozenberg, H.; Shimon, L. J. W.; Milstein, D. *J. Am. Chem. Soc.* **2003**, *125*, 4714-4715.

(24)   Wen, T. B.; Cheung, Y. K.; Yao, J.; Wong, W.-T.; Zhou, Z. Y.; Jia, G. *Organometallics* **2000**, *19*, 3803-3809.

(25)   Wen, T. B.; Zhou, Z. Y.; Jia, G. *Angew. Chem. Int. Ed.* **2006**, *45*, 5842-5846.

(26)   Caskey, S. R.; Stewart, M. H.; Ahn, Y. J.; Johnson, M. J. A.; Rowsell, J. L. C.; Kampf, J. W. *Organometallics* **2007**, *26*, 1912-1923.

Chapter 5

Hydrogenation Kinetics of *trans*-5-decene with (^{tBu}PCP)IrH$_2$

Abstract

The reaction of *trans*-5-decene with (^{tBu}PCP)IrH$_2$ was studied over the temperature range of 40 ºC to 100 ºC. The rate constant showed small changes over the temperature range. An Eyring plot, yielded an activation enthalpy ($\Delta H^{\ddagger}$) of 2.6(0.6) kcal/mol, an activation entropy ($\Delta S^{\ddagger}$) of –63.5(1.7) cal/mol·K and a room temperature activation energy (Ea) of 3.2(0.3) kcal/mol. The rate constant (k) and activation energy at 125 ºC were also extrapolated and found to be 4.0 x 10^{-3}(1.6) M^{-1}s^{-1} and 3.4(0.3) kcal/mol, respectively. The reaction to product does not proceed cleanly, with one major olefin bound product and four minor olefin-bound products observed.

5.1 Introduction

The addition of H_2 to metals has long been known. In 1955, Cu^{2+} was found to heterolytically cleave H_2 to give $[CuH]^+ + H^+$.[1,2] The first example of oxidative addition of H_2 to a metal complex was reported in 1962, when Vaska found that $Ir(CO)(Cl)(PPh_3)_2$ added H_2 to give the dihydride complex as shown in Scheme 5.1.[3] Since H_2 could be broken, the possibility of using transition metal complexes to catalyze the hydrogenation of a double bond seemed possible. Indeed this was the case in 1965, when Wilkinson reported that $Rh(PPh_3)_3X$ catalyzed the hydrogenation of 1-hexene and acetylenes according to the proposed mechanism in Figure 5.1. [4,5]

Scheme 5.1: First example of oxidative addition of H_2 to a metal complex[3]
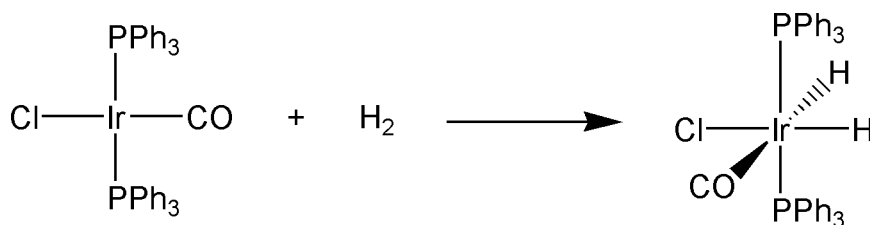
Figure 5.1: Proposed cycle of hydrogenation by Wilkinson's catalyst[4,5]
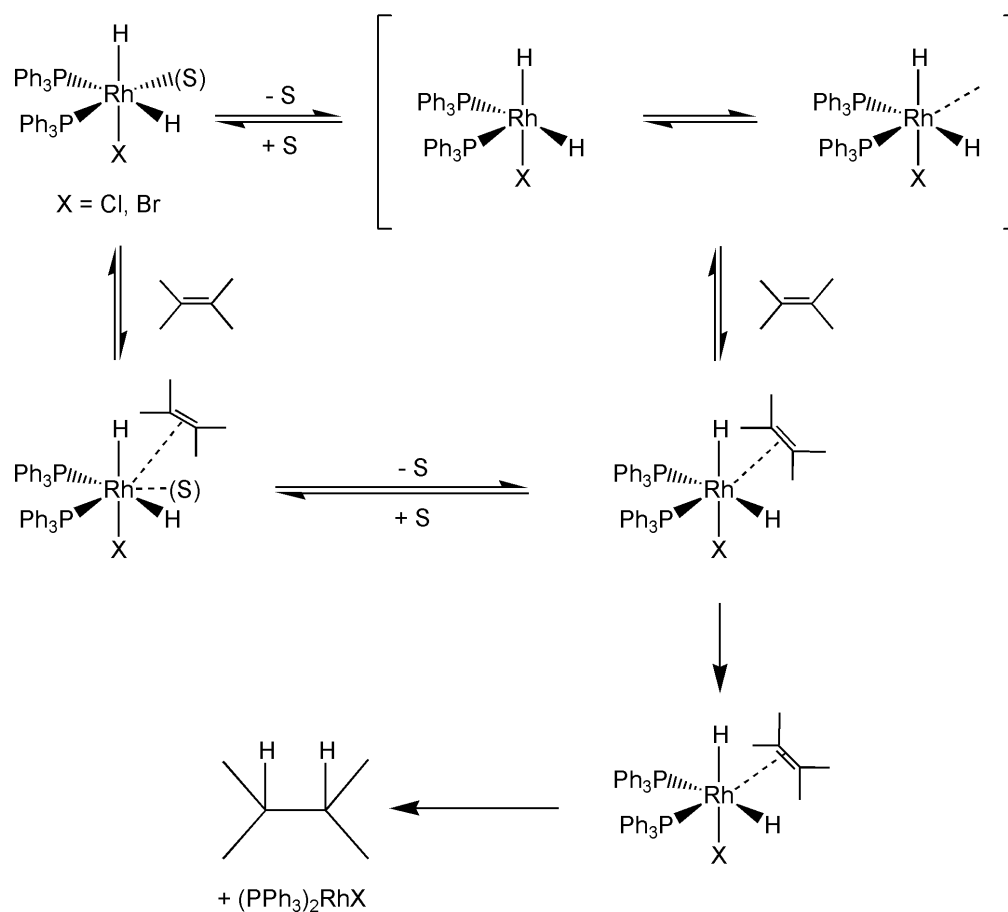
In the field of petroleum research there has been much interest in "rearranging" alkanes. Recently, Goldman and Brookhart have published a key paper describing a tandem catalytic system for alkane metathesis.[6] In this system, ([R]PCP)Ir complexes dehydrogenate an alkane to an alkene, a Schrock based molybdenum catalyst metathesizes two alkenes, and ([R]PCP)IrH$_2$ complex then hydrogenates the newly formed alkene to an alkane, thus regenerating the ([R]PCP)Ir catalyst (Figure 5.2).[6] Unlike previous systems for alkane metathesis, this system has been shown to be selective for the production of alkanes of a specific carbon number.[7,8]

Figure 5.2: Mechanism of tandem dehydrogenation-olefin metathesis[6]

$R = {}^tBu$ or ${}^iPr$, $E = C$, $X = H$ or OMe

$R = {}^tBu$, $E = O$, $X = H$
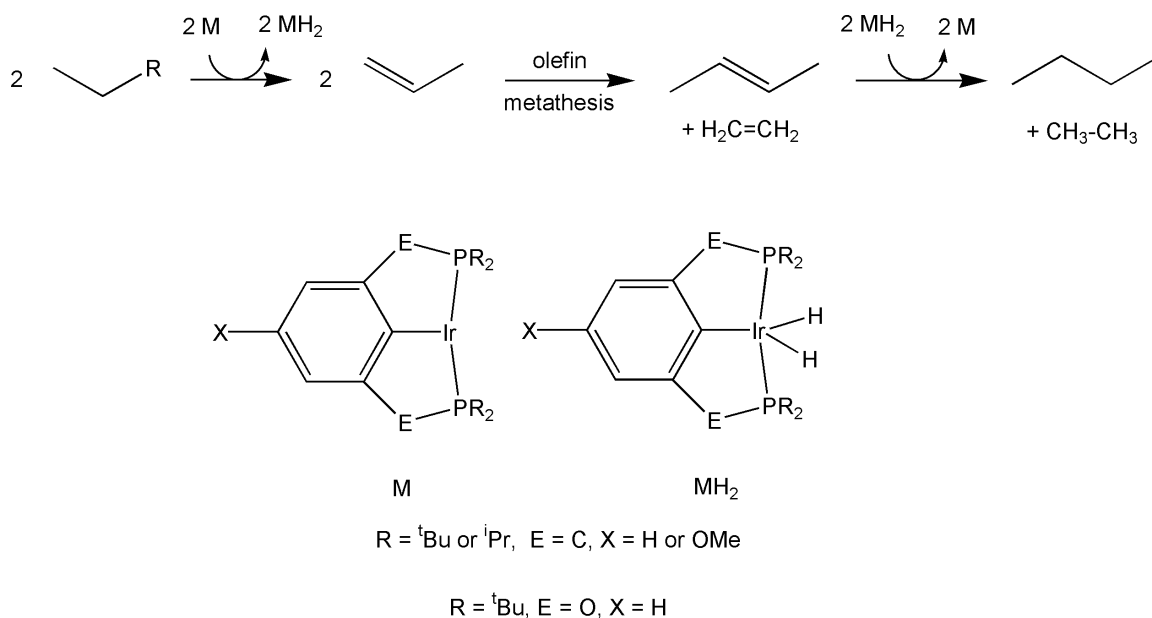
Work is ongoing in the Brookhart and Goldman labs to find ways to improve the catalytic system. An important component of these efforts involves mechanistic studies.

The selectivity of the system is highly dependent on conditions and the nature of the catalyst. Presumably isomerization of olefinic intermediates leads to decreased selectivity for alkane carbon numbers. Thus, one element of the catalytic cycle to examine is the rate of hydrogenation versus the rate of isomerization. "$({}^{tBu}PCP)Ir$", the active catalyst in the cycle, has been shown to promote isomerization of double bonds in addition to dehydrogenation.[9] At the temperature that the tandem catalysis takes place both isomerization and dehydrogenation are possibilities. In order to improve the tandem catalytic cycle, the rate of hydrogenation would ideally be maximized while that of isomerization would be minimized.

This chapter presents NMR experiments that were carried out to determine the rate of hydrogenation of *trans*-5-decene. Using Arrhenius and Eyring plots, the activation energy, transition state enthalpy and transition state entropy were determined. The rate constant of the reaction at 125 ºC was also determined.

5.2 Results and Discussion

(^{tBu}PCP)IrH$_2$ was reacted with *trans*-5-decene and the reaction was monitored by ^{31}P{^{1}H} NMR spectoscopy. Although the tandem catalysis reactions take place at 125 ºC, due to instrument limitations, the highest temperature at which the reaction could be monitored was 100 ºC. Although the reaction followed second order kinetics, the reaction was designed so that the signal due to the disappearance of (^{tBu}PCP)IrH$_2$ followed psuedo-first order kinetics. Although, as expected, the reaction at 100 ºC was fastest there was only a small variation in the second order rate constants with temperature (Table 5.1).

Table 5.1: Second order rate constants at various temperatures

Rate Constant (k) M^{-1}sec^{-1}	Temperature (ºC)
3.27 x 10^{-3}	100
2.23 x 10^{-3}	80
1.60 x 10^{-3}	60
1.40 x 10^{-3}	40

An Eyring plot was made using the rate constants from the different experiments (Figure 5.3). Since we are particularly interested in reactions that occur at 125 ºC, or greater, the graph was extrapolated to obtain a second order rate constant of 4.0 x 10^{-3}(1.6) $M^{-1}s^{-1}$ at this temperature.   The plot was used to calculate the enthalpy of activation ($\Delta H^{\ddagger}$). Using equation 5, $\Delta H^{\ddagger}$ was calculated to be 2.6 (0.6) kcal/mol.

$$\text{Slope} = - \Delta H^{\ddagger} / R \qquad (R = 1.9872 \text{ cal/mol·K}) \qquad (5)$$

Figure 5.3: Eyring plot for the reaction of (^{tBu}PCP)IrH$_2$ (24 mM) with trans-5-decene (144 mM)
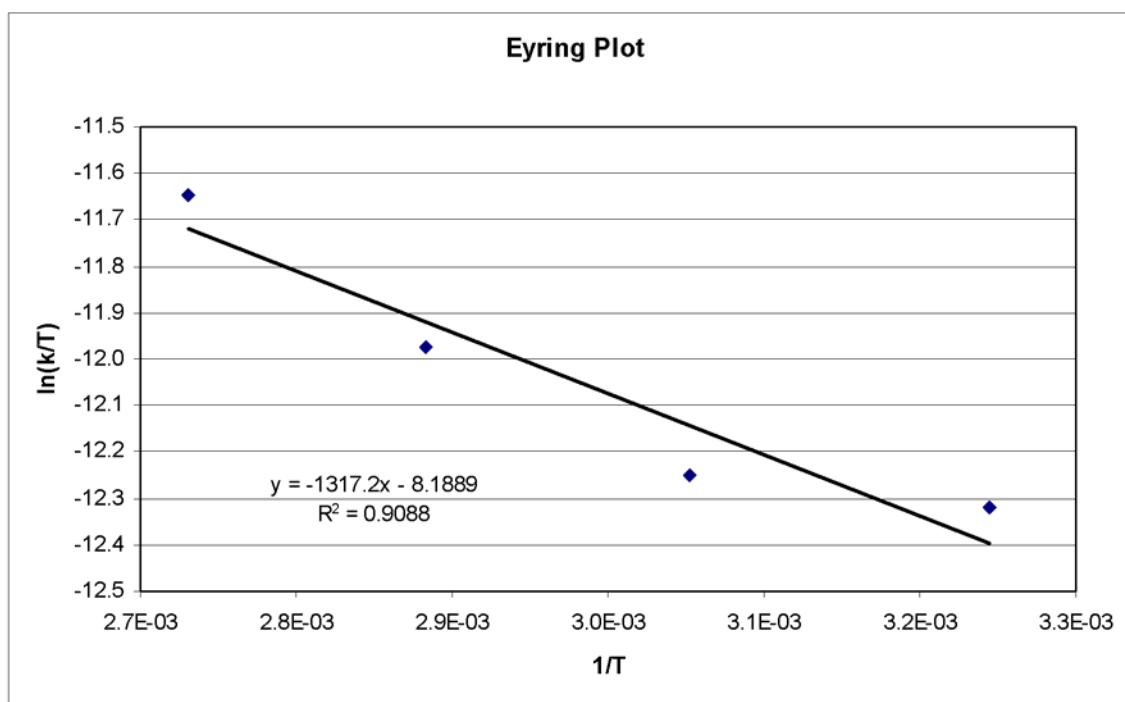
The y-intercept of the Eyring plot is used to find the entropy of activation ($\Delta S^{\ddagger}$) according to equation 6. For this equation K_b is the Boltzmann constant, 3.298×10^{-24} cal/K, and h is Plank's constant, 1.583×10^{-34} cal·s. The calculated $\Delta S^{\ddagger}$ value was $-63.5(1.7)$ cal/mol·K. This remarkably negative value may suggest the possibility of non-classical behavior such as the involvement of quantum tunneling. This proposal is further supported by the observation that reactions where tunneling occurs are largely temperature independent, similar to what is observed in this reaction.[10-12] These values are summarized in Table 5.2.

$$\text{y-intercept} = \text{Ln} (K_b / h) + (\Delta S^{\ddagger} / R) \qquad (6)$$

Table 5.2: Comparison of values obtained from Eyring and Arrhenius plots.

	Eyring Values	Arrhenius Values
Rate constant (k) at 125 ºC	$4.0 \times 10^{-3}(1.6)$ M^{-1}s^{-1}	$4.0 \times 10^{-3}(1.6)$ M^{-1}s^{-1}
$\Delta H^{\ddagger}$	2.6 (0.6) kcal /mol	
$\Delta S^{\ddagger}$	-63.5(1.7) cal / mol · K	
Ea (25 ºC)	3.2 (0.3) kcal / mol	3.3 (0.6) kcal / mol
Ea (125 ºC)	3.4 (0.3) kcal / mol	

The activation free energy ($\Delta G^{\ddagger}$) is related to the activation enthalpy and activation entropy by equation 7.

$$\Delta G^{\ddagger} = \Delta H^{\ddagger} - T\Delta S^{\ddagger} \qquad\qquad (7)$$

At 298 K (25 ºC) and 398 (125 ºC), the $T\Delta S^{\ddagger}$ quantity is calculated to be 18.92 kcal/mol and 25.27 kcal/mol, respectively. In both cases these values are much greater than the $\Delta H^{\ddagger}$ value of 2.6(0.6) kcal/mol, indicating that the majority of the barrier to the transition state is due to entropic factors.

An Arrhenius plot was also made (Figure 5.4). As was the case with the Eyring plot, the Arrhenius plot was extrapolated to 125 ºC to determine a rate constant of 4.0 x 10^{-3}(1.6) M^{-1}s^{-1} at this temperature. Unlike the Eyring plot, the Arrhenius plot ignores temperature in the calculation of activation energy, which is obtained directly from the slope. Using equation 8, the activation energy was found to be 3.3(0.6) kcal/mol. Table 2, compares these values with the values obtained from the Eyring plot.

$$\text{Slope} = -E_a / R \qquad (R = 1.9872 \text{ cal/mol·K}) \qquad (8)$$

Figure 5.4: Arrhenius plot for the reaction of (^{tBu}PCP)IrH$_2$ (24 mM) with trans-5-decene (144 mM)
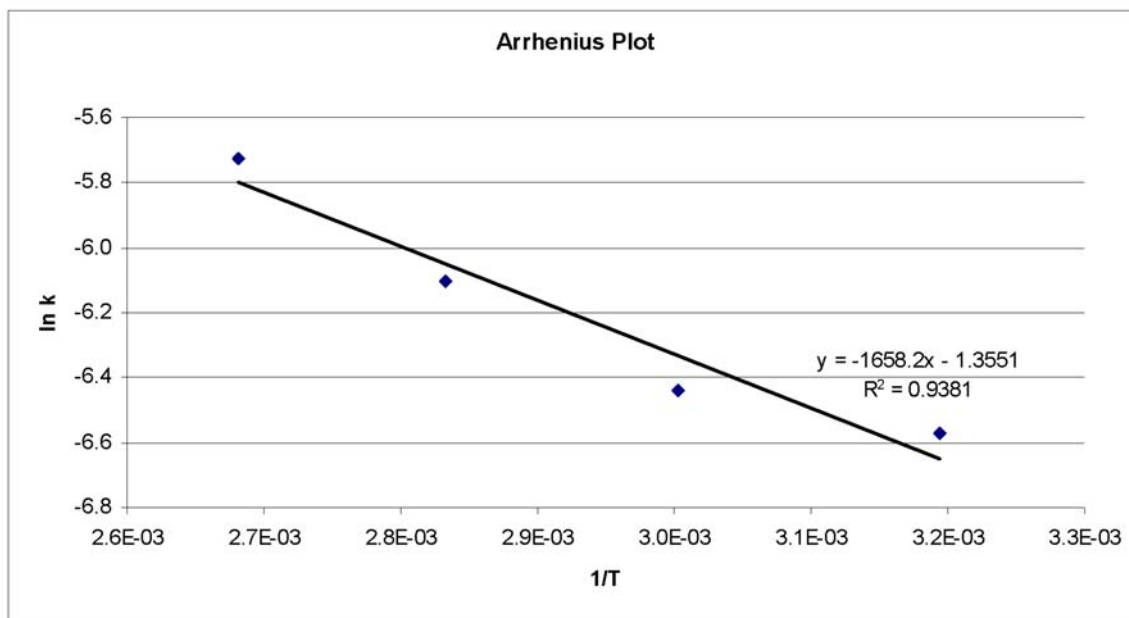
The formation of five different (^{tBu}PCP)Ir(olefin) signals were observed, with what was labeled as olefin-A (δ = 59.90 ppm) as the major (^{tBu}PCP)Ir(olefin) in each case. At 40 ºC growth of (^{tBu}PCP)Ir(olefin-A) followed a very neat first order kinetic increase (Figure 5.5), unlike the other (^{tBu}PCP)Ir(olefin) complexes that remained approximately linear over the course of the reaction. Also at 100 ºC (Figure 5.6), (^{tBu}PCP)Ir(olefin-A) is still the major product and does seem to still be following a first order rise; however the reaction gives less of a clean conversion.

Figure 5.5: Graph of the reaction of (^{tBu}PCP)IrH$_2$ (24 mM) and trans-5-decene (144 mM) at 40 ºC, showing the first order disappearance of (^{tBu}PCP)IrH$_2$ and first order appearance of (^{tBu}PCP)Ir(olefin-A)
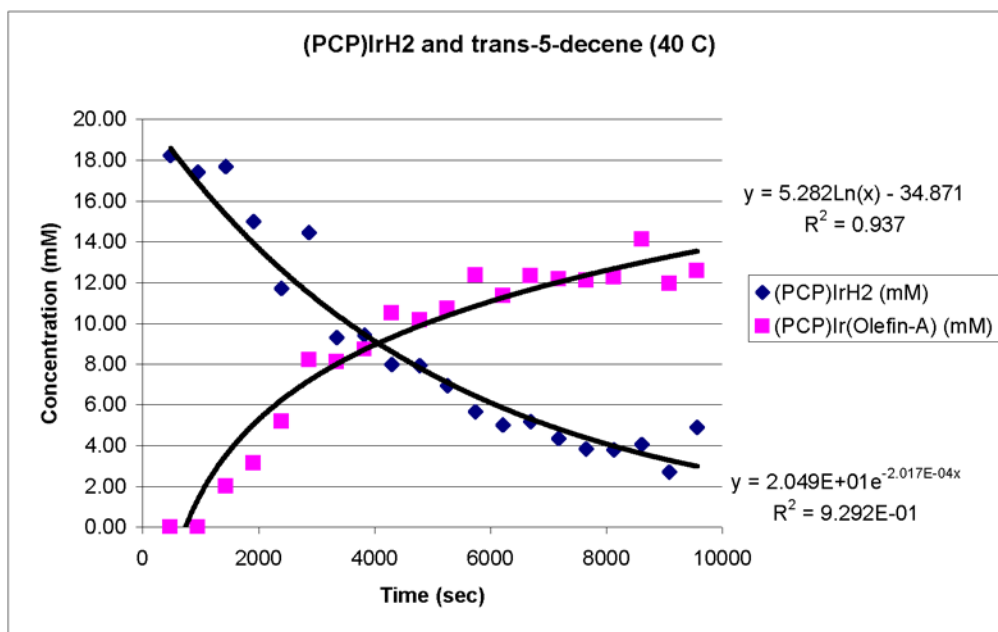
Figure 5.6: Graph of the reaction of (^{tBu}PCP)IrH$_2$ (24 mM) and trans-5-decene (144 mM) at 100 ºC, showing the first order disappearance of (^{tBu}PCP)IrH$_2$ and first order appearance of (^{tBu}PCP)Ir(olefin-A)
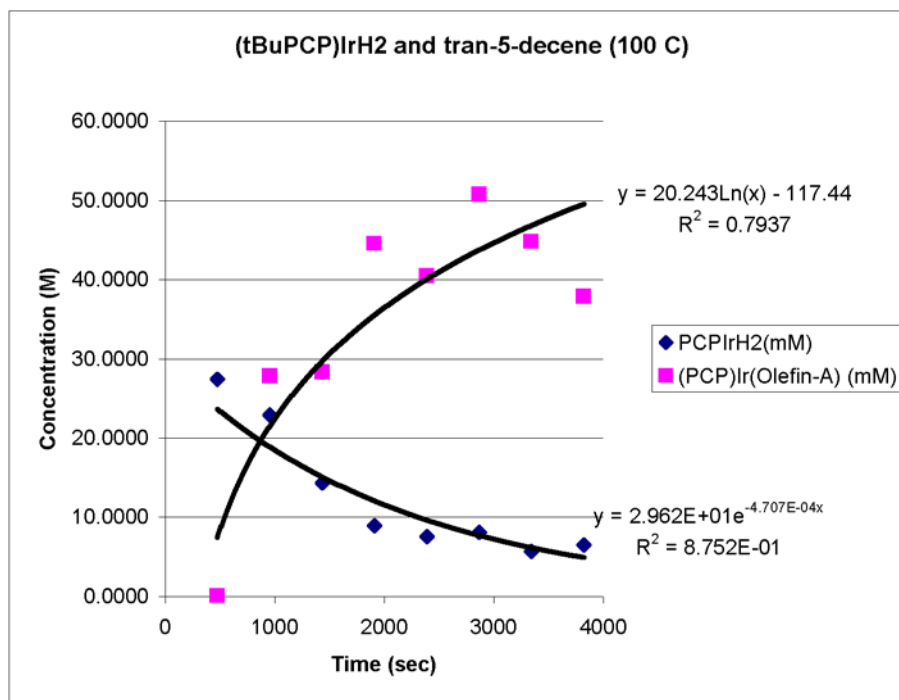
(^{tBu}PCP)Ir-η^2-5-decene seemed the most likely form of (^{tBu}PCP)Ir(olefin-A); however, the possibility that alkane dehydrogenation was taking place to give 1-decene that was binding to the Ir to give (^{tBu}PCP)Ir-η^2-1-decene could not be ignored (Scheme 5.2). To determine if the olefins could be identified, (^{tBu}PCP)Ir(NBE) (NBE = norbornene) was reacted with *trans*-5-decene and 1-decene separately. The chemical shift of each product showed only a slight difference in the NMR, meaning that the two species could not be distinguished by NMR and that the identity of (^{tBu}PCP)Ir(olefin-A) could also not be definitively determined by NMR methods.

Scheme 5.2: Mechanism to convert (PCP)Ir trans-5-decene (PCP)Ir 1-decene
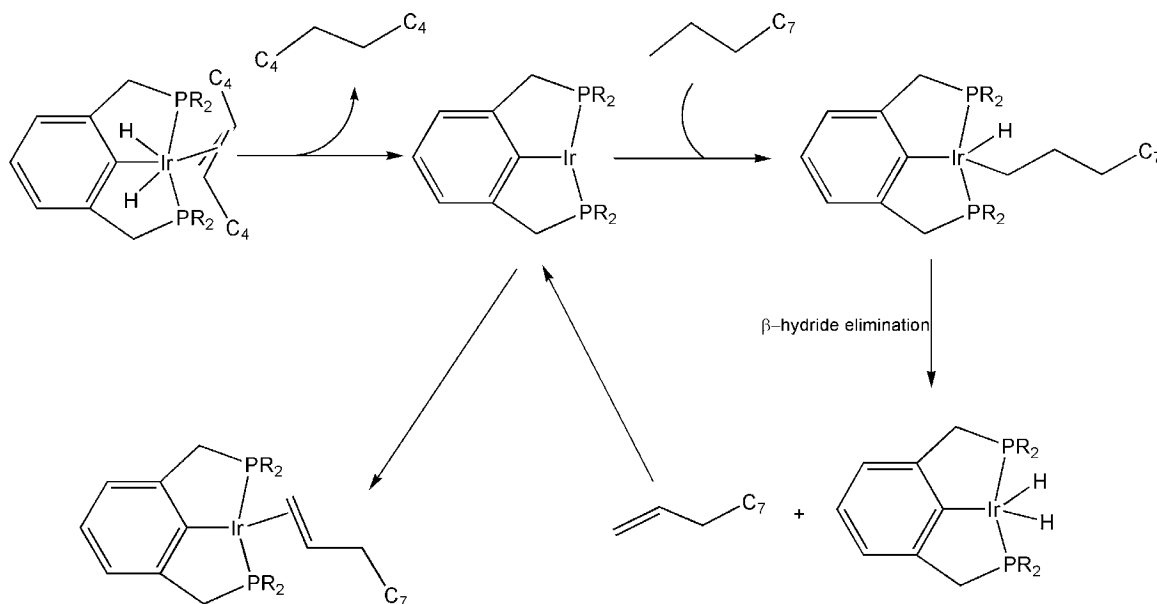
5.3 Conclusions

The reaction of $(^{tBu}PCP)IrH_2$ with *trans*-5-decene follows second order kinetics in the disappearance of $(^{tBu}PCP)IrH_2$ and the appearance of the major olefin bound product. From an Eyring plot, the rate constant and activation energy at 125 °C were extrapolated to be 4.0 x 10^{-3}(1.6) $M^{-1}s^{-1}$ and 3.4(0.3) kcal/mol, respectively. Also from the plot, the enthalpy of activation was found to be 2.6(0.6) kcal/mol and the entropy of activation was −63.5(1.7) cal/mol. The large difference between these two values indicates that the barrier to the transition state is mainly due to entropic factors. The remarkably negative value found for the entropy of activation is a strong indication that non-classical behavior such as quantum tunneling might be occurring in the reaction. The room temperature

energy of activation, 3.2(0.3) kcal/mol was slightly lower than the energy of activation at 125 ºC. The rate constants showed little change between 40 ºC and 125 ºC, meaning that the reaction rate was largely temperature independent. The small difference in values of activation energy obtained from the Eyring [3.2(0.3) kcal/mol] and Arrhenius [3.3(0.6) kcal/mol] plots supports this conclusion.

5.4 Experimental

All reactions were conducted under an argon atmosphere unless otherwise noted. All solvents were purchased as anhydrous from Aldrich and degassed with argon. NMR spectra were recorded on a 400-MHz spectrometer. ^{31}P NMR signals are calibrated with an external reference, a capillary with a solution of para-xylene-d_{10} and PMe$_3$ (δ −62.4 ppm). Unless otherwise noted the solvents used were not deuterated.

Kinetic measurements: Stock solutions of (^{tBu}PCP)IrH$_2$ (48 mM) and *trans*-5-decene (288 mM) in mesitylene were made. 0.15 mL of each solution was injected via syringe into an NMR tube resulting in final concentrations of 24 mM for (^{tBu}PCP)IrH$_2$ and 144 mM for *trans*-5-decene. The NMR tube was immediately placed in a liquid nitrogen filled dewar and brought to the 400-MHz NMR instrument. The NMR instrument was heated to the desired temperature and the experiment set to take spectra every 5 minutes, before the sample was thawed and inserted.

5.5 References

(1)   Halpern, J.; Peters, E. *J. Chem. Phys.* **1955**, *23*, 605.

(2)   Peters, E.; Halpern, J. *J. Phys. Chem.* **1955**, *59*, 793-796.

(3)   Vaska, L.; DiLuzio, J. W. *J. Am. Chem. Soc.* **1962**, *84*, 679-680.

(4)   Young, J. F.; Osborn, J. A.; Jardine, F. H.; Wilkinson, G. *Chem. Commun.* **1965**, *7*, 131-132.

(5)   Jardine, F. H.; Osborn, J. A.; Wilkinson, G. *J. Chem. Soc. (A): Inorg. Phys. Theor.* **1967**, *10*, 1574-1578.

(6)   Goldman, A. S.; Roy, A. H.; Huang, Z.; Ahuja, R.; Schinski, W.; Brookhart, M. *Science* **2006**, *312*, 257-261.

(7)   Burnet, R. L.; Hughes, T. R. *J. Catalysis* **1973**, *31*, 55.

(8)   Basset, J. M.; Coperet, C.; Lefort, L.; Maunders, B. M.; Maury, O.; Le Roux, E.; Saggio, G.; Soignier, S.; Soulivong, D.; Sunley, G. J.; Taoufik, M.; Thivolle-Cazat, J. *J. Am. Chem. Soc.* **2005**, 8604 and references therein.

(9)   Liu, F.; Pak, E. B.; Singh, B.; Jensen, C. M.; Goldman, A. S. *J. Am. Chem. Soc.* **1999**, *121*, 4086-4087.

(10)   Sheridan, R. S. *Rev. React. Intermed. Chem.* **2007**, 415-463.

(11)   Moss, R. A.; Sauers, R. R.; Sheridan, R. S.; Tian, J.; Zuev, P. S. *J. Am. Chem. Soc.* **2004**, *126*, 10196-10197.

(12)   Zuev, P. S.; Sheridan, R. S.; Albu, T. V.; Truhlar, D. G.; Hrovat, D. A. *Science* **2003**, *299*, 867-870.

Chapter 6

($^{\text{tBu}}$PCP)IrH(μ^2Cl)$_2$Ir(COD): A Side Product in the Synthesis of ($^{\text{tBu}}$PCP)IrHCl

Abstract

($^{\text{tBu}}$PCP)IrHCl is a key intermediate in the synthesis of the highly active dehydrogenation catalyst ($^{\text{tBu}}$PCP)IrH$_4$. During the synthesis of ($^{\text{tBu}}$PCP)IrHCl a side product, ($^{\text{tBu}}$PCP)IrH(μ^2Cl)$_2$Ir(COD), was isolated and fully characterized. ($^{\text{tBu}}$PCP)IrH(μ^2Cl)$_2$Ir(COD) can be viewed as the product of oxidative addition where PCP displaces COD and coordinates, via C-H oxidative, addition to one center of [Ir(COD)Cl]$_2$. The signals of the $^{\text{tBu}}$PCP ligand were clearly visible in the ^{1}H NMR; however only one set of COD signals were found due to overlap with solvent and the *tert*-butyl signals of the $^{\text{tBu}}$PCP ligand. X-ray diffraction showed that the complex was a dimer and that the hydride was coordinated to the iridium atom bound to the PCP ligand. The Ir-Cl bond lengths are consistent with the bond lengths for other mixed Ir(I) and Ir(III) complexes. One half of a hexane molecule was also crystalized in the unit cell, however there were no significant interactions between the hydrogens on the hexane and those in the iridium dimer.

6.1 Introduction

In 1976, Moulton and Shaw first published the synthesis of 1,3-bis[(di-*tert*-butyl phosphino)methyl]benzene or ^{tBu}PCP-H, shown in Figure 6.1.[1] In recent years there has been great interest in the development of pincer complexes with both the original ^{tBu}PCP pincer and other pincer ligands that have been derived from the PCP pincer, some of which are shown in Figure 6.2.

Figure 6.1: Structure of 1,3-bis[(di-tert-butyl phosphino)methyl]benzene (^{tBu}PCP)
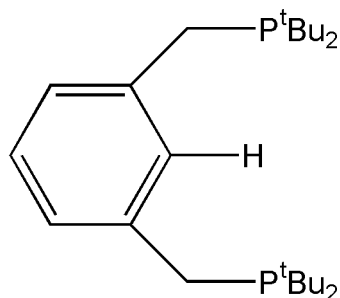
Derivatives of (^{tBu}PCP)Ir are currently some of the most active catalysts for the dehydrogenation of alkanes.[2-6]   Previous research in our group has shown that (^{tBu}PCP)IrH$_2$ is an especially noteworthy catalyst as it not only dehydrogenates alkanes efficently, but is also selective for the production of α-olefins.[3]   In addition to their dehydrogenation abilities, (^{R}PCP)Ir complexes have also been found to be active catalysts for other bond transforming processes such as N-H activation,[7,8] and C-C coupling reactions.[8,9] Recently, our group, in collaboration with the Brookhart group, has shown that (^{R}PCP)Ir catalysts when combined with Shrock-type catalysts will effect the

metathesis of *n*-alkanes. Unlike previously reported systems this catalytic combination is effective with higher alkanes (C > 4) and in some cases with selectivity for specific product carbon numbers.[10]

Figure 6.2:   Pincer Complexes   a. Original (^{tBu}PCP)Ir complex[5]   b. (^{iPr}PCP)Rh complex[11] c. MeO-(^RPCP)Ir complex[2]   d. Ferrocenyl-(^RPCP)Pd complex[12]   e. para-X-(POCOP)Ir complex[13]
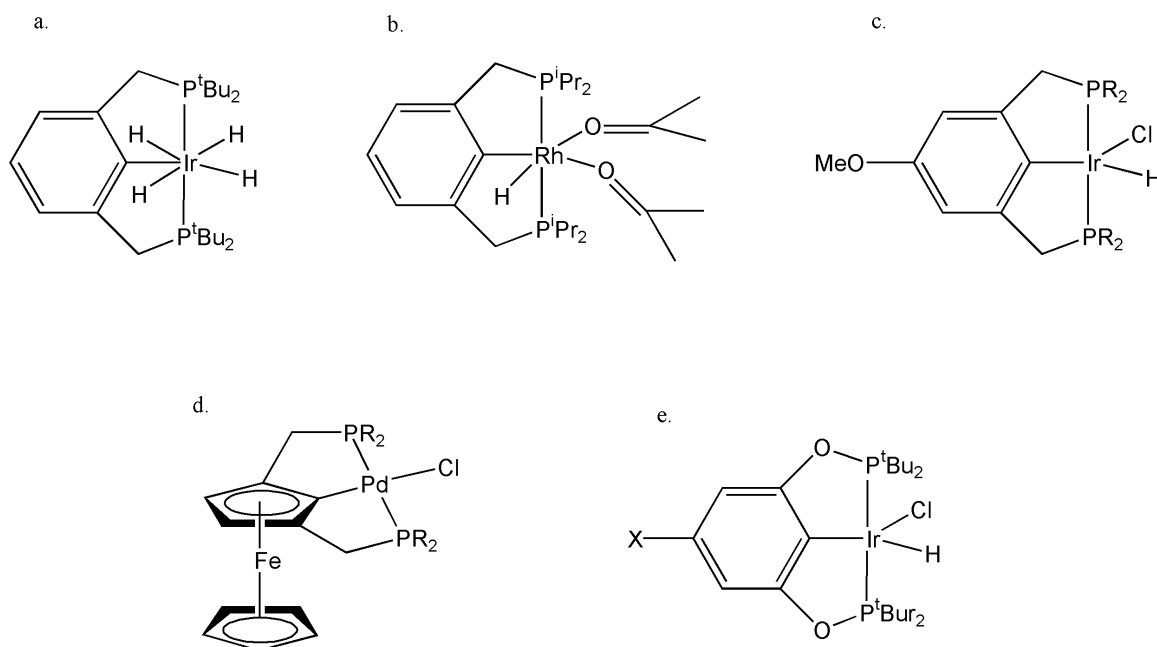
The synthetic precursor to the versatile (^{tBu}PCP)IrH$_2$ is (^{tBu}PCP)IrHCl (Scheme 6.1). In the synthesis of (^{tBu}PCP)IrHCl one side product that may form, especially if the ratio of PCP to Ir$_2$ is less than 2:1, is the bright yellow hexanuclear iridium η^4-2,5-cyclooctadiene complex [(COD)Ir]$_2${η^6-{κ^4-C$_6$H$_2$(CH$_2$P^{t}Bu$_2$)$_2$]Ir$_2$H$_2$Cl$_3$}$_2$ (COD = 2,5-cyclooctadiene) which has been previously isolated and characterized.[14]   When the synthesis of (^{tBu}PCP)IrHCl was attempted according to Scheme 6.1, a second side

product of the reaction was isolated as orange/red crystals. These were characterized by NMR spectroscopy and x-ray diffraction and identified as $(^{tBu}PCP)IrH(\mu^2-Cl)_2Ir(COD)$ (**6**). This chapter will present the synthesis of **6** as well as the x-ray and NMR data used to identify this complex.

Scheme 6.1: Synthesis of $(^{tBu}PCP)IrH_4^{5,6}$
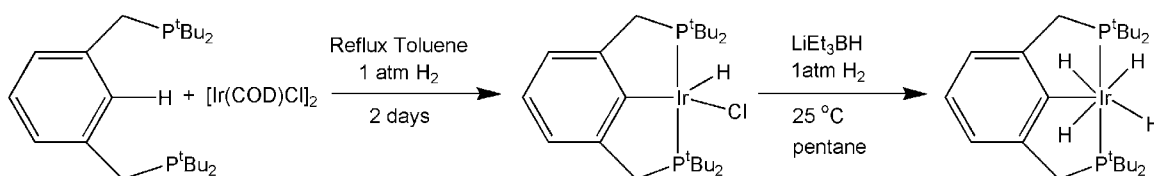
6.2 Results and Discussion

Complex **6** was isolated from cold hexane as a by-product of the reaction of (^{tBu}PCP) with $[Ir(COD)Cl]_2$. The complex formed as large red/orange crystals coated with a red/orange powder. ^1H and ^{31}P NMR spectra of the crystals showed that they were primarily **6**, however a significant amount of $(^{tBu}PCP)IrHCl$ was also present. The ^{31}P NMR spectrum showed one signal at δ 67.75 ppm for the $(^{tBu}PCP)IrHCl$ signal and a larger signal at δ 54.89 ppm for compound **6** (Figure 6.3).

The ^1H NMR spectrum was more difficult to interpret because of the large number of protons in the complex and the overlap of some protons with the solvent molecule (Figure 6.4). Aside from the aryl protons on the PCP ligand that overlapped with the solvent signals, all other signals for the PCP portion of **6** were found and

assigned based on integration and chemical shift. Each set of methylene protons appeared as a doublet of triplets, one centered at δ 3.29 ppm and the second at δ 2.86 ppm, while the *tert*-butyl signals appeared as two triplets, one at δ 1.73 ppm and the second at δ 1.22 ppm. In the COD portion of the complex, only the vinyl protons were found as a broad doublet centered at δ 3.94 ppm. Of the other two sets of aryl signals, one was overlapped with the toluene-d$_8$ or p-xylene-d$_{10}$ solvent and the second overlapped with the *tert*-butyl groups of both the PCP ligand on complex **6** and the (^{tBu}PCP)IrHCl that was also present in solution.

Figure 6.3: $^{31}P\{^{1}H\}$ *NMR of (*^{tBu}*PCP)IrH(μ^{2}-Cl)$_2$Ir(COD) (**6**)*

(^{tBu}PCP)IrH(μ^{2}Cl)$_2$(COD)

(^{tBu}PCP)IrHCl

Figure 6.4: ^1H *NMR of* $(^{tBu}PCP)IrH(\mu^2\text{-}Cl)_2Ir(COD)$ *(6)*
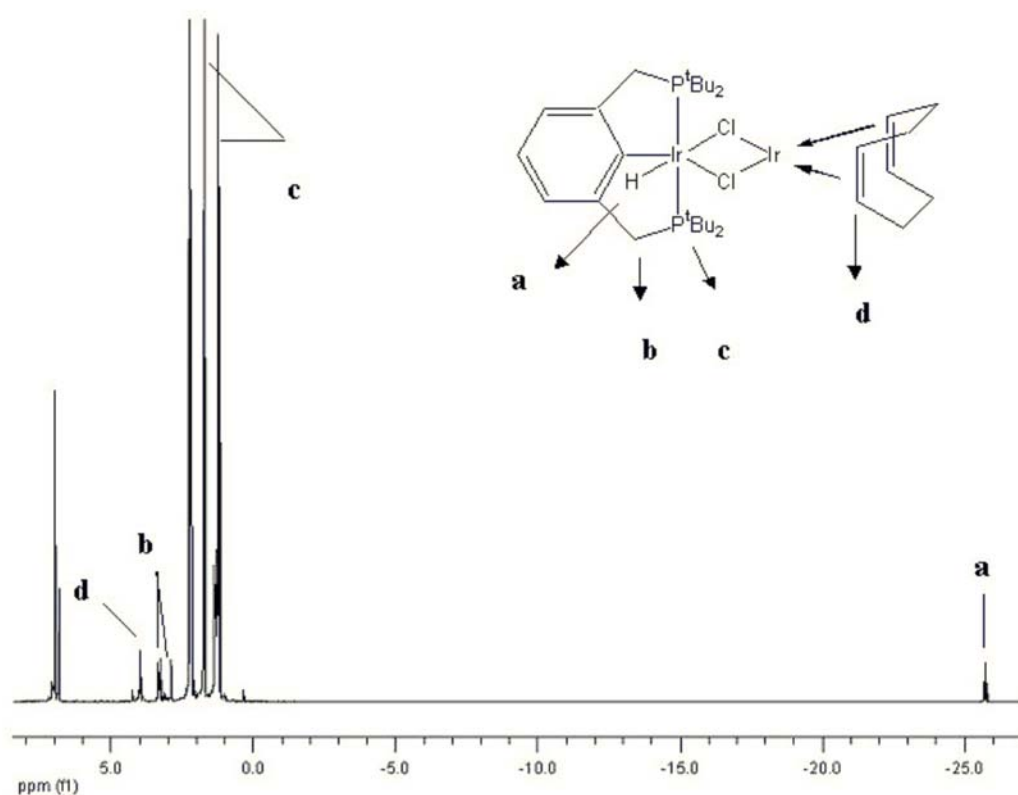
In addition to the NMR data, complex **6** was also characterized by solid state x-ray diffraction. The crystal was found to be monoclinic and in the P2(1)/c space group. The ORTEP diagram is shown in Figure 6.5, with crystallographic details in Table 6.1 and selected bond lengths and angles in Table 6.2. Full crystallographic details may be found in the Appendix.

Figure 6.5: (^{tBu}PCP)IrH(μ^2-Cl)$_2$Ir(COD) (6)
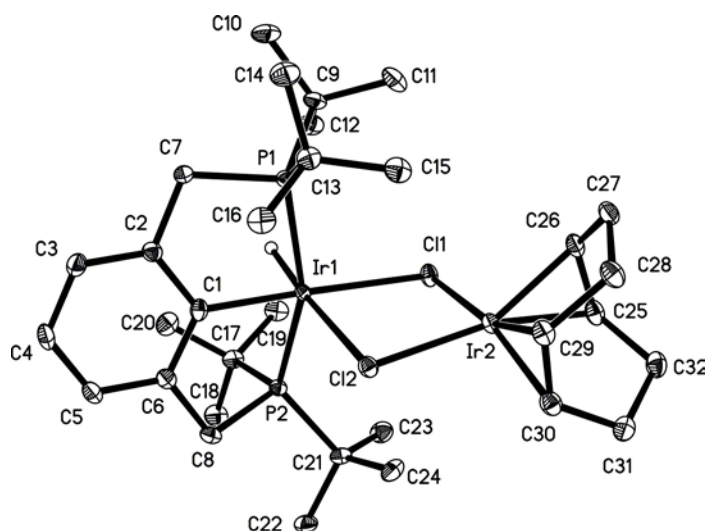
Table 6.1: Crystallographic Data for (^{tBu}PCP)IrH(μ^2-Cl)$_2$Ir(COD) (**6**)

Identification code	irhco_bad
Empirical formula	C35 H63 Cl2 Ir2 P2
Formula weight	1001.09
Temperature	293(2) K
Wavelength	0.71073 Å
Crystal system	Monoclinic
Space group	P2(1)/c
Unit cell dimensions	a = 14.8424(7) Å α= 90°
	b = 11.6735(5) Å β= 99.416(1)°
	c = 22.0589(10) Å γ = 90°
Volume	3770.5(3) Å^3
Z	4
Density (calculated)	1.764 Mg/m^3
Absorption coefficient	7.301 mm^{-1}
F(000)	1964
Crystal size	0.19 x 0.12 x 0.08 mm^3
Theta range for data collection	1.87 to 30.61°.
Index ranges	-21<=h<=21, -16<=k<=16, -31<=l<=31
Reflections collected	42778
Independent reflections	11498 [R(int) = 0.0332]
Completeness to theta = 30.61°	99.0 %
Absorption correction	Semi-empirical from equivalents
Max. and min. transmission	0.9999 and 0.7589
Refinement method	Full-matrix least-squares on F^2
Data / restraints / parameters	11498 / 1 / 398
Goodness-of-fit on F^2	1.003
Final R indices [I>2sigma(I)]	R1 = 0.0263, wR2 = 0.0603
R indices (all data)	R1 = 0.0317, wR2 = 0.0622
Largest diff. peak and hole	2.638 and -0.928 e.Å^{-3}

Table 6.2: Selected bond lengths (Å) and angles (º) for (^{tBu}PCP)IrH(μ^2-Cl)$_2$Ir(COD) (**6**)

Ir(1)-C(1)	2.013(3)	Ir(1)-H(1)	1.587(10)
Ir(1)-P(2)	2.3284(8)	Ir(1)-P(1)	2.3261(8)
Ir(1)-Cl(2)	2.5912(7)	Ir(1)-Cl(1)	2.5070(8)
Ir(2)-C(26)	2.090(3)	Ir(2)-C(30)	2.100(3)
Ir(2)-C(25)	2.108(3)	Ir(2)-C(29)	2.113(3)
Ir(2)-Cl(1)	2.3831(8)	Ir(2)-Cl(2)	2.4071(7)
P(1)-C(7)	1.843(3)	P(1)-C(9)	1.891(3)
P(1)-C(13)	1.891(3)	P(2)-C(8)	1.845(3)
P(2)-C(21)	1.890(3)	P(2)-C(17)	1.896(3)

C(1)-Ir(1)-P(1)	83.27(9)	C(1)-Ir(1)-P(2)	81.21(9)
P(1)-Ir(1)-P(2)	158.83(3)	C(1)-Ir(1)-Cl(1)	176.78(9)
P(1)-Ir(1)-Cl(1)	97.23(3)	P(2)-Ir(1)-Cl(1)	99.07(3)
C(1)-Ir(1)-Cl(2)	96.80(9)	P(1)-Ir(1)-Cl(2)	99.77(3)
P(2)-Ir(1)-Cl(2)	96.29(3)	Cl(1)-Ir(1)-Cl(2)	79.98(2)
C(1)-Ir(1)-H(1)	86.8(14)	P(1)-Ir(1)-H(1)	79.1(14)
P(2)-Ir(1)-H(1)	85.8(14)	Cl(1)-Ir(1)-H(1)	96.4(14)
Cl(2)-Ir(1)-H(1)	176.0(14)	C(26)-Ir(2)-C(30)	99.15(13)
C(26)-Ir(2)-C(25)	39.25(13)	C(30)-Ir(2)-C(25)	81.94(13)
C(26)-Ir(2)-C(29)	82.10(13)	C(30)-Ir(2)-C(29)	39.27(13)
C(25)-Ir(2)-C(29)	90.49(13)	C(26)-Ir(2)-Cl(1)	89.84(9)
C(30)-Ir(2)-Cl(1)	160.23(10)	C(25)-Ir(2)-Cl(1)	94.45(9)

C(29)-Ir(2)-Cl(1)	160.48(9)	C(26)-Ir(2)-Cl(2)	154.80(10)
C(30)-Ir(2)-Cl(2)	92.57(9)	C(25)-Ir(2)-Cl(2)	165.92(10)
C(29)-Ir(2)-Cl(2)	93.42(9)	Cl(1)-Ir(2)-Cl(2)	86.33(3)
C(7)-P(1)-Ir(1)	99.55(10)	C(9)-P(1)-Ir(1)	116.13(11)
C(13)-P(1)-Ir(1)	121.36(11)	C(8)-P(2)-Ir(1)	99.44(10)
C(21)-P(2)-Ir(1)	125.05(11)	C(17)-P(2)-Ir(1)	111.51(10)
Ir(2)-Cl(1)-Ir(1)	97.43(3)	Ir(2)-Cl(2)-Ir(1)	94.60(2)
C(6)-C(1)-Ir(1)	121.3(2)	C(2)-C(1)-Ir(1)	121.5(2)
C(26)-C(25)-Ir(2)	69.70(19)	C(32)-C(25)-Ir(2)	114.2(2)
Ir(2)-C(25)-H(25)	112(3)	C(25)-C(26)-Ir(2)	71.04(19)
C(27)-C(26)-Ir(2)	111.0(2)	Ir(2)-C(26)-H(26)	106(3)
C(30)-C(29)-Ir(2)	69.85(19)	C(28)-C(29)-Ir(2)	113.4(2)
Ir(2)-C(29)-H(29)	107(2)	C(29)-C(30)-Ir(2)	70.88(19)
C(31)-C(30)-Ir(2)	112.0(2)	Ir(2)-C(30)-H(30)	105(3)

The complex is best viewed as the di(chloride-bridged) mixed valence addition product of (PCP)IrHCl and "Ir(COD)Cl", where "Ir(COD)Cl" can be considered a monomeric unit of [Ir(COD)Cl]$_2$ which has been previously characterized crystallographically.[15] The hydride in **6** was found using electron difference maps. Because of its close proximity to the iridium atom, the hydride distance was restrained to 1.60 A, which is the Ir-H distance found by neutron diffraction in other iridium hydride complexes.[16-18]

The pincer bound Ir(1) atom is best considered as formally being in the +3 oxidation state. The Ir(1)-C(1) distance of 2.012(3) Å is similar to those found in other Ir(I) and Ir(III) PCP complexes.[19] Support for the character of the Ir(1) atom being in the +3 oxidation state comes from an examination of the Ir-P bond lengths. The Ir-P bond lengths of 2.326(1) Å and 2.328(1) Å are consistent with the Ir-P bond lengths of other PCP pincer complexes, where the Ir atom is in the +3 oxidation state and somewhat longer than the range of values (2.27 Å – 2.30 Å) reported for PCP pincer complexes, where the Ir atom is in the +1 oxidation state.[19] As with other (PCP)Ir complexes, the P-Ir-P angle is notably not linear, with both phosphorus atoms being bent away from the Cl ligand cis to the PCP aryl C-Ir bond. This results in a P(1)-Ir-P(2) angle of 158.83(3)° and P-Ir(1)-Cl(2) angles of 99.77(3)° and 96.29(3)°.

The COD-bound Ir(2) atom is best considered as being in the +1 oxidation state. If the centers of the coordinating C-C double bonds are considered to be single coordination points, the geometry around the Ir(2) atom can be viewed as square planar. The Ir(COD)Cl$_2$ portion of **6** has a geometry that is consistent with either Ir(COD)Cl$_2$ unit of the previously characterized [Ir(COD)Cl]$_2$. In [Ir(COD)Cl]$_2$, the dihedral angle

Ir(1)-Cl(1)-Cl(2)-Ir(2) is 86° and the Ir---Ir distance is 2.910(1) Å.[15] In **6,** the dihedral angle is only 13.04(4)° which corresponds to an increase in the Ir---Ir distance to 3.6754(2) Å. The significant difference in values between **6** and [Ir(COD)Cl]$_2$ most likely comes from the steric bulk of the ^{tBu}PCP ligand which inhibits folding about the Cl-Cl vector.

The Ir-Cl bond lengths for the trivalent Ir(1) are noticeably longer (average = 2.55 Å) than those for the monovalent Ir(2) (average = 2.40 Å) or those found in the [Ir(COD)Cl]$_2$ dimer (average = 2.40 Å),[15] where each iridium atom is in a monovalent state. The two Ir(2)-Cl distances are reasonably similar to each other (2.383(1) Å vs. 2.407(1) Å) a result of each chlorine atom being trans to a double bond on the symmetrical COD ligand. In contrast, the Ir(1)-Cl distances are distinctly different from each other. The Ir(1)-Cl(1) distance is 2.507(1) Å, while the Ir(1)-Cl(2) distance is much longer at 2.591(1) Å due to this chloride being opposite a hydride, which is a strong trans influence ligand.

Although there is ample room around the chlorides for weak inter and intra molecular interactions, very few occur. The shortest distance between a chloride and a hydrogen from a *tert*-butyl group is 2.66 Å from Cl(2) to H(16A). Given that the next shortest distances between a chloride and *tert*-butyl hydrogen are several that measure 2.79 Å, the Cl(2)---H(16A) interaction is noticeably shorter although it is unclear as to why this is the case. The hemi-hexane solvate appears to have no interactions with the chlorides in the dimer and only long H---H interactions with the other hydrogens in the molecule.

6.3 Conclusion

A side product in the synthesis of $(^{tBu}PCP)IrHCl$, $[(^{tBu}PCP)IrH(\mu^2\text{-}Cl)_2Ir(COD)]$ was isolated and characterized. The complex is an iridium (I)/(III) dimer. The Ir(I)-Cl bond lengths are significantly shorter than the Ir(III)-Cl bond lengths. The Ir(III)-Cl bond lengths are also noticeably different from each other with the Ir-Cl bond trans to carbon being shorter than the Ir-Cl bond trans to hydride, which is the result of hydride being a strong trans influence ligand. The dihedral angle Ir(1)-Cl(1)-Cl(2)-Ir(2) in $[(^{tBu}PCP)IrH(\mu^2\text{-}Cl)_2Ir(COD)]$ is only 13º, as compared with 86º for $[Ir(COD)Cl]_2$ which is most likely due to the steric bulk of the *tert*-butyl groups on the PCP ligand that prevents folding about the Cl---Cl vector.

6.4 Experimental

The synthesis was performed under an argon atmosphere using standard Schlenk and glove-box techniques. All solvents were purchased as anhydrous from Aldrich and degassed with argon. NMR spectra were recorded on a Varian 400-MHz spectrometer. ^{1}H NMR signals are calibrated using the residual proton peaks of the deuterated solvent (they are referenced to TMS). ^{31}P NMR signals are calibrated with an external reference, a capillary with a solution of para-xylene-d_{10} and PMe_3 (δ −62.4 ppm). X-ray diffraction by Dr. Thomas Emge (Rutgers) was obtained from an oil coated crystal mounted on a glass fiber. X-Ray intensity measurements were made using a Bruker-AXS Smart APEX

CCD diffractometer with graphite monochromatized Mo Kα radiation at 100 K. ^{tBu}PCP was synthesized according to a method published by Moulton and Shaw.[1]

[(^{tBu}PCP)IrH(μ²-Cl)₂Ir(COD)] (6): ^{tBu}PCP-H (2.000 g, 5.068 mmol) was dissolved in toluene (100 mL) and [Ir(COD)Cl]₂ (1.660 g, 2.472 mmol) was added. The resulting solution was refluxed under argon for 2 days after which time the solution was cooled to room temperature and the solvent removed by vacuum. Hexane (50 mL) was then added to the resulting solid. The red solution was pipetted away from the yellow insoluble material and filtered through glass wool before being placed in a freezer for one week. The resulting solid material (0.4299 g) contained large red crystals of **6** as well as a significant amount of microcrystalline (^{tBu}PCP)IrHCl. ^{1}H NMR (400 MHz, p-xylene-d$_{10}$): δ 3.953 (d, J = 7, 4H, COD), 3.291 (dt, J$_{P-H}$ = 16, J$_{H-H}$ = 3, 2H, CH₂), 2.857 (dt, J$_{P-H}$ = 16, J$_{H-H}$ = 4, 2H, CH₂), 1.733 (t, J = 6, 18H, *tert*-butyl), 1.220 (t, J = 6, 18H, *tert*-butyl), -25.732 (t, J$_{P-H}$ = 15, Hydride). ^{31}P{^{1}H) NMR (161 MHz, toluene-d$_{10}$): δ 67.754 (^{tBu}PCPIrHCl), 54.892 (**6**).

6.5 References

(1)   Moulton, C. J.; Shaw, B. L. *J. Chem. Soc. Dalt. Trans.* **1976**, *11*, 1020-1024.

(2)   Zhu, K.; Achord, P. D.; Zhang, X.; Krogh-Jespersen, K.; Goldman, A. S. *J. Am. Chem. Soc.* **2004**, *126*, 13044-13053.

(3)   Liu, F.; Pak, E. B.; Singh, B.; Jensen, C. M.; Goldman, A. S. *J. Am. Chem. Soc.* **1999**, *121*, 4086-4087.

(4)   Xu, W.-W.; Rosini, G. P.; Krogh-Jespersen, K.; Goldman, A. S.; Gupta, M.; Jensen, C. M.; Kaska, W. C. *Chem. Commun.* **1997**, *23*, 2273-2274.

(5)   Gupta, M.; Hagen, C.; Kaska, W. C.; Cramer, R. E.; Jensen, C. M. *J. Am. Chem. Soc.* **1997**, *119*, 840-841.

(6)   Gupta, M.; Hagen, C.; Flesher, R. J.; Kaska, W. C.; Jensen, C. M. *Chem. Commun.* **1996**, 2083-2084.

(7)   Kanzelberger, M.; Zhang, X.; Emge, T. J.; Goldman, A. S.; Zhao, J.; Incarvito, C.; Hartwig, J. F. *J. Am. Chem. Soc.* **2003**, *125*, 13644-13645.

(8)   van der Boom, M. E.; Milstein, D. *Chem. Rev.* **2003**, *103*, 1759-1792.

(9)   Ghosh, R.; Xiawei, Z.; Achord, P. D.; Emge, T. J.; Krogh-Jespersen, K.; Goldman, A. S. *J. Am. Chem. Soc.* **2007**, *129*, 853-866.

(10)   Goldman, A. S.; Roy, A. H.; Huang, Z.; Ahuja, R.; Schinski, W.; Brookhart, M. *Science* **2006**, *312*, 257-261.

(11)   Montag, M.; Schwartsburd, L.; Cohen, R.; Leitus, G.; Ben-David, Y.; Martin, J. M. L.; Milstein, D. *Angew. Chem. Int. Ed.* **2007**, *46*, 1901-1904.

(12)   Koridze, A. A.; Kuklin, S. A.; Sheloumov, A. M.; Dolgushin, F. M.; Lagunova, V. Y.; Petukhova, I. I.; Vorontsov, E. V.; Baya, M.; Poli, R. *Organometallics* **2004**, *23*, 4585-4593.

(13)   Gottker-Schnetmann, I.; White, P.; Brookhart, M. *J. Am. Chem. Soc.* **2004**, *126*, 1804-1811.

(14)   Zhang, X.; Emge, T. J.; Goldman, A. S. *Inorg. Chim. Acta.* **2004**, *357*, 3014-3018.

(15)   Cotton, F. A.; Lahuerta, P.; Sanau, M.; Schwotzer, W. *Inorg. Chim. Acta.* **1986**, *120*, 153-157.

(16)   Eckert, J.; Jensen, C. M.; Koetzle, T. F.; Husebo, T. L.; Nicol, J.; Wu, P. *J. Am. Chem. Soc.* **1995**, *117*, 7271-7272.

(17)   Bau, R.; Schwerdtfeger, C. J.; Garlaschelli, L.; Koetzle, T. F. *J. Chem. Soc., Dalt. Trans.: Inorg. Chem.* **1993**, *22*, 3359-3362.

(18)   Garlaschelli, L.; Khan, S. I.; Bau, R.; Longoni, G.; Koetzle, T. F. *J. Am. Chem. Soc.* **1985**, *107*, 7212-7213.

(19)   Pelczar, E. M.; Emge, T. J.; Goldman, A. S. *Acta Cryst. Sec. C* **2007**, *C63*, m323-m326.

Appendix

Full Cyrstallographic Details
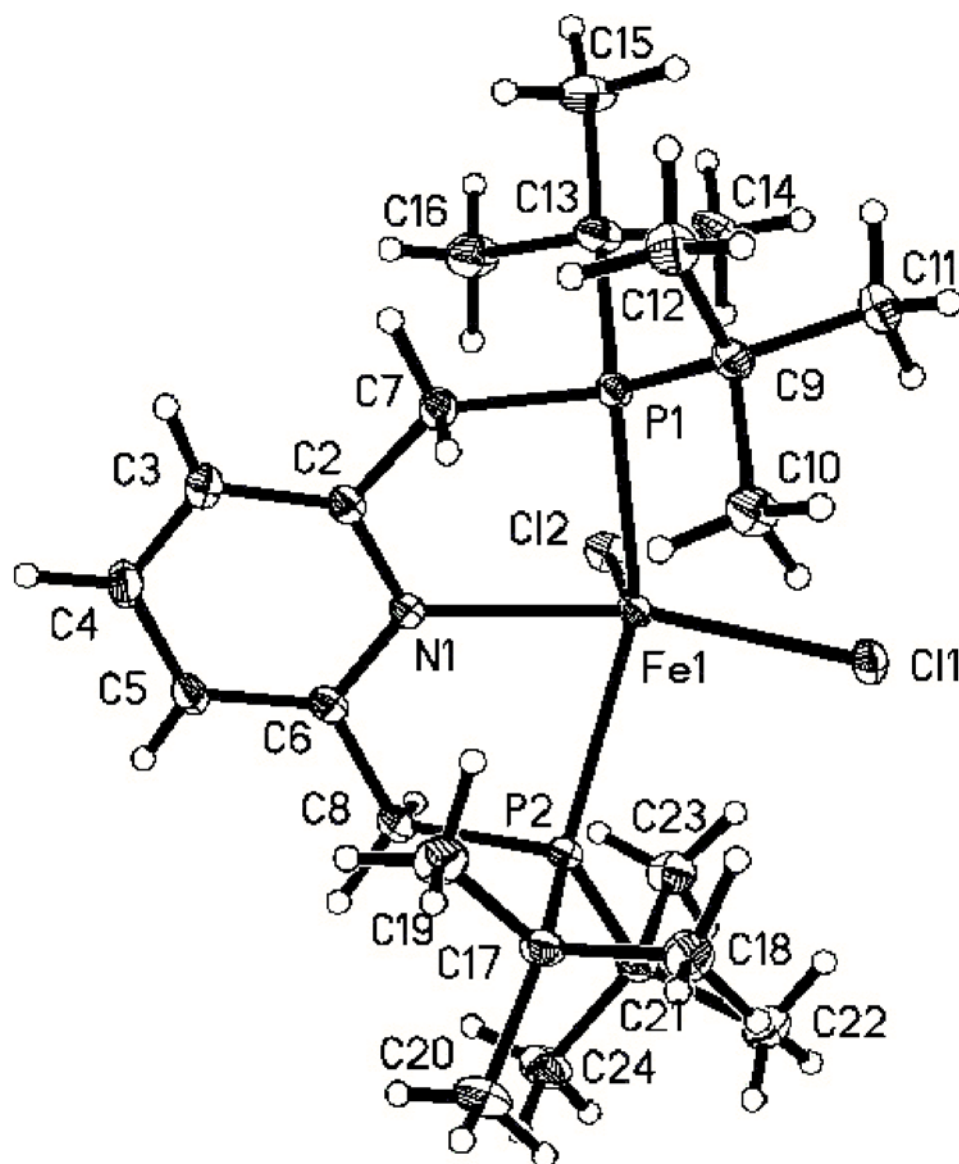
Table 1. Crystal data and structure refinement for Fe(PNP)Cl2.

Identification code	fecl2pnp
Empirical formula	C23 H43 Cl2 Fe N P2
Formula weight	522.27
Temperature	100(2) K
Wavelength	0.71073 Å
Crystal system	Monoclinic
Space group	P2(1)/n
Unit cell dimensions	a = 12.0831(9) Å $\alpha= 90°$.
	b = 15.5084(12) Å $\beta= 91.093(2)°$.
	c = 14.5049(11) Å $\gamma = 90°$.
Volume	2717.6(4) $Å^3$
Z	4
Density (calculated)	1.277 Mg/m^3
Absorption coefficient	0.880 mm^{-1}
F(000)	1112
Crystal size	0.21 x 0.06 x 0.03 mm^3
Theta range for data collection	1.92 to 30.57°.
Index ranges	-17<=h<=17, -22<=k<=22, -20<=l<=20
Reflections collected	31924
Independent reflections	8292 [R(int) = 0.0456]
Completeness to theta = 30.57°	99.4 %
Absorption correction	Semi-empirical from equivalents
Max. and min. transmission	0.9999 and 0.8338
Refinement method	Full-matrix least-squares on F^2
Data / restraints / parameters	8292 / 0 / 434
Goodness-of-fit on F^2	1.012
Final R indices [I>2sigma(I)]	R1 = 0.0349, wR2 = 0.0753
R indices (all data)	R1 = 0.0534, wR2 = 0.0823
Largest diff. peak and hole	0.618 and -0.300 e.$Å^{-3}$

Table 2. Atomic coordinates (x 10^4) and equivalent isotropic displacement parameters (Å^{2}x 10^3) for Fe(PNP)Cl2. U(eq) is defined as one third of the trace of the orthogonalized U^{ij} tensor.

	x	y	z	U(eq)
Fe(1)	8902(1)	1834(1)	2298(1)	13(1)
Cl(1)	8608(1)	2923(1)	3425(1)	20(1)
Cl(2)	8730(1)	2469(1)	867(1)	19(1)
P(1)	7206(1)	916(1)	2484(1)	13(1)
P(2)	10955(1)	1773(1)	2619(1)	13(1)
N(1)	9490(1)	482(1)	1808(1)	13(1)
C(2)	8794(1)	-194(1)	1749(1)	15(1)
C(3)	9046(1)	-930(1)	1246(1)	19(1)
C(4)	10064(1)	-988(1)	830(1)	20(1)
C(5)	10802(1)	-314(1)	935(1)	17(1)
C(6)	10498(1)	412(1)	1426(1)	14(1)
C(7)	7772(1)	-171(1)	2327(1)	17(1)
C(8)	11313(1)	1140(1)	1592(1)	16(1)
C(9)	6593(1)	837(1)	3661(1)	15(1)
C(10)	7587(2)	882(1)	4339(1)	21(1)
C(11)	5855(2)	1621(1)	3833(1)	21(1)
C(12)	5950(2)	6(1)	3844(1)	22(1)
C(13)	6114(1)	1012(1)	1552(1)	19(1)
C(14)	5786(2)	1964(1)	1461(1)	24(1)
C(15)	5083(2)	452(1)	1692(1)	26(1)
C(16)	6662(2)	723(1)	652(1)	26(1)
C(17)	11459(1)	1121(1)	3641(1)	18(1)
C(18)	11005(2)	1531(1)	4521(1)	24(1)
C(19)	10964(2)	211(1)	3560(1)	22(1)
C(20)	12720(2)	1040(1)	3730(1)	25(1)
C(21)	11799(1)	2785(1)	2480(1)	18(1)
C(22)	11831(2)	3290(1)	3385(1)	26(1)
C(23)	11167(2)	3335(1)	1764(1)	24(1)
C(24)	12976(2)	2632(1)	2138(2)	27(1)

Table 3.   Bond lengths [Å] and angles [°] for Fe(PNP)Cl2.

_____

Fe(1)-Cl(2)	2.3028(5)	C(11)-H(11C)	0.94(2)
Fe(1)-N(1)	2.3286(13)	C(12)-H(12A)	0.96(2)
Fe(1)-Cl(1)	2.3816(5)	C(12)-H(12B)	0.99(2)
Fe(1)-P(1)	2.5149(5)	C(12)-H(12C)	0.96(2)
Fe(1)-P(2)	2.5168(5)	C(13)-C(14)	1.533(3)
P(1)-C(7)	1.8351(16)	C(13)-C(15)	1.535(2)
P(1)-C(9)	1.8772(16)	C(13)-C(16)	1.541(2)
P(1)-C(13)	1.8774(17)	C(14)-H(14A)	0.97(2)
P(2)-C(8)	1.8438(17)	C(14)-H(14B)	0.97(2)
P(2)-C(21)	1.8843(17)	C(14)-H(14C)	0.943(19)
P(2)-C(17)	1.8851(17)	C(15)-H(15A)	0.998(19)
N(1)-C(2)	1.346(2)	C(15)-H(15B)	1.00(2)
N(1)-C(6)	1.3520(19)	C(15)-H(15C)	0.96(2)
C(2)-C(3)	1.392(2)	C(16)-H(16A)	0.98(2)
C(2)-C(7)	1.507(2)	C(16)-H(16B)	0.96(2)
C(3)-C(4)	1.383(2)	C(16)-H(16C)	0.98(2)
C(3)-H(3)	0.917(19)	C(17)-C(20)	1.531(2)
C(4)-C(5)	1.382(2)	C(17)-C(19)	1.537(2)
C(4)-H(4)	0.967(19)	C(17)-C(18)	1.538(2)
C(5)-C(6)	1.385(2)	C(18)-H(18A)	1.00(2)
C(5)-H(5)	0.912(19)	C(18)-H(18B)	1.02(2)
C(6)-C(8)	1.514(2)	C(18)-H(18C)	0.95(2)
C(7)-H(7A)	0.95(2)	C(19)-H(19A)	0.94(2)
C(7)-H(7B)	0.95(2)	C(19)-H(19B)	0.96(2)
C(8)-H(8A)	0.97(2)	C(19)-H(19C)	0.97(2)
C(8)-H(8B)	0.982(19)	C(20)-H(20A)	0.95(2)
C(9)-C(12)	1.531(2)	C(20)-H(20B)	0.93(2)
C(9)-C(11)	1.532(2)	C(20)-H(20C)	0.96(2)
C(9)-C(10)	1.539(2)	C(21)-C(22)	1.530(3)
C(10)-H(10A)	0.96(2)	C(21)-C(24)	1.533(2)
C(10)-H(10B)	0.96(2)	C(21)-C(23)	1.537(2)
C(10)-H(10C)	0.96(2)	C(22)-H(22A)	0.94(2)
C(11)-H(11A)	0.98(2)	C(22)-H(22B)	0.95(2)
C(11)-H(11B)	1.00(2)	C(22)-H(22C)	0.97(2)

C(23)-H(23A)	0.96(2)	C(24)-H(24A)	0.97(2)
C(23)-H(23B)	0.96(2)	C(24)-H(24B)	0.97(2)
C(23)-H(23C)	1.02(2)	C(24)-H(24C)	0.98(2)
Cl(2)-Fe(1)-N(1)	97.61(3)	C(5)-C(4)-H(4)	120.6(11)
Cl(2)-Fe(1)-Cl(1)	107.628(17)	C(3)-C(4)-H(4)	120.6(11)
N(1)-Fe(1)-Cl(1)	153.95(3)	C(4)-C(5)-C(6)	119.66(15)
Cl(2)-Fe(1)-P(1)	106.190(16)	C(4)-C(5)-H(5)	121.7(12)
N(1)-Fe(1)-P(1)	77.13(3)	C(6)-C(5)-H(5)	118.7(12)
Cl(1)-Fe(1)-P(1)	101.249(16)	N(1)-C(6)-C(5)	121.73(15)
Cl(2)-Fe(1)-P(2)	104.774(16)	N(1)-C(6)-C(8)	117.59(14)
N(1)-Fe(1)-P(2)	73.59(3)	C(5)-C(6)-C(8)	120.62(14)
Cl(1)-Fe(1)-P(2)	93.402(16)	C(2)-C(7)-P(1)	113.70(11)
P(1)-Fe(1)-P(2)	139.582(16)	C(2)-C(7)-H(7A)	105.7(12)
C(7)-P(1)-C(9)	101.98(7)	P(1)-C(7)-H(7A)	107.1(12)
C(7)-P(1)-C(13)	104.04(8)	C(2)-C(7)-H(7B)	110.1(12)
C(9)-P(1)-C(13)	112.11(7)	P(1)-C(7)-H(7B)	114.3(12)
C(7)-P(1)-Fe(1)	101.54(5)	H(7A)-C(7)-H(7B)	105.2(16)
C(9)-P(1)-Fe(1)	118.08(5)	C(6)-C(8)-P(2)	111.32(11)
C(13)-P(1)-Fe(1)	116.14(5)	C(6)-C(8)-H(8A)	109.3(12)
C(8)-P(2)-C(21)	102.74(7)	P(2)-C(8)-H(8A)	103.1(12)
C(8)-P(2)-C(17)	105.80(8)	C(6)-C(8)-H(8B)	109.7(11)
C(21)-P(2)-C(17)	111.33(7)	P(2)-C(8)-H(8B)	113.2(11)
C(8)-P(2)-Fe(1)	96.66(5)	H(8A)-C(8)-H(8B)	110.0(16)
C(21)-P(2)-Fe(1)	118.84(5)	C(12)-C(9)-C(11)	109.97(14)
C(17)-P(2)-Fe(1)	117.92(5)	C(12)-C(9)-C(10)	108.67(14)
C(2)-N(1)-C(6)	118.54(13)	C(11)-C(9)-C(10)	108.01(14)
C(2)-N(1)-Fe(1)	121.78(10)	C(12)-C(9)-P(1)	115.00(12)
C(6)-N(1)-Fe(1)	118.70(10)	C(11)-C(9)-P(1)	109.71(11)
N(1)-C(2)-C(3)	122.02(14)	C(10)-C(9)-P(1)	105.18(11)
N(1)-C(2)-C(7)	117.67(14)	C(9)-C(10)-H(10A)	110.0(12)
C(3)-C(2)-C(7)	120.02(14)	C(9)-C(10)-H(10B)	112.0(12)
C(4)-C(3)-C(2)	119.14(16)	H(10A)-C(10)-H(10B)	104.1(16)
C(4)-C(3)-H(3)	123.0(12)	C(9)-C(10)-H(10C)	111.6(12)
C(2)-C(3)-H(3)	117.8(12)	H(10A)-C(10)-H(10C)	105.5(16)
C(5)-C(4)-C(3)	118.72(15)	H(10B)-C(10)-H(10C)	113.2(16)

C(9)-C(11)-H(11A)	111.0(12)	C(20)-C(17)-C(19)	108.45(15)
C(9)-C(11)-H(11B)	109.2(12)	C(20)-C(17)-C(18)	109.54(14)
H(11A)-C(11)-H(11B)	109.7(17)	C(19)-C(17)-C(18)	107.36(15)
C(9)-C(11)-H(11C)	109.5(12)	C(20)-C(17)-P(2)	114.61(12)
H(11A)-C(11)-H(11C)	106.9(17)	C(19)-C(17)-P(2)	108.27(11)
H(11B)-C(11)-H(11C)	110.5(18)	C(18)-C(17)-P(2)	108.37(12)
C(9)-C(12)-H(12A)	108.1(12)	C(17)-C(18)-H(18A)	113.2(12)
C(9)-C(12)-H(12B)	113.3(12)	C(17)-C(18)-H(18B)	112.4(12)
H(12A)-C(12)-H(12B)	107.9(17)	H(18A)-C(18)-H(18B)	106.0(17)
C(9)-C(12)-H(12C)	112.8(12)	C(17)-C(18)-H(18C)	108.8(13)
H(12A)-C(12)-H(12C)	106.8(16)	H(18A)-C(18)-H(18C)	106.5(17)
H(12B)-C(12)-H(12C)	107.8(17)	H(18B)-C(18)-H(18C)	109.7(17)
C(14)-C(13)-C(15)	110.29(15)	C(17)-C(19)-H(19A)	109.5(14)
C(14)-C(13)-C(16)	108.82(15)	C(17)-C(19)-H(19B)	111.2(12)
C(15)-C(13)-C(16)	108.04(15)	H(19A)-C(19)-H(19B)	108.3(18)
C(14)-C(13)-P(1)	108.40(12)	C(17)-C(19)-H(19C)	113.6(12)
C(15)-C(13)-P(1)	114.86(12)	H(19A)-C(19)-H(19C)	104.9(18)
C(16)-C(13)-P(1)	106.22(11)	H(19B)-C(19)-H(19C)	108.9(16)
C(13)-C(14)-H(14A)	108.9(13)	C(17)-C(20)-H(20A)	108.8(13)
C(13)-C(14)-H(14B)	113.2(13)	C(17)-C(20)-H(20B)	112.3(13)
H(14A)-C(14)-H(14B)	107.1(18)	H(20A)-C(20)-H(20B)	108.8(18)
C(13)-C(14)-H(14C)	112.4(12)	C(17)-C(20)-H(20C)	111.1(12)
H(14A)-C(14)-H(14C)	107.1(17)	H(20A)-C(20)-H(20C)	107.6(18)
H(14B)-C(14)-H(14C)	107.9(17)	H(20B)-C(20)-H(20C)	108.1(18)
C(13)-C(15)-H(15A)	111.2(11)	C(22)-C(21)-C(24)	110.43(15)
C(13)-C(15)-H(15B)	110.9(11)	C(22)-C(21)-C(23)	107.41(15)
H(15A)-C(15)-H(15B)	110.3(15)	C(24)-C(21)-C(23)	108.62(15)
C(13)-C(15)-H(15C)	106.9(12)	C(22)-C(21)-P(2)	109.81(12)
H(15A)-C(15)-H(15C)	108.7(16)	C(24)-C(21)-P(2)	114.43(12)
H(15B)-C(15)-H(15C)	108.7(16)	C(23)-C(21)-P(2)	105.80(11)
C(13)-C(16)-H(16A)	105.1(12)	C(21)-C(22)-H(22A)	112.1(13)
C(13)-C(16)-H(16B)	112.7(13)	C(21)-C(22)-H(22B)	110.0(14)
H(16A)-C(16)-H(16B)	109.1(17)	H(22A)-C(22)-H(22B)	110.8(19)
C(13)-C(16)-H(16C)	113.2(12)	C(21)-C(22)-H(22C)	109.0(12)
H(16A)-C(16)-H(16C)	109.0(17)	H(22A)-C(22)-H(22C)	108.3(17)
H(16B)-C(16)-H(16C)	107.7(17)	H(22B)-C(22)-H(22C)	106.4(18)

C(21)-C(23)-H(23A)	110.6(12)
C(21)-C(23)-H(23B)	111.7(13)
H(23A)-C(23)-H(23B)	111.5(17)
C(21)-C(23)-H(23C)	107.5(11)
H(23A)-C(23)-H(23C)	108.4(16)
H(23B)-C(23)-H(23C)	106.9(16)
C(21)-C(24)-H(24A)	108.5(12)
C(21)-C(24)-H(24B)	110.4(13)
H(24A)-C(24)-H(24B)	106.6(17)
C(21)-C(24)-H(24C)	110.7(14)
H(24A)-C(24)-H(24C)	108.8(18)
H(24B)-C(24)-H(24C)	111.7(19)

Table 4.   Anisotropic displacement parameters (Å^2x 10^3) for Fe(PNP)Cl2. The anisotropic

displacement factor exponent takes the form: $-2\pi^2[\, h^2\, a^{*2}U^{11} + ... \; + 2\, h\, k\, a^*\, b^*\, U^{12}\,]$

	U^{11}	U^{22}	U^{33}	U^{23}	U^{13}	U^{12}
Fe(1)	10(1)	12(1)	16(1)	1(1)	1(1)	1(1)
Cl(1)	19(1)	15(1)	25(1)	-4(1)	2(1)	3(1)
Cl(2)	17(1)	20(1)	18(1)	4(1)	0(1)	0(1)
P(1)	11(1)	13(1)	14(1)	0(1)	2(1)	0(1)
P(2)	10(1)	14(1)	15(1)	-1(1)	0(1)	1(1)
N(1)	11(1)	13(1)	15(1)	-1(1)	0(1)	1(1)
C(2)	13(1)	15(1)	17(1)	0(1)	0(1)	2(1)
C(3)	20(1)	15(1)	22(1)	-3(1)	1(1)	0(1)
C(4)	21(1)	17(1)	21(1)	-4(1)	0(1)	5(1)
C(5)	15(1)	20(1)	15(1)	-1(1)	1(1)	5(1)
C(6)	13(1)	17(1)	14(1)	2(1)	0(1)	2(1)
C(7)	16(1)	13(1)	22(1)	-2(1)	3(1)	-1(1)
C(8)	11(1)	19(1)	19(1)	-1(1)	3(1)	1(1)
C(9)	14(1)	17(1)	16(1)	2(1)	3(1)	1(1)
C(10)	21(1)	26(1)	17(1)	3(1)	-1(1)	1(1)
C(11)	19(1)	22(1)	22(1)	-2(1)	5(1)	4(1)
C(12)	22(1)	20(1)	22(1)	4(1)	7(1)	-3(1)
C(13)	13(1)	27(1)	16(1)	2(1)	0(1)	-1(1)
C(14)	16(1)	32(1)	25(1)	8(1)	1(1)	6(1)
C(15)	16(1)	37(1)	24(1)	1(1)	-2(1)	-7(1)
C(16)	21(1)	38(1)	17(1)	-3(1)	0(1)	-4(1)
C(17)	14(1)	21(1)	18(1)	0(1)	-3(1)	2(1)
C(18)	24(1)	29(1)	18(1)	-1(1)	-1(1)	4(1)
C(19)	26(1)	21(1)	20(1)	4(1)	-5(1)	0(1)
C(20)	16(1)	32(1)	27(1)	5(1)	-4(1)	4(1)
C(21)	13(1)	17(1)	24(1)	0(1)	0(1)	-2(1)
C(22)	23(1)	22(1)	33(1)	-6(1)	-4(1)	-3(1)
C(23)	22(1)	18(1)	31(1)	5(1)	-2(1)	-3(1)
C(24)	15(1)	27(1)	40(1)	3(1)	4(1)	-3(1)

Table 5. Hydrogen coordinates (x 10^4) and isotropic displacement parameters ($Å^2$x 10 ^{3}) for Fe(PNP)Cl2.

	x	y	z	U(eq)
H(3)	8521(16)	-1356(13)	1206(13)	22(5)
H(4)	10266(16)	-1502(12)	494(13)	21(5)
H(5)	11491(16)	-333(12)	690(13)	19(5)
H(7A)	7999(16)	-375(12)	2920(14)	21(5)
H(7B)	7247(16)	-584(13)	2105(14)	27(5)
H(8A)	11242(16)	1554(13)	1097(14)	22(5)
H(8B)	12070(16)	908(12)	1619(13)	22(5)
H(10A)	7335(16)	865(12)	4960(14)	24(5)
H(10B)	7970(16)	1419(14)	4299(14)	26(5)
H(10C)	8063(16)	392(13)	4278(13)	24(5)
H(11A)	5185(17)	1601(13)	3444(14)	25(5)
H(11B)	6279(18)	2158(14)	3699(15)	33(6)
H(11C)	5626(16)	1618(13)	4447(15)	27(5)
H(12A)	5743(16)	4(13)	4482(14)	21(5)
H(12B)	6384(17)	-521(14)	3730(14)	31(6)
H(12C)	5274(17)	-33(13)	3483(14)	24(5)
H(14A)	5257(19)	2025(14)	949(16)	36(6)
H(14B)	6410(19)	2341(14)	1333(15)	35(6)
H(14C)	5438(16)	2174(12)	1993(14)	19(5)
H(15A)	4659(15)	649(12)	2237(13)	18(5)
H(15B)	5291(16)	-172(13)	1761(13)	23(5)
H(15C)	4622(17)	516(13)	1147(14)	27(5)
H(16A)	6116(17)	851(14)	162(15)	33(6)
H(16B)	6824(17)	119(15)	645(14)	29(6)
H(16C)	7351(18)	1034(14)	526(14)	33(6)
H(18A)	10189(18)	1637(13)	4486(14)	29(5)
H(18B)	11361(18)	2116(15)	4665(15)	34(6)
H(18C)	11131(17)	1147(14)	5025(15)	30(6)
H(19A)	11134(18)	-104(15)	4098(16)	38(6)
H(19B)	11258(16)	-95(13)	3041(14)	22(5)

H(19C)	10163(18)	205(13)	3513(14)	28(5)
H(20A)	12896(18)	645(15)	4215(16)	35(6)
H(20B)	13059(17)	1564(14)	3858(14)	29(6)
H(20C)	13026(16)	815(13)	3176(14)	25(5)
H(22A)	12303(18)	3033(14)	3831(16)	35(6)
H(22B)	11106(19)	3350(14)	3612(16)	36(6)
H(22C)	12095(16)	3867(14)	3268(14)	26(5)
H(23A)	10452(17)	3492(13)	1987(14)	25(5)
H(23B)	11110(17)	3052(13)	1179(15)	28(6)
H(23C)	11612(16)	3884(13)	1667(14)	25(5)
H(24A)	13337(17)	3188(14)	2069(14)	28(6)
H(24B)	12954(18)	2369(15)	1532(16)	37(6)
H(24C)	13405(19)	2283(15)	2583(16)	41(6)

Table 6. Torsion angles [°] for Fe(PNP)Cl2.

Cl(2)-Fe(1)-P(1)-C(7)	105.57(6)
N(1)-Fe(1)-P(1)-C(7)	11.26(7)
Cl(1)-Fe(1)-P(1)-C(7)	-142.14(6)
P(2)-Fe(1)-P(1)-C(7)	-33.06(7)
Cl(2)-Fe(1)-P(1)-C(9)	-144.00(6)
N(1)-Fe(1)-P(1)-C(9)	121.70(7)
Cl(1)-Fe(1)-P(1)-C(9)	-31.71(6)
P(2)-Fe(1)-P(1)-C(9)	77.37(6)
Cl(2)-Fe(1)-P(1)-C(13)	-6.51(6)
N(1)-Fe(1)-P(1)-C(13)	-100.82(7)
Cl(1)-Fe(1)-P(1)-C(13)	105.78(6)
P(2)-Fe(1)-P(1)-C(13)	-145.14(6)
Cl(2)-Fe(1)-P(2)-C(8)	-57.79(6)
N(1)-Fe(1)-P(2)-C(8)	35.94(6)
Cl(1)-Fe(1)-P(2)-C(8)	-167.03(6)
P(1)-Fe(1)-P(2)-C(8)	81.18(6)
Cl(2)-Fe(1)-P(2)-C(21)	50.74(6)
N(1)-Fe(1)-P(2)-C(21)	144.47(7)
Cl(1)-Fe(1)-P(2)-C(21)	-58.50(6)
P(1)-Fe(1)-P(2)-C(21)	-170.29(6)
Cl(2)-Fe(1)-P(2)-C(17)	-169.64(6)
N(1)-Fe(1)-P(2)-C(17)	-75.91(7)
Cl(1)-Fe(1)-P(2)-C(17)	81.13(6)
P(1)-Fe(1)-P(2)-C(17)	-30.66(7)
Cl(2)-Fe(1)-N(1)-C(2)	-100.96(11)
Cl(1)-Fe(1)-N(1)-C(2)	93.31(13)
P(1)-Fe(1)-N(1)-C(2)	3.99(11)
P(2)-Fe(1)-N(1)-C(2)	155.81(12)
Cl(2)-Fe(1)-N(1)-C(6)	67.57(11)
Cl(1)-Fe(1)-N(1)-C(6)	-98.16(12)
P(1)-Fe(1)-N(1)-C(6)	172.52(11)
P(2)-Fe(1)-N(1)-C(6)	-35.66(10)
C(6)-N(1)-C(2)-C(3)	-5.2(2)

Fe(1)-N(1)-C(2)-C(3)	163.34(12)
C(6)-N(1)-C(2)-C(7)	168.58(14)
Fe(1)-N(1)-C(2)-C(7)	-22.87(19)
N(1)-C(2)-C(3)-C(4)	3.1(3)
C(7)-C(2)-C(3)-C(4)	-170.52(15)
C(2)-C(3)-C(4)-C(5)	0.5(3)
C(3)-C(4)-C(5)-C(6)	-1.9(2)
C(2)-N(1)-C(6)-C(5)	3.7(2)
Fe(1)-N(1)-C(6)-C(5)	-165.18(12)
C(2)-N(1)-C(6)-C(8)	-173.33(14)
Fe(1)-N(1)-C(6)-C(8)	17.76(18)
C(4)-C(5)-C(6)-N(1)	-0.2(2)
C(4)-C(5)-C(6)-C(8)	176.79(15)
N(1)-C(2)-C(7)-P(1)	33.51(19)
C(3)-C(2)-C(7)-P(1)	-152.57(13)
C(9)-P(1)-C(7)-C(2)	-148.41(12)
C(13)-P(1)-C(7)-C(2)	94.87(13)
Fe(1)-P(1)-C(7)-C(2)	-26.10(13)
N(1)-C(6)-C(8)-P(2)	21.16(18)
C(5)-C(6)-C(8)-P(2)	-155.93(13)
C(21)-P(2)-C(8)-C(6)	-164.36(11)
C(17)-P(2)-C(8)-C(6)	78.79(12)
Fe(1)-P(2)-C(8)-C(6)	-42.74(11)
C(7)-P(1)-C(9)-C(12)	-43.06(14)
C(13)-P(1)-C(9)-C(12)	67.66(14)
Fe(1)-P(1)-C(9)-C(12)	-153.25(10)
C(7)-P(1)-C(9)-C(11)	-167.62(12)
C(13)-P(1)-C(9)-C(11)	-56.90(13)
Fe(1)-P(1)-C(9)-C(11)	82.19(12)
C(7)-P(1)-C(9)-C(10)	76.43(12)
C(13)-P(1)-C(9)-C(10)	-172.85(11)
Fe(1)-P(1)-C(9)-C(10)	-33.76(12)
C(7)-P(1)-C(13)-C(14)	-166.07(11)
C(9)-P(1)-C(13)-C(14)	84.51(13)
Fe(1)-P(1)-C(13)-C(14)	-55.43(12)
C(7)-P(1)-C(13)-C(15)	70.08(14)

C(9)-P(1)-C(13)-C(15)	-39.34(15)
Fe(1)-P(1)-C(13)-C(15)	-179.28(11)
C(7)-P(1)-C(13)-C(16)	-49.27(14)
C(9)-P(1)-C(13)-C(16)	-158.69(12)
Fe(1)-P(1)-C(13)-C(16)	61.37(13)
C(8)-P(2)-C(17)-C(20)	67.31(14)
C(21)-P(2)-C(17)-C(20)	-43.58(15)
Fe(1)-P(2)-C(17)-C(20)	173.95(11)
C(8)-P(2)-C(17)-C(19)	-53.87(13)
C(21)-P(2)-C(17)-C(19)	-164.77(11)
Fe(1)-P(2)-C(17)-C(19)	52.77(13)
C(8)-P(2)-C(17)-C(18)	-170.03(12)
C(21)-P(2)-C(17)-C(18)	79.08(13)
Fe(1)-P(2)-C(17)-C(18)	-63.39(13)
C(8)-P(2)-C(21)-C(22)	-165.99(12)
C(17)-P(2)-C(21)-C(22)	-53.16(14)
Fe(1)-P(2)-C(21)-C(22)	88.92(12)
C(8)-P(2)-C(21)-C(24)	-41.17(15)
C(17)-P(2)-C(21)-C(24)	71.67(15)
Fe(1)-P(2)-C(21)-C(24)	-146.25(12)
C(8)-P(2)-C(21)-C(23)	78.37(13)
C(17)-P(2)-C(21)-C(23)	-168.79(12)
Fe(1)-P(2)-C(21)-C(23)	-26.71(14)
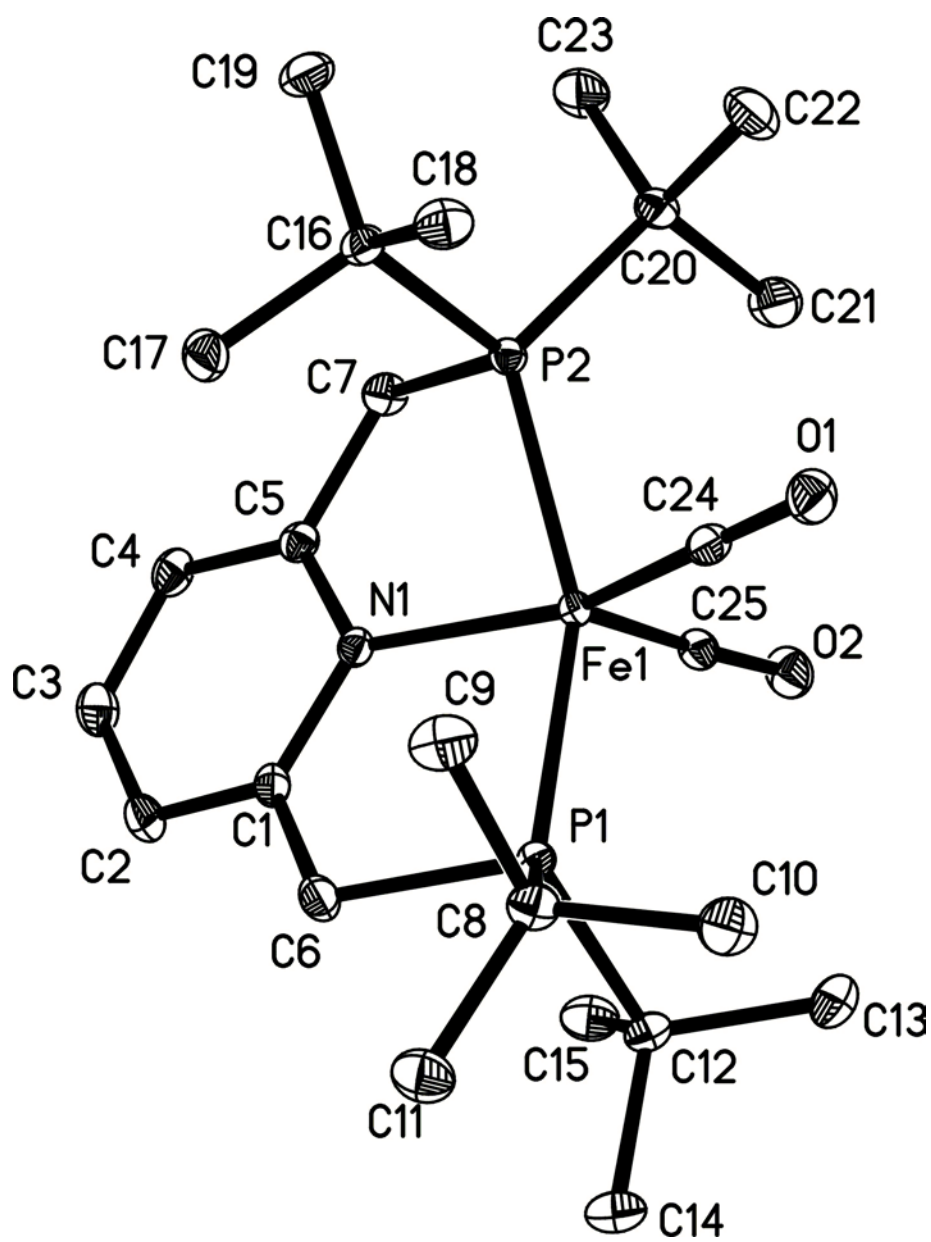
Table 1. Crystal data and structure refinement for PNP-Fe(CO)2.

Identification code	fehco
Empirical formula	C25 H43 Fe N O2 P2
Formula weight	507.39
Temperature	100(2) K
Wavelength	0.71073 Å
Crystal system	Orthorhombic
Space group	P2(1)2(1)2(1)
Unit cell dimensions	a = 11.7404(12) Å $\alpha= 90°$.
	b = 14.5944(14) Å $\beta= 90°$.
	c = 15.3327(15) Å $\gamma = 90°$.
Volume	2627.2(4) Å^3
Z	4
Density (calculated)	1.283 Mg/m^3
Absorption coefficient	0.717 mm^{-1}
F(000)	1088
Crystal size	0.29 x 0.25 x 0.18 mm^3
Theta range for data collection	1.93 to 30.56°.
Index ranges	-16<=h<=16, -20<=k<=20, -21<=l<=21
Reflections collected	31387
Independent reflections	8025 [R(int) = 0.0228]
Completeness to theta = 30.56°	99.9 %
Absorption correction	Semi-empirical from equivalents
Max. and min. transmission	0.9999 and 0.9146
Refinement method	Full-matrix least-squares on F^2
Data / restraints / parameters	8025 / 0 / 335
Goodness-of-fit on F^2	1.041
Final R indices [I>2sigma(I)]	R1 = 0.0219, wR2 = 0.0561
R indices (all data)	R1 = 0.0230, wR2 = 0.0565
Absolute structure parameter	0.002(6)
Largest diff. peak and hole	0.362 and -0.180 e.Å^{-3}

Table 2. Atomic coordinates (x 10^4) and equivalent isotropic displacement parameters ($Å^2$x 10^3) for PNP-Fe(CO)2. U(eq) is defined as one third of the trace of the orthogonalized U^{ij} tensor.

	x	y	z	U(eq)
Fe(1)	3493(1)	4841(1)	9565(1)	9(1)
P(1)	2067(1)	5699(1)	9055(1)	10(1)
P(2)	5170(1)	4168(1)	9449(1)	10(1)
N(1)	3159(1)	4041(1)	8496(1)	10(1)
C(1)	2293(1)	4234(1)	7931(1)	12(1)
C(2)	1947(1)	3624(1)	7289(1)	16(1)
C(3)	2524(1)	2802(1)	7180(1)	17(1)
C(4)	3448(1)	2624(1)	7717(1)	16(1)
C(5)	3742(1)	3242(1)	8367(1)	12(1)
C(6)	1801(1)	5174(1)	7981(1)	14(1)
C(7)	4723(1)	3068(1)	8967(1)	14(1)
C(8)	2292(1)	6946(1)	8743(1)	13(1)
C(9)	3489(1)	7025(1)	8344(1)	19(1)
C(10)	2236(1)	7554(1)	9555(1)	19(1)
C(11)	1447(1)	7309(1)	8056(1)	19(1)
C(12)	639(1)	5577(1)	9622(1)	14(1)
C(13)	767(1)	5821(1)	10594(1)	20(1)
C(14)	-346(1)	6139(1)	9240(1)	19(1)
C(15)	310(1)	4556(1)	9548(1)	19(1)
C(16)	6179(1)	4661(1)	8607(1)	13(1)
C(17)	5556(1)	4679(1)	7724(1)	18(1)
C(18)	6463(1)	5661(1)	8835(1)	17(1)
C(19)	7292(1)	4124(1)	8485(1)	19(1)
C(20)	6023(1)	3804(1)	10437(1)	14(1)
C(21)	5177(1)	3552(1)	11164(1)	24(1)
C(22)	6769(1)	4589(1)	10781(1)	22(1)
C(23)	6768(1)	2949(1)	10267(1)	22(1)
C(24)	4126(1)	5771(1)	10071(1)	13(1)
O(1)	4551(1)	6377(1)	10452(1)	18(1)
C(25)	2844(1)	4198(1)	10409(1)	13(1)
O(2)	2449(1)	3862(1)	11030(1)	19(1)

Table 3.   Bond lengths [Å] and angles [°] for PNP-Fe(CO)2.

_____

Fe(1)-C(24)	1.7310(12)	C(10)-H(10C)	0.9800
Fe(1)-C(25)	1.7708(12)	C(11)-H(11A)	0.9800
Fe(1)-N(1)	2.0503(9)	C(11)-H(11B)	0.9800
Fe(1)-P(2)	2.2066(4)	C(11)-H(11C)	0.9800
Fe(1)-P(1)	2.2322(3)	C(12)-C(14)	1.5340(16)
P(1)-C(6)	1.8427(11)	C(12)-C(13)	1.5404(17)
P(1)-C(12)	1.8974(11)	C(12)-C(15)	1.5428(16)
P(1)-C(8)	1.8985(12)	C(13)-H(13A)	0.9800
P(2)-C(7)	1.8439(12)	C(13)-H(13B)	0.9800
P(2)-C(20)	1.8930(12)	C(13)-H(13C)	0.9800
P(2)-C(16)	1.8939(12)	C(14)-H(14A)	0.9800
N(1)-C(1)	1.3648(14)	C(14)-H(14B)	0.9800
N(1)-C(5)	1.3664(14)	C(14)-H(14C)	0.9800
C(1)-C(2)	1.3885(16)	C(15)-H(15A)	0.9800
C(1)-C(6)	1.4905(16)	C(15)-H(15B)	0.9800
C(2)-C(3)	1.3878(17)	C(15)-H(15C)	0.9800
C(2)-H(2)	0.9500	C(16)-C(19)	1.5342(16)
C(3)-C(4)	1.3859(18)	C(16)-C(18)	1.5370(16)
C(3)-H(3)	0.9500	C(16)-C(17)	1.5399(16)
C(4)-C(5)	1.3871(15)	C(17)-H(17A)	0.9800
C(4)-H(4)	0.9500	C(17)-H(17B)	0.9800
C(5)-C(7)	1.4965(16)	C(17)-H(17C)	0.9800
C(6)-H(6A)	0.9900	C(18)-H(18A)	0.9800
C(6)-H(6B)	0.9900	C(18)-H(18B)	0.9800
C(7)-H(7A)	0.9900	C(18)-H(18C)	0.9800
C(7)-H(7B)	0.9900	C(19)-H(19A)	0.9800
C(8)-C(10)	1.5296(17)	C(19)-H(19B)	0.9800
C(8)-C(9)	1.5375(17)	C(19)-H(19C)	0.9800
C(8)-C(11)	1.5413(16)	C(20)-C(22)	1.5365(17)
C(9)-H(9A)	0.9800	C(20)-C(21)	1.5377(17)
C(9)-H(9B)	0.9800	C(20)-C(23)	1.5452(16)
C(9)-H(9C)	0.9800	C(21)-H(21A)	0.9800
C(10)-H(10A)	0.9800	C(21)-H(21B)	0.9800
C(10)-H(10B)	0.9800	C(21)-H(21C)	0.9800

C(22)-H(22A)	0.9800	C(23)-H(23B)	0.9800
C(22)-H(22B)	0.9800	C(23)-H(23C)	0.9800
C(22)-H(22C)	0.9800	C(24)-O(1)	1.1717(14)
C(23)-H(23A)	0.9800	C(25)-O(2)	1.1679(14)
C(24)-Fe(1)-C(25)	105.78(5)	C(4)-C(3)-C(2)	118.15(11)
C(24)-Fe(1)-N(1)	152.52(5)	C(4)-C(3)-H(3)	120.9
C(25)-Fe(1)-N(1)	101.57(4)	C(2)-C(3)-H(3)	120.9
C(24)-Fe(1)-P(2)	90.13(4)	C(3)-C(4)-C(5)	120.01(11)
C(25)-Fe(1)-P(2)	101.94(4)	C(3)-C(4)-H(4)	120.0
N(1)-Fe(1)-P(2)	81.55(3)	C(5)-C(4)-H(4)	120.0
C(24)-Fe(1)-P(1)	92.21(4)	N(1)-C(5)-C(4)	122.26(11)
C(25)-Fe(1)-P(1)	103.35(4)	N(1)-C(5)-C(7)	116.23(10)
N(1)-Fe(1)-P(1)	84.04(3)	C(4)-C(5)-C(7)	121.51(10)
P(2)-Fe(1)-P(1)	152.917(13)	C(1)-C(6)-P(1)	111.32(7)
C(6)-P(1)-C(12)	102.72(5)	C(1)-C(6)-H(6A)	109.4
C(6)-P(1)-C(8)	101.37(5)	P(1)-C(6)-H(6A)	109.4
C(12)-P(1)-C(8)	109.18(5)	C(1)-C(6)-H(6B)	109.4
C(6)-P(1)-Fe(1)	101.92(4)	P(1)-C(6)-H(6B)	109.4
C(12)-P(1)-Fe(1)	116.69(4)	H(6A)-C(6)-H(6B)	108.0
C(8)-P(1)-Fe(1)	121.45(4)	C(5)-C(7)-P(2)	108.48(8)
C(7)-P(2)-C(20)	103.07(5)	C(5)-C(7)-H(7A)	110.0
C(7)-P(2)-C(16)	103.63(5)	P(2)-C(7)-H(7A)	110.0
C(20)-P(2)-C(16)	108.70(5)	C(5)-C(7)-H(7B)	110.0
C(7)-P(2)-Fe(1)	99.58(4)	P(2)-C(7)-H(7B)	110.0
C(20)-P(2)-Fe(1)	122.20(4)	H(7A)-C(7)-H(7B)	108.4
C(16)-P(2)-Fe(1)	116.38(4)	C(10)-C(8)-C(9)	108.60(10)
C(1)-N(1)-C(5)	117.24(9)	C(10)-C(8)-C(11)	109.19(10)
C(1)-N(1)-Fe(1)	122.15(7)	C(9)-C(8)-C(11)	106.84(10)
C(5)-N(1)-Fe(1)	120.37(7)	C(10)-C(8)-P(1)	110.21(8)
N(1)-C(1)-C(2)	122.33(11)	C(9)-C(8)-P(1)	107.42(8)
N(1)-C(1)-C(6)	116.48(10)	C(11)-C(8)-P(1)	114.37(8)
C(2)-C(1)-C(6)	120.96(10)	C(8)-C(9)-H(9A)	109.5
C(3)-C(2)-C(1)	119.83(11)	C(8)-C(9)-H(9B)	109.5
C(3)-C(2)-H(2)	120.1	H(9A)-C(9)-H(9B)	109.5
C(1)-C(2)-H(2)	120.1	C(8)-C(9)-H(9C)	109.5

H(9A)-C(9)-H(9C)	109.5	H(15A)-C(15)-H(15C)	109.5
H(9B)-C(9)-H(9C)	109.5	H(15B)-C(15)-H(15C)	109.5
C(8)-C(10)-H(10A)	109.5	C(19)-C(16)-C(18)	109.15(10)
C(8)-C(10)-H(10B)	109.5	C(19)-C(16)-C(17)	107.80(10)
H(10A)-C(10)-H(10B)	109.5	C(18)-C(16)-C(17)	106.62(9)
C(8)-C(10)-H(10C)	109.5	C(19)-C(16)-P(2)	114.97(8)
H(10A)-C(10)-H(10C)	109.5	C(18)-C(16)-P(2)	109.96(8)
H(10B)-C(10)-H(10C)	109.5	C(17)-C(16)-P(2)	107.99(8)
C(8)-C(11)-H(11A)	109.5	C(16)-C(17)-H(17A)	109.5
C(8)-C(11)-H(11B)	109.5	C(16)-C(17)-H(17B)	109.5
H(11A)-C(11)-H(11B)	109.5	H(17A)-C(17)-H(17B)	109.5
C(8)-C(11)-H(11C)	109.5	C(16)-C(17)-H(17C)	109.5
H(11A)-C(11)-H(11C)	109.5	H(17A)-C(17)-H(17C)	109.5
H(11B)-C(11)-H(11C)	109.5	H(17B)-C(17)-H(17C)	109.5
C(14)-C(12)-C(13)	108.59(9)	C(16)-C(18)-H(18A)	109.5
C(14)-C(12)-C(15)	107.44(9)	C(16)-C(18)-H(18B)	109.5
C(13)-C(12)-C(15)	108.62(11)	H(18A)-C(18)-H(18B)	109.5
C(14)-C(12)-P(1)	116.19(8)	C(16)-C(18)-H(18C)	109.5
C(13)-C(12)-P(1)	109.57(8)	H(18A)-C(18)-H(18C)	109.5
C(15)-C(12)-P(1)	106.19(8)	H(18B)-C(18)-H(18C)	109.5
C(12)-C(13)-H(13A)	109.5	C(16)-C(19)-H(19A)	109.5
C(12)-C(13)-H(13B)	109.5	C(16)-C(19)-H(19B)	109.5
H(13A)-C(13)-H(13B)	109.5	H(19A)-C(19)-H(19B)	109.5
C(12)-C(13)-H(13C)	109.5	C(16)-C(19)-H(19C)	109.5
H(13A)-C(13)-H(13C)	109.5	H(19A)-C(19)-H(19C)	109.5
H(13B)-C(13)-H(13C)	109.5	H(19B)-C(19)-H(19C)	109.5
C(12)-C(14)-H(14A)	109.5	C(22)-C(20)-C(21)	107.32(11)
C(12)-C(14)-H(14B)	109.5	C(22)-C(20)-C(23)	109.74(10)
H(14A)-C(14)-H(14B)	109.5	C(21)-C(20)-C(23)	107.18(10)
C(12)-C(14)-H(14C)	109.5	C(22)-C(20)-P(2)	111.53(8)
H(14A)-C(14)-H(14C)	109.5	C(21)-C(20)-P(2)	107.75(8)
H(14B)-C(14)-H(14C)	109.5	C(23)-C(20)-P(2)	113.04(8)
C(12)-C(15)-H(15A)	109.5	C(20)-C(21)-H(21A)	109.5
C(12)-C(15)-H(15B)	109.5	C(20)-C(21)-H(21B)	109.5
H(15A)-C(15)-H(15B)	109.5	H(21A)-C(21)-H(21B)	109.5
C(12)-C(15)-H(15C)	109.5	C(20)-C(21)-H(21C)	109.5

H(21A)-C(21)-H(21C)	109.5	C(20)-C(23)-H(23A)	109.5
H(21B)-C(21)-H(21C)	109.5	C(20)-C(23)-H(23B)	109.5
C(20)-C(22)-H(22A)	109.5	H(23A)-C(23)-H(23B)	109.5
C(20)-C(22)-H(22B)	109.5	C(20)-C(23)-H(23C)	109.5
H(22A)-C(22)-H(22B)	109.5	H(23A)-C(23)-H(23C)	109.5
C(20)-C(22)-H(22C)	109.5	H(23B)-C(23)-H(23C)	109.5
H(22A)-C(22)-H(22C)	109.5	O(1)-C(24)-Fe(1)	176.68(10)
H(22B)-C(22)-H(22C)	109.5	O(2)-C(25)-Fe(1)	171.87(10)

Table 4.   Anisotropic displacement parameters (Å^2x 10^3) for PNP-Fe(CO)2. The anisotropic
displacement factor exponent takes the form: $-2\pi^2[\ h^2\ a^{*2}U^{11} + ... \ + 2\ h\ k\ a^*\ b^*\ U^{12}\ ]$

	U^{11}	U^{22}	U^{33}	U^{23}	U^{13}	U^{12}
Fe(1)	9(1)	10(1)	9(1)	-1(1)	0(1)	0(1)
P(1)	9(1)	10(1)	10(1)	-1(1)	0(1)	0(1)
P(2)	10(1)	10(1)	10(1)	0(1)	0(1)	0(1)
N(1)	11(1)	11(1)	9(1)	-1(1)	1(1)	-1(1)
C(1)	13(1)	14(1)	9(1)	-1(1)	1(1)	-1(1)
C(2)	18(1)	19(1)	12(1)	-2(1)	-3(1)	-1(1)
C(3)	22(1)	16(1)	15(1)	-4(1)	-1(1)	-3(1)
C(4)	18(1)	13(1)	16(1)	-4(1)	3(1)	-1(1)
C(5)	11(1)	12(1)	13(1)	0(1)	2(1)	-2(1)
C(6)	16(1)	15(1)	11(1)	-1(1)	-3(1)	1(1)
C(7)	14(1)	9(1)	17(1)	-2(1)	-1(1)	1(1)
C(8)	14(1)	10(1)	16(1)	1(1)	-1(1)	1(1)
C(9)	17(1)	17(1)	25(1)	6(1)	3(1)	0(1)
C(10)	20(1)	13(1)	23(1)	-4(1)	-2(1)	1(1)
C(11)	19(1)	17(1)	21(1)	5(1)	-2(1)	2(1)
C(12)	10(1)	15(1)	16(1)	0(1)	2(1)	1(1)
C(13)	19(1)	25(1)	17(1)	-1(1)	5(1)	2(1)
C(14)	12(1)	21(1)	25(1)	1(1)	0(1)	3(1)
C(15)	13(1)	18(1)	25(1)	3(1)	-1(1)	-3(1)
C(16)	10(1)	15(1)	14(1)	-1(1)	2(1)	-1(1)
C(17)	17(1)	23(1)	13(1)	2(1)	1(1)	-4(1)
C(18)	14(1)	14(1)	22(1)	0(1)	1(1)	-2(1)
C(19)	13(1)	22(1)	21(1)	-2(1)	3(1)	2(1)
C(20)	13(1)	18(1)	13(1)	2(1)	-2(1)	3(1)
C(21)	20(1)	34(1)	16(1)	8(1)	1(1)	4(1)
C(22)	20(1)	24(1)	21(1)	-2(1)	-8(1)	1(1)
C(23)	21(1)	21(1)	23(1)	2(1)	-4(1)	8(1)
C(24)	11(1)	15(1)	13(1)	0(1)	1(1)	2(1)
O(1)	17(1)	18(1)	18(1)	-5(1)	1(1)	-3(1)
C(25)	13(1)	14(1)	13(1)	-2(1)	-2(1)	0(1)
O(2)	19(1)	24(1)	15(1)	4(1)	1(1)	-4(1)

Table 5. Hydrogen coordinates (x 10^4) and isotropic displacement parameters (Å^2x 10^3)
for PNP-Fe(CO)2.

	x	y	z	U(eq)
H(2)	1317	3768	6925	18(4)
H(3)	2293	2373	6749	29(4)
H(4)	3879	2079	7641	21(4)
H(6A)	970	5144	7876	15(3)
H(6B)	2143	5562	7520	13(3)
H(7A)	5364	2792	8639	23(4)
H(7B)	4493	2637	9433	24(4)
H(9A)	3628	7661	8168	22(4)
H(9B)	3543	6625	7832	34(5)
H(9C)	4059	6840	8777	21(4)
H(10A)	2535	8163	9415	33(5)
H(10B)	2695	7280	10021	20(4)
H(10C)	1444	7608	9748	15(4)
H(11A)	668	7256	8280	20(4)
H(11B)	1520	6949	7519	36(5)
H(11C)	1617	7954	7931	33(5)
H(13A)	910	6480	10653	33(5)
H(13B)	1407	5479	10843	28(4)
H(13C)	66	5661	10905	34(5)
H(14A)	-1062	5954	9519	19(4)
H(14B)	-396	6029	8611	28(4)
H(14C)	-211	6791	9348	20(4)
H(15A)	-324	4425	9944	15(4)
H(15B)	966	4175	9706	31(5)
H(15C)	81	4420	8947	30(4)
H(17A)	6026	5002	7293	19(4)
H(17B)	4826	4997	7789	26(4)
H(17C)	5421	4050	7526	25(4)
H(18A)	6854	5683	9399	18(4)
H(18B)	5757	6018	8868	24(4)

H(18C)	6958	5919	8383	27(4)
H(19A)	7709	4372	7984	34(5)
H(19B)	7116	3477	8381	24(4)
H(19C)	7760	4182	9011	40(5)
H(21A)	5596	3331	11675	23(4)
H(21B)	4663	3070	10955	31(5)
H(21C)	4731	4094	11323	40(5)
H(22A)	6308	5146	10837	24(4)
H(22B)	7397	4701	10374	27(4)
H(22C)	7079	4422	11353	27(4)
H(23A)	7328	3088	9812	35(5)
H(23B)	6283	2440	10076	31(5)
H(23C)	7165	2777	10805	39(5)

Table 6. Torsion angles [°] for PNP-Fe(CO)2.

_____

C(24)-Fe(1)-P(1)-C(6)	144.06(5)	C(5)-N(1)-C(1)-C(6)	-169.65(9)
C(25)-Fe(1)-P(1)-C(6)	-109.16(6)	Fe(1)-N(1)-C(1)-C(6)	15.93(13)
N(1)-Fe(1)-P(1)-C(6)	-8.64(5)	N(1)-C(1)-C(2)-C(3)	-3.12(18)
P(2)-Fe(1)-P(1)-C(6)	49.44(5)	C(6)-C(1)-C(2)-C(3)	171.17(11)
C(24)-Fe(1)-P(1)-C(12)	-104.96(6)	C(1)-C(2)-C(3)-C(4)	-0.79(18)
C(25)-Fe(1)-P(1)-C(12)	1.83(6)	C(2)-C(3)-C(4)-C(5)	2.71(18)
N(1)-Fe(1)-P(1)-C(12)	102.34(5)	C(1)-N(1)-C(5)-C(4)	-2.87(16)
P(2)-Fe(1)-P(1)-C(12)	160.42(4)	Fe(1)-N(1)-C(5)-C(4)	171.65(9)
C(24)-Fe(1)-P(1)-C(8)	32.64(6)	C(1)-N(1)-C(5)-C(7)	177.09(10)
C(25)-Fe(1)-P(1)-C(8)	139.43(6)	Fe(1)-N(1)-C(5)-C(7)	-8.38(13)
N(1)-Fe(1)-P(1)-C(8)	-120.06(5)	C(3)-C(4)-C(5)-N(1)	-0.89(18)
P(2)-Fe(1)-P(1)-C(8)	-61.98(5)	C(3)-C(4)-C(5)-C(7)	179.15(11)
C(24)-Fe(1)-P(2)-C(7)	176.47(5)	N(1)-C(1)-C(6)-P(1)	-22.69(12)
C(25)-Fe(1)-P(2)-C(7)	70.30(5)	C(2)-C(1)-C(6)-P(1)	162.70(9)
N(1)-Fe(1)-P(2)-C(7)	-29.82(5)	C(12)-P(1)-C(6)-C(1)	-102.66(8)
P(1)-Fe(1)-P(2)-C(7)	-88.41(5)	C(8)-P(1)-C(6)-C(1)	144.46(8)
C(24)-Fe(1)-P(2)-C(20)	64.30(6)	Fe(1)-P(1)-C(6)-C(1)	18.56(8)
C(25)-Fe(1)-P(2)-C(20)	-41.86(6)	N(1)-C(5)-C(7)-P(2)	-20.12(12)
N(1)-Fe(1)-P(2)-C(20)	-141.99(5)	C(4)-C(5)-C(7)-P(2)	159.84(9)
P(1)-Fe(1)-P(2)-C(20)	159.42(5)	C(20)-P(2)-C(7)-C(5)	161.49(8)
C(24)-Fe(1)-P(2)-C(16)	-73.02(6)	C(16)-P(2)-C(7)-C(5)	-85.24(8)
C(25)-Fe(1)-P(2)-C(16)	-179.18(5)	Fe(1)-P(2)-C(7)-C(5)	35.06(8)
N(1)-Fe(1)-P(2)-C(16)	80.69(5)	C(6)-P(1)-C(8)-C(10)	165.99(8)
P(1)-Fe(1)-P(2)-C(16)	22.10(5)	C(12)-P(1)-C(8)-C(10)	58.07(10)
C(24)-Fe(1)-N(1)-C(1)	-85.57(13)	Fe(1)-P(1)-C(8)-C(10)	-82.31(9)
C(25)-Fe(1)-N(1)-C(1)	100.18(9)	C(6)-P(1)-C(8)-C(9)	-75.86(9)
P(2)-Fe(1)-N(1)-C(1)	-159.27(9)	C(12)-P(1)-C(8)-C(9)	176.22(8)
P(1)-Fe(1)-N(1)-C(1)	-2.27(8)	Fe(1)-P(1)-C(8)-C(9)	35.85(9)
C(24)-Fe(1)-N(1)-C(5)	100.18(12)	C(6)-P(1)-C(8)-C(11)	42.54(10)
C(25)-Fe(1)-N(1)-C(5)	-74.07(9)	C(12)-P(1)-C(8)-C(11)	-65.39(10)
P(2)-Fe(1)-N(1)-C(5)	26.48(8)	Fe(1)-P(1)-C(8)-C(11)	154.24(7)
P(1)-Fe(1)-N(1)-C(5)	-176.52(8)	C(6)-P(1)-C(12)-C(14)	-66.90(10)
C(5)-N(1)-C(1)-C(2)	4.88(16)	C(8)-P(1)-C(12)-C(14)	40.10(10)
Fe(1)-N(1)-C(1)-C(2)	-169.54(9)	Fe(1)-P(1)-C(12)-C(14)	-177.42(7)

C(6)-P(1)-C(12)-C(13)	169.60(8)
C(8)-P(1)-C(12)-C(13)	-83.40(9)
Fe(1)-P(1)-C(12)-C(13)	59.09(9)
C(6)-P(1)-C(12)-C(15)	52.47(9)
C(8)-P(1)-C(12)-C(15)	159.48(8)
Fe(1)-P(1)-C(12)-C(15)	-58.04(9)
C(7)-P(2)-C(16)-C(19)	-66.51(9)
C(20)-P(2)-C(16)-C(19)	42.62(10)
Fe(1)-P(2)-C(16)-C(19)	-174.65(7)
C(7)-P(2)-C(16)-C(18)	169.84(8)
C(20)-P(2)-C(16)-C(18)	-81.03(9)
Fe(1)-P(2)-C(16)-C(18)	61.70(8)
C(7)-P(2)-C(16)-C(17)	53.87(9)
C(20)-P(2)-C(16)-C(17)	163.00(8)
Fe(1)-P(2)-C(16)-C(17)	-54.27(9)
C(7)-P(2)-C(20)-C(22)	163.05(8)
C(16)-P(2)-C(20)-C(22)	53.54(9)
Fe(1)-P(2)-C(20)-C(22)	-86.59(9)
C(7)-P(2)-C(20)-C(21)	-79.41(9)
C(16)-P(2)-C(20)-C(21)	171.08(9)
Fe(1)-P(2)-C(20)-C(21)	30.95(10)
C(7)-P(2)-C(20)-C(23)	38.83(10)
C(16)-P(2)-C(20)-C(23)	-70.68(10)
Fe(1)-P(2)-C(20)-C(23)	149.19(7)
C(25)-Fe(1)-C(24)-O(1)	18.6(17)
N(1)-Fe(1)-C(24)-O(1)	-155.6(17)
P(2)-Fe(1)-C(24)-O(1)	-83.9(17)
P(1)-Fe(1)-C(24)-O(1)	123.1(17)
C(24)-Fe(1)-C(25)-O(2)	8.3(7)
N(1)-Fe(1)-C(25)-O(2)	-174.4(7)
P(2)-Fe(1)-C(25)-O(2)	101.9(7)
P(1)-Fe(1)-C(25)-O(2)	-87.9(7)
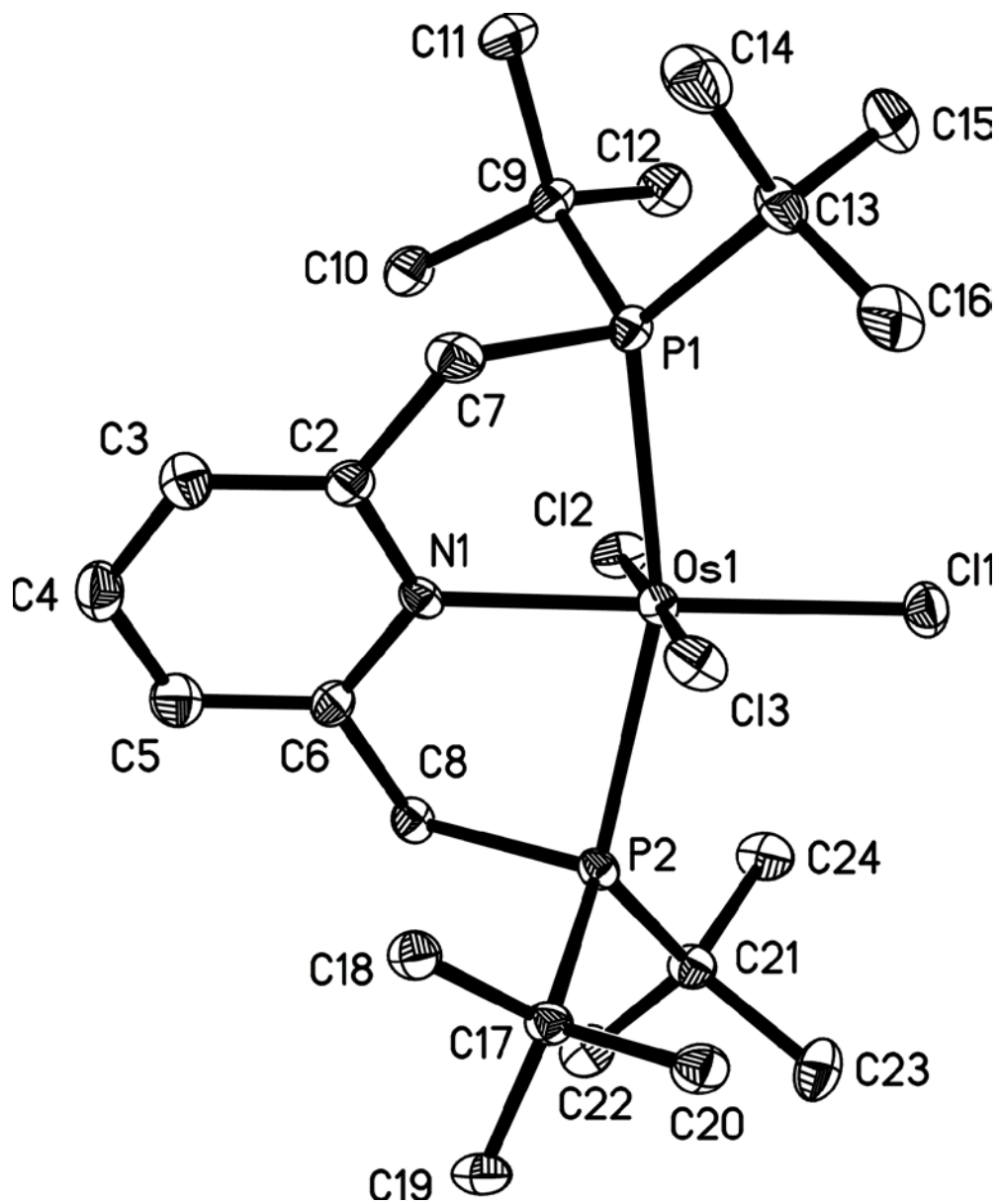
Table 1. Crystal data and structure refinement for Os(PNP)Cl3.

Identification code	ospnpcl
Empirical formula	C23 H43 Cl3 N Os P2
Formula weight	692.07
Temperature	100(2) K
Wavelength	0.71073 Å
Crystal system	Orthorhombic
Space group	P2(1)2(1)2(1)
Unit cell dimensions	a = 13.1011(6) Å $\quad\quad\quad$ $\alpha= 90°$.
	b = 14.1488(7) Å $\quad\quad\quad$ $\beta= 90°$.
	c = 15.0599(7) Å $\quad\quad\quad$ $\gamma = 90°$.
Volume	2791.6(2) Å^3
Z	4
Density (calculated)	1.647 Mg/m^3
Absorption coefficient	4.981 mm^{-1}
F(000)	1380
Crystal size	0.16 x 0.09 x 0.04 mm^3
Theta range for data collection	1.97 to 30.51°.
Index ranges	-18<=h<=18, -20<=k<=20, -21<=l<=21
Reflections collected	33378
Independent reflections	8522 [R(int) = 0.0388]
Completeness to theta = 30.51°	99.9 %
Absorption correction	None
Refinement method	Full-matrix least-squares on F^2
Data / restraints / parameters	8522 / 0 / 283
Goodness-of-fit on F^2	1.004
Final R indices [I>2sigma(I)]	R1 = 0.0396, wR2 = 0.0889
R indices (all data)	R1 = 0.0426, wR2 = 0.0903
Absolute structure parameter	0.007(7)
Largest diff. peak and hole	7.495 and -2.106 e.Å^{-3}

Table 2. Atomic coordinates (x 10^4) and equivalent isotropic displacement parameters (Å^2x 10^3) for Os(PNP)Cl3. U(eq) is defined as one third of the trace of the orthogonalized U^{ij} tensor.

	x	y	z	U(eq)
Os(1)	6298(1)	664(1)	2059(1)	13(1)
Cl(1)	6466(1)	1872(1)	3146(1)	21(1)
Cl(2)	6140(1)	1822(1)	928(1)	20(1)
Cl(3)	6462(1)	-513(1)	3160(1)	20(1)
P(1)	4451(1)	437(1)	2145(1)	14(1)
P(2)	8081(1)	486(1)	1630(1)	13(1)
N(1)	6140(4)	-382(3)	1111(3)	14(1)
C(2)	5313(4)	-980(4)	1131(4)	16(1)
C(3)	5222(5)	-1701(4)	521(4)	20(1)
C(4)	5937(5)	-1795(4)	-143(4)	23(1)
C(5)	6753(5)	-1179(4)	-180(4)	22(1)
C(6)	6854(4)	-492(4)	455(3)	17(1)
C(7)	4530(4)	-822(4)	1845(4)	20(1)
C(8)	7773(4)	162(4)	472(3)	15(1)
C(9)	3597(4)	943(4)	1237(4)	17(1)
C(10)	4025(4)	632(5)	330(3)	21(1)
C(11)	2490(4)	571(5)	1266(4)	26(1)
C(12)	3579(5)	2030(4)	1282(4)	22(1)
C(13)	3705(5)	446(4)	3231(4)	21(1)
C(14)	2903(6)	-346(5)	3265(5)	31(2)
C(15)	3214(5)	1415(5)	3363(4)	26(1)
C(16)	4422(5)	296(5)	4012(4)	26(1)
C(17)	8845(4)	-582(3)	2026(3)	15(1)
C(18)	8223(4)	-1480(4)	1814(4)	18(1)
C(19)	9880(4)	-704(5)	1553(4)	21(1)
C(20)	9026(4)	-539(4)	3049(4)	20(1)
C(21)	8991(4)	1522(4)	1527(4)	18(1)
C(22)	9684(5)	1464(4)	699(4)	22(1)
C(23)	9640(5)	1589(5)	2385(4)	26(1)
C(24)	8396(5)	2455(4)	1474(5)	23(1)

Table 3.   Bond lengths [Å] and angles [°] for Os(PNP)Cl3.

_____

Os(1)-N(1)	2.066(4)	C(3)-C(4)	1.377(8)
Os(1)-Cl(3)	2.3597(12)	C(4)-C(5)	1.381(9)
Os(1)-Cl(2)	2.3721(12)	C(5)-C(6)	1.369(8)
Os(1)-Cl(1)	2.3777(13)	C(6)-C(8)	1.519(8)
Os(1)-P(2)	2.4374(14)	C(9)-C(12)	1.540(7)
Os(1)-P(1)	2.4440(13)	C(9)-C(10)	1.541(8)
P(1)-C(7)	1.841(6)	C(9)-C(11)	1.544(8)
P(1)-C(9)	1.905(6)	C(13)-C(16)	1.521(9)
P(1)-C(13)	1.906(6)	C(13)-C(15)	1.526(8)
P(2)-C(8)	1.848(5)	C(13)-C(14)	1.537(9)
P(2)-C(21)	1.896(6)	C(17)-C(19)	1.542(7)
P(2)-C(17)	1.908(5)	C(17)-C(18)	1.542(7)
N(1)-C(6)	1.370(7)	C(17)-C(20)	1.560(7)
N(1)-C(2)	1.375(7)	C(21)-C(24)	1.536(8)
C(2)-C(3)	1.378(8)	C(21)-C(22)	1.543(8)
C(2)-C(7)	1.502(8)	C(21)-C(23)	1.550(8)
N(1)-Os(1)-Cl(3)	89.43(12)	C(9)-P(1)-C(13)	108.2(3)
N(1)-Os(1)-Cl(2)	89.41(12)	C(7)-P(1)-Os(1)	93.32(18)
Cl(3)-Os(1)-Cl(2)	178.78(5)	C(9)-P(1)-Os(1)	119.60(18)
N(1)-Os(1)-Cl(1)	179.53(14)	C(13)-P(1)-Os(1)	123.5(2)
Cl(3)-Os(1)-Cl(1)	90.82(5)	C(8)-P(2)-C(21)	104.6(2)
Cl(2)-Os(1)-Cl(1)	90.35(5)	C(8)-P(2)-C(17)	102.3(2)
N(1)-Os(1)-P(2)	80.75(13)	C(21)-P(2)-C(17)	108.0(2)
Cl(3)-Os(1)-P(2)	91.52(5)	C(8)-P(2)-Os(1)	93.81(17)
Cl(2)-Os(1)-P(2)	87.95(5)	C(21)-P(2)-Os(1)	123.02(18)
Cl(1)-Os(1)-P(2)	99.65(5)	C(17)-P(2)-Os(1)	120.07(16)
N(1)-Os(1)-P(1)	81.00(13)	C(6)-N(1)-C(2)	119.0(5)
Cl(3)-Os(1)-P(1)	87.73(5)	C(6)-N(1)-Os(1)	120.8(4)
Cl(2)-Os(1)-P(1)	92.43(5)	C(2)-N(1)-Os(1)	120.3(4)
Cl(1)-Os(1)-P(1)	98.61(5)	N(1)-C(2)-C(3)	120.6(5)
P(2)-Os(1)-P(1)	161.74(4)	N(1)-C(2)-C(7)	117.5(5)
C(7)-P(1)-C(9)	102.8(2)	C(3)-C(2)-C(7)	121.9(5)
C(7)-P(1)-C(13)	104.2(2)	C(4)-C(3)-C(2)	119.8(5)

C(3)-C(4)-C(5)	119.6(6)	C(16)-C(13)-P(1)	110.2(4)
C(6)-C(5)-C(4)	119.7(6)	C(15)-C(13)-P(1)	109.4(4)
C(5)-C(6)-N(1)	121.2(5)	C(14)-C(13)-P(1)	112.0(4)
C(5)-C(6)-C(8)	121.4(5)	C(19)-C(17)-C(18)	106.1(4)
N(1)-C(6)-C(8)	117.4(5)	C(19)-C(17)-C(20)	109.0(4)
C(2)-C(7)-P(1)	111.0(4)	C(18)-C(17)-C(20)	108.5(4)
C(6)-C(8)-P(2)	109.9(4)	C(19)-C(17)-P(2)	113.9(4)
C(12)-C(9)-C(10)	109.2(5)	C(18)-C(17)-P(2)	108.1(3)
C(12)-C(9)-C(11)	108.9(5)	C(20)-C(17)-P(2)	111.0(3)
C(10)-C(9)-C(11)	105.7(4)	C(24)-C(21)-C(22)	107.7(5)
C(12)-C(9)-P(1)	110.7(4)	C(24)-C(21)-C(23)	105.6(5)
C(10)-C(9)-P(1)	108.4(4)	C(22)-C(21)-C(23)	110.7(5)
C(11)-C(9)-P(1)	113.8(4)	C(24)-C(21)-P(2)	110.4(4)
C(16)-C(13)-C(15)	106.6(5)	C(22)-C(21)-P(2)	113.2(4)
C(16)-C(13)-C(14)	107.1(5)	C(23)-C(21)-P(2)	108.9(4)
C(15)-C(13)-C(14)	111.3(5)		

Table 4. Anisotropic displacement parameters ($Å^2$x 10^3) for Os(PNP)Cl3. The anisotropic displacement factor exponent takes the form: $-2\pi^2[\ h^2\ a^{*2}U^{11} + ... \ + 2\ h\ k\ a^*\ b^*\ U^{12}\ ]$

	U^{11}	U^{22}	U^{33}	U^{23}	U^{13}	U^{12}
Os(1)	16(1)	13(1)	11(1)	2(1)	-1(1)	3(1)
Cl(1)	25(1)	19(1)	19(1)	-4(1)	-3(1)	5(1)
Cl(2)	19(1)	20(1)	20(1)	9(1)	-3(1)	1(1)
Cl(3)	22(1)	21(1)	16(1)	8(1)	2(1)	7(1)
P(1)	16(1)	14(1)	12(1)	1(1)	-1(1)	-2(1)
P(2)	14(1)	12(1)	13(1)	1(1)	1(1)	2(1)
N(1)	14(2)	14(2)	12(2)	2(2)	1(2)	4(2)
C(2)	16(2)	19(2)	14(2)	2(2)	-3(2)	2(2)
C(3)	23(3)	17(3)	20(3)	1(2)	2(2)	-1(2)
C(4)	28(3)	22(3)	18(3)	-4(2)	-3(2)	2(2)
C(5)	23(3)	29(3)	15(3)	0(2)	1(2)	2(2)
C(6)	17(2)	20(3)	14(2)	-1(2)	-4(2)	2(2)
C(7)	17(2)	17(3)	27(3)	2(2)	4(2)	-3(2)
C(8)	18(3)	17(2)	10(2)	2(2)	2(2)	1(2)
C(9)	15(2)	18(2)	18(2)	-1(2)	-2(2)	-3(2)
C(10)	20(2)	26(3)	15(2)	2(2)	-6(2)	2(2)
C(11)	16(2)	29(3)	32(3)	-4(3)	-4(2)	-2(2)
C(12)	24(3)	17(2)	25(3)	3(2)	-4(2)	4(2)
C(13)	22(2)	21(2)	19(2)	-1(2)	7(2)	-1(2)
C(14)	32(3)	28(3)	32(3)	1(3)	14(3)	-4(3)
C(15)	30(3)	28(3)	19(3)	-2(2)	5(2)	8(3)
C(16)	29(3)	39(4)	11(3)	8(2)	7(2)	2(3)
C(17)	15(2)	14(2)	17(2)	1(2)	-1(2)	3(2)
C(18)	17(2)	14(2)	24(3)	1(2)	-1(2)	0(2)
C(19)	13(2)	20(2)	29(3)	3(2)	-1(2)	1(2)
C(20)	20(2)	19(3)	21(3)	3(2)	-3(2)	4(2)
C(21)	16(2)	16(2)	22(3)	0(2)	1(2)	-1(2)
C(22)	23(3)	18(3)	25(3)	5(2)	1(2)	-7(2)
C(23)	31(3)	23(3)	26(3)	-5(2)	-3(3)	-8(2)
C(24)	19(3)	12(2)	37(3)	2(2)	2(2)	-4(2)

Table 5.   Hydrogen coordinates (x 10^4) and isotropic displacement parameters ($Å^2$x 10 ^{3})
for Os(PNP)Cl3.

	x	y	z	U(eq)
H(3)	4668	-2132	559	24
H(4)	5869	-2281	-574	28
H(5)	7243	-1232	-642	27
H(7A)	4715	-1196	2377	25
H(7B)	3855	-1043	1634	25
H(8A)	7623	739	125	18
H(8B)	8366	-158	197	18
H(10A)	3647	949	-145	31
H(10B)	3953	-54	267	31
H(10C)	4749	804	292	31
H(11A)	2153	801	1806	39
H(11B)	2495	-121	1267	39
H(11C)	2118	799	744	39
H(12A)	4280	2269	1322	33
H(12B)	3193	2232	1806	33
H(12C)	3254	2281	746	33
H(14A)	3247	-961	3270	46
H(14B)	2460	-304	2742	46
H(14C)	2491	-280	3804	46
H(15A)	2952	1465	3970	39
H(15B)	2651	1492	2941	39
H(15C)	3725	1909	3261	39
H(16A)	4039	350	4569	39
H(16B)	4962	775	3999	39
H(16C)	4728	-335	3973	39
H(18A)	8550	-2029	2091	27
H(18B)	8196	-1571	1169	27
H(18C)	7529	-1410	2047	27
H(19A)	10351	-209	1751	31
H(19B)	9782	-655	910	31

H(19C)	10166	-1325	1698	31
H(20A)	8383	-389	3350	30
H(20B)	9532	-49	3183	30
H(20C)	9278	-1153	3258	30
H(22A)	9261	1382	168	33
H(22B)	10148	925	759	33
H(22C)	10081	2048	646	33
H(23A)	10036	2177	2378	39
H(23B)	10107	1049	2415	39
H(23C)	9189	1584	2904	39
H(24A)	8000	2542	2021	34
H(24B)	7932	2438	964	34
H(24C)	8875	2982	1405	34

Table 6. Torsion angles [°] for Os(PNP)Cl3.

		P(1)-Os(1)-N(1)-C(6)	156.7(4)
N(1)-Os(1)-P(1)-C(7)	30.7(2)	Cl(3)-Os(1)-N(1)-C(2)	64.4(4)
Cl(3)-Os(1)-P(1)-C(7)	-59.04(19)	Cl(2)-Os(1)-N(1)-C(2)	-115.9(4)
Cl(2)-Os(1)-P(1)-C(7)	119.75(19)	Cl(1)-Os(1)-N(1)-C(2)	-56(17)
Cl(1)-Os(1)-P(1)-C(7)	-149.52(19)	P(2)-Os(1)-N(1)-C(2)	156.1(4)
P(2)-Os(1)-P(1)-C(7)	28.9(3)	P(1)-Os(1)-N(1)-C(2)	-23.4(4)
N(1)-Os(1)-P(1)-C(9)	-76.0(2)	C(6)-N(1)-C(2)-C(3)	2.3(8)
Cl(3)-Os(1)-P(1)-C(9)	-165.73(19)	Os(1)-N(1)-C(2)-C(3)	-177.5(4)
Cl(2)-Os(1)-P(1)-C(9)	13.06(19)	C(6)-N(1)-C(2)-C(7)	-178.4(5)
Cl(1)-Os(1)-P(1)-C(9)	103.79(19)	Os(1)-N(1)-C(2)-C(7)	1.7(6)
P(2)-Os(1)-P(1)-C(9)	-77.8(2)	N(1)-C(2)-C(3)-C(4)	-3.4(8)
N(1)-Os(1)-P(1)-C(13)	140.2(2)	C(7)-C(2)-C(3)-C(4)	177.4(5)
Cl(3)-Os(1)-P(1)-C(13)	50.5(2)	C(2)-C(3)-C(4)-C(5)	1.6(9)
Cl(2)-Os(1)-P(1)-C(13)	-130.8(2)	C(3)-C(4)-C(5)-C(6)	1.2(9)
Cl(1)-Os(1)-P(1)-C(13)	-40.0(2)	C(4)-C(5)-C(6)-N(1)	-2.3(9)
P(2)-Os(1)-P(1)-C(13)	138.4(2)	C(4)-C(5)-C(6)-C(8)	176.3(5)
N(1)-Os(1)-P(2)-C(8)	31.3(2)	C(2)-N(1)-C(6)-C(5)	0.5(8)
Cl(3)-Os(1)-P(2)-C(8)	120.51(17)	Os(1)-N(1)-C(6)-C(5)	-179.6(4)
Cl(2)-Os(1)-P(2)-C(8)	-58.39(17)	C(2)-N(1)-C(6)-C(8)	-178.1(5)
Cl(1)-Os(1)-P(2)-C(8)	-148.40(17)	Os(1)-N(1)-C(6)-C(8)	1.8(6)
P(1)-Os(1)-P(2)-C(8)	33.2(2)	N(1)-C(2)-C(7)-P(1)	30.9(6)
N(1)-Os(1)-P(2)-C(21)	141.5(3)	C(3)-C(2)-C(7)-P(1)	-149.9(5)
Cl(3)-Os(1)-P(2)-C(21)	-129.3(2)	C(9)-P(1)-C(7)-C(2)	81.4(4)
Cl(2)-Os(1)-P(2)-C(21)	51.8(2)	C(13)-P(1)-C(7)-C(2)	-165.8(4)
Cl(1)-Os(1)-P(2)-C(21)	-38.2(2)	Os(1)-P(1)-C(7)-C(2)	-40.0(4)
P(1)-Os(1)-P(2)-C(21)	143.3(2)	C(5)-C(6)-C(8)-P(2)	-147.7(5)
N(1)-Os(1)-P(2)-C(17)	-75.2(2)	N(1)-C(6)-C(8)-P(2)	30.9(6)
Cl(3)-Os(1)-P(2)-C(17)	13.94(19)	C(21)-P(2)-C(8)-C(6)	-165.9(4)
Cl(2)-Os(1)-P(2)-C(17)	-164.97(19)	C(17)-P(2)-C(8)-C(6)	81.6(4)
Cl(1)-Os(1)-P(2)-C(17)	105.03(19)	Os(1)-P(2)-C(8)-C(6)	-40.3(4)
P(1)-Os(1)-P(2)-C(17)	-73.4(2)	C(7)-P(1)-C(9)-C(12)	-170.6(4)
Cl(3)-Os(1)-N(1)-C(6)	-115.5(4)	C(13)-P(1)-C(9)-C(12)	79.5(4)
Cl(2)-Os(1)-N(1)-C(6)	64.2(4)	Os(1)-P(1)-C(9)-C(12)	-69.3(4)
Cl(1)-Os(1)-N(1)-C(6)	124(17)	C(7)-P(1)-C(9)-C(10)	-50.9(4)
P(2)-Os(1)-N(1)-C(6)	-23.8(4)	C(13)-P(1)-C(9)-C(10)	-160.8(4)

Os(1)-P(1)-C(9)-C(10)	50.4(4)
C(7)-P(1)-C(9)-C(11)	66.3(4)
C(13)-P(1)-C(9)-C(11)	-43.5(5)
Os(1)-P(1)-C(9)-C(11)	167.6(3)
C(7)-P(1)-C(13)-C(16)	85.9(5)
C(9)-P(1)-C(13)-C(16)	-165.3(4)
Os(1)-P(1)-C(13)-C(16)	-18.0(5)
C(7)-P(1)-C(13)-C(15)	-157.2(4)
C(9)-P(1)-C(13)-C(15)	-48.4(5)
Os(1)-P(1)-C(13)-C(15)	98.9(4)
C(7)-P(1)-C(13)-C(14)	-33.3(5)
C(9)-P(1)-C(13)-C(14)	75.5(5)
Os(1)-P(1)-C(13)-C(14)	-137.2(4)
C(8)-P(2)-C(17)-C(19)	66.4(4)
C(21)-P(2)-C(17)-C(19)	-43.6(4)
Os(1)-P(2)-C(17)-C(19)	168.2(3)
C(8)-P(2)-C(17)-C(18)	-51.2(4)
C(21)-P(2)-C(17)-C(18)	-161.2(4)
Os(1)-P(2)-C(17)-C(18)	50.6(4)
C(8)-P(2)-C(17)-C(20)	-170.1(3)
C(21)-P(2)-C(17)-C(20)	79.9(4)
Os(1)-P(2)-C(17)-C(20)	-68.3(4)
C(8)-P(2)-C(21)-C(24)	87.8(4)
C(17)-P(2)-C(21)-C(24)	-163.7(4)
Os(1)-P(2)-C(21)-C(24)	-16.7(5)
C(8)-P(2)-C(21)-C(22)	-33.0(5)
C(17)-P(2)-C(21)-C(22)	75.5(4)
Os(1)-P(2)-C(21)-C(22)	-137.5(3)
C(8)-P(2)-C(21)-C(23)	-156.6(4)
C(17)-P(2)-C(21)-C(23)	-48.2(5)
Os(1)-P(2)-C(21)-C(23)	98.8(4)
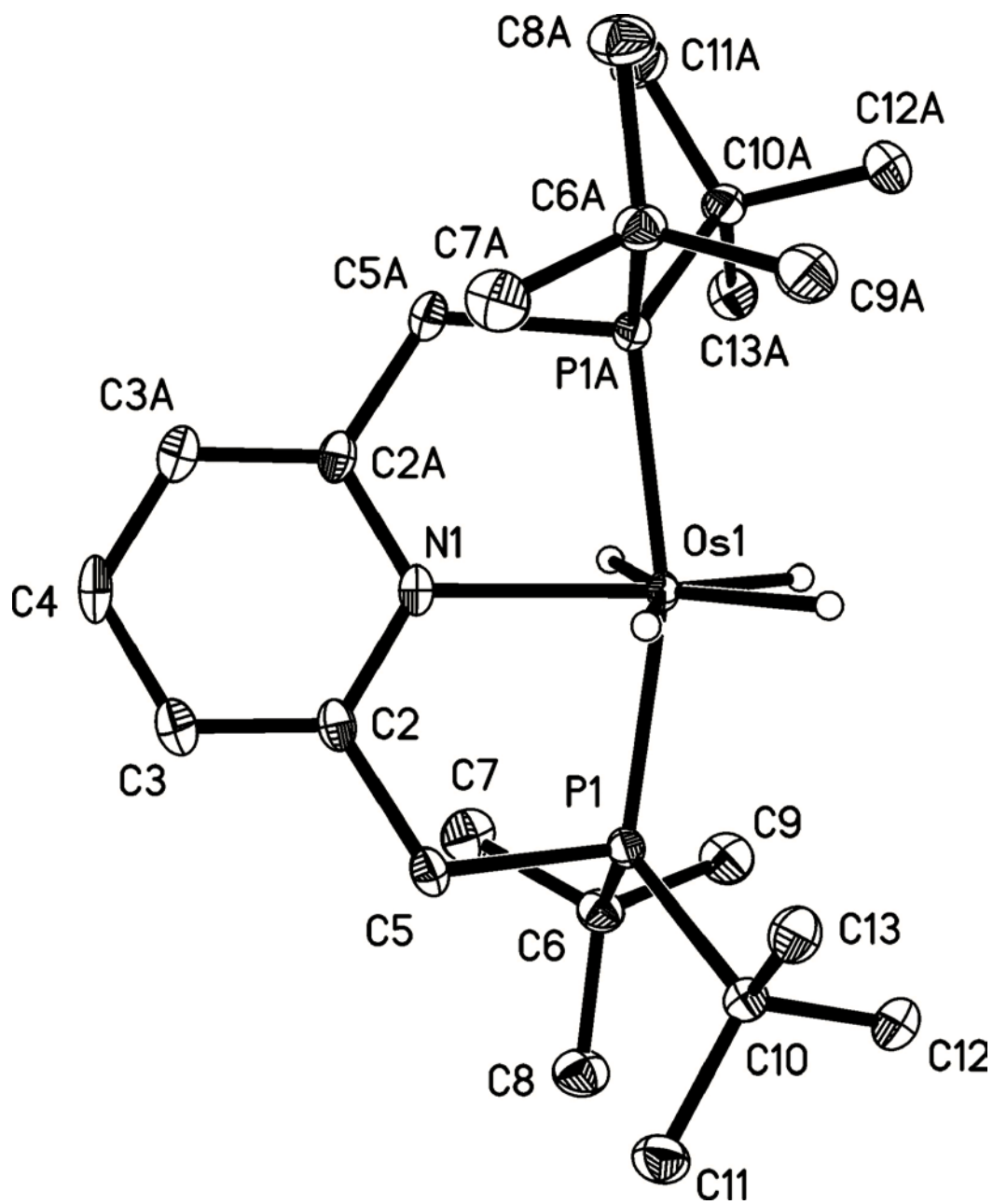
Table 1. Crystal data and structure refinement for OsH4(PNP).

Identification code	osh4
Empirical formula	C23 H47 N Os P2
Formula weight	589.76
Temperature	100(2) K
Wavelength	0.71073 Å
Crystal system	Tetragonal
Space group	$P4_2$ (#77)

Unit cell dimensions	a = 11.6422(10) Å	α= 90°.
	b = 11.6422 Å	β= 90°.
	c = 9.4519(8) Å	γ = 90°.

Volume	1281.12(15) Å^3
Z	2
Density (calculated)	1.529 Mg/m^3
Absorption coefficient	5.110 mm^{-1}
F(000)	596
Crystal size	0.30 x 0.15 x 0.07 mm^3
Theta range for data collection	1.75 to 30.49°.
Index ranges	-16<=h<=16, -16<=k<=16, -13<=l<=13
Reflections collected	15756
Independent reflections	3901 [R(int) = 0.0224]
Completeness to theta = 30.49°	100.0 %
Absorption correction	Semi-empirical from equivalents
Max. and min. transmission	0.7324 and 0.3093
Refinement method	Full-matrix least-squares on F^2
Data / restraints / parameters	3901 / 1 / 218
Goodness-of-fit on F^2	1.007
Final R indices [I>2sigma(I)]	R1 = 0.0129, wR2 = 0.0352
R indices (all data)	R1 = 0.0147, wR2 = 0.0362
Absolute structure parameter	0.022(7)
Largest diff. peak and hole	0.927 and -0.264 e.Å^{-3}

Table 2. Atomic coordinates (x 10^4) and equivalent isotropic displacement parameters (Å^{2}x 10^3) for OsH4(PNP). U(eq) is defined as one third of the trace of the orthogonalized U^{ij} tensor.

	x	y	z	U(eq)
Os(1)	5000	0	-25(1)	11(1)
P(1)	6454(1)	-1296(1)	288(1)	12(1)
N(1)	5000	0	2253(3)	14(1)
C(2)	5880(1)	-491(1)	2983(2)	15(1)
C(3)	5875(2)	-525(1)	4447(2)	19(1)
C(4)	5000	0	5196(4)	21(1)
C(5)	6875(1)	-951(2)	2138(2)	16(1)
C(6)	6063(1)	-2878(1)	379(2)	18(1)
C(7)	5258(2)	-3023(2)	1652(2)	23(1)
C(8)	7061(2)	-3721(2)	560(2)	24(1)
C(9)	5385(2)	-3182(2)	-956(3)	24(1)
C(10)	7863(1)	-1129(1)	-693(2)	16(1)
C(11)	8909(1)	-1602(2)	99(2)	23(1)
C(12)	7753(2)	-1694(2)	-2154(2)	23(1)
C(13)	8073(2)	158(2)	-942(3)	21(1)

Table 3. Bond lengths [Å] and angles [°] for OsH4(PNP).

_____

Os(1)-N(1)	2.153(3)	C(7)-H(7A)	1.02(2)
Os(1)-P(1)#1	2.2864(4)	C(7)-H(7B)	0.93(2)
Os(1)-P(1)	2.2865(4)	C(7)-H(7C)	0.86(3)
Os(1)-H(1)	1.62(2)	C(8)-H(8A)	0.93(2)
Os(1)-H(2)	1.846(19)	C(8)-H(8B)	0.96(2)
P(1)-C(5)	1.8592(17)	C(8)-H(8C)	0.95(2)
P(1)-C(10)	1.8953(16)	C(9)-H(9A)	1.05(3)
P(1)-C(6)	1.8985(15)	C(9)-H(9B)	0.92(2)
N(1)-C(2)	1.361(2)	C(9)-H(9C)	1.07(2)
N(1)-C(2)#1	1.361(2)	C(10)-C(11)	1.531(2)
C(2)-C(3)	1.384(2)	C(10)-C(12)	1.535(2)
C(2)-C(5)	1.506(2)	C(10)-C(13)	1.537(3)
C(3)-C(4)	1.382(3)	C(11)-H(11A)	0.97(2)
C(3)-H(3)	0.941(19)	C(11)-H(11B)	0.96(2)
C(4)-C(3)#1	1.383(3)	C(11)-H(11C)	0.984(19)
C(4)-H(4)	0.89(9)	C(12)-H(12A)	1.019(17)
C(5)-H(5A)	0.97(2)	C(12)-H(12B)	0.92(2)
C(5)-H(5B)	0.95(2)	C(12)-H(12C)	0.98(2)
C(6)-C(9)	1.529(3)	C(13)-H(13A)	0.96(3)
C(6)-C(8)	1.531(2)	C(13)-H(13B)	0.99(3)
C(6)-C(7)	1.534(3)	C(13)-H(13C)	0.97(2)
N(1)-Os(1)-P(1)#1	82.555(17)	C(10)-P(1)-C(6)	109.21(7)
N(1)-Os(1)-P(1)	82.556(17)	C(5)-P(1)-Os(1)	100.04(5)
P(1)#1-Os(1)-P(1)	165.11(3)	C(10)-P(1)-Os(1)	120.65(5)
N(1)-Os(1)-H(1)	145.2(8)	C(6)-P(1)-Os(1)	117.93(5)
P(1)#1-Os(1)-H(1)	97.2(6)	C(2)-N(1)-C(2)#1	119.1(3)
P(1)-Os(1)-H(1)	95.0(6)	C(2)-N(1)-Os(1)	120.47(13)
N(1)-Os(1)-H(2)	80.2(9)	C(2)#1-N(1)-Os(1)	120.47(13)
P(1)#1-Os(1)-H(2)	92.0(6)	N(1)-C(2)-C(3)	121.03(18)
P(1)-Os(1)-H(2)	85.4(6)	N(1)-C(2)-C(5)	117.32(17)
H(1)-Os(1)-H(2)	65.0(12)	C(3)-C(2)-C(5)	121.61(14)
C(5)-P(1)-C(10)	102.09(7)	C(4)-C(3)-C(2)	120.1(2)
C(5)-P(1)-C(6)	103.34(8)	C(4)-C(3)-H(3)	123.4(11)

C(2)-C(3)-H(3)	116.5(11)	C(12)-C(10)-C(13)	107.06(16)
C(3)-C(4)-C(3)#1	118.4(3)	C(11)-C(10)-P(1)	114.34(11)
C(3)-C(4)-H(4)	120.78(15)	C(12)-C(10)-P(1)	108.92(12)
C(3)#1-C(4)-H(4)	120.78(15)	C(13)-C(10)-P(1)	108.23(12)
C(2)-C(5)-P(1)	111.91(11)	C(10)-C(11)-H(11A)	115.4(13)
C(2)-C(5)-H(5A)	110.7(12)	C(10)-C(11)-H(11B)	111.1(12)
P(1)-C(5)-H(5A)	115.5(12)	H(11A)-C(11)-H(11B)	103.4(17)
C(2)-C(5)-H(5B)	106.6(15)	C(10)-C(11)-H(11C)	116.2(10)
P(1)-C(5)-H(5B)	102.7(14)	H(11A)-C(11)-H(11C)	104.3(17)
H(5A)-C(5)-H(5B)	108.6(19)	H(11B)-C(11)-H(11C)	105.1(16)
C(9)-C(6)-C(8)	109.59(15)	C(10)-C(12)-H(12A)	108.6(10)
C(9)-C(6)-C(7)	107.86(15)	C(10)-C(12)-H(12B)	107.0(14)
C(8)-C(6)-C(7)	107.75(15)	H(12A)-C(12)-H(12B)	105.9(18)
C(9)-C(6)-P(1)	108.12(13)	C(10)-C(12)-H(12C)	112.4(12)
C(8)-C(6)-P(1)	116.41(12)	H(12A)-C(12)-H(12C)	106.1(17)
C(7)-C(6)-P(1)	106.79(11)	H(12B)-C(12)-H(12C)	116.4(19)
C(6)-C(7)-H(7A)	111.2(13)	C(10)-C(13)-H(13A)	108.0(16)
C(6)-C(7)-H(7B)	109.0(12)	C(10)-C(13)-H(13B)	106.4(13)
H(7A)-C(7)-H(7B)	110.7(18)	H(13A)-C(13)-H(13B)	104(2)
C(6)-C(7)-H(7C)	114.0(18)	C(10)-C(13)-H(13C)	113.0(13)
H(7A)-C(7)-H(7C)	106(2)	H(13A)-C(13)-H(13C)	114(2)
H(7B)-C(7)-H(7C)	106(2)	H(13B)-C(13)-H(13C)	111.3(17)
C(6)-C(8)-H(8A)	107.7(12)		
C(6)-C(8)-H(8B)	111.4(12)		
H(8A)-C(8)-H(8B)	104.1(16)	Symmetry transformations used to generate	
C(6)-C(8)-H(8C)	115.0(13)	equivalent atoms: #1 -x+1,-y,z	
H(8A)-C(8)-H(8C)	106.8(17)		
H(8B)-C(8)-H(8C)	111.0(16)		
C(6)-C(9)-H(9A)	108.3(14)		
C(6)-C(9)-H(9B)	115.2(14)		
H(9A)-C(9)-H(9B)	102(2)		
C(6)-C(9)-H(9C)	109.7(12)		
H(9A)-C(9)-H(9C)	114(2)		
H(9B)-C(9)-H(9C)	107.1(17)		
C(11)-C(10)-C(12)	110.58(14)		
C(11)-C(10)-C(13)	107.42(15)		

Table 4. Anisotropic displacement parameters (Å^2x 10^3) for OsH4(PNP). The anisotropic displacement factor exponent takes the form: $-2\pi^2[h^2 a^{*2}U^{11} + ... + 2 h k a^* b^* U^{12}]$

	U^{11}	U^{22}	U^{33}	U^{23}	U^{13}	U^{12}
Os(1)	14(1)	12(1)	8(1)	0	0	1(1)
P(1)	14(1)	13(1)	11(1)	1(1)	-1(1)	0(1)
N(1)	18(1)	15(1)	9(1)	0	0	-3(1)
C(2)	19(1)	14(1)	11(1)	2(1)	-1(1)	-4(1)
C(3)	21(1)	21(1)	14(1)	3(1)	-3(1)	-4(1)
C(4)	28(1)	27(1)	8(3)	0	0	-8(1)
C(5)	17(1)	19(1)	12(1)	1(1)	-3(1)	-1(1)
C(6)	19(1)	14(1)	20(1)	0(1)	-1(1)	1(1)
C(7)	24(1)	18(1)	27(1)	5(1)	6(1)	-4(1)
C(8)	26(1)	17(1)	30(1)	5(1)	2(1)	4(1)
C(9)	29(1)	16(1)	26(1)	-4(1)	-2(1)	0(1)
C(10)	14(1)	19(1)	16(1)	1(1)	1(1)	1(1)
C(11)	16(1)	29(1)	25(1)	6(1)	0(1)	2(1)
C(12)	24(1)	29(1)	18(1)	-2(1)	4(1)	4(1)
C(13)	19(1)	24(1)	21(1)	4(1)	4(1)	-2(1)

Table 5.   Hydrogen coordinates (x 10^4) and isotropic displacement parameters ($Å^2$x 10 ^{3})
for OsH4(PNP).

	x	y	z	U(eq)
H(1)	5547(18)	574(18)	-1430(30)	37(6)
H(2)	6106(16)	1103(15)	310(30)	25(5)
H(3)	6490(16)	-913(15)	4880(19)	19(5)
H(4)	5000	0	6140(100)	50(20)
H(5A)	7259(17)	-1559(19)	2640(20)	18(5)
H(5B)	7400(20)	-330(20)	2020(20)	18(6)
H(7A)	5688(19)	-2912(19)	2580(20)	26(6)
H(7B)	4924(16)	-3749(18)	1620(20)	14(5)
H(7C)	4700(30)	-2540(20)	1670(30)	28(7)
H(8A)	6750(16)	-4450(18)	690(20)	24(5)
H(8B)	7479(17)	-3575(16)	1420(20)	18(5)
H(8C)	7566(18)	-3772(19)	-230(20)	28(6)
H(9A)	5100(20)	-4040(20)	-870(30)	35(7)
H(9B)	5811(18)	-3200(20)	-1780(20)	22(5)
H(9C)	4710(20)	-2570(20)	-1110(20)	28(6)
H(11A)	9102(19)	-1209(18)	970(30)	34(6)
H(11B)	9596(17)	-1530(16)	-460(20)	23(5)
H(11C)	8874(14)	-2418(16)	370(30)	25(5)
H(12A)	8445(16)	-1463(15)	-2751(18)	12(4)
H(12B)	7130(20)	-1370(20)	-2590(20)	33(7)
H(12C)	7769(19)	-2530(20)	-2100(20)	34(6)
H(13A)	8820(20)	240(20)	-1360(30)	36(8)
H(13B)	8156(18)	512(18)	10(30)	39(6)
H(13C)	7466(19)	522(18)	-1480(20)	24(5)

Table 6. Torsion angles [°] for OsH4(PNP).

_____

N(1)-Os(1)-P(1)-C(5)	-20.01(5)
P(1)#1-Os(1)-P(1)-C(5)	-20.01(5)
N(1)-Os(1)-P(1)-C(10)	-130.63(6)
P(1)#1-Os(1)-P(1)-C(10)	-130.63(6)
N(1)-Os(1)-P(1)-C(6)	91.03(7)
P(1)#1-Os(1)-P(1)-C(6)	91.03(7)
P(1)#1-Os(1)-N(1)-C(2)	-167.44(7)
P(1)-Os(1)-N(1)-C(2)	12.56(7)
P(1)#1-Os(1)-N(1)-C(2)#1	12.57(7)
P(1)-Os(1)-N(1)-C(2)#1	-167.43(7)
C(2)#1-N(1)-C(2)-C(3)	1.82(11)
Os(1)-N(1)-C(2)-C(3)	-178.17(11)
C(2)#1-N(1)-C(2)-C(5)	-175.85(15)
Os(1)-N(1)-C(2)-C(5)	4.15(15)
N(1)-C(2)-C(3)-C(4)	-3.7(2)
C(5)-C(2)-C(3)-C(4)	173.92(12)
C(2)-C(3)-C(4)-C(3)#1	1.79(11)
N(1)-C(2)-C(5)-P(1)	-23.54(17)
C(3)-C(2)-C(5)-P(1)	158.80(13)
C(10)-P(1)-C(5)-C(2)	153.43(11)
C(6)-P(1)-C(5)-C(2)	-93.21(12)
Os(1)-P(1)-C(5)-C(2)	28.85(12)
C(5)-P(1)-C(6)-C(9)	164.19(13)
C(10)-P(1)-C(6)-C(9)	-87.72(14)
Os(1)-P(1)-C(6)-C(9)	55.01(14)
C(5)-P(1)-C(6)-C(8)	-72.01(15)
C(10)-P(1)-C(6)-C(8)	36.09(16)
Os(1)-P(1)-C(6)-C(8)	178.82(11)
C(5)-P(1)-C(6)-C(7)	48.35(14)
C(10)-P(1)-C(6)-C(7)	156.44(12)
Os(1)-P(1)-C(6)-C(7)	-60.83(14)
C(5)-P(1)-C(10)-C(11)	40.49(14)
C(6)-P(1)-C(10)-C(11)	-68.45(14)
Os(1)-P(1)-C(10)-C(11)	150.01(10)

C(5)-P(1)-C(10)-C(12)	164.74(12)
C(6)-P(1)-C(10)-C(12)	55.81(13)
Os(1)-P(1)-C(10)-C(12)	-85.73(12)
C(5)-P(1)-C(10)-C(13)	-79.18(14)
C(6)-P(1)-C(10)-C(13)	171.88(14)
Os(1)-P(1)-C(10)-C(13)	30.34(15)

Symmetry transformations used to generate equivalent atoms: #1 -x+1,-y,z
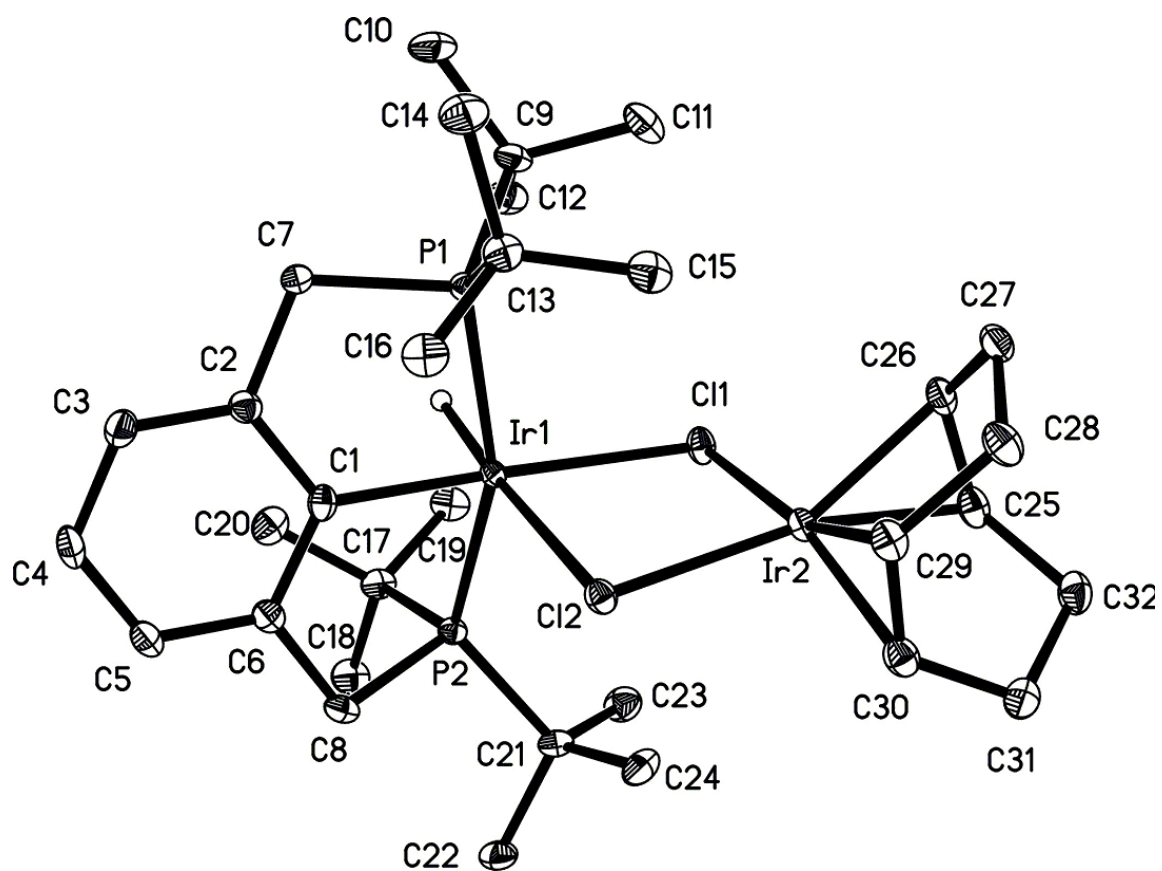
Table 1. Crystallographic Data for irhco_bad

Identification code	irhco_bad
Empirical formula	C35 H63 Cl2 Ir2 P2
Formula weight	1001.09
Temperature	293(2) K
Wavelength	0.71073 Å
Crystal system	Monoclinic
Space group	P2(1)/c
Unit cell dimensions	a = 14.8424(7) Å $\quad$ $\alpha = 90°$
	b = 11.6735(5) Å $\quad$ $\beta = 99.416(1)°$
	c = 22.0589(10) Å $\quad$ $\gamma = 90°$
Volume	3770.5(3) Å^3
Z	4
Density (calculated)	1.764 Mg/m^3
Absorption coefficient	7.301 mm^{-1}
F(000)	1964
Crystal size	0.19 x 0.12 x 0.08 mm^3
Theta range for data collection	1.87 to 30.61°.
Index ranges	-21<=h<=21, -16<=k<=16, -31<=l<=31
Reflections collected	42778
Independent reflections	11498 [R(int) = 0.0332]
Completeness to theta = 30.61°	99.0 %
Absorption correction	Semi-empirical from equivalents
Max. and min. transmission	0.9999 and 0.7589
Refinement method	Full-matrix least-squares on F^2
Data / restraints / parameters	11498 / 1 / 398
Goodness-of-fit on F^2	1.003
Final R indices [I>2sigma(I)]	R1 = 0.0263, wR2 = 0.0603
R indices (all data)	R1 = 0.0317, wR2 = 0.0622
Largest diff. peak and hole	2.638 and -0.928 e.Å^{-3}

Table 3. Bond lengths [Å] and angles [º] for irhco_bad.

_____

Ir(1)-C(1)	2.013(3)	C(9)-C(10)	1.535(5)
Ir(1)-P(1)	2.3261(8)	C(9)-C(11)	1.542(5)
Ir(1)-P(2)	2.3284(8)	C(10)-(H10A)	0.9600
Ir(1)-Cl(1)	2.5070(8)	C(10)-H(10B)	0.9600
Ir(1)-Cl(2)	2.5912(7)	C(10)-H(10C)	0.9600
Ir(1)-H(1)	1.587(10)	C(11)-H(11A)	0.9600
Ir(2)-C(26)	2.090(3)	C(11)-H(11B)	0.9600
Ir(2)-C(30)	2.100(3)	C(11)-H(11C)	0.9600
Ir(2)-C(25)	2.108(3)	C(12)-H(12A)	0.9600
Ir(2)-C(29)	2.113(3)	C(12)-H(12B)	0.9600
Ir(2)-Cl(1)	2.3831(8)	C(12)-H(12C)	0.9600
Ir(2)-Cl(2)	2.4071(7)	C(13)-C(15)	1.536(5)
P(1)-C(7)	1.843(3)	C(13)-C(14)	1.539(5)
P(1)-C(9)	1.891(3)	C(13)-C(16)	1.542(5)
P(1)-C(13)	1.891(3)	C(14)-H(14A)	0.9600
P(2)-C(8)	1.845(3)	C(14)-H(14B)	0.9600
P(2)-C(21)	1.890(3)	C(14)-H(14C)	0.9600
P(2)-C(17)	1.896(3)	C(15)-H(15A)	0.9600
C(1)-C(6)	1.412(4)	C(15)-H(15B)	0.9600
C(1)-C(2)	1.4204(4)	C(15)-H(15C)	0.9600
C(2)-C(3)	1.394(5)	C(16)-H(16A)	0.9600
C(2)-C(7)	1.511(4)	C(16)-H(16B)	0.9600
C(3)-C(4)	1.392(5)	C(16)-H(16C)	0.9600
C(3)-H(3)	0.9300	C(17)-H(20)	1.534(5)
C(4)-C(5)	1.319(5)	C(17)-C(18)	1.537(5)
C(4)-H(4)	0.9300	C(17)-C(19)	1.546(5)

C(5)-H(5)	0.9300	C(18)-H(18B)	0.9600
C(6)-C(8)	1.516(4)	C(18)-H(18C)	0.9600
C(7)-H(7A)	0.9700	C(19)-H(19A)	0.9600
C(7)-H(7B)	0.9700	C(19)-H(19B)	0.9600
C(8)-H(8A)	0.9700	C(19)-H(19C)	0.9600
C(8)-H(8B)	0.9700	C(20)-H(20A)	0.9600
C(9)-C(12)	1.531(5)	C(20)-H(20B)	0.9600
C(20)-H(20C)	0.9600	C(28)-H(28A)	0.9700
C(21)-C(24)	1.527(5)	C(28)-H(28B)	0.9700
C(21)-C(23)	1.536(5)	C(29)-C(30)	1.416(5)
C(21)-C(22)	1.543(5)	C(29)-H(29)	0.96(4)
C(22)-H(22A)	0.9600	C(30)-C(31)	1.520(5)
C(22)-H(22B)	0.9600	C(30)-H(30)	0.87(4)
C(22)-H(22C)	0.9600	C(31)-C(32)	1.540(5)
C(23)-H(23A)	0.9600	C(31)-H(31A)	0.9700
C(23)-H(23B)	0.9600	C(31)-H(31B)	0.9600
C(23)-H(23C)	0.9600	C(32)-H(32A)	0.9700
C(24)-H(24A)	0.9600	C(32)-H(32B)	0.9700
C(24)-H(24B)	0.9600	C(33)-C(33)#1	1.514(14)
C(24)-H(24C)	0.9600	C(33)-C(34)	1.529(11)
C(25)-C(26)	1.410(5)	C(33)-H(33A)	0.9700
C(25)-C(32)	1.531(5)	C(33)-H(33B)	0.9700
C(25)-H(25)	0.91(4)	C(34)-C(35)	1.542(12)
C(26)-C(27)	1.512(5)	C(34)-H(34A)	0.9700
C(26)-H(26)	0.94(4)	C(34)-H(34B)	0.9700
C(27)-C(28)	1.528(5)	C(35)-H(35A)	0.9600
C(27)-H(27A)	0.9700	C(35)-H(35B)	0.9600
C(27)-H(27B)	0.9700	C(35)-H(35C)	0.9600

C(28)-C(29)	1.520(4)		

C(1)-Ir(1)-P(1)	83.27(9)	Cl(1)-Ir(1)-H(1)	96.4(14)
C(1)-Ir(1)-P(2)	81.21(9)	Cl(2)-Ir(1)-H(1)	176.0(14)
P(1)-Ir(1)-P(2)	158.83(3)	C(26)-Ir(2)-C(30)	99.15(13)
C(1)-Ir(1)-Cl(1)	176.78(9)	C(26)-Ir(2)-C(25)	39.25(13)
P(1)-Ir(1)-Cl(1)	97.23(3)	C(30)-Ir(2)-C(25)	81.94(13)
P(2)-Ir(1)-Cl(1)	99.07(3)	C(26)-Ir(2)-C(29)	82.10(13)
C(1)-Ir(1)-Cl(2)	96.80(9)	C(30)-Ir(2)-C(29)	39.27(13)
P(1)-Ir(1)-Cl(2)	99.77(3)	C(25)-Ir(2)-C(29)	90.49(13)
P(2)-Ir(1)-Cl(2)	96.29(3)	C(26)-Ir(2)-Cl(1)	89.84(9)
Cl(1)-Ir(1)-Cl(2)	79.98(2)	C(30)-Ir(2)-Cl(1)	160.23(10)
Cl(1)-Ir(1)-H(1)	86.8(14)	C(25)-Ir(2)-Cl(1)	94.45(9)
P(1)-Ir(1)-H(1)	79.1(14)	C(29)-Ir(2)-Cl(1)	160.48(9)
P(2)-Ir(1)-H(1)	85.8(14)	C(26)-Ir(2)-Cl(2)	154.80(10)
C(30)-Ir(2)-Cl(2)	92.57(9)	C(2)-C(7)-P(1)	109.1(2)
C(25)-Ir(2)-Cl(2)	165.92(10)	C(2)-C(7)-H(7A)	109.9
C(29)-Ir(2)-Cl(2)	93.42(9)	P(1)-C(7)-H(7A)	109.9
Cl(1)-Ir(2)-Cl(2)	86.33(3)	C(2)-C(7)-H(7B)	109.9
C(7)-P(1)-C(9)	103.74(15)	P(1)-C(7)-H(7B)	109.9
C(7)-P(1)-C(13)	103.07(15)	H(7A)-C(7)-H(7B)	108.3
C(9)-P(1)-C(13)	109.74(15)	C(6)-C(8)-P(2)	107.1(2)
C(7)-P(1)-Ir(1)	99.55(10)	C(6)-C(8)-H(8A)	110.3
C(9)-P(1)-Ir(1)	116.13(11)	P(2)-C(8)-H(8A)	110.3
C(13)-P(1)-Ir(1)	121.36(11)	C(6)-C(8)-H(8B)	110.3
C(8)-P(2)-C(21)	104.31(14)	P(2)-C(8)-H(8B)	110.3
C(8)-P(2)-C(17)	105.66(15)	H(8A)-C(8)-H(8B)	108.5
C(21)-P(2)-C(17)	108.52(15)	C(12)-C(9)-C(10)	107.9(3)

C(8)-P(2)-Ir(1)	99.44(10)	C(12)-C(9)-C(11)	107.3(3)
C(21)-P(2)-Ir(1)	125.05(11)	C(10)-C(9)-C(11)	109.8(3)
C(17)-P(2)-Ir(1)	111.51(10)	C(12)-C(9)-P(1)	109.5(2)
Ir(2)-Cl(1)-Ir(1)	97.43(3)	C(10)-C(9)-P(1)	112.2(2)
Ir(2)-Cl(2)-Ir(1)	94.60(2)	C(11)-C(9)-P(1)	110.0(2)
C(6)-C(1)-C(2)	117.0(3)	C(9)-C(10)-H(10A)	109.5
C(6)-C(1)-Ir(1)	121.3(2)	C(9)-C(10)-H(10B)	109.5
C(2)-C(1)-Ir(1)	121.5(2)	H(10A)-C(10)-H(10B)	109.5
C(3)-C(2)-C(1)	120.9(3)	C(9)-C(10)-H(10C)	109.5
C(3)-C(2)-C(7)	121.4(3)	H(10A)-C(10)-H(10C)	109.5
C(1)-C(2)-C(7)	117.6(3)	H(10B)-C(10)-H(10C)	109.5
C(4)-C(3)-C(2)	120.6(3)	C(9)-C(11)-H(11A)	109.5
C(4)-C(3)-H(3)	119.7	C(9)-C(11)-H(11B)	109.5
C(2)-C(3)-H(3)	119.7	H(11A)-C(11)-H(11B)	109.5
C(5)-C(4)-C(3)	119.3(3)	C(9)-C(11)-H(11C)	109.5
C(5)-C(4)-H(4)	120.4	H(11A)-C(11)-H(11C)	109.5
C(3)-C(4)-H(4)	120.4	H(11B)-C(11)-H(11C)	109.5
C(6)-C(5)-C(4)	120.7(3)	C(9)-C(12)-H(12A)	109.5
C(6)-C(5)-H(5)	119.7	C(9)-C(12)-H(12B)	109.5
C(4)-C(5)-H(5)	119.7	H(12A)-C(12)-H(12B)	109.5
C(5)-C(6)-C(1)	121.2(3)	C(9)-C(12)-H(12C)	109.5
C(5)-C(6)-C(8)	120.5(3)	H(12A)-C(12)-H(12C)	109.5
C(1)-C(6)-C(8)	118.1(3)	H(12B)-C(12)-H(12C)	109.5
C(15)-C(13)-C(14)	108.4(3)	C(17)-C(19)-H(19A)	109.5
C(15)-C(13)-C(16)	108.6(3)	C(17)-C(19)-H(19B)	109.5
C(14)-C(13)-C(16)	107.8(3)	H(19A)-C(19)-H(19B)	109.5
C(15)-C(13)-P(1)	110.9(2)	C(17)-C(19)-H(19C)	109.5
C(14)-C(13)-P(1)	115.2(2)	H(19A)-C(19)-H(19C)	109.5

C(16)-C(13)-P(1)	105.8(2)	H(19B)-C(19)-H(19C)	109.5
C(13)-C(14)-H(14A)	109.5	C(17)-C(20)-H(20A)	109.5
C(13)-C(14)-H(14B)	109.5	C(17)-C(20)-H(20B)	109.5
H(14A)-C(14)-H(14B)	109.5	H(20A)-C(20)-H(20B)	109.5
C(13)-C(14)-H(14C)	109.5	C(17)-C(20)-H(20C)	109.5
H(14A)-C(14)-H(14C)	109.5	H(20A)-C(20)-H(20C)	109.5
H(14B)-C(14)-H(14C)	109.5	H(20B)-C(20)-H(20C)	109.5
C(13)-C(15)-H(15A)	109.5	C(24)-C(21)-C(23)	107.2(3)
C(13)-C(15)-H(15B)	109.5	C(24)-C(21)-C(22)	107.0(3)
H(15A)-C(15)-H(15B)	109.5	C(23)-C(21)-C(22)	110.3(3)
C(13)-C(15)-H(15C)	109.5	C(24)-C(21)-P(2)	107.9(2)
H(15A)-C(15)-H(15C)	109.5	C(23)-C(21)-P(2)	111.7(2)
H(15B)-C(15)-H(15C)	109.5	C(22)-C(21)-P(2)	112.6(2)
C(13)-C(16)-H(16A)	109.5	C(21)-C(22)-H(22A)	109.5
C(13)-C(16)-H(16B)	109.5	C(21)-C(22)-H(22B)	109.5
H(16A)-C(16)-H(16B)	109.5	H(22A)-C(22)-H(22B)	109.5
C(13)-C(16)-H(16C)	109.5	C(21)-C(22)-H(22C)	109.5
H(16A)-C(16)-H(16C)	109.5	H(22A)-C(22)-H(22C)	109.5
H(16B)-C(16)-H(16C)	109.5	H(22B)-C(22)-H(22C)	109.5
C(20)-C(17)-C(18)	106.8(3)	C(21)-C(23)-H(23A)	109.5
C(20)-C(17)-C(19)	107.6(3)	C(21)-C(23)-H(23B)	109.5
C(18)-C(17)-C(19)	109.6(3)	H(23A)-C(23)-H(23B)	109.5
C(20)-C(17)-P(2)	110.4(2)	C(21)-C(23)-H(23C)	109.5
C(18)-C(17)-P(2)	113.1(2)	H(23A)-C(23)-H(23C)	109.5
C(19)-C(17)-P(2)	109.3(2)	H(23B)-C(23)-H(23C)	109.5
C(17)-C(18)-H(18A)	109.5	C(21)-C(24)-H(24A)	109.5
C(17)-C(18)-H(18B)	109.5	C(21)-C(24)-H(24B)	109.5
H(18A)-C(18)-H(18B)	109.5	H(24A)-C(24)-H(24B)	109.5

C(17)-C(18)-H(18C)	109.5	C(21)-C(24)-H(24C)	109.5
H(18A)-C(18)-H(18C)	109.5	H(24A)-C(24)-H(24C)	109.5
H(18B)-C(18)-H(18C)	109.5	H(24B)-C(24)-(H24C)	109.5
C(26)-C(25)-C(32)	123.4(3)	C(29)-C(30)-H(30)	116(3)
C(26)-C(25)-Ir(2)	67.70(19)	C(31)-C(30)-H(30)	116(3)
C(32)-C(25)-Ir(2)	114.2(2)	Ir(2)-C(30)-H(30)	105(3)
C(26)-C(25)-H(25)	107(3)	C(30)-C(31)-C(32)	112.0(3)
C(32)-C(25)-H(25)	120(3)	C(30)-C(31)-H(31A)	109.2
Ir(2)-C(25)-H(25)	112(3)	C(32)-C(31)-H(31A)	109.2
C(25)-C(26)-C(27)	125.2(3)	C(30)-C(31)-H(31B)	109.2
C(25)-C(26)-Ir(2)	71.04(19)	C(32)-C(31)-H(31B)	109.2
C(27)-C(26)-Ir(2)	111.0(2)	H(31A)-C(31)-H(31B)	107.9
C(25)-C(26)-H(26)	114(3)	C(25)-C(32)-C(31)	111.3(3)
C(27)-C(26)-H(26)	117(3)	C(25)-C(32)-H(32A)	109.4
Ir(2)-C(26)-H(26)	106(3)	C(31)-C(32)-H(32A)	109.4
C(26)-C(27)-C(28)	112.3(3)	C(25)-C(32)-H(32B)	109.4
C(26)-C(27)-H(27A)	109.1	C(31)-C(32)-H(32B)	109.4
C(28)-C(27)-H(27A)	109.1	H(32A)-C(32)-H(32B)	108.0
C(26)-C(27)-H(27B)	109.1	C(33)#1-C(33)-C(34)	114.8(6)
C(28)-C(27)-H(27B)	109.1	C(33)#1-C(33)-H(33A)	108.6
H(27A)-C(27)-H(27B)	107.9	C(34)-C(33)-H(33A)	108.6
C(29)-C(28)-C(27)	111.3(3)	C(33)#1-C(33)-H(33B)	108.6
C(29)-C(28)-H(28A)	109.4	C(34)-C(33)-H(33B)	108.6
C(27)-C(28)-H(28A)	109.4	H(33A)-C(33)-H(33B)	107.5
C(29)-C(28)-H(28B)	109.4	C(33)-C(34)-C(35)	114.7(5)
C(27)-C(28)-H(28B)	109.4	C(33)-C(34)-H(34A)	108.6
H(28A)-C(28)-H(28B)	108.0	C(35)-C(34)-H(34A)	108.6
C(30)-C(29)-C(28)	123.7(3)	C(33)-C(34)-H(34B)	108.6

C(30)-C(29)-Ir(2)	69.85(19)	C(35)-C(34)-H(34B)	108.6
C(28)-C(29)-Ir(2)	113.4(2)	H(34A)-C(34)-H(34B)	107.6
C(30)-C(29)-H(29)	117(2)	C(34)-C(35)-H(35A)	109.5
C(28)-C(29)-H(29)	114(2)	C(34)-C(35)-H(35B)	109.5
Ir(2)-C(29)-H(29)	107(2)	H(35A)-C(35)-H(35B)	109.5
C(29)-C(30)-C(31)	124.3(3)	C(34)-C(35)-H(35C)	109.5
C(29)-C(30)-Ir(2)	70.88(19)	H(35A)-C(35)-H(35C)	109.5
C(31)-C(30)-Ir(2)	112.02(2)	H(35B)-C(35)-H(35C)	109.5

Symmetry transformations used to generate equivalent atoms: #1 -x+2, -y+1, -z

Curriculum Vita

Elizabeth Marie Pelczar

Education:

2001 – 2007   Ph.D. Department of Chemistry and Chemical Biology
Rutgers University, New Brunswick, NJ
Thesis: *Studies of PNP and PCP Pincer Systems: Synthesis and C-H Activation Potential of PNP Pincer Complexes and a PCP Pincer Complex Applied to Alkene Hydrogenation.*

1999-2001   M.S. Department of Chemistry
Dartmouth College, Hanover, NH
Thesis: *Ligand Study of Dismesitylphosphine in Platinum and Palladium Complexes.*

1995-1999   B.S. Chemistry and Biology
University of Hartford, West Hartford, CT

Publications:

1.   Pelczar, Elizabeth M.; Emge, Thomas J.; Krogh-Jespersen, Karsten; Goldman, Alan S. *Iron Containing PNP-Pincer complexes with unusual structural and spectroscopic features*. (In preparation).

2.   Laviska, David; Pelczar, Elizabeth; Goldman, Alan S. *An interactive high school-university program for outreach and integrated education on greenhouse gases and global warming.* (In preparation.)

3.   Pelczar, Elizabeth M.; Emge, Thomas J.; Goldman, Alan S. *A mixed-valence chloride-bridged (pincer)IrIII-(diene)IrI complex.*   Acta Crystallographica, Section C: Crystal Structure Communications (2007), C63(7), m323-m326.

4.   Pelczar, Elizabeth M.; Nytko, Emily A.; Zhuravel, Michael A.; Smith, Jeremy M.; Glueck, David S.; Sommer, Roger; Incarvito, Christopher D.; Rheingold, Arnold L.   *Synthesis and structure of platinum and palladium complexes of dimesitylphosphine*. Polyhedron (2002), 21(23), 2409-2419.

Presentations:

1.   Pelczar, Elizabeth M.; Emge, Thomas J.; Krogh-Jespersen, K.; Goldman, Alan S. *Iron and osmium pincer complexes*. Middle Atlantic Regional Meeting of the American Chemical Society, Collegeville, PA, United States, May 16-18,

2007. **(Oral)**

2. Pelczar, Elizabeth M.; Emge, Thomas J.; Goldman, Alan S. *A Series of Iron and Osmium Pincer Complexes*. Abstracts, 37th Middle Atlantic Regional Meeting of the American Chemical Society, New Brunswick, NJ, United States, May 22-25, 2005. **(Oral)**

3. Pelczar, Elizabeth M.; Goldman, Alan S. *Iron and osmium pincer complexes: Synthesis and characterization*. Abstracts of Papers, 228th ACS National Meeting, Philadelphia, PA, United States, August 22-26, 2004. INOR-222.

4. Pelczar, Elizabeth M.; Goldman, Alan S. *Synthesis and characterization of a paramagnetic iron pincer complex*. Abstracts of Papers, 226th ACS National Meeting, New York, NY, United States, September 7-11, 2003. INOR-438.

5. Pelczar, Elizabeth M.; Glueck, David S. *Synthesis of palladium and platinum complexes containing dimesitylphosphine ligands*. Abstracts of Papers, 221st ACS National Meeting, San Diego, CA, United States, April 1-5, 2001. INOR-249.

6. Pence, Laura E.; Pink, Courtney C.; Pelczar, Elizabeth M.; Broyles, Nicole M.; Whitehead, Joyce P. *Preparation and characterization of a series of trinuclear ruthenium carboxylates*. Abstracts of Papers, 220th ACS National Meeting, Washington, DC, United States, August 20-24, 2000. INOR-191.

7. Pelczar, Elizabeth M.; Pence, Laura E. *Building blocks for ruthenium coordination clusters*. Book of Abstracts, 216th ACS National Meeting, Boston, MA, United States, August 23-27, 1998. CHED-242.